Mechanisms for Maintaining the Telomere Cap in Eukaryotic Cells

Eva-Maria Holstein

Thesis submitted to the University of Newcastle upon Tyne for the degree of Doctor of Philosophy

May 2012

Institute for Ageing and Health
Institute for Cell and Molecular Biosciences, Medical School
Newcastle University

Abstract

Telomeres are found at the end of linear eukaryotic chromosome ends and contribute to genetic stability. It is crucial that telomeres are not perceived and treated as double-strand breaks by checkpoint and DNA repair proteins in order to prevent potentially lethal consequences, such as cellular ageing and cancer formation in mammalian cells (Murnane, 2006; Shin et al., 2006; Gilley et al., 2005). Hence, eukaryotic chromosome ends are masked by various telomere-binding proteins. Two crucial telomere capping proteins in *Saccharomyces cerevisiae* are Cdc13 and Yku70. Cdc13 forms a complex with Stn1 and Ten1 and binds specifically to single-stranded telomeric DNA (Grandin *et al.*, 2001). Yku70 is a subunit of the Yku complex that is found at double-stranded telomeric DNA (Tuteja and Tuteja, 2000). A temperature-sensitive allele of *CDC13*, known as *cdc13-1*, or a null-mutation of *YKU70* is used in this study to induce telomere uncapping and to study its consequences *in vivo*.

This work looks into the puzzling observation that components of the nonsense-mediated mRNA decay pathway (Upf1, Upf2, Upf3) suppress one form of telomere capping defect (*yku70*Δ), but enhance another (*cdc13-1*) (Addinall *et al.*, 2011). The same effect can be seen in Ebs1, which has previously been linked to NMD (Azzalin *et al.*, 2007). Here it is shown that Ebs1, like components of nonsense-mediated decay (NMD), regulate transcript levels of the two telomere binding proteins Stn1 and Ten1. Interestingly, increased levels of Stn1, but not Ten1, suppress the *yku70*Δ capping defect, but enhance the *cdc13-1* capping defect, indicating that NMD and Ebs1 influence Cdc13- and Yku70-dependent telomere capping through modification of Stn1 levels. It is also shown that increase in Stn1 levels alters stochiometry of the Cdc13/Stn1/Ten1 (CST) complex. Cdc13 association to telomeres is significantly reduced at the presence of increased levels of Stn1.

Inefficient telomere protection allows resection of telomeric DNA and the generation of ssDNA tracts triggers cell cycle arrest (Booth et al., 2001; Garvik et al., 1995; Lydall and Weinert, 1995; Weinert and Hartwell, 1993). It is shown that Upf2 and Ebs1 do not affect checkpoint activation in response to *cdc13-1* uncapped telomeres, but are required

for efficient G1 to S phase progression. Furthermore, Upf2 contributes to ssDNA generation at *cdc13-1* uncapped telomeres in a parallel pathway to the exonuclease Exo1 and the checkpoint protein Rad24. Remarkably, elimination of Upf2 and Exo1 or Upf2 and Rad24 allows viability of cells in the absence of the otherwise essential telomere capping protein Cdc13.

Acknowledgments

I would like to thank everyone who has helped me throughout my PhD. In particular I would like to say thanks to my supervisor David Lydall for giving me the opportunity to work in his lab and for all his support and guidance. I really appreciate that his door was always open when I had questions or wanted to discuss a certain result. A very special thank you to Alan Leake for all the chats we had and for preparing a majority of the stock solutions and media. His assistance was invaluable and allowed me to focus on the experiments. A special thanks to the past and current members of the lab for all their support and for providing an enjoyable work environment. I'm very grateful for the BBSRC, ONDEX and the Wellcome Trust for funding my studies. Last but not least I would like to thank my family and friends for all their support throughout the last couple of years, especially Meli, Sabine, Karen and Kelly who believed in me and supported me throughout my PhD. Thank you!

Table of Content

Table of Figures

Table of Tables

List of Abbreviations

ANOVA: Analysis of variance between groups
bp: base pairs
BSA: Bovine serum albumin
DAPI: 4',6-Diamidino-2-phenylindole
DDR: DNA damage respone
dNTP: deoxyribonucleotide triphosphate
DSB: double strand break
dsDNA: double-stranded DNA
DTT: dithiothreitol
g: acceleration caused by gravity
HR: homologous recombination
HU: hydroxyurea
kb: kilobases
L: litre
ml: milliliter
MMS: methyl methane sulphonate
MPT: maximum permissive temperature
MQ: Milli-Q (filtrated and deionised)
NHEJ: non-homologous end joining
NMD: nonsense-mediated decay
PMSF: phenylmethanesulfonyl fluoride
QAOS: quantitative amplification of ssDNA
RPA: replication protein A
rpm: revolutions per minute
RRM: RNA recognition motif
SDS: sodium dodecyl sulfate
ssDNA: single-stranded DNA
TAE: Tris-acetate/EDTA
TBE: Tris/Borate/EDTA
TBS: Tris-Buffered Saline
TE: Tris/EDTA

TMPyP4: Tetra(N-methyl-4-pyridyl)-porphyrin chloride

w/v: mass/volume

YEPD: yeast extract/peptone/dextrose

Budding yeast nomenclature

CDC13: Wild type gene

cdc13-1: Mutant allele

*cdc13*Δ: Null allele

Cdc13: Protein encoded by wild type gene

1. Introduction

1.1 Telomeres

Telomeres are located at the end of linear eukaryotic chromosomes. Chromosomes allow DNA to be organized and packed into the nucleus through formation of nucleosomes by wrapping the DNA around octamers of histones (two copies of H2A, H2B, H3 and H4) (Polo and Almouzni, 2006; Davey et al., 2002; Luger et al., 1997). The nucleosomes themselves are further condensed into higher-order structures and generally two types of chromatins exist: euchromatin and heterochromatin (Tamaru, 2010). Euchromatin is decondensed, rich in genes and transcriptionally active, whereas heterochromatin is tightly packed, poor in genes and transcriptionally inactive. The DNA replication fork is thought to displace histones during replication. Histones are then, together with newly synthesized histones, redistributed on the newly synthesized daughter strands and the replicated parental strands (Groth et al., 2007).

Eukaryotic genomes have multiple linear chromosomes, whereas most prokaryotic genomes have circular DNA. Two exceptions are the spirochaete *Borrelia* or the Gram-positive *Streptomyces*, both of which contain linear chromosomes (Casjens, 1999; Lin et al., 1993; Saint Girons et al., 1992). The exposed DNA ends of linear chromosomes have to be capped in order to ensure genomic integrity. Protection against DNA degradation and chromosome instability is provided by telomeres that are found at the end of eukaryotic chromosomes (Hug and Lingner, 2006; Chan and Blackburn, 2004). Telomeres are organized in nucleoprotein complexes that are known to have a crucial role in preventing cellular cancer formation and ageing (Murnane, 2006; Shin et al., 2006; Gilley et al., 2005).

Telomeres are extensively studied in various organisms. The overall telomeric DNA structure is conserved in eukaryotes, with few exceptions such as the fruit fly *Drosophila* that uses arrays of retrotransposons as telomeres (Figure 1). A better understanding of the activities taking place at telomeres will have notable implications for human ageing and cancer processes (Wellinger and Sen, 1997; Biessmann et al., 1990). Over the past decades, the yeasts *Saccharomyces cerevisae* and

Schizosaccharomyces pombe became successful model organisms for studying fundamental aspects of human biology as yeasts share many basic properties with higher eukaryotes and addressing cellular functions in yeast instead of human cells has clear benefits. Ease of genetic manipulation, simplicity of growth as well as a short generation time makes yeast a simple and powerful model organism (Bitterman et al., 2003; Botstein and Fink, 1988).

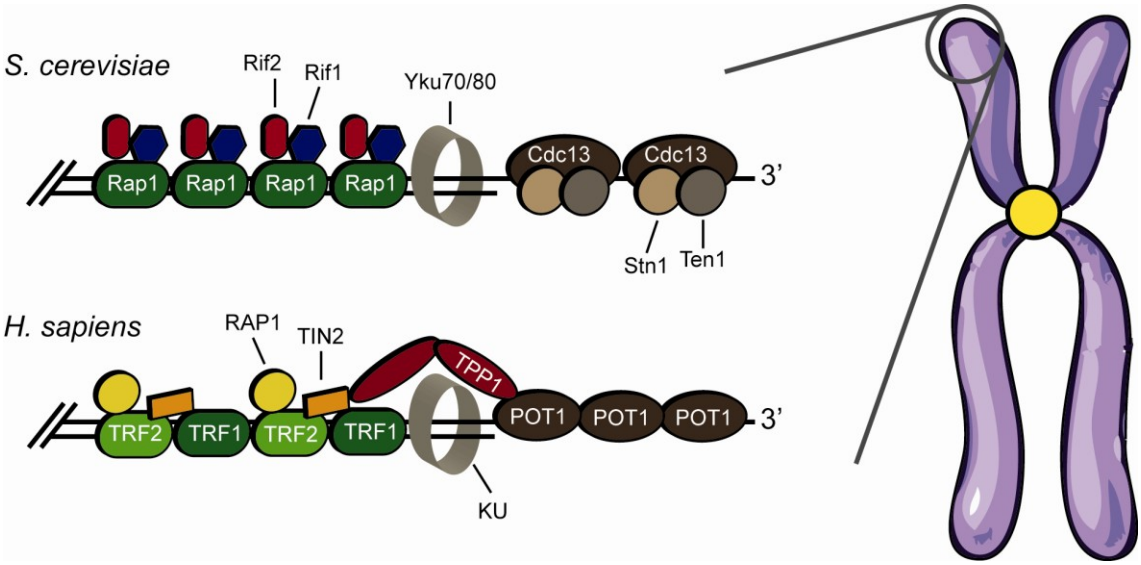

Figure 1. Schematic representation of yeast and human telomeres.

Telomeres, located at the end of eukaryotic chromosome, consist of repetitive DNA sequences and terminate in a 3' ssDNA overhang. Binding of various protein complexes to double-stranded and single-stranded telomeric DNA prevents telomeres from being recognized and treated as DNA double-strand breaks and regulates elongation of telomeres by telomerase. Double-stranded telomeric repeats in *S. cerevisiae* are bound by the Yku heterodimer and Rap1, the latter of which in turn recruits Rif1 and Rif2 to the telomere. ssDNA overhangs are bound by the CST complex consisting of Cdc13, Stn1 and Ten1. Human telomeric dsDNA is bound by TRF1 and TRF2. The two proteins are connected by TIN2 and TRF2 recruits RAP1 to the telomere. The human KU complex also binds to dsDNA. Telomeric ssDNA is bound by POT1 in conjunction with TPP1 and the complex is linked to the TRF1-TRF2-RAP1 complex through TIN2, forming a single complex known as shelterin. See text for details.

1.2 Telomere Structure

Telomeres form complexes at the end of chromosomes, consisting of DNA and various associated DNA binding proteins (Figure 1). The overall telomeric DNA structure is conserved in eukaryotes and is generally composed of tandem TG/AC repeats of variable length depending on the organism. Mammalian telomere length ranges from 5 to 15kb long TTAGGG repeats, whereas telomeric DNA sequences in the budding yeast *Saccharomyces cerevisiae* comprise considerably shorter (250-400bp) and more heterogeneous $G_{2-3}(TG)_{1-6}$ repeats (de Lange, 2005; Larrivee et al., 2004; Wang and Zakian, 1990). Telomeres of both organisms terminate in a 3' single-stranded overhang; however, they feature diverse organisation and length. 150-300nt long overhangs, often called G-tails, are detectable throughout the cell-cycle in mammalian telomeres and have the ability to fold back to form telomere loops (t-loop) (Huffman et al., 2000; Wright et al., 1997). In addition, the single-stranded overhangs can also invade adjacent subtelomeric double-stranded DNA repeats and replace the formerly bound 3'-strand by binding to the opposite DNA strand, resulting in a protective structure known as displacement loop (d-loop). It is proposed that t-loop formation may contribute to telomere capping by protecting DNA termini from being recognised as DNA double-strand breaks (Stansel et al., 2001; Griffith et al., 1999).

So far, distinct loop formations have not yet been observed in budding yeast. Telomeres in *Saccharomyces cerevisiae* are considerably shorter compared to mammalian telomeres with variable length depending on the stage of the cell cycle. Overhangs of a 50-100nt length can be detected transiently during telomere replication in late S phase. However, outside of S phase the average length is 12-14nt (Wellinger *et al.*, 1993). The short 3' overhang in combination with the more heterogeneous telomeric DNA sequences may impede strand invasion and therefore hinder t-loop formation. However, it has been shown that t-loop like structures can be obtained in an *in vitro* study in fission yeast, where Taz1 binding to an artificial telomere with elongated 3' overhangs induced t-loop formation to a moderate extent (Tomaska *et al.*, 2004). In addition, a mutant containing elongated telomeres in yeast *Klyveromyces lactis* featured a similar phenotype and de Bruin et al, 2001 claims that yeast telomeres can loop and that loop formation is mediated by SIR proteins (Cesare et al., 2008; de Bruin et al., 2001).

Other structures proposed to form at eukaryotic telomeres are G-quadruplexes. Telomeres are rich in guanine and allow formation of G-quartets consisting of 4 hydrogen-bonded guanines. Stacking of several G-quartets leads to formation of a G-quadruplex (Burge et al., 2006; Sen and Gilbert, 1988). The structures of G-quadruplexes have been well studied *in vitro* but not *in vivo*.However, recent *in vivo* studies in yeast demonstrate G-quadruplex forming potential (QFP), and a role for G4-DNA in telomere regulation has been proposed by various studies (Zhang et al., 2010; Tsai et al., 2007; Hayashi and Murakami, 2002).

Recent data demonstrates that mammalian and various eukaryotic telomeric DNA is not transcriptionally silent as previously thought and can be transcribed into telomeric repeat-containing RNA (TERRA) (Azzalin *et al.*, 2007). TERRA remains associated with telomeres and several potential functions in telomere regulations have been proposed (Redon et al., 2010; Luke and Lingner, 2009).

In yeast chromosomes, an approximately 25kb long subtelomeric region resides immediately adjacent to the telomeric repeats, consisting of middle repetitive repeat sequences which exhibit considerable variation in number and type among species and even between chromosome ends within a single strain. Subtelomeric repeats in *S. cerevisae* can roughly be divided into two regions, referred to as X and Y' repeats (Pryde and Louis, 1997). A small core X element of 473bp is present in all chromosomes and can be adjacent to the telomeric repeats or is accompanied by smaller subtelomeric repeats (STR) A, B, C and D (Louis, 1995). However, up to two-third of chromosomes exhibit a second subtelomeric region in addition to the X repeat, known as Y' elements, with up to 4 copies of tandem repeats located between the X element and the DNA termini. The Y' repeats can vary highly in sequence content, organization and overall size between the chromosomes and the number of Y' tandem repeats and their distribution can change considerably in response to telomere replication defects (Riethman et al., 2005; Lundblad and Blackburn, 1993).

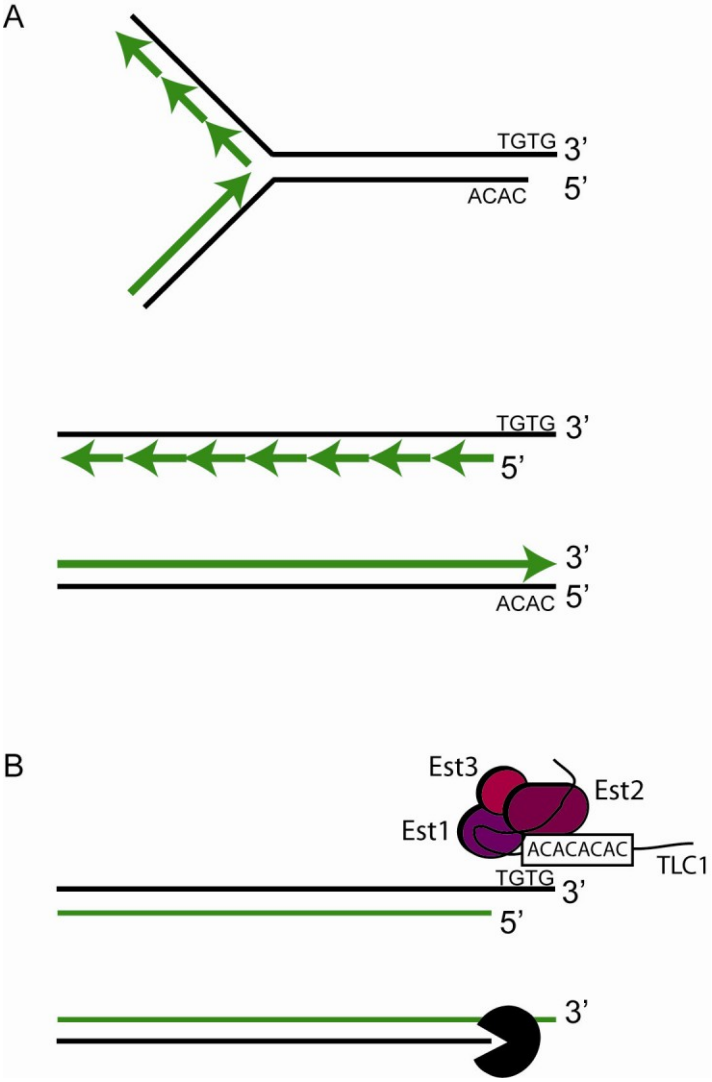

Figure 2. Schematic representation of telomere replication.

A DNA polymerases replicate the 5' to 3' leading strand from one DNA primer, whereas replication of the 3' to 5' lagging strand occurs from continuous RNA primers. The lagging strand cannot be replicated all the way to the end of the chromosome, leading to telomere shortening during each round of replication.

B Replication of the lagging strand generates a ssDNA overhang after removal of the last RNA primer, whereas leading strand replication results in a blunt chromosome end. A ssDNA overhang is generated by resection of the C-strand after replication. Telomerase can elongate 3' single-stranded DNA overhangs through reverse transcription in late S phase using the RNA moiety TLC1. See text for details.

1.3 Telomere end processing

Independent of the high variation of subtelomeric regions on different chromosomes, the subtelomeric elements have a common property: they are responsible for initiation of telomere replication, as initiation of replication cannot occur at the chromosome ends (Makovets et al., 2004; Wellinger et al., 1993).

The entire genome is duplicated during each cell division by DNA polymerases to provide a full set of chromosomes for the new cell. Replication of the two parental strands however occurs through different mechanisms as DNA polymerases are only able to add new nucleotides in a 5' to 3' direction by elongating short RNA primers (Figure 2). Replication of the 3' to 5' lagging strand proceeds from continuously added RNA primers and removal of the last RNA primer on the 5' strand generates a short 3' single-stranded overhang at the outmost chromosome end that cannot be replicated by the conventional replication machinery and is known as "the end replication problem" (Chan and Blackburn, 2004; Diffley and Labib, 2002; Lingner et al., 1997b). In contrast, the leading 5' to 3' strand can be replicated without any interruptions from one DNA primer resulting in a blunt DNA end. A recent study suggests that nucleolytic resection of the generated C-strand occurs to generate the 3' ssDNA overhang after replication of the leading strand (Faure *et al.*, 2010). The nuclease activity of the heterotrimeric MRX (Mre11-Rad50-Xrs2) complex in *S. cerevisiae* or the MRN (Mre11-Rad50-Nbs1) complex in humans have been considered as the suitable factors for G-tail processing and the theory is supported by the fact that MRX has been shown to only bind to leading strand telomeres (Faure *et al.*, 2010). However, although the complexes have been shown to have a role in 3' overhang generation, G-tail formation is not completely abolished in the absence of MRX, suggesting that other nucleases may be part of the telomere end processing (Chai et al., 2006; Clerici et al., 2006; Larrivee et al., 2004).

1.4 Telomere binding proteins

1.41 CST complex (Cdc13, Stn1, Ten1)

Cdc13, Stn1 and Ten1 are essential telomere-binding proteins that bind specifically to single-stranded telomeric 3' overhangs through Cdc13 (Figure 1) (Gao et al., 2007; Hughes et al., 2000). Like Cdc13, Stn1 is able to bind telomeric ssDNA and has been shown to interact with Ten1 through its N-terminus and with Cdc13 through its C-terminus. Ten1 seems to possess only a weak DNA binding activity, but enhances the DNA binding activity of Cdc13, indicating that all three proteins bind to telomeres in a complex (Qian et al., 2009; Puglisi et al., 2008; Gao et al., 2007). The CST complex has two crucial roles at telomeres: one is to protect telomeres by limiting the extent of telomere resection and the other is to maintain telomeres by regulating telomerase (described in detail in 1.6 and 1.8) (Nugent et al., 1996; Garvik et al., 1995).

As mentioned above, Cdc13 is an essential protein. Binding of Cdc13 alone is not sufficient for telomere protection as cells containing only the DNA binding domain (DBD) of Cdc13 are not viable (Pennock *et al.*, 2001). Fusion of Stn1 to the Cdc13 DBD in cells lacking *CDC13* restores viability, indicating that Stn1 provides efficient telomere capping. However, DBD_{CDC13}-Stn1 cells lacking *CDC13* have shortenend telomeres and eventually enter senescence. Addition of a ~15 kDa telomerase recruitment domain of Cdc13 to DBD_{CDC13}-Stn1 however restores telomere replication, indicating that recruitment of the telomerase subunit Est1 to telomeres is sufficient for telomere maintenance. These data suggests that the role of Cdc13 at telomeres is to bind to telomeric ssDNA and to recruit other factors that enable efficient telomere protection and telomere maintenance. Consistent with these data, over-expression of Stn1 and Ten1 restores the viability of cells lacking Cdc13, indicating that the essential role of Cdc13 is to recruit telomere factors to the telomere (Petreaca *et al.*, 2006). In addition, deletion of several nucleases and checkpoint components bypasses the requirement for Cdc13 and the CST complex does not seem to be required in non-dividing cells if other telomere capping proteins (Yku70 and Rap1) are present (Ngo and Lydall, 2010; Vodenicharov *et al.*, 2010).

Recent data demonstrates that Cdc13 binds to telomeres as a homodimer, and dimerization seems to be required for its DNA binding activity and efficient telomerase recruitment (Mitchell *et al.*, 2010). Several studies argue that the CST complex may form a telomere-specific RPA-like complex as several domains of Stn1 and Ten1 possess striking structural similarities to domains found in RPA proteins (Gelinas et al., 2009; Sun et al., 2009; Gao et al., 2007). But despite structural similarities, analysis of the two complexes shows functional differences. RPA binds with high affinity but low specificity to ssDNA and is involved in pathways that include single-stranded DNA intermediates, occurring in DNA repair, recombination and repair, whereas the CST complex has a role in telomere protection and telomere maintenance (Iftode et al., 1999; Wold, 1997). However, interaction between the CST and the RPA complex does occur as the RPA complex enables binding of the telomerase subunit Est1 to Cdc13 in S phase, suggesting a synergistic interaction of Cdc13 and RPA in telomerase recruitment (Schramke et al., 2004).

Binding of Cdc13 to Pol1 (the catalytic subunit of DNA polymerase α) and binding of Stn1 to Pol12 (B subunit of DNA polymerase α) suggests a potential link between replication of the C-strand and binding of the CST complex to the generated G-tail (Puglisi et al., 2008; Qi and Zakian, 2000). It has been shown that lack of interaction between Cdc13 and Pol1 through point-mutations does not affect growth but leads to elongated telomeres, supporting the idea that replication of telomeres and telomerase regulation may be linked (Qi and Zakian, 2000). Binding of Cdc13 to telomeric DNA occurs throughout the cell cycle. However, highest association of Cdc13 to the 3' overhang is detected in late S phase when the length of the single-stranded overhang is maximal, coinciding with the time when Cdc13 functions in telomerase recruitment (Schramke et al., 2004; Taggart et al., 2002).

Telomeric ssDNA in mammalian cells is bound by POT1 in conjunction with TPP1 (Figure 1) (Baumann and Cech, 2001). Separate complexes bind to ssDNA and dsDNA at telomeres in budding yeast (such as CST, Yku, Rap1-Rif1-Rif2 complexes), whereas mammalian POT1-TPP1 is linked to the telomeric dsDNA binding complex RAP1-TRF1-TRF2 through TIN2, forming a single complex known as the shelterin complex (de Lange, 2005; Houghtaling et al., 2004; Liu et al., 2004b; Ye et al., 2004b; Kim et

al., 1999). No obvious sequence similarity exists between mammalian POT1-TPP1 and the budding yeast CST complex, although structural similarities in the DNA-binding domains of Cdc13 and POT1 have been found (Linger and Price, 2009; Mitton-Fry et al., 2002). However, the CST complex in budding yeast seems to have more structural similarities with the RPA complex than POT1-TPP1 (Sun et al., 2009; Gao et al., 2007). Miyake et al. (2009) argues that CST and POT1 have redundant roles in telomere protection. Interestingly, a recent study shows that RPA and POT1 binding to telomeric ssDNA is regulated by TERRA (telomeric repeat-containing RNA), leading to displacement of RPA in late S phase and promotion of POT1 binding after S phase (Flynn *et al.*, 2011).

Orthologues of the budding yeast CST complex have been found in mammalian cells consisting of CTC1 and a STN1 and TEN1 homolog (Miyake *et al.*, 2009). The complex has no specific affinity to telomeric ssDNA and binding to telomeres is independent of POT1. A recent study in mice proposes that the mammalian CST complex is not involved in telomere capping, but facilitates restart of stalled replication forks, thereby aiding telomere replication (Gu *et al.*, 2012). However, the same group showed that similar to Cdc13 in yeast, loss of CTC1 results in telomere shortening and acute single-stranded DNA accumulation. Various data indicate that CST and shelterin complex cooperate to protect telomeres. A study from 2009 proposes that human CST associates with the shelterin complex and both POT1 and CST compete with RPA for binding to the G tail (Wan et al., 2009; Griffith et al., 1999).

1.4.2 Yku complex

The heterodimeric Yku70/Yku80 complex binds to double-strand breaks as well as double-stranded telomeric repeats and plays a crucial role in telomere protection and telomere maintenance (Figure 1) (described in detail in 1.6 and 1.8). Like Cdc13, Ku contributes to telomere maintenance by mediating telomerase recruitment to telomeres. In G1 phase of the cell cycle, telomerase recruitment is dependent on Ku and occurs through interaction of Ku with TLC1, the RNA component of telomerase (Stellwagen et al., 2003; Peterson et al., 2001; Porter et al., 1996). Yku plays a role in telomere capping

by protecting telomeres from degradation with several studies indicating that Yku limits nucleolytic degradation of the telomeric C-strand by Exo1 and perhaps other nucleases (Bertuch and Lundblad, 2004; Maringele and Lydall, 2002). In addition to limiting resection of telomeres, Yku protects telomeres from inappropriate amplification of subtelomeric Y' elements through homologous recombination (Fellerhoff *et al.*, 2000).

The Yku complex plays a key role in DNA repair of DSBs and recombination pathways via NHEJ by interacting with the DNA ligase IV (Wilson *et al.*, 1997). Ku stabilizes the DNA ends for ligation and aids ligation by recruiting the ligase complex and additional repair proteins to DSBs (Ramsden and Gellert, 1998; Pang et al., 1997).

Moreover, Ku is crucial for enabling telomere position effect by facilitating co-localization of the silent information regulator proteins Sir2, Sir3 and Sir4 with Rap1. Loss of Ku almost completely abolishes transcriptional silencing at telomeres (Boulton and Jackson, 1998). Sir binding is promoted through Ku by counteracting the binding of the competing Rif1 and Rif2 proteins and the interplay of Sir4 and Ku seems to be required for recruitment of the other proteins of the Sir complex to the telomere (Roy et al., 2004; Tsukamoto et al., 1997).

A role of Ku at anchoring telomeres to the nuclear periphery in a cell cycle dependent manner has been proposed in several studies. Telomeres seem to delocalize from the nuclear envelope upon telomere replication by repressing the Ku-mediated positioning mechanism. One reason for keeping telomeres close to the nuclear periphery might be that several proteins involved in telomere position effect (TPE) are clustered there (Ebrahimi and Donaldson, 2008; Taddei and Gasser, 2004; Hediger et al., 2002; Tham et al., 2001).

1.5 Telomerase and telomere replication

As mentioned in 1.3, replication of the 3' to 5' lagging strand occurs from continuously added RNA primers, resulting in a short 3' single-stranded overhang at the chromosome end after removal of the last RNA primer (Figure 2). The end replication problem leaves the cell with the predicament that telomeres shorten progressively with every cell cycle, eventually leading to either loss of genomic information or senescence, the loss of being able to divide. Consequently, maintaining telomere length homeostasis is fundamental for genomic integrity. On the one hand, the telomere itself supports genomic integrity by providing a buffer of non-coding repeats that can be shortened during cell divisions without losing any genetic information. One the other hand, critically short telomeres either initiate cell cycle arrest or telomere elongation. Many eukaryotes are able to bypass the progressive shortening by using a reverse transcriptase called telomerase. The enzyme is composed of several subunits including a RNA moiety, known as *TLC1* in *S. cerevisiae* or hTERT in mammalian cells, which serves as a template for elongating 3' single-stranded DNA overhangs through reverse transcription in late S phase (Figure 2) (Greider and Blackburn, 1985). The four subunits of yeast telomerase are encoded by *TLC1, EST1, EST2* and *EST3* (Lendvay et al., 1996; Lundblad and Szostak, 1989).

It is believed that telomerase activity is coupled to the C-rich strand synthesis by the conventional DNA replication machinery, as inactivation of the DNA polymerase α and DNA polymerase δ inhibits telomerase-dependent G-strand elongation in *S. cerevisiae* (Diede and Gottschling, 1999). So far, little is known about coordination between G-strand and C-strand synthesis in mammalian cells, however, inactive DNA polymerase α in mammalian cells leads to elongated 3' overhangs, indicating that the coordination between telomerase action and conventional DNA replication machinery might be a common attribute in eukaryotes (Nakamura *et al.*, 2005).

In the absence of telomerase, telomeres gradually shorten and enter senescence when a critical telomere length is reached. Occasionally, cells can overcome senescence and maintain telomere length by using homologous recombination (HR) to amplify either subtelomeric or telomeric repeats. These cells are called survivors and telomere

elongation in these cells is known as alternative lengthening of telomeres (ALT) (Teng and Zakian, 1999; Lundblad and Blackburn, 1993). Telomerase is not detectable in most human somatic cells, leading to telomere shortening and subsequent senenscence through a persistent DNA damage response which provides a potent barrier to cancer by limiting the number of cell divisions (Blasco, 2007; d'Adda di Fagagna et al., 2003). However, human stem cells express telomerase and in approximately 85% of cancers telomerase is up-regulated, allowing ongoing telomere maintenance and subsequent continued proliferation required for oncogenesis. Similar to yeast survivors, a small percent of human cancers maintain their telomeres through alternative lengthening of telomeres (ALT) using homologous recombination (Cesare and Reddel, 2010).

Regulation of telomerase activity and recruitment to telomeres is primarily obtained by telomeric factors. For instance, the repetitive structure of telomeres allows formation of G-quadruplex structures in human cells (Parkinson *et al.*, 2002) which potentially hinder efficient replication of the outmost chromosome ends. Recent data reveals TERRA as an inhibitor of telomerase (Redon *et al.*, 2010). *In vitro* data demonstrated that TERRA associates with telomerase by binding to the RNA template sequence of telomerase RNA. However, further studies are required to show how TERRA inhibits telomere elongation.

It has been demonstrated that telomeric factors such as the RecQ-like helicase WRN are required for efficient telomere replication. Loss of function of WRN leads to premature senescence, telomere shortening and consequently to loss of genomic information (Crabbe *et al.*, 2004). The disorder, known as Werner syndrome, demonstrates the importance of the proficient interaction of telomeric factors, telomerase and the DNA replication machinery to ensure efficient telomere replication. In addition, telomere binding proteins play a crucial role in telomerase regulation as described in detail in the next chapter.

1.6 Role of Telomere-Binding Proteins in Telomerase Regulation

Besides G-quadruplexes and other telomeric factors, telomere binding proteins are crucial factors for regulating telomerase. One way of regulating telomerase activity is provided by controlling telomerase recruitment to the telomeres. In *S. cerevisiae* access of telomerase to telomeres is controlled by telomeres being able to switch between extendable and non-extendable states. Telomerase does not elongate every telomere during each cell cycle, but preferentially extends short telomeres probably due to two mechanisms: earlier replication of short telomeres, thus allowing telomerase more time to amplify the telomere and the "protein-counting model" which depends on several telomere binding proteins (Puglisi et al., 2008; Teixeira et al., 2004). The latter is due to Rap1 binding to telomeres (Figure 1). Rap1 is known to negatively control telomere length by recruiting the telomerase inhibitors Rif1 and Rif2 (Levy and Blackburn, 2004; Hardy et al., 1992; Conrad et al., 1990). In fact, the amount of Rap1 bound to the telomere is proportional to the length of telomeric repeats, thereby allowing increased binding of Rif1 and Rif2. Thus, shorter telomeres are more likely to be elongated by telomerase (Marcand *et al.*, 1997).

Telomeric double-stranded DNA in mammalian cells is bound by the so-called shelterin complex, consisting of Rap1 along with Trf1, Trf2, Tin2, Tpp1 and the ssDNA and dsDNA binding protein Pot1 (Liu *et al.*, 2004a). It has been shown that each component of the complex acts as a repressor of telomerase, in agreement with the protein-counting mechanism shown in *S. cerevisiae*. Long telomeres are bound by additional proteins, thus increasing the negative effect on telomerase activity (Ye et al., 2004a; Li and de Lange, 2003; Loayza and De Lange, 2003; Smogorzewska et al., 2000). A similar mechanism has been shown in fission yeast, where Taz1, the orthologue of Trf1 and Trf2, is responsible for recruiting telomerase inhibitors, suggesting an overall conserved mechanism in eukaryotes (Cooper *et al.*, 1997).

DsDNA binding proteins are crucial for maintaining telomere length, but proteins bound to the 3' ssDNA overhang are also important for coordinated telomerase recruitment and telomerase activity. The essential protein Cdc13 in *Saccharomyces cerevisae* binds specifically to the exposed single-stranded TG_{1-3} overhangs in

conjunction with Stn1 and Ten1 and binding plays a decisive role in promoting telomerase recruitment to its site of action (Pennock et al., 2001; Grandin et al., 2000; Grandin et al., 1997; Nugent et al., 1996). Est1, a subunit of telomerase is recruited and bound by Cdc13 in late S phase, when telomerase action occurs. The complex is then thought to promote telomere elongation by either recruiting the remaining components of telomerase to the telomere or by activating the bound telomerase (Chan et al., 2008; Bianchi et al., 2004; Nugent et al., 1996). Taggart et al. (2002) demonstrated that association of the catalytic telomerase subunit Est2 to telomeres is considerably reduced in a *cdc13-2* mutant strain during S phase, supporting the idea of a function of Cdc13 in telomerase recruitment (Taggart *et al.*, 2002). Moreover, the same group demonstrated that Est1 levels increased 2-3 fold during changeover from G_1 to S phase; the same pattern has been demonstrated for telomere association, at which binding of Est1 to telomeres during S phase shows an impressive increase of 15- to 30- fold (Schramke *et al.*, 2004). In contrast, Est2 association to telomeres appears to be continuous throughout the cell cycle until mitosis (Smith *et al.*, 2003). An interesting study of Bianchi et al. (2004) demonstrated that relocation of Cdc13 or Est1 to non-telomeric sites results in telomerase recruitment as long as the Cdc13 –Est1 interaction is intact (Bianchi *et al.*, 2004). Several studies have shown that defects of Cdc13 binding Est1 results in failure of telomerase recruitment (Pennock et al., 2001; Lingner et al., 1997a; Nugent et al., 1996). Overall, these results suggest an active recruitment of telomerase to telomeres in a Cdc13-dependent manner and reinforce the importance of Cdc13 interaction with the telomerase subunit in order to enable efficient telomerase action. In addition, phosphorylation of Cdc13 by the cyclin-dependent kinase Cdk1 and/or the Tel1 and Mec1 checkpoint kinases results in a switch from Cdc13 binding Stn1 and Ten1 to Cdc13 binding Est1 instead (Li et al., 2009; Tseng et al., 2006). Moreover, Cdc13 was found to maintain the complex balance between positive regulation through Est1 recruitment and negatively controlling telomerase through Cdc13 interaction with Stn1 and Ten1. It is argued that this balance may be achieved through direct competition between Stn1 and Est1 for Cdc13 binding; reassembly of the CST complex would then lead to dissociation of telomerase from the telomere (Evans and Lundblad, 2000; Grandin *et al.*, 2000). It is thought that reassembly of the CST complex is caused by dephosphorylation of Cdc13 and is coupled to C-strand synthesis (Li et al., 2009; Smogorzewska and de Lange, 2004).

Several publications have shown that Cdc13, as well as Stn1, demonstrate direct interaction with subunits of the DNA polymerase α / primase complex. Telomerase activity is abolished in the absence of DNA polymerase α / primase and DNA polymerase δ, suggesting that completion of lagging strand synthesis and telomere elongation by telomerase may be co-regulated and mediated by Cdc13 and Stn1, followed by subsequent dissociation of telomerase from the telomere by Stn1 binding to Cdc13 (Puglisi et al., 2008; Grossi et al., 2004; Diede and Gottschling, 1999). The fact that telomerase activity at telomeres requires the DNA polymerases α and δ supports the idea of a linked interaction between telomere replication of the lagging strand and telomerase activity (Diede and Gottschling, 1999). Lastly, Est1 has been shown to convert single-stranded telomeric DNA to a G-quadruplex structure, thereby limiting telomerase binding to the 3' terminus (Zhang *et al.*, 2010).

Single-stranded telomeric overhangs in mammalian cells are predominately bound by POT1, which is part of the shelterin complex, and similar to Cdc13 in budding yeast, hPOT1 negatively regulates telomerase. Binding of POT1 to single-stranded telomeric DNA inhibits telomerase activity, presumably by limiting access of telomerase to telomeres (Churikov and Price, 2008; Kelleher et al., 2005). On the other hand, POT1 seems to be able to disrupt G-quadruplex structures, thus facilitating telomerase access to the telomere (Torigoe, 2007; Zaug et al., 2005). Similar to budding yeast, telomere elongation by telomerase in fission yeast seems to be coupled to DNA polymerase α and δ dependent lagging strand replication (Moser *et al.*, 2009).

The Yku complex contributes to telomere maintenance in *S. cerevisiae* by recruiting telomerase to telomeres in G1 through physical interaction with the telomerase RNA subunit TLC1 (Fisher *et al.*, 2004). Recruitment in G1 is independent of Cdc13 and in addition, Ku promotes telomerase activity in late S phase by recruiting Est1 to Cdc13 (Fisher et al., 2004; Diede and Gottschling, 1999). In the absence of Ku, Est2 cannot be detected in G1 and only approximately 50% of Est2 wild-type levels are associated with telomeres in late S phase, probably due to Cdc13 (Fisher *et al.*, 2004). Recruitment of telomerase to telomeres by Yku and binding of Yku to telomeres seems to be independent of telomere length (Bianchi and Shore, 2007; Sabourin *et al.*, 2007).

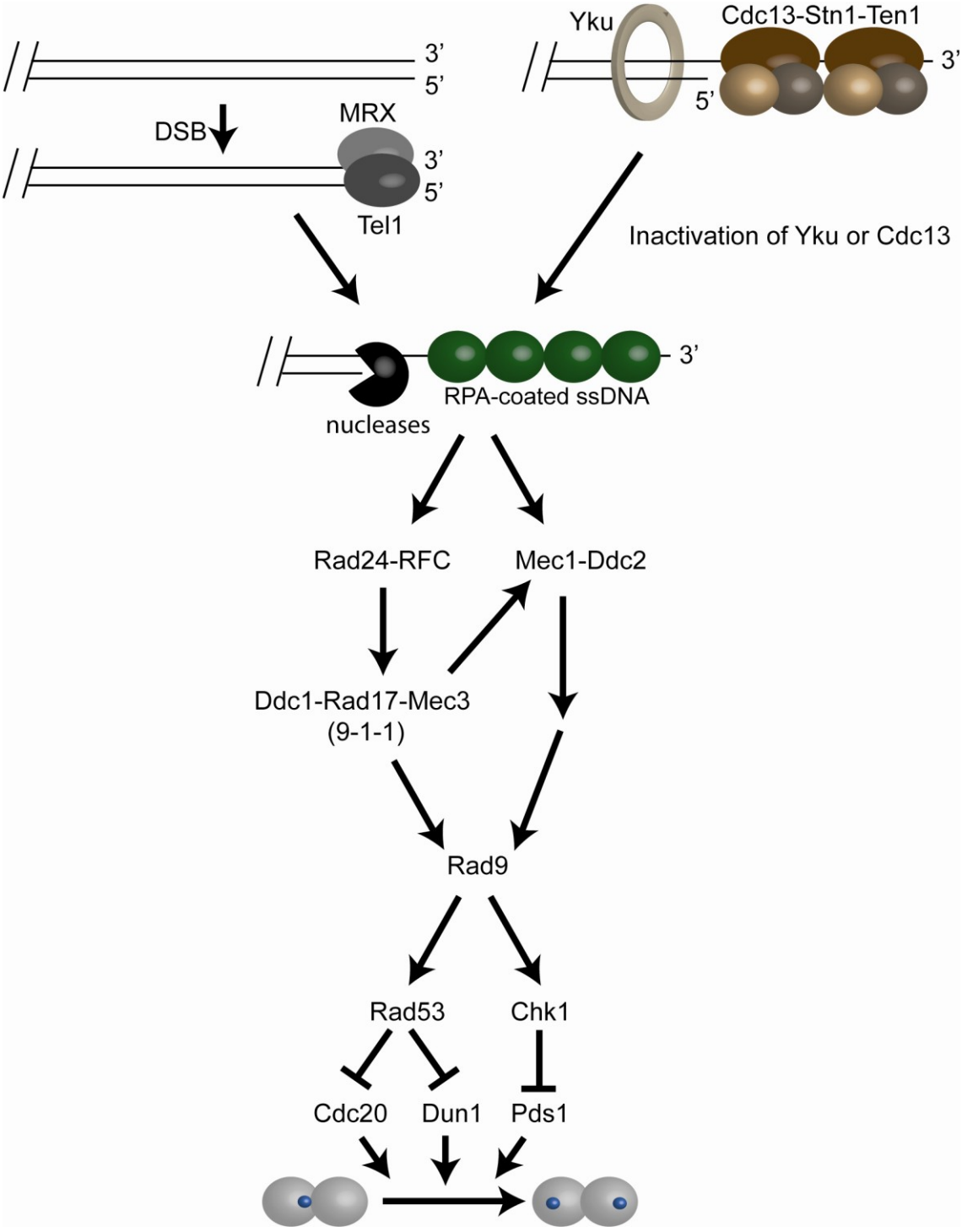

Figure 3. Schematic representation of the DNA damage response pathway at DSBs and uncapped telomeres in *S. cerevisiae* (see text for details).

1.7 DNA Damage Responses

DNA double-strand breaks within a chromosome trigger a cascade of DNA damage checkpoint and DNA repair pathways, resulting in a cell cycle arrest until the damage is repaired. This surveillance mechanism is crucial for the cell as continued cell cycle progression with unrepaired DNA double-strand breaks can cause accumulation of DNA changes with catastrophic consequences, such as chromosome instability or even cell death (Longhese *et al.*, 2006; Shiloh, 2006). DNA damage checkpoint action and subsequent G_2/M cell cycle arrest is well conserved between humans and yeast. The ATM and ATR-related PIKKs Tel1 and Mec1 in *S. cerevisiae* are key players in DNA damage checkpoint response that transmit and amplify the DNA damage signal through binding to the site of damage (Figure 3) (Longhese *et al.*, 2006; Shiloh, 2006). Tel1 binding to DNA DSBs and its subsequent checkpoint activation is initiated upon binding of the MRX (Mre11-Rad50-Xrs1) complex to the unprocessed break. MRX then instigates resection of the DNA to generate 3' overhangs (Falck et al., 2005; Nakada et al., 2003). Human ATM activation, analogous to yeast, results from association to MRN (Mre11-Rad50-Nbs1). The generated 3' overhang is bound by the RPA complex, which in turn is recognized by Mec1 and Ddc2 in yeast or ATR in mammalian cells (Zou and Elledge, 2003). RPA is also responsible for recruiting homologous recombination proteins such as Rad51 and Rad52 in yeast. Mec1 dependent checkpoint activation is enhanced by binding of the 9-1-1 complex Ddc1-Rad17-Mec3 through a replication factor C (RF-C)-like complex in conjunction with Rad24 (Majka *et al.*, 2006). Transmission of the DNA damage signal is mediated through Rad9, allowing activation of Rad53 or Chk1 via autophosphorylation and resulting in a subsequent cell cycle arrest at the G_2/M checkpoint (Sweeney et al., 2005; Gilbert et al., 2001).

The arrest then enables repair of the DNA damage mainly through homologous recombination (HR) or non-homologous end joining (NHEJ) (Usui *et al.*, 2001). The former requires the initial nucleolytic resection of the DSB in order to allow invasion of homologous sequences by the generated 3' single-stranded overhangs. Resection is initiated by the nuclease Sae2 and the MRX complex to generate a small overhang. The nucleases Exo1, DNA2 and the helicase Sgs1 are required for extensive resection of the DSB ends to activate cell cycle arrest and allow homologous recombination of the break

(Bonetti et al., 2009; Mimitou and Symington, 2008; Zhu et al., 2008; Tsubouchi and Ogawa, 2000).

NHEJ is largely used in higher eukaryotes and is achieved through direct ligation of the processed DNA overhangs without sequence homology (Hefferin and Tomkinson, 2005; Haber, 2000a; Haber, 2000b). In yeast, the MRX complex and the Yku70/80 complex are part of the NHEJ repair pathway. The Yku complex not only stabilizes DNA ends for ligation and protects them of extensive nucleolytic degradation, but also facilitates ligation by recruiting the ligase complex and additional repair proteins to DSBs (Ramsden and Gellert, 1998; Pang et al., 1997).

1.8 Dysfunctional Telomeres

ssDNA overhangs play a crucial role in DNA checkpoint and DNA repair pathways, which leaves the cell with the challenge to maintain 3' ssDNA overhangs as part of an intact telomere as well as to prevent activation of DNA checkpoint, repair and recombination pathways in response to single-stranded telomeric DNA. It is of extreme importance that telomeres are not recognized and treated as DSBs in order to prevent the lethal consequences caused by extensive DNA degradation or end-to-end joining events. A wide range of telomeric factors ensure efficient telomere capping in order to circumvent activation of the DNA damage machinery. Several studies in mammalian and yeast systems propose that binding of Pot1 or the CST complex to ssDNA at telomeric overhangs inhibits localisation of RPA to telomeres, thereby preventing activation of DNA damage responses at telomeric termini (Denchi and de Lange, 2007; Hirano and Sugimoto, 2007). Other telomere binding factors, such as the Yku and the Rap1/Rif1/Rif2 complex also function in preventing telomeres from being treated as DSBs.

Dysfunctional telomere capping caused by loss of function, modification or defects in essential telomere-binding proteins, as well as critically short telomeres due to defects in telomere homeostasis, can activate a DNA damage response at telomeres with disastrous consequences for the cell. End-to-end fusions between telomeres caused by recombination and NHEJ events as well as nucleolytic resection of telomeric DNA can lead to telomere loss, genomic instability and subsequent permanent cell cycle arrest and cell death. One fatal consequence of dysfunctional telomeres is tumorigenesis, caused by loss of genomic integrity and consequent mis-regulation of genes involved in growth control (Artandi and DePinho, 2000; DePinho, 2000).

Consequences of dysfunctional telomere capping can for instance be observed in *S. cerevisae*. *cdc13-1* mutants containing a temperature-sensitive mutant allele of the telomere capping protein Cdc13. No capping defect can be observed in *cdc13-1* cells growing below 26°C (permissive temperature) and cells proliferate as well as wild-type cells. However, temperature shift of *cdc13-1* mutants to 26°C or higher (non-permissive temperature) causes telomere uncapping, exposure of the G-tail and binding of RPA to

the unprotected ssDNA. Bound RPA is then able to activate the DNA damage response machinery, resulting in a Rad9-dependent cell cycle arrest in G_2/M phase, nucleolytic C-strand resection and subsequent ssDNA accumulation (>30 kilobases) (Figure 3) (Booth et al., 2001; Garvik et al., 1995; Lydall and Weinert, 1995; Weinert and Hartwell, 1993). Temperature-sensitive *cdc13-1* allows conditional telomere uncapping, thus making it a great tool to study telomere uncapping under controlled experimental conditions.

The important role of the DNA damage checkpoint protein Rad9 in mediating cell cycle arrest has been demonstrated in *cdc13-1 rad9*Δ double mutants (Garvik *et al.*, 1995). Unlike *cdc13-1* mutants, *cdc13-1 rad9*Δ mutants do not halt cell cycle progression upon temperature shift, but continue cycling until accumulated DNA damage eventually causes cell death. Interestingly, Rad9 does not only arrest cells on the basis of ssDNA generation, but appears to also influence the amount of ssDNA (Lydall and Weinert, 1995). Zubko et al (2004) demonstrated that to some extent the checkpoint protein can inhibit C-strand resection by the exonuclease Exo1 at subtelomeric regions. The 5'-3' exonuclease has been shown to play a critical role in extensive telomeric DNA degradation at uncapped telomeres, which extends beyond the telomeric regions (Zubko et al., 2004; Garvik et al., 1995; Lydall and Weinert, 1995).

Exo1 is almost entirely responsible for single-stranded DNA generation at telomeres dysfunctional in Ku (Maringele and Lydall, 2002). Although resection at *cdc13-1* uncapped telomeres is mainly dependent on Exo1 activity, deletion of the exonuclease does not completely abolish generation of ssDNA. Zubko et al (2004) demonstrated that the remaining ssDNA is reduced but not completely abolished in *exo1*Δ mutants in the absence of the checkpoint protein Rad24. Hence, a Rad24-dependent nuclease and a further third nuclease are likely to be involved in C-strand resection at *cdc13-1* uncapped telomeres. Recent data suggests that the helicase Pif1 plays a role in resection. Pif1 resects telomeric DNA independently of Exo1 and deletion of both *PIF1* and *EXO1* abolishes ssDNA generation (Dewar and Lydall, 2010).

Similar results can be seen at dysfunctional telomeres in *S. pombe* or mammalian cells. Loss of function of fission yeast Pot1 or hPOT1 results in chromosome circularisation

(Baumann and Cech, 2001). Two POT1 genes exist in mice, POT1a and POT1b. POT1a is essential and loss of POT1a leads to cell cycle arrest, accumulation of telomeric ssDNA and chromosome instability (Wu *et al.*, 2006). POT1b is not essential but lack of POT1b has also shown to increase telomeric ssDNA (Hockemeyer *et al.*, 2006). Knockdown of human POT1 using siRNA, leads to apoptosis, senescence and chromosome instability, indicating striking similarities between yeast Cdc13 and POT1 in response to telomere uncapping (Veldman *et al.*, 2004). Interaction between mammalian POT1 and the shelterin protein TPP1, and the fission yeast Pot1 and Tpz1, is required for efficient protection of telomeres, showing that POT1/Pot1 just like budding yeast Cdc13 needs other telomere factors to ensure telomere capping (Miyoshi et al., 2008; Hockemeyer et al., 2006). Similarly, elimination of mammalian or plant CST complexes results in telomere degradation and ssDNA accumulation (Miyake *et al.*, 2009; Surovtseva *et al.*, 2009).

As described earlier, Cdc13 is crucial for protecting the chromosome ends from unregulated extensive nucleolytic degradation. Efficient telomere capping is ensured through interaction of Cdc13 with two proteins, Stn1 and Ten1. Loss of any component results in catastrophic loss of telomere integrity through degradation of the exposed DNA termini and single-stranded DNA accumulation, an indicator for a pronounced defect in telomere capping (Grandin et al., 2001; Grandin et al., 1997).

A recent study argues that the essential role of Cdc13 can be bypassed by co-over-expressing Ten1 and Stn1, as long as the interaction between Stn1 and Pol12 (the polymerase α-primase regulatory subunit) is still intact. In this case, telomere capping appears to be maintained by a chromosome end protection mechanism that is coupled to conventional DNA replication (Petreaca et al., 2006; Grossi et al., 2004). In addition, a recent study observed that the interaction of Stn1 with Ten1 is sufficient to maintain telomere capping; the direct interaction of Stn1 with Cdc13 does not seem to be required (Petreaca *et al.*, 2007). However, the direct interaction of Ten1 with Cdc13 may still be required for chromosome end protection and does not rule out a crucial role of Cdc13 in telomere capping.

In addition to playing an essential role in processing DSBs, Ku carries out a wide range of functions at telomeres. Ku was observed to restrain telomeric DNA degradation of the 5' strand caused by nuclease activity at telomeres. Elimination of the heterodimeric Ku results in telomere shortening and a temperature-sensitive growth defect that can partially be suppressed by over-expressing subunits of telomerase (Teo and Jackson, 2001; Feldmann and Winnacker, 1993). Similar to *cdc13-1*, cells lacking any of the two subunits of the Yku complex undergo telomere uncapping, leading to resection, ssDNA accumulation and cell cycle arrest (Maringele and Lydall, 2002). Interestingly, less ssDNA is generated in *yku70*Δ mutants compared to *cdc13-1* mutants at non-permissive temperature (Zubko et al., 2004; Maringele and Lydall, 2002). Unlike *cdc13-1* mutants, cell cycle arrest in *yku70*Δ mutants is independent of the 9-1-1 complex (Rad17, Mec3, Ddc1) and the complex has no role in resection of *yku70*Δ telomeres. Resection seem to be almost entirely dependent on Exo1 as no ssDNA can be detected in *yku70*Δ *exo1*Δ mutants and cells are able to grow at high temperatures (37°C) (Maringele and Lydall, 2002). However, there are some similarities to *cdc13-1*; just like in *cdc13-1* mutants, Rad9 and MRX complex inhibit resection in *yku70*Δ mutants (Foster et al., 2006; Maringele and Lydall, 2002).

Similarly to the Yku and the CST complex, telomerase supports telomere capping which seems to be independent of both complexes. Recent data indicates that the ability of the telomerase subunit Est1 to form G-quadruplexes at telomeres is essential for the telomerase capping function (Tong et al., 2011; Zhang et al., 2010). Deletion of any of the telomerase subunits leads to telomere shortening, activation of DNA damage response and ssDNA accumulation. The additional deletion of the Yku complex is synthetically lethal, indicating that telomerase has a role in telomere protection in addition to its role in telomere elongation (Hackett and Greider, 2003; Nautiyal et al., 2002; Gravel et al., 1998; Nugent and Lundblad, 1998; Polotnianka et al., 1998). Furthermore, deletion of *EST1* results in recombination of subtelomeric Y' elements (Tong *et al.*, 2011).

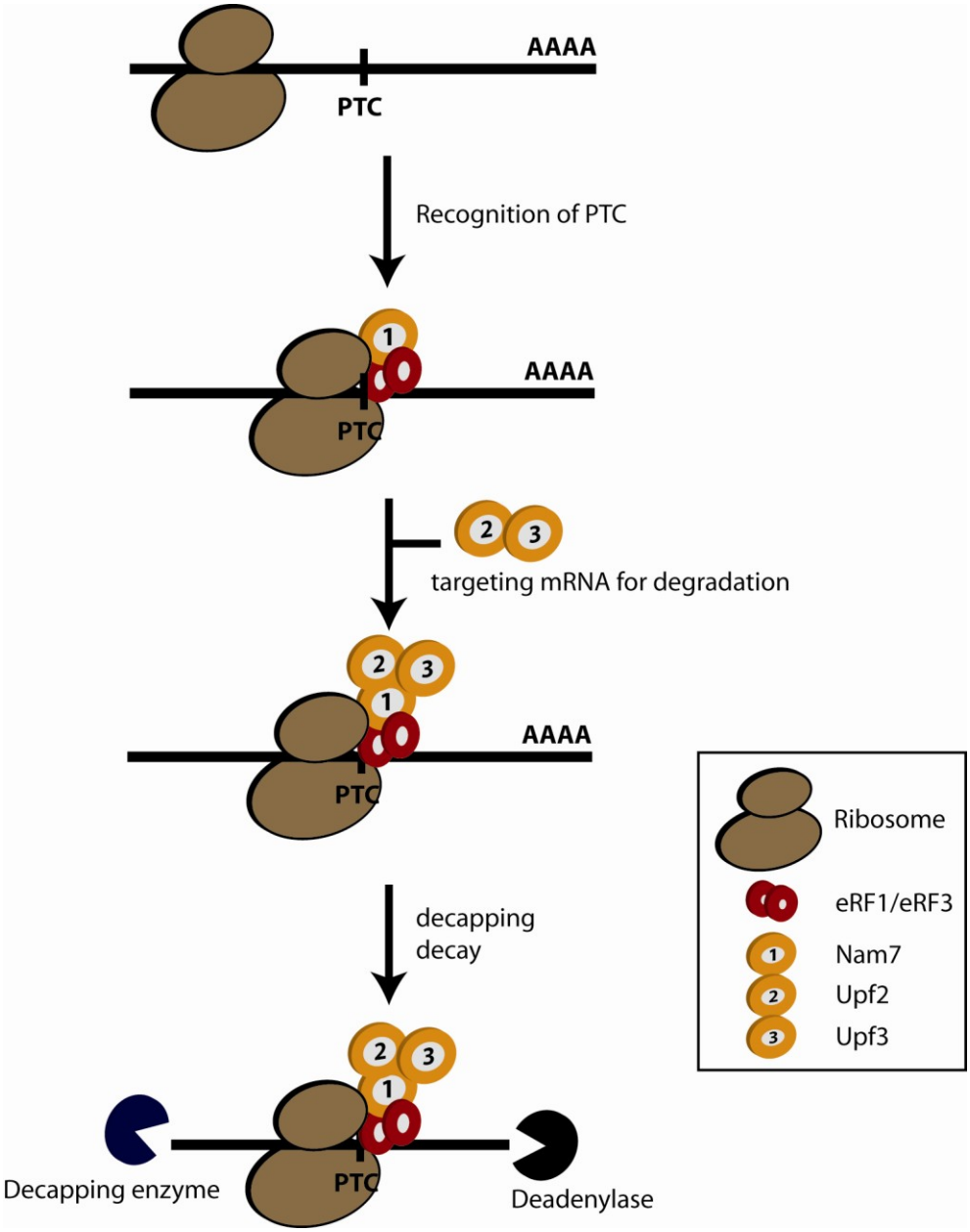

Figure 4. Simplified model for the nonsense-mediated mRNA decay pathway in *S. cerevisiae*.

Eukaryotic release factors eRF1 and eRF3 associate with the ribosome after the ribosome encounters a premature termination codon (PTC) on the mRNA. Nam7 binds to the complex, targets the mRNA to processing bodies (P-bodies) and subsequent Upf2 and Upf3 binding triggers decay of the mRNA through exosome-mediated 3'-5' decay or through decapping and Sep1-mediated 5'-3' decay. See text for details.

1.9 Nonsense-Mediated Decay

1.9.1 Overview

Telomere homeostasis requires a tight control of telomere association of the various factors involved in telomere capping or telomere length regulation. Interaction of proteins with telomeres can for instance be cell cycle regulated and be dependent on telomere replication, activity of cyclin-dependent kinases such as CDK or the overall structure of telomeres (Vodenicharov and Wellinger, 2006). Moreover, regulation of the amount of proteins associating with telomeres can already occur at the transcriptional level by regulating mRNA levels of telomeric factors by the nonsense-mediated mRNA decay (NMD) pathway. NMD is a surveillance mechanism that degrades mRNAs containing a premature translation-termination codon (PTC) in order to prevent translation of truncated and potentially harmful proteins. However, it has also been shown that NMD controls mRNA levels of various wild-type genes, including genes involved in telomere maintenance (Lejeune and Maquat, 2005; Holbrook et al., 2004; Dahlseid et al., 2003). Premature translation-termination codons can arise from various mutations, such as nonsense mutations, for instance a termination codon generated by base substitutions. Other examples are frameshifts caused by random nucleotide insertions and deletions or errors in pre-mRNA splicing. In addition, the termination codon of short upstream open reading frames (uORFs) can be recognized as a PTC and inefficiently spliced RNAs have been shown to be a target of NMD (Sayani et al., 2008; Chang et al., 2007).

Recognition and targeting of mRNAs for decay is carried out by three proteins in *S. cerevisiae*: Nam7 (alias Upf1), Nmd2 (alias Upf2) and Upf3, whereas the mammalian orthologues UPF1-3 are accompanied by SMG1 and SMG5-7 (Serin et al., 2001; Lykke-Andersen et al., 2000; Perlick et al., 1996; Cui et al., 1995; Leeds et al., 1992). In *S. cerevisiae,* poly(A)-binding protein Pab1 binds to 3' untranslated regions (UTRs) near natural stop codons and interaction between terminating ribosomes and Pab1 through eukaryotic release factor eRF3 supports efficient translation termination (Amrani et al., 2004; Mangus et al., 2003). Ribosomes at premature termination codons, however, cannot interact with Pab1. Consistent with this model, most yeast 3' UTRs are a similar length (~100 nucleotides), whereas aberrant mRNA with long 3'UTRs are targeted by NMD (Muhlrad and Parker, 1999). In this case Nam7 is recruited to the

translation termination factors eRF1 and eRF3 that are bound to ribosomes and recognize stop codons in eukaryotes (Figure 4) (Wang et al., 2001; Czaplinski et al., 1998). Nam7 targets bound mRNA to special cytoplasmic compartments known as processing bodies (P-bodies) and subsequent binding of Upf2 and Upf3 to Nam7 is then thought to trigger degradation, which can proceed from both ends, by exosome-mediated 3'-5' decay as well as by decapping through DCP2 and Sep1-mediated 5'-3' decay (Garneau et al., 2007; Sheth and Parker, 2006; Parker and Song, 2004). A similar mechanism for targeting mRNAs for degradation has been shown in mammalian cells for UPF1-3. However, PTCs recognition occurs through the positioning of an exon junction complex (EJC) to exon-exon boundaries, and phosphorylation and dephosphorylation of UPF1 by SMG1, SMG5, SMG6 and SMG7 is required for efficient nonsense-mediated decay (Chiu *et al.*, 2003; Ohnishi *et al.*, 2003). The cellular location of degradation in mammalian cells is believed to be in the cytoplasm in loci similar to the P bodies shown in *S. cerevisiae* (Eulalio *et al.*, 2007).

As mentioned before, NMD is not only restricted to degradation of transcripts containing premature translation-termination codons, but has further been reported to regulate 3-10% of all mRNAs in eukaryotes (Rehwinkel et al., 2005; Mendell et al., 2004; He et al., 2003). Moreover, NMD factors have been implicated in enhancing translation in mammalian cells, although it is still not fully understood how NMD regulates the level of expression and at what point a transcript becomes a NMD substrate (Nott *et al.*, 2004). Targets of NMD include, amongst others, mRNAs with uORFs in the 5' UTR, mRNAs encoding selenoproteins (UGA codon can be interpreted as a PTC) and mRNAs with introns in the 3' UTRs (Rehwinkel *et al.*, 2006).

The surveillance mechanism of mRNA degradation by NMD has a huge impact on severity of various diseases. Approximately 30% of mutations that cause human genetic diseases carry a PTC and expression of these nonsense mRNAs can have various consequences for the cell, ranging from beneficial to potentially deleterious effects (Frischmeyer and Dietz, 1999). NMD has been shown to beneficially influence β-thalassemic disorders, in which production of haemoglobin is affected (Hall and Thein, 1994). The disorder is mostly caused by generation of PTCs and the ability of NMD in recognizing and targeting these PTC-containing mRNAs for degradation has been

shown to beneficially influence the severity of the disease. Furthermore, NMD can protect organisms from developing cancer by degrading transcripts of mutated tumour suppressor proteins. Mutations in the tumour suppressor proteins BRCA1, WT1 and p53 can convert the proteins into oncoproteins, leading to tumorigenicity (Wolf et al., 2005; Holbrook et al., 2004; Noensie and Dietz, 2001; Frischmeyer and Dietz, 1999). On the other hand, patients with muscular dystrophy feature severe symptoms when expression of the nonsense mRNAs is inhibited by NMD and the amount of the truncated, yet still functional protein is not sufficient in the cell (Kerr *et al.*, 2001). Drugs aiming at read-through of PTCs to allow synthesis of full-length proteins have been attempted.

1.9.2 Role of Nonsense-Mediated Decay at telomeres

Intriguingly, NMD factors have not only been associated with various genetic disorders, but appear to contribute to genome stability and telomere maintenance. Human SMG1 and UPF1 have been implicated in the DNA damage response (Azzalin and Lingner, 2006; Brumbaugh et al., 2004). The kinase activity of SMG1 is required for optimal activation of the cell cycle protein p53 in response to ionizing radiation (IR) damage and depletion of SMG1 leads to spontaneous DNA damage, cell cycle arrest in early S phase and induction of an ATR-dependent DNA damage response (Azzalin and Lingner, 2006; Brumbaugh et al., 2004). In fact, both, SMG1 and ATM have been shown to phosphorylate p53 as well as UPF1 in response to γ-irradiation (Brumbaugh *et al.*, 2004). Furthermore, UPF1 physically interacts with the DNA polymerase δ and accumulates at chromatin during S phase and upon DNA damage, suggesting a role for UPF1 and SMG1 in DNA replication and DNA damage response (Azzalin and Lingner, 2006). SMG5, SMG6 and SMG7 are homologs of yeast Est1, the regulatory subunit of telomerase. For this reason, SMG5, SMG6 and SMG7 are also known as EST1B, EST1A and EST1C. Interestingly, EST1A/SMG6 and EST1B/SMG5 associate with active telomerase in HeLa cell extracts and a hTERT interaction module has been identified in EST1A. In addition, SMG6, like Est1, can bind ssDNA and is believed to contribute to telomere capping as over-expression of SMG6 leads to telomere fusions and telomere shortening (Sealey et al., 2011; Reichenbach et al., 2003; Snow et al., 2003).

Remarkably, several SMG proteins were found to be concentrated at telomeres, where they promote dissociation of TERRA (telomeric repeat-containing) (Azzalin *et al.*, 2007). Elimination of NMD in yeast *S. cerevisiae* leads to an increase of TERRA transcripts (Feuerhahn et al., 2010; Luke and Lingner, 2009). However, potential functions of TERRA and NMD factors in organizing telomere structure or heterochromatin assembly are not yet clear and will require further studies. One hypothesis is that human UPF1 may displace TERRA from telomeres during S phase to ensure efficient DNA replication as TERRA association with telomeres decreases in S phase, reaching its lowest level at late S and G2 phase (Porro *et al.*, 2010). Furthermore, nonsense-mediated decay may regulate succession of DNA replication and telomere elongation through TERRA, as TERRA has been shown to negatively regulate telomerase activity (Redon *et al.*, 2010).

Studies in *S. cerevisiae* demonstrate that NMD and telomere metabolism may indeed be more closely linked than previously thought. Loss of function of NMD core factors Nam7, Nmd2 or Upf3 results in telomere shortening and reduced telomeric silencing (Lew *et al.*, 1998). Further studies revealed that NMD regulates the mRNA levels of several telomere related factors involved in either telomere elongation, such as subunits of telomerase (Est1 and Est2), telomere capping (Stn1 and Ten1) or telomeric silencing (Sas2 and Orc5) and demonstrated that the phenotypes observed in *upf*Δ mutants were indistinguishable from phenotypes obtained by overexpressing *STN1* in combination with *TEN1* (reduced telomere length) or *EST2* (reduced telomeric silencing) (Dahlseid *et al.*, 2003). Other studies revealed that proteins involved in DNA repair and telomere maintenance (yeast Tel1 and fruit fly ATM) are regulated by NMD (Rehwinkel et al., 2005; He et al., 2003). Furthermore, delayed senescence is detected in NMD deficient strains lacking components of telomerase with increased levels of Stn1 being responsible for the delay, suggesting that NMD accelerates senescence by modifying the telomere cap organization (Enomoto *et al.*, 2004).

A recent genome-wide screen of enhancers and suppressors of *cdc13-1* strains revealed that all three core NMD factors are strong suppressors of growth defects obtained in

cdc13-1 mutants containing uncapped telomeres, although *CDC13* mRNA is no target of the nonsense-mediated decay (Addinall et al., 2011; Addinall et al., 2008; Dahlseid et al., 2003). Interestingly, studies demonstrated that over-expression of *STN1* in conjunction with *TEN1* (both targets of NMD) efficiently suppresses any *cdc13-1* associated telomere-capping defects which might explain the phenotypes (Petreaca *et al.*, 2006). In conclusion, the data demonstrates that the NMD pathway in yeast as well as in higher eukaryotes not only regulates decay of PTC-containing nonsense mRNAs, but is intimately connected with telomere maintenance.

Another Est1-like protein involved in NMD has been discovered several years ago in yeast. Ebs1 was first characterized in 1999 due to a sequence similarity with Est1, which is most pronounced in a presumed RNA recognition motif (RRM) in Ebs1 (Zhou *et al.*, 2000). It has been shown that RRMs can directly interact with single-stranded RNA and the Est1 binding to the TLC1 RNA occurs in fact via an RRM. Furthermore, many studies demonstrated that many RRMs are also capable of binding to single-stranded DNA and in particular to telomeric ssDNA (Ding et al., 1999; Johnston et al., 1999; Reim et al., 1999; Lin and Zakian, 1994). However, although Ebs1 is not essential for telomerase activity, contribution of Ebs1 to telomere maintenance via association to telomeric DNA and potential interaction with Cdc13 cannot be excluded (Zhou *et al.*, 2000).

Interestingly, deletion of either *EST1* or *EBS1* leads to a short-telomere phenotype; however, unlike *est1*Δ mutants, cells lacking *EBS1* do not undergo senescence, suggesting that the observed phenotypes are caused by different mechanisms (Zhou et al., 2000; Lundblad and Szostak, 1989). It is not known whether the observed telomere shortening is caused by partially disrupted NMD in *ebs1*Δ mutants as Ebs1 was identified as a component of yeast NMD. Ebs1 contains a 14-3-3 domain that has striking similarity to the UPF1-interacting domain in human SMG5, SMG6 and SMG7, with highest similarity to SMG7 (Luke *et al.*, 2007). In addition, the same study demonstrates that EBS1 physically interacts with NAM7 and over-expression of *EBS1*, SMG5 or SMG7 leads to localisation of UPF1 to P-bodies. Furthermore, slight changes in transcript levels of NMD targets have been demonstrated for strains lacking SMG7 or *EBS1*. However, neither SMG7 nor EBS1 are essential for NMD in human and yeast,

respectively (Luke *et al.*, 2007). One study proposed that the NMD defects observed in yeast cells lacking functional Ebs1 are a consequence of loss of proper translation regulation (Ford *et al.*, 2006). The group argues that Ebs1 acts as a global translation inhibitor through physical interaction with the mRNA cap binding and translation initiation factor eIF-4E (Cdc33). However, two years later, another study by Luke et al. 2007 argued that Ebs1 does not function as a translation regulator. In conclusion, data of the past ten years suggest a close connection between nonsense-mediated decay and telomere metabolism in yeast as well as in higher eukaryotes.

1.10 Aims

One aim of this study was to understand the puzzling observation that components of the nonsense-mediated mRNA decay pathway (Upf1, Upf2, Upf3) suppress one form of telomere capping defect (*yku70*Δ), but enhance another (*cdc13-1*) (Addinall *et al.*, 2011). The same effect can be seen in Ebs1, which has previously been linked to NMD (Azzalin *et al.*, 2007).

- What causes the opposite growth phenotypes in *upf2*Δ *cdc13-1*Δ and *upf2*Δ *yku70*Δ mutants in the presence of uncapped telomeres?
- How can NMD have the opposite growth effect on two forms of telomere uncapping?
- What is the difference between Yku70- and Cdc13-mediated telomere protection?
- Does Ebs1 work in the same pathway as NMD in regards to telomere regulation?
- What role does NMD play at telomeres?
- Do other mutants with similar growth phenotypes as NMD mutants affect Cdc13- and Yku70-mediated through the same mechanism as NMD?

The other aim was to try and understand if NMD has a role in DNA damage response or checkpoint activation in response to uncapped telomeres as a lot of proteins involved in telomere protection have been shown to also play a role in DNA damage response pathways.

- Does NMD have a role in cell cycle checkpoint control?
- Does NMD have a role in resection at telomeres?

2. Methods

2.1 Yeast Strains

2.1.1 Strains used in this study

All strains (except DLY26 and DLY2440) used in this study were in the W303 background and contained the following mutations: *ade2-1 can1-100 trp1-1 leu2-3,112 his3-11,15 ura3 GAL*$^{+}$ *psi*$^{+}$ *ssd1-d2 RAD5*$^{+}$. Due to the *ade2-1* YEPD (yeast extract/ peptone/ dextrose) medium was supplemented with 50 mg/l adenine. *cdc13-1* mutation was integrated by plasmid rather than back-crossing and is indicated as '*int'* in the table.

*generated in this study

Strain (DLY)	Genotype	Source
26	*MATa ade1 arg4 aro2 his7 lys5 met4 ura2*	D. Jenness
640	*MATa*	R. Rothstein
1108	*MATa cdc13-1 int*	D. Lydall
1195	*MATalpha cdc13-1 int*	D. Lydall
1255	*MATa cdc13-1 int rad9::HIS3*	D. Lydall
1256	*MATalpha cdc13-1 int rad9::HIS3*	D. Lydall
1258	*MATalpha cdc13-1 int rad24::TRP1*	D. Lydall
1522	*MATa cdc13-1 int rad24::TRP1*	D. Lydall
1696	*MATalpha cdc13-1 int exo1::LEU2 rad24::TRP1*	D. Lydall
1839	*MATalpha sgs1 ::KanMX*	D. Lydall
2234	*MATa rad9 ::LEU2*	D. Lydall
2440	*MATalpha ade1 arg4 aro2 his7 lys5 met4 ura2*	D. Jenness
2560	*MATalpha cdc13-1 int exo1::LEU2*	D. Lydall
2561	*MATa cdc13-1 int exo1::LEU2*	D. Lydall
2764	*MATa ebs1::URA3*	D. Lydall
2787	*MATalpha yku70::LEU2*	D. Lydall
2824	*MATa ebs1::KanMX*	D. Lydall
2889	*MATa yku70::LEU2 ebs1::KanMX*	D. Lydall
2890	*MATalpha yku70::LEU2 ebs1::KanMX*	D. Lydall

2901	*MATa ebs1::KanMX exo1::LEU2 rad24::TRP1*	D. Lydall
3001	*MATalpha*	R. Rothstein
3113	*MATa yku80::KanMX*	D. Lydall
3186	*MATa sep1::URA3 cdc13-1 int*	D. Lydall
3225	*MATalpha yku80::HIS3 ebs1::KanMX*	D. Lydall
3258	*MATalpha sep1::URA3*	D. Lydall
3360	*MATa sep1::URA3 yku70::HIS3*	D. Lydall
4309	*MATa yku70::LEU2*	D. Lydall
4413	*MATalpha yku70::HIS3*	D. Lydall
4528	*MATa nmd2::HIS3*	D. Lydall
4557	*MATa cdc13-1 int*	D. Lydall
4576	*MATa cdc13-1 int ebs1::KanMX*	D. Lydall
4577	*MATalpha cdc13-1 int ebs1::KanMX*	D. Lydall
4624	*MATa cdc13-1 int nmd2::HIS3*	D. Lydall
4625	*MATa cdc13-1 int nmd2::HIS3*	D. Lydall
4626	*MATalpha cdc13-1 int ebs1::KanMX nmd2::HIS3*	D. Lydall
4627	*MATa cdc13-1 int ebs1::KanMX nmd2::HIS3*	D. Lydall
4763*	*MATa*	4528 x 4674
4764*	*MATa ebs1::KanMX*	4528 x 4674
4765*	*MATa nmd2::HIS3*	4528 x 4674
4766*	*MATalpha nmd2::HIS3*	4528 x 4674
4674*	*MATalpha ebs1::KanMX*	2833 x 2889
4780*	*MATa*	4528 x 4674
4781*	*MATa ebs1::KanMX*	4528 x 4674
4782*	*MATa ebs1::KanMX*	4528 x 4674
4783*	*MATa nmd2::HIS3*	4528 x 4674
4784*	*MATa nmd2::HIS3*	4528 x 4674
4801	*MATa ede1::KanMX*	D.Lydall
4868*	*MATa ebs1::KanMX rad9::NatMX cdc13-1 int*	4576 transformed with NatMX
4869*	*MATa ebs1::KanMX rad9::NatMX cdc13-1 int*	4576 transformed with NatMX

5007*	*MATalpha yku70::LEU2 nmd2::HIS3*	2787 x 4765
5008*	*MATa yku70::LEU2 nmd2::HIS3*	2787 x 4765
5038*	*MATa CEN pVECT*	640 transformed with pDL1265
5039*	*MATa 2μ pSTN1*	640 transformed with pDL1261
5040*	*MATa 2μ pVECT*	640 transformed with pDL1262
5042*	*MATa CEN pSTN1*	640 transformed with pDL1264
5043*	*MATalpha cdc13-1 int 2μ pSTN1*	1195 transformed with pDL1261
5044*	*MATalpha cdc13-1 int 2μ pVECT*	1195 transformed with pDL1262
5046*	*MATalpha cdc13-1int CEN pSTN1*	1195 transformed with pDL1264
5047*	*MATalpha cdc13-1int CEN pVECT*	1195 transformed with pDL1265
5048*	*MATalpha yku70::HIS3 2μ pSTN1*	4413 transformed with pDL1261
5049*	*MATalpha yku70::HIS3 2μ pVECT*	4413 transformed with pDL1262
5051*	*MATalpha yku70::HIS3 CEN pSTN1*	4413 transformed with pDL1264
5052*	*MATalpha yku70::HIS3 CEN pVECT*	4413 transformed with pDL1265
5107*	*MATalpha nmd2::HIS3 cdc13-1 int*	4557 x4766
5232*	*MATalpha yku80::HIS3 ebs1::KanMX*	3225 x 2889
5233*	*MATa yku80::HIS3 ebs1::KanMX*	3225 x 2889
5234*	*MATa yku80::HIS3 ebs1::KanMX yku70::LEU2*	3225 x 2889
5235*	*MATa yku80::HIS3 ebs1::KanMX yku70::LEU2*	3225 x 2889
5236*	*MATa yku70::LEU2 nmd2::HIS3*	5007 x 3113
5237*	*MATa yku70::LEU2 nmd2::HIS3 yku80::LEU2*	5007 x 3113
5238*	*MATalpha cdc13-1 int ebs1::KanMX nmd2::HIS3*	1696 x 4627
5239*	*MATalpha cdc13-1 int ebs1::KanMX nmd2::HIS3*	1696 x 4627
5240*	*MATalpha yku80::KanMX nmd2::HIS3*	5007 x 3113
5241*	*MATa yku80::KanMX nmd2::HIS3*	5007 x 3113
5242*	*MATalpha yku70::LEu2 ebs1::KanMX nmd2::HIS3*	2889 x 4766
5243*	*MATa cdc13-1 int ebs1::KanMX rad24::TRP1*	1696 x 4627
5244*	*MATa cdc13-1 int ebs1::KanMX rad24::TRP1*	1696 x 4627
5245*	*MATalpha cdc13-1 int ebs1::KanMX exo1::LEU2*	1696 x 4627

5246*	*MATalpha cdc13-1 int ebs1::KanMX exo1::LEU2*	1696 x 4627
5247*	*MATa yku70::HIS3 rad24::TRP1 ebs1::KanMX*	4413 x 2901
5248*	*MATa ebs1::KanMX yku70::HIS3 exo1::LEU2*	4413 x 2901
5249*	*MATa yku70::LEU2 nmd2::HIS3*	5007 x 3113
5250*	*MATalpha yku70::LEU2 nmd2::HIS3 yku80::KanMX*	5007 x 3113
5251*	*MATa yku70::LEU2 ebs1::KanMX nmd2::HIS3*	2889 x 4766
5255*	*MATalpha rad9::LEU2 nmd2::HIS3 cdc13-1 int*	4627 x 1718
5256*	*MATalpha rad9::LEU2 nmd2::HIS3 cdc13-1 int*	4627 x 1718
5757*	*MATa STN1-C-MYC::TRP1 yku70::LEU2*	5756 x 5757
5758*	*MATa STN1-C-MYC::TRP1 ebs1::KanMX*	5756 x 5757
5759*	*MATa STN1-C-MYC::TRP1 nmd2::HIS3*	5756 x 5757
5760*	*MATalpha STN1-C-MYC::TRP1 cdc13-1 int*	5756 x 5757
5761*	*MATa STN1-C-MYC::TRP1*	5756 x 5757
5762*	*MATa STN1-C-MYC::TRP1 yku70::HIS3*	5756 x 5757
5763*	*MATa STN1-C-MYC::TRP1 ebs1::KANMX cdc13-1 int*	5756 x 5757
5764*	*MATalpha STN1-C-MYC::TRP1 ebs1::KANMX yku70Δ::LEU2*	5756 x 5757
5765*	*MATa STN1-C-MYC::TRP1 nmd2::HIS3 yku70::LEU2*	5756 x 5757
5766*	*MATα STN1-C-MYC::TRP1 nmd2::HIS3 cdc13-1 int*	5756 x 5757
6000*	*MATa STN1-C-MYC::TRP1 sep1::URA3*	5761 x 3258
6001*	*MATa STN1-C-MYC::TRP1 sep1::URA3*	5761 x 3258
6005*	*MATa STN1-C-MYC::TRP1 chk1::HIS3*	5760 x 1095
6007*	*MATa STN1-C-MYC::TRP1 rif1::URA3*	4452 x 5761
6008*	*MATa STN1-C-MYC::TRP1 rif1::URA3*	4452 x 5761
6585	*MATa rad24::TRP1*	D. Lydall
6656*	*MATa nam7::KanMX*	DDY227 transformed with pDL1042
6808*	*MATalpha nam7::KanMX yku70::LEU2*	6656 x 2984
6809*	*MATa nam7::KanMX yku70::LEU2 ebs1::TRP1*	6656 x 2984
6810*	*MATalpha nam7::KanMX cdc13-1 int*	6656 x 1256
6811*	*MATa upf3::KanMX*	DDY227 transformed with pDL1042
6812*	*MATalpha yku70::LEU2 upf3::KanMX*	6811 x 2984

6813*	*MATalpha yku70::LEU2 ebs1::TRP1*	6811 x 2984
6814*	*MATa cdc13-1 int upf3::KanMX*	6811 x 1256
6856	*MATa mec1::TRP1 sml1::URA3*	D. Lydall
6867*	*MATa nam7::KanMX nmd2::HIS3*	6810 x 6866
6868*	*MATalpha nam7::KanMX nmd2::HIS3*	6810 x 6866
6974*	*MATalpha nmd2::HIS3 nam7::KANMX yku70::LEU2*	5007 x 6656
6975*	*MATa nmd2::HIS3 nam7::KANMX yku70::LEU2*	5007 x 6656
6976*	*MATa nmd2::HIS3 nam7::KANMX*	5007 x 6656
6977*	*MATa Est2-13Myc::HIS3 RAD5*	6737 x 6741
6978*	*MATalpha nmd2::HIS3 Est2-13Myc::HIS3*	6737 x 6741
6979*	*MATa nmd2::HIS3 yku70::LEU2 Est2-13Myc::HIS3*	6737 x 6741
6980*	*MATa yku70::LEU2 Est2-13Myc::HIS3*	6737 x 6741
7273*	*MATalpha Cdc13-C-MYC::HIS3*	6736 x 6741
7274*	*MATa Cdc13-C-MYC::HIS3 nmd2::URA3*	6736 x 6741
7275*	*MATalpha Cdc13-C-MYC::HIS3 yku70::LEU2*	6736 x 6741
7276*	*MATa Cdc13-C-MYC::HIS3 nmd2::URA3 yku70::LEU2*	6736 x 6741
7747*	*MAT cdc13-1 int exo1::LEU2 nmd2::URA3*	7745x7759
7749*	*MAT cdc13-1int rad24::TRP1 nmd2::URA3*	7745x7759
7751*	*MAT cdc13-1 int rad24::TRP1 exo1::LEU2*	7745x7759
7753*	*MAT cdc13-1 int rad24::TRP1 exo1::LEU2 nmd2::URA3*	7745x7759
7755*	*MAT cdc13-1 int rad24::TRP1 exo1::LEU2 nmd2::URA3 rad9::HIS3*	7745x7759
7757*	*MAT cdc13-1 int rad24::TRP1 nmd2::URA3 rad9::HIS3*	7745x7759
7759*	*MAT cdc13-1int exo1::LEU2 nmd2::URA3 rad9::HIS3*	7745x7759

Table1. Strains used in this study

2.1.2 Conditional mutants used in this study

cdc13-1

cdc13-1 is a temperature-sensitive allele of the essential gene *CDC13*, that encodes for the telomere capping protein Cdc13. *cdc13-1* is functional and shows growth comparable to wild type strains at 23°C (permissive temperature), but causes a temperature-sensitive telomere capping defect at temperatures above 26°C and growth gradually decreases with rise in temperature (semi-permissive temperature). At 36°C, *cdc13-1* mutants show now growth at all (non-permissive temperature). *cdc13-1* allows controlled induction of telomere uncapping at semi- and non-permissive temperature, leading to activation of a G2/M checkpoint response (Garvik et al., 1995; Weinert and Hartwell, 1993).

*yku70*Δ

The *yku70*Δ mutation is a null-mutation of the Yku70 subunit of the Ku complex. *yku70*Δ causes a temperature-sensitive telomere capping defect. *yku70*Δ mutants are able to grow at the permissive temperature of 30°C, but growth gradually decreases at temperatures above 33°C, due to telomere uncapping and activation of the DNA damage response pathway (Maringele and Lydall, 2002; Nugent and Lundblad, 1998; Barnes and Rio, 1997).

cdc15-2

cdc15-2 is a temperature-sensitive allele of the gene *CDC15*, that encodes for a protein kinase required for mitotic exit. At the non-permissive temperature of 36°C, cells containing the *cdc15-2* mutation cannot finish mitosis, but arrest during late nuclear division (Lydall and Weinert, 1995).

2.2 Recipes For Yeast Media

All reagents were from Sigma or Formedium unless otherwise stated.

2.2.1 Yeast extract, peptone, dextrose (YEPD)

1% yeast extract, 2% bacto peptone, 2% dextrose, 50 mg/L adenine

For 1 L media: 10 g of yeast extract and 20 g of bacto peptone (and 20 g of bacto agar for solid media) were made up to 935 ml with MQ water, autoclaved for 12 min at 121°C and cooled to 60°C before 50 ml sterile 40% (w/v) dextrose and 15 ml of sterile 0.5% (w/v) adenine was added.

For solid media, 20g agar was added prior to autoclaving.

2.2.2 YEPD + G418

Same recipe as for YEPD (2.2.1) except 1 ml of 200 mg/ml G418 was added following autoclaving once cooled down to 60°C.

2.2.3 Synthetic media

0.13% amino acids, 0.17% yeast nitrogen base, 0.5% ammonium sulphate.

For 1 L media: 1.3 g of amino acid drop out powder (2.5g adenine, 1.2g argenine, 6.0g aspartic acid, 6.0g glutamic acid, 1.2g histidine, 3.6g leucine, 1.8g lysine, 1.2g methionine, 3.0g phenylalanine. 22.5g serine, 12.0g threonine, 2.4g tryptophan, 1.8g tyrosine, 9.0g valine, 1.2g uracil), 5 g of ammonium sulphate and 1.7 g of yeast nitrogen base were made up to 500 ml with MQ water, autoclaved and 500 ml of autoclaved MQ water was added.

For solid media, 20 g agar was added to 500 ml MQ water prior to autoclaving.

2.2.3. –Histidine/-Leucine/-Tryptophane/-Uracil media

Same recipe as for synthetic media (2.2.3), but the appropriate amino acid(s) were excluded from the drop out powder.

2.2.4 TMPyP4/HU/MMS media

Same recipe as for YEPD (2.2.1), except sterile TMPyP4 (50 mg/ml stock in water, final concentration of 150 μM), 10 ml of 2 M HU (final concentration 100 mM) or MMS (final concentration of 0.01 or 0.02%) were added following autoclaving once cooled down to 60°C.

2.3 Yeast Genetic Methods

2.3.1 Mating, sporulation and tetrad analysis

MATa and *MATalpha* parental strains were mixed on a YEPD plate using a toothpick and incubated at 23°C overnight to mate. Diploids were selected on selective plates that allow growth of diploids, but not haploids (2.2.3). Selective plates were incubated for 2 days at 23°C.

Diploids were selected by picking zygotes whenever selection on selective media was not possible (e.g. mating of a *cdc13-1* strain with a strain that is unable to grow at high temperature). Strains were grown separately on a YEPD plate overnight at 23°C. Strains were then mixed on a YEPD plate and incubated for 4 h at 23°C. Zygotes were isolated to a clean area using a micro-needle designed for tetrad dissection.

Diploid colonies were inoculated in 2 ml of YEPD and grown overnight at 23°C. 0.5 ml of the culture was centrifuged for 3 min at 2000 rpm in a bench microcentrifuge, washed twice with sterile water and re-suspended in 2 ml of 1% potassium acetate (KOAc) to allow sporulation. Cultures were incubated on a wheel at 23°C for 2-3 days and presence of spores was examined by phase contrast microscopy (40x). Cultures were centrifuged for 3 min at 2000 rpm, washed twice with 3 ml sterile water, re-suspended in 1 ml sterile water and stored in a 1.5 ml Eppendorf tube at 4°C.

20 µl of sporulated culture was transferred to a new 1.5 ml Eppendorf tube and incubated together with 1.2 µl glusulase enzyme in a water bath for 13 min at 30°C to allow digestion of the sack around the tetrads. Spores were then kept on ice and 0.5 ml sterile water was added carefully. 50 µl of digested spores were spread onto a YEPD plate along a marked line. Tetrads were dissected using a Microtec tetrad microscope and dissected spores were allowed to germinate and form colonies at 23°C for 3-5 days.

Grown colonies were transferred to a new YEPD plate and grown overnight at 23°C. The YEPD plate was then replica plated onto appropriate selective plates (2.2.3) for

genotype identification. The mating type was identified by mating with DLY26 (*MATa ade1 arg4 aro2 his7 lys5 met4 ura2*) and DLY2440 (*MATalpha ade1 arg4 aro2 his7 lys5 met4 ura2*) overnight at 23°C and replica plating onto selective plates that only allowed growth of the diploids (2.2.3). Scoring for growth took place after 3 days of incubation at 23°C. *cdc13-1* mutation was scored by replica plating onto a new YEPD plate and incubation for 2 days at 36°C. Only heterozygotes containing a wild-type *CDC13* copy are able to grow. *cdc15-2* mutation was assessed by mating with DLY349 (*MATa cdc15-2*) and DLY350 (*MATalpha cdc15-2*) overnight at 23°C. Cells were replica plated onto a new YEPD plate and incubated for 2-3 days at 36°C. Only diploids containing a wild-type *CDC15* copy are able to grow.

2.3.2 Gene deletion

Genes were deleted by replacing the gene of interest with an antibiotic resistance cassette. Gene deletion constructs were amplified from plasmids by PCR as previously described (Longtine *et al.*, 1998). Primers used for amplification of the gene deletion constructs were designed to only replace the ORF of the gene of interest (Table 2). Amplified gene deletion constructs were transformed into yeast strains by Lithium acetate transformation (see 2.3.3). Correct integration of the construct was confirmed by colony PCR.

2.3.3 High efficiency lithium acetate transformation

Stationary phase culture was diluted to a cell density of 5 x 10^6 cells/ml in 50 ml of YEPD. Cells were grown in a shaking water bath at 180 rpm for 3-5 hours until cells reached a concentration of 2 x 10^7 cells/ml. Cells were harvested in a sterile 50 ml centrifuge tube at 1,500 rpm for 3 min in a bench microcentrifuge, washed in sterile water and re-suspended in 1 ml of 0.1 M lithium acetate (LiAc). Cell suspension was transferred to a 1.5 ml eppendorf tube, centrifuged at 13,000 rpm for 15 sec and re-suspended in 0.4 ml of 0.1M LiAc by vortexing. 50 µl of cell suspension was transferred to a new eppendorf tube for each transformation, spun down at 13,000 rpm for 15 sec and kept on ice. Following reagents were added in the following order and mixed vigorously by vortexing:

240 µl of 50% Polyethylene glycol 400

36 µl of 1 M LiAc

10 µl of 10 mg/ml salmon sperm DNA (sonicated and prior to use DNA was denatured by boiling for 5 minutes at 95°C and cooled rapidly on ice)

50 - 100 µl transforming DNA in water (0.1 – 10 µg)

The suspension was incubated in a 30°C water bath for 30 min followed by a 20 min heat shock at 42°C. Cells were spun down at 6,000 rpm for 15 sec and pellet was re-suspended in 200 µl sterile water. To select for auxotrophy, the suspension was plated onto a selective plate. To select for antibiotic resistance, the suspension was plated onto YEPD at 23°C overnight and replica-plated onto an antibiotic-containing plate the next day. Transformants were allowed to form colonies for 4-5 days at 23°C.

2.3.4 One step transformation

Freshly grown cells on YEPD plates were re-suspended in 100 µl of one-step buffer. 1 µl of transforming DNA (obtained by plasmid miniprep) and 5.3 µl of 10 mg/ml salmon sperm DNA was added and mixed vigorously by vortexing. The suspension was incubated at 45°C for 30 min and then plated onto selective plates. Transformants were allowed to form colonies for 3-5 days at 23°C.

<u>One-step buffer:</u>

0.2 M Lithium Acetate, 40% PEG, 100 mM DTT

2.3.5 DNA isolation from Yeast (Yale Quick Method)

1.5 ml of stationary phase culture was spun down in a bench microcentrifuge at 13,000 rpm for 1 minute and re-suspended in 0.25 ml digestion buffer (250 µl 0.1 M EDTA (pH7.5), 1:1000 dilution ß-Mercaptoethanol containing 2.5 mg/ml zymolase 20T). Cells were incubated at 37°C for about 1 hour until spheroblasted (monitored by microscopy).

55 µl of lysis buffer (0.25 M EDTA (ph 8.5), 0.5 M Tris Base, 2.5% SDS) was added to lyse the cells and the suspension was incubated in a water bath at 65°C for 30 min. 68 µl of potassium acetate was used to neutralize lysis buffer, followed by incubation on ice for 30 min. Proteins were removed by centrifugation for 20 min at 13,000 rpm. DNA in the supernatant was precipitated by adding 720 µl of 100% ethanol and following centrifugation for 10 min at 13,000 rpm. Existing RNA was eliminated by incubation at 37°C for 35 min in 130 µl of TE containing 1 mg/ml RNAse A. DNA was then re-precipitated in 130 µl of isopropanol and centrifugation for 20 min at 13,000 rpm. 100 µl of 70% ethanol (vol/vol) to remove existing salts and DNA was then pelleted by centrifugation for 5 min at 13,000 rpm. Pellets were air dried for 30 min, re-suspended in 40 µl TE and incubated at 37°C for 30 min. Samples contained approximately 10 µg of genomic DNA and were stored at -20°C.

2.3.6 Growth assays

Single colonies were inoculated in 2 ml of YEPD and grown to saturation at 23°C. 40 µl of saturated culture was added to 160 µl of sterile water and a 5-fold dilution series was prepared in a 96 well plate from this dilution by adding 40 µl culture to 160 µl of sterile water at a time. The dilution series was then spotted onto YEPD plates using a sterilised 48-prong replica plating device (Sigma).

2.3.7 Telomere uncapping in asynchronous cell cultures

Exponentially dividing *yku70*Δ mutants at 23°C were shifted to 37°C at a concentration of $1x10^7$ cells/ml. Every 1.5 hours, cell density was determined using a hemocytometer and cultures were, when necessary, diluted using 37°C pre-warmed YEPD.

2.3.8 Telomere uncapping in synchronous cell cultures

Synchronization of cell cultures using alpha factor was performed similarly to previously described (Zubko *et al.*, 2006). Exponentially growing *cdc13-1 cdc15-2 bar1*Δ mutants at 23°C were diluted to 250 ml of 8×10^6 cells/ml. Cells were allowed to divide once by cultivating them at a shaking water bath at 23°C for 2.5 h. Cells were

arrested in G1 using alpha factor to 20 nM and incubation at 23°C for 2.5 h in a shaking water bath. Arrest and schmoo formation of cells was monitored by microscopy. Cells were released from Alpha factor arrest by spinning cultures at 1000 rpm for 4 min in 250 ml centrifuge tubes. Supernatant was discarded (Time was noted as -40 min) and cell pellets were washed twice in 50 ml YEPD and spun in 50 ml Falcon tubes for 3 min at 2000 rpm. Pellet was re-suspended in 150 ml of YEPD and was left at room temperature until 40 min after cells were first spun down. 125 ml of 51°C YEPD was added and cell cultures were transferred to 36°C shaking water bath to induce telomere uncapping. Samples were collected over a time course of 4 h.

2.3.9 Determination of cell viability

Samples for cell viability were collected every 40 min. 20 µl of cell culture was diluted in an eppendorf tube containing 1.98 ml of water. 20 µl were transferred from each tube to a new tube containing 1.98 ml of water. 100 µl of this 10000-fold dilution was spread onto each half of a YEPD plate. Colonies were counted after incubation for 3 days at 23°C. As viability can decrease massively at later time points, the 100-fold dilution was plated as well from the 160 min time point onwards.

2.3.10 Determination of cell cycle position

1 ml of cell culture was spun at 13200 rpm for 7 s and cell pellet was re-suspended in 0.5 ml of 70% ethanol. Cells could be stored at 4°C. Cells were washed twice in 0.5 ml water and re-spun at 13200 rpm for 10 s. Cell pellet was re-suspended in 300 µl of 0.2 µg/ml DAPI (4,6-diamidino-2-phenylindole) in the dark. Cells were sonicated at an amplitude of 5 microns for 1-10 s to separate cell clumps and 3 µl of sonicated cell culture was examined under a fluorescence microscope (Nicon eclips 50i, 60x objective). 100 cells were counted and scored as G1 (no bud), S phase (single nucleus and bud <50% diameter of mother cell), methaphase (Single nucleus and bud >50% diameter of mother cell) or anaphase (two nuclei).

2.4 Molecular Biology

2.4.1 Primer design

Primers for QAOS were designed according to Holstein and Lydall et al., 2011). Primers for PCR and RT-PCR were designed to be 18-23 bp in length with a T_m of 55-59°C. Primer3 (http://fokker.wi.mit.edu/primer3/) was used to select primers.

2.4.2 Oligonucleotides

Lyophilised oligonucleotides (Sigma Genosys) were adjusted to 200 µM using 1X TE and were stored at -20°C. CY5-labelled oligonucleotides were stored in Sigma H_2O instead of TE.

Oligo Number	**Primer Sequence**	**Target**
M417	ATGGGCGCAGGGCCTGGATTC	Tag for QAOS
M418	ATGCTCGCAGAGCCCCTGGATCT	Tag for QAOS
M1114	AGCGTCGACTATTGTGGGATA	*BAR1*
M1156	AATAATCGATGTGGTCGCGTA	*BAR1*
M1157	CATATCCGCACCTCCTCAA	*hisG*
M1158	CTCTGTGCCATCTCACCGT	*hisG*
M1172	CAGACCGAACTCGGTGATTT	*BUD6*
M1173	TTTTAGCGGGCTGAGACCTA	*BUD6*
M1362	CGCACTTAACTTCGCATCTGGGC	*KANMX*
M1509	CAAGAAATGGGAACCTCCATTAAGATTAGCAA	*RET2*
M1510	AGCGCACCTGCATCGTTGGCAGCAA	*RET2*
M1511	ATGGGCGCAGGGCCTGGATTCATATGGAGCTT	*RET2*
M1514	TGACTTTCCAAGATGCCTTGAACACTAGTGTC	*DUG1*
M1515	AATGAGCACCATCATCGCCTCTAC	*DUG1*
M1516	ATGCTCGCAGAGCCCCTGGATCTTCATACCACCA	*DUG1*

M1734	TCGAGCAACTGCAAGAAGAA	*STN1*
M1735	CGAAATGACAAGGAATGCAC	*STN1*
M1794	ATACACCAAAGTCCGCCAAT	*TEN1*
M1795	CACCAAGTGGTGATTTGACA	*TEN1*
M1792	AATTTGACGCTGCAAAAGCTA	*EST2*
M1793	AGTCCAATACGGTCCCTTCC	*EST2*
M1809	AAGAGCCTGAGTGTCCTCCA	*CDC13*
M1810	ACGAATTGCACGGGAACTAT	*CDC13*
M2046	AATATACTTTTATATTACATCAATCATTGTCATTAT CAACGGATCCCCGGGTTAATTAA	*NAM7*
M2047	AAGCCAAGTTTAACATTTTATTTTAACAGGGTTCAC CGAAGAATTCGAGCTCGTTTAAAC	*NAM7*
M2048	ATCAGGAAAGAAGGAAGGGC	*NAM7*
M2049	CCGGAAAAGTAAAAAAAGTT	*NAM7*
M2050	GAGGGACTTACATTTCTGCTGAAATATATAGTAATC TATCCGGATCCCCGGGTTAATTAA	*UPF3*
M2051	TGTATTCCATATATAATATATAAGAAGCCATGAGCT TTTAGAATTCGAGCTCGTTTAAAC	*UPF3*
M2052	TTATCATCCCTTTATTTATT	*UPF3*
M2053	AAAATCATTAAATACGAAAC	*UPF3*
M2188	[CY5] CCCACCACACACACCCACACCC	*TG ssDNA*
M2243	AAACTCCGCAAGCACCAAGT	*PDI1*
M2244	CTGAAGACTCCGCTGTCGTTAA	*PDI1*
M2245	CGTATGCTAAAGTATATATTACTTCACTCCATT	*VI-R telomere*
M2246	TCCGAACTCAGTTACTATTGATGGAA	*VI-R telomere*

Table 2. Oligonucleotides used in this study

2.4.3 Plasmids

Plasmids used in this study are described in table 3 and stored at -20°C in 1X TE.

Plasmid Number	**Details**	**Source**
pDL698	Plasmid for amplification of hphMX4 gene deletion cassette by PCR.	pAG32 (Goldstein and McCusker, 1999)
pDL888	Plasmid for disrupting HIS3 cassette with URA3 cassette.	pHU10 (Cross, 1997)
pDL1042	Plasmid for amplification of kanMX6 gene deletion cassette by PCR	pFA6a-kanMX6 (Longtine *et al.*, 1998)
pDL1056	Centromeric plasmid expressing native *EBS1*	pAF15 (Ford *et al.*, 2006)
pDL1071	Centromeric plasmid expressing EBS1[R208]	Daniel Durocher lab
pDL1261	2μ plasmid expressing native *STN1*	pVL1066 (Gasparyan *et al.*, 2009)
pDL1262	Vector only control for pDL1261	YEplac181 (Gasparyan *et al.*, 2009)
pDL1264	Centromeric plasmid expressing native *STN1*	pVL1045 (Gasparyan *et al.*, 2009)
pDL1265	Vector only control for pDL1264	.YCplac111 (Gasparyan *et al.*, 2009)
pDL1306	Centromeric plasmid expressing native *TEN1*	pCN284 (Gasparyan *et al.*, 2009)
pDL1307	2μ plasmid expressing native *TEN1*	pPC4 (Gasparyan *et al.*, 2009)
pDL1309	Vector only control for pDL1306	YCplac22 (Gasparyan *et al.*, 2009)
pDL1310	Vector only control for pDL1307	YEplac195 (Gasparyan *et al.*, 2009)

Table 3. Plasmids used in this study

2.4.4 Restriction digests:

A mastermix containing 1.8 µl of 10X buffer, 0.18 µl of 100X BSA, 1 µl of restriction enzyme (all from New England Biolabs) and 12 µl of sterile H_2O were added to 5 µl of DNA sample. DNA was digested at 37°C and digest was stopped by incubating the mixture at 62°C for 20 min.

2.4.5 Polymerase chain reaction (PCR)

Per single reaction:

Stock Concentration	Volume µl	Final Concentration
Template DNA	1 µl	
Forward primer (30 µM)	0.2 µl	0.3 µM
Reverse primer (30 µM)	0.2 µl	0.3 µM
dNTP mix (2.5mM)	1.92 µl	0.24 mM
Ex Taq Buffer (10X)	2 µl	1X
Ex Taq (5 U/µl)	0.2 µl	0.05 U/µl
Sigma water	14.5 µl	

Template DNA was either 1 µl of 1/50 dilution of plasmid, 1 µl of 1/25 dilution of yeast genomic DNA prep or 1 µl of colony lysate (single colony added to 20 µl of TE and lysed for 10 min at 95°C).

Typical PCR programme:

95°C for 5 min

35 cycles of:

94°C for 30 s

55°C for 30 s

72°C for 1 min/ kb product size

1 cycle of:

72°C for 10 min

2 µl of PCR product was run on an agarose gel to visualise amplified PCR product.

2.4.6 Agarose gel electrophoresis

Agarose gels were prepared at concentrations of 0.8-2% in 1X TAE buffer. Agarose was dissolved in a microwave and the molten agarose was cooled to 50°C before adding 10 µl of SYBR SAFE (10000X) per 100 ml of molten agarose and pouring the agarose into a casting tray. A final concentration of 1X loading buffer (6X blue loading buffer or 6X orange loading buffer) was added to DNA or RNA samples and agarose gels were run at 25-100 V along with 3 µl of 1 KB DNA ladder (Invitrogen). Bands were visualised using the Fuji LAS 4000 imager.

Blue loading buffer (6X)

0.25% bromophenol blue, 0.25% xylene cyanol, 15% ficoll, 120 mM EDTA pH 8.0 in dH_2O.

Orange loading buffer (6X)

0.25% Orange G, 15% ficoll, 120 mM EDTA pH 8.0

2.4.7 Isolation of RNA and quantification of RNA by qRT-PCR

RNA isolation was performed as previously described (Greenall *et al.*, 2008). Single colonies were inoculated into 50 ml YEPD and grown overnight at 23°C in a water bath. Grown cells were then diluted to a concentration of 2 x 10^6 cells/ml and returned to the water bath until a cell density of 7 x 10^6 was obtained. All samples taken at a given time point were spun at the same time for 3 min at 3000 rpm at room temperature and pellets were snap frozen in liquid nitrogen and stored at -80°C.

For RNA isolation, pellets were thawed on ice, re-suspended in 1 ml of pre-chilled sterile water and spun for 10 sec at 13000 rpm in a table centrifuge. 750 µl of TES (10 mM Tris (pH 7.5), 10 mM EDTA (pH 8.0), 0.5% SDS) and 750 µl of acidic phenol chloroform was added to the pellet and the suspension was vortexed and incubated in a 65°C water bath for 1 h. During incubation, samples were vortexed every 10 min for 10 s. Samples were then placed on ice for 1 min, vortexed for 20 s and spun down for 15

min at 13000 rpm at 4°C. The aqueous phase was transferred to Eppendorf phase lock gel tubes and mixed with 700 µl acidic phenol chloroform by inversion. Samples were spun for 5 min and the water phase was transferred to a new Eppendorf phase lock gel tube, mixed with 600 µl phenol chloroform:isoamyl alcohol (24:1) by inversion and spun for 5 min. The water phase was transferred to an Eppendorf tube containing 1 ml of 100% Ethanol (-20°C) and 50 µl of 3 M Sodium Acetate (pH 5.2). The suspension was vortexed for 10 s and the RNA was precipitated at -80°C for 30 min.

The mixture was spun for 10 min at room temperature and the pellet was washed with 70% Ethanol (4°C) and re-spun for 1 min. RNA was purified using the Qiagen RNeasy kit and eluted in sterile water. RNA was quantified by OD measurement (OD260) and diluted to 1 µg/µl and stored at -80°C. 0.5 µg of each sample was run on a TBE (22.5 mM Tris Base, 22.5 mM Boric Acid, 0.5 mM EDTA) agarose gel to confirm the 28S and 18S ribosomal bands.

RNA was treated with DNAse I (Invitrogen) by adding 2 µl of 10X DNAse buffer, 2 µl of DNAse and 10 µl of sterile water to 5 µl of each 1 µg/µl sample. The mixture was incubated at 37°C for 30 min. 2 µl of 25 mM EDTA was added followed by incubation at 65°C for 10 min to stop the DNAse. Each sample was diluted by adding 80 µl of sterile water.

Transcript levels were analysed by qRT-PCR using the Invitrogen Superscript III Platinum SYBR green one-step qRT-PCR kit. PCR primers used (table 3 in section 2.4.2) amplify a 100 bp region within the target gene and each measurement was performed in triplicate. Per reaction 12 µl of mastermix was added to each 8 µl of RNA sample in a 96 well reaction plate (Applied Biosystems). Correction factors to normalize RNA concentrations of each sample were generated by quantification and calculation of the geometric means of the loading control *BUD6* using dsDNA standards (2 ng/µl; 0.2 ng/µl; 0.02 ng/µl) (see Zubko et al., 2004).

Mastermix per single reaction:

Superscript III Platinum Taq Mix: 0.4 µl

2X SYBR Green Reaction Mix: 10 µl

Forward primer (10 µM): 0.4 µl

Reverse primer (10 µM): 0.4 µl

ROX Reference DYE: 0.4 µl

dH_2O: 0.4 µl

PCR programme:

50°C for 3 min

95°C for 5 min

40 cycles of:

95°C for 15 s

60°C for 30 s

40°C for 1 min

Followed by melting curve analysis

2.4.8 Chromatin immunoprecipitation

10^6 cells/ml containing Myc-tagged proteins were grown in 50 ml of YEPD in a shaking water bath overnight at 23°C, diluted to 10^7 cells/ml in the morning and incubated for another 2.5 h at 23°C. 1.1 ml of 36.5% Formaldehyde were added to 40 ml of cell culture and the culture was left on the bench for 15 min before adding 6 ml of 2.5 M Glycine for 5 min to stop cross-linking. Cells were spun for 2 min at 3500 rpm at 4°C and the pellet was washed twice each with 40 ml ice cold 1X TBS and re-spinning as above. Cell pellet was re-suspended in 15 ml of FA lysis buffer and spun for 5 min at 3500 rpm. Cell pellet could be frozen at -80°C at this stage. Thawed cell pellet was re-

suspended in 800 µl of FA lysis buffer containing 2 mM PMSF (from 100 mM stock solution, stored at -80°C). The cell suspension was transferred to a 2 ml screw cap tube and spun for 7 s at 13200 rpm. Cell pellet was re-suspended in 600 µl of FA lysis/PMSF buffer. Ice cold glass beads were added up to 0.75 ml and cells were lysed during 3 breakage cycles for 1 min at 6500 power setting using a Precellys24 lysis and homogenization ribolyser (Bertin technologies). Tubes were incubated on ice-water in between cycles. Bottom of the tube was punctured using a 21 gauge syringe needle and tube was placed in a 1.5 ml eppendorf tube (cap was removed using dog nail clippers). Both tubes were placed in a 15 ml falcon tube and the tubes were spun at 2000 rpm for 2 min at 4°C. Beads were washed with 300 µl of FA lysis/PMSF buffer and eppendorf tube with the collected sample was spun for 15 min at 13200 rpm at 4°C. Pellet was re-suspended in 1 ml FA lysis buffer and the sample was sonicated 5 times for 15 s per cycle at power setting 7 using a Soniprep150 (Sanyo). Tubes were kept on ice during sonication. Sample was spun for 30 min at 13200 rpm at 4°C and the supernatant was transferred to a 15 ml falcon tube containing 3 ml of FA lysis buffer. 800 µl of sample were aliquoted for IP and Background measurement and 80 µl for Input measurement. Input sample was frozen at -80°C.

3 µg of primary anti-MYC antibody (Mouse anti-MYC, 9E10) was added to IP sample and 3 µg of secondary antibody (monoclonal goat anti-mouse) was added to Background sample. Both samples were incubated on an end-over-end rotator at 4°C at speed setting 20. For each sample 50 µl of protein G dynabeads were added to a 1.5 ml eppendorf tube and beads were washed 3 times for 10 min in 250 µl of FA lysis buffer on the wheel at 4°C. A magnet was used to hold the beads when the buffer was poured off after each wash. Washed beads and IP and Background samples containing antibodies were combined and kept on the end-over-end rotator at 4°C overnight.

In the afternoon the supernatant was poured off using the magnet to hold the beads. Beads were washed 5 times for 3 min each with 700 µl of FA lysis buffer. 100 µl of ChIP elution buffer was added to the beads and tubes were incubated at 65°C for 10 min. 100 µl of the supernatant of each Input or Background samples was then added to 80 µl of TE and 20 µl of proteinase K (20 mg/ml stock). Frozen Input samples were thawn on ice and were added to 100 µl of ChIP elution buffer, 100 µl of TE and 20 µl of

proteinase K. Samples were incubated at 37°C for 2 h and then at 62°C overnight. Qiagen PCR purification kit was used to purify the DNA samples. 1 ml of PB buffer was added to IP and Background samples and 1.5 ml to Input samples. Samples were added to the spin columns and the columns were spun for 30 s at 13200 rpm. Flow through was discarded and columns were washed using 750 µl of PE buffer. Columns were spun for 1 min at 13200 rpm. Flow through was discarded and columns were re-spun for 1 min. DNA was eluted using 160 µl of TE and spinning for 1 min. Samples were stored at -20°C until used for RT-PCR measurement.

2.4.9 RT-PCR for ChIP measurement

Input, IP and Background samples were measured in triplicate. 15 µl of mastermix was added to 5 µl of sample in a 96 well reaction plate (Applied Biosystems).

Mastermix (per reaction):

Platinum SYBR Green qPCR SuperMix-UDG with ROX: 10 µl

Forward primer (10 µM): 0.4 µl

Reverse primer (10 µM): 0.4 µl

dH_2O: 4.2 µl

PCR programme:

50°C for 2 min hold

95°C for 2 min hold

40 cycles of:

95°C for 15 s

60°C for 30 s

Melting curve analysis

10X TBS (1 L):

87.6 g NaCl

12.1 g TrisBase

700 ml dH_2O

pH was adjuted to 7.5 using HCl and solution was topped up to 1 litre with dH_2O.

FA lysis buffer (1 L):

11.9 g HEPES (powder), diluted in 700 ml of dH_2O. pH was adjusted to 7.5 using KOH.

30 ml 5 M NaCl

2 ml 0.5 M EDTA, pH7.6

10 ml 100% Triton-X

1 g Sodium deoxycholate

10 ml 10% SDS

Solution was topped up to 1 litre with dH_2O.

ChIP elution buffer (50 ml):

2.5 ml 1 M Tris-HCl, pH 7.5

1 ml 0.5 M EDTA, pH 7.6

5 ml 10% SDS

Solution was topped up to 50 ml with dH_2O.

2.4.10 FACS

Cells were grown as described in 2.3.8. For each time point 1 ml of cell culture was spun at 13200 rpm for 7 s and cell pellet was re-suspended in 0.5 ml of 70% ethanol. Cells could be stored at 4°C. Cells were prepared according to the Breeden FACS protocol with a few exceptions (http://labs.fhcrc.org/breeden/Methods/index.html). Cells were washed twice in 1 ml of water, spun at 13200 rpm for 10 s and re-suspended in 0.5 ml of 50 mM Tris (pH 8.0). 10 µl of 10 mg/ml RNAse A was added to each sample and the mixture was incubated for 4 h at 37°C. The cell suspension was spun for 30 s at 13200 rpm and the pellet was re-suspended in 0.5 ml of 50 mM Tris (pH 7.5) containing 2 mg/ml proteinase K. After incubation at 50°C for 40 min, the suspension was spun at 13200 rpm for 30 s and the pellet was re-suspended in 0.5 m of FACS buffer (200 mM Tris/HCL pH 7.5; 200 mM NaCl; 78 mM $MgCl_2$). 10 µl of cell suspension was transferred to a new eppendorf tube. 1 ml of 1X Sytox Green in 50 mM Tris pH 7.5 (2 µl of 5 mM Sytox Green in DMSO (5000X); 10 µl of Tris pH7.5) were added to stain the nucleus and the mixture was sonicated at an amplitude of 5 microns for 10 s and samples were analysed using a Partec PAS flow cytometer.

2.4.11 TCA extraction of proteins

TCA (Trichloroacetic acid) extractions were performed as previously described (Foiani *et al.*, 1994). 10^8 of exponentially growing cells were spun down for 3 min at 1500 rpm, washed with 10 ml sterile water, spun again and re-suspended in 10 ml 20% TCA. Cells were re-spun and re-suspended in 100 µl of 20% TCA and transferred to a 2 ml screw cap tube. Cells could be stored at -20°C at this stage. An equal volume of glass beads was added to each tube and tubes were vortexed for 4 min. 100 µl of extract was transferred to a fresh eppendorf tube and glass beads were washed twice with 100 µl of 5% TCA. After each wash 100 µl of cell extract was transferred to get a final volume of 300 µl of extract. The mixture was spun at 3000 rpm for 10 min and the pellet was re-suspended in 100 µl Laemmli loading buffer. 50 µl of 2 M Tris was added to neutralize the sample and the extract was boiled for 3 min, spun for 10 min at 3000 rpm. The supernatant was used for Western blot analysis and could be stored at -20°C.

2.4.12 Western blot analysis

10 µl of TCA extract was run on a 7.5% Tris-glycine Ready gel (Bio-Rad) at 100 V in running buffer. A Hybond-ECL nitrocellulose membrane and 4 sheets of Whatman paper were cut to the size of the gel and soaked in transfer buffer together with two fibre pads. Two Whatman papers were placed on top of on fibre pad, followed by the nitrocellulose membrane, the gel, another two pieces of Whatman paper and the second fibre pad. Air bubbles were removed using a glass test tube. The sandwich was inserted into the transfer cassette with the gel being arranged between the membrane and the negative electrode. The transfer cassette was placed into the tank filled with transfer buffer. Transfer occurred over 2 hours at 100 V.

The membrane was removed from the cassette after completion of the transfer and was quickly rinsed in water before being blocked in 5% milk (powdered milk; Marvel) in PBST for 1 h on a rocking table. The membrane was then incubated with 10 ml of primary antibody solution in 1% milk overnight at 4°C on a rocking table. The primary antibody solution was poured off; the membrane was briefly rinsed in tap water and washed five times with 80 ml of PBST for 10 min each wash on a rocking table at room temperature. Blot was incubated with 10 ml of secondary antibody solution in 1% milk for 2 h at room temperature. The membrane was washed five times with 80 ml of PBST for 10 min each wash. The membrane was then incubated with 5 ml of peroxide and 5 ml of luminal solutions (SuperSignal Wet Pico Chemiluminescent substrate) for 5 min. The membrane was placed on a glass plate, covered with cling film and chemiluminescent bands were detected using a chemiluminescent imager (Fuji LAS 4000).

<u>Running buffer (1 L):</u>

100 ml 10X Tris/Glycine/SDS buffer (Bio-Rad)

900 ml MQ water

Transfer buffer (1 L):

100 ml 10X Tris/Glycine buffer (Bio-Rad)

200 ml methanol

700 ml MQ water

PBST (1 L):

999 ml MQ water

5 PBS tablets (Sigma)

1 ml Tween 20

Primary antibodies used:

9E10 mouse anti-MYC

Mouse anti-tubulin

Rabbit anti-Rad53

Rabbit anti-H2A phosphorylated at Serine129

Secondary antibodies used:

Goat anti-mouse conjugated to HRP

Goat anti-rabbit conjugated to HRP

2.4.13 Fluorescent In-Gel Assay

In-gel assay was performed as previously described (Dewar and Lydall, 2010). 25 ml of exponentially dividing cells (2 x 10^7 cells/ml) were harvested by spinning cells in a pre-chilled centrifuge for 5 min at 2000 rpm at 4°C. Pellets were re-suspended in 1 ml ice cold dH_2O and suspension was transferred to 1.5 ml Eppendorf tubes. Cells were pelleted at 4°C in a microcentrifuge for 15 sec at 13,000 rpm, supernatant was poured off, and cells were re-spun for 10 sec. Remaining liquid was aspirated and cell pellets could be stored at -80°C.

To isolate DNA from cell pellets, cells were thawn on ice and then re-suspended in 200 µl of lysis buffer. 0.3 g of acid-washed glass beads (Stratech) were added to a 2 ml skirted screw top tube (Sarstedt) for each sample and re-suspended cell pellet was added to the screw tube. 200µl of phenol:chloroform:isoamyl alcohol (25:24:1) was added to each tube and tubes were inverted to mix. Cells were lysed at 5.5 power setting for 20 sec using a Precellys 24 automated homogeniser. This step was repeated twice and cells were chilled on ice-water in between breakage cycles. 200 µl of TE was added to each tube after cell lysis and the suspension was mixed by vortexing. Tubes were spun in a microcentrifuge for 5 min at 13,000 rpm at 4°C. 750 µl of the aqueous phase was transferred to a 2 ml phase lock gel containing 750 µl of phenol:chloroform:isoamyl alcohol (25:24:1). Suspension was mixed by inversion and tubes were spun in a microcentrifuge for 5 min at 13,000 rpm at 4°C. The aqueous phase was transferred to a fresh 2 ml Eppendorf tube and 100% ethanol was added to fill the tube. The suspension was mixed by inversion and left to precipitate for 5 min at room temperature. Tubes were then spun in a microcentrifuge for 3 min at 13,000 rpm, supernatant was poured off and tubes were re-spun for another 15 sec. Residual ethanol was removed by aspiration and pellet were dried in a fume hood for 5 min. 400 µl of TE and 3 µl of RNase A (10 mg/ml) were added to each tube and tubes were incubated in a 37°C water bath for 30 min. 13 µl of NaAc (3M, pH 5.2) was added and tube was filled with 100% ethanol. DNA was left to precipitate at room temperature for 15 min. DNA was then pelleted in a microcentrifuge for 3 min at 13,000 rpm. Supernatant was decanted, tubes were re-spun for 15 sec and residual ethanol was aspirated. DNA pellets were dried in the fume hood for 30 min and then re-suspended in 25 µl TE by incubation in a 37°C water bath for 30 min. DNA was equilibrated by incubating tubes on ice for 1 hour.

DNA samples were quantified by spectroscopy using a nanodrop (NanoVue Plus, GE Healthcare), adjusted to the sample with the lowest concentration using TE and stored at -80°C. 10 µl of DNA sample was cut with Xho1 (1.5 µl Xho1 (20 units/ µl), 2 µl NEB Buffer 4 (10X), 0.2 µl BSA (100X), 5.8 µl dH_2O) in a 37°C water bath overnight. The next day, tubes were incubated at 65°C for 20 min to heat-inactivate Xho1. Tubes were then placed on ice and 1 µl of CY5-labelled AC probe (500 nM) was added to each tube. Tubes were flicked to mix, incubated at 37°C for 10 min to anneal the probe to TG ssDNA and then kept on ice for 30 min.

5 µl of orange loading dye (6X) was added to each tube and samples were run on a 1% agarose gel in 0.5X TBE alongside 1 KB DNA ladder in orange loading buffer. Gel was run at 5 V/cm for 90 min and signal was then detected on a Typhoon Trio Imager (GE Healthcare) at maximum resolution and sensitivity.

Gel was post-stained for 1 hour using 1X SYBR Safe in 0.5X TBE buffer and total DNA was detected using a FUJI LAS-4000 imager.

ssDNA of the CY5 image was quantified using ImageJ. The mean pixel intensity of each lane (between 0.8 and 12 kb) was quantified and the mean pixel intensitiy between the lanes (between 0.8 and 12 kb) were quantified to determine background signal. Background signal was then substracted from quantified signal of each lane.

Lysis buffer:

2% Triton X-100, 1% SDS, 100 mM NaCl, 10 mM Tris (pH 8.0), 1 mM EDTA (pH 8.0)

2.4.14 Quantitative Amplification of ssDNA (QAOS)

Quantitative Amplification of ssDNA was performed as described in Holstein and Lydall (in press). The protocol is attached to this thesis.

3 The role of Nmd2 and Ebs1 in telomere capping

3.1 Introduction

Telomere-binding proteins protect telomeres from being recognised and treated as double-strand breaks, thereby preventing telomere degradation and DNA repair events that can contribute to chromosome instability and cancer in mammalian cells. Dysfunctional telomeres and their effects on the cell can be studied in yeast using mutations in genes encoding for telomere capping proteins. Mutants containing a deletion of the *YKU70* gene or a point-mutation in the essential gene *CDC13* have been used in this work to study responses to telomere uncapping in *Saccharomyces cerevisiae*. Both *yku70*Δ and *cdc13-1* mutants are temperature-sensitive and growth at non-permissive temperature have been shown to lead to resection of telomeres, ssDNA accumulation and subsequent cell cycle arrest (Maringele and Lydall, 2002; Weinert and Hartwell, 1993) (Figure 5). Genome-wide high-throughput screens of strains carrying either the *yku70*Δ or the *cdc13-1* mutation were carried out in our lab by combining these two strains with a library of more than 4000 single gene deletion mutants (Addinall *et al.*, 2011). Growth of double mutants compared to single mutants at non-permissive temperature (27°C for *cdc13-1* and 37.5 °C for *yku70*Δ) was analysed using Quantitative Fitness Analysis (QFA) (Figure 6).

Various gene deletions in the Addinall et al., 2011 screen suppressed or enhanced both *yku70*Δ and *cdc13-1* telomere capping defects. However, many gene deletions suppressed one telomere capping defect, but enhanced the other, despite Cdc13 and Yku70 both having a role in telomere capping. Gene deletions affecting the nonsense-mediated mRNA decay pathway, including *upf1*Δ*, upf2*Δ and *upf3*Δ*,* were some of the strongest suppressors of the *cdc13-1* temperature-sensitivity whilst being one of the strongest enhancer of the *yku70*Δ temperature-sensitivity.

The aim of this chapter was to investigate how deletion of any of the Nonsense-Mediated Decay (NMD) genes can have opposite growth effects on two forms of telomere uncapping, thus allowing a better understanding of telomere uncapping and the

cellular responses to dysfunctional telomeres. Ebs1 was included in the study as Ebs1 has proposed roles in both telomere regulation and NMD pathway and showed less strong, but similar growth phenotypes to NMD genes in the QFA screen (Figure 6).

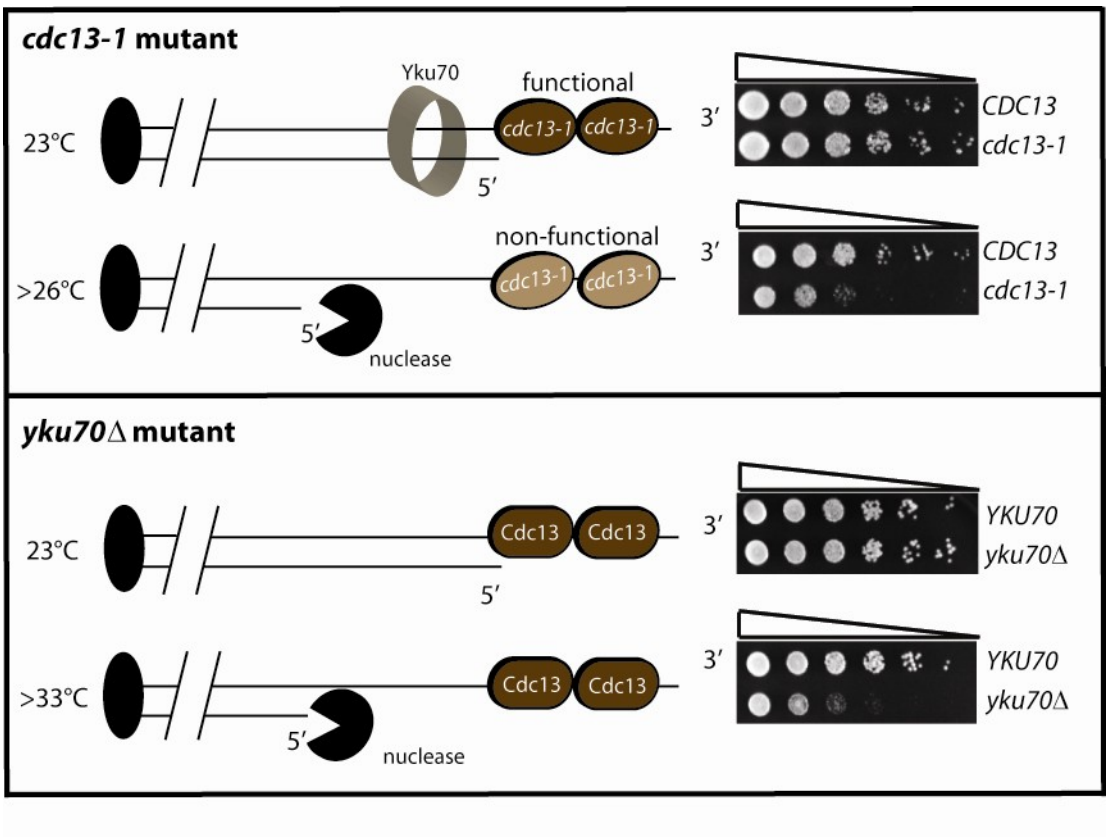

Figure 5. *cdc13-1* and *yku70*Δ-dependent telomere uncapping.

cdc13-1 is a temperature-sensitive allele of the essential gene *CDC13*. *CDC13* encodes for the telomere capping protein Cdc13 and binding of Cdc13 to single-stranded telomeric overhangs prevents telomeres from being recognized as DNA damage (Nugent et al., 1996). A *cdc13-1* mutant can grow at 23°C and telomeres are not recognized as DNA damage. However, growth gradually decreases at temperatures above 26°C due to telomere uncapping and a subsequent G2-M checkpoint response leading to cell cycle arrest (Weinert and Hartwell., 1993). Yku70 protects telomeres from being recognized as DNA damage by binding to double-stranded telomeric repeats. Mutants containing a *yku70*Δ null-mutation are temperature-sensitive and growth gradually decreases at temperatures above 33°C, due to telomere uncapping and activation of the DNA damage reponse pathway (Nugent et al., 1998; Barnes and Rio., 1997; Maringele and Lydall 2002). Temperature-sensitive *cdc13-1* and *yku70*Δ mutants provide a great tool to study the role of a gene of interest at uncapped telomeres. See text for details.

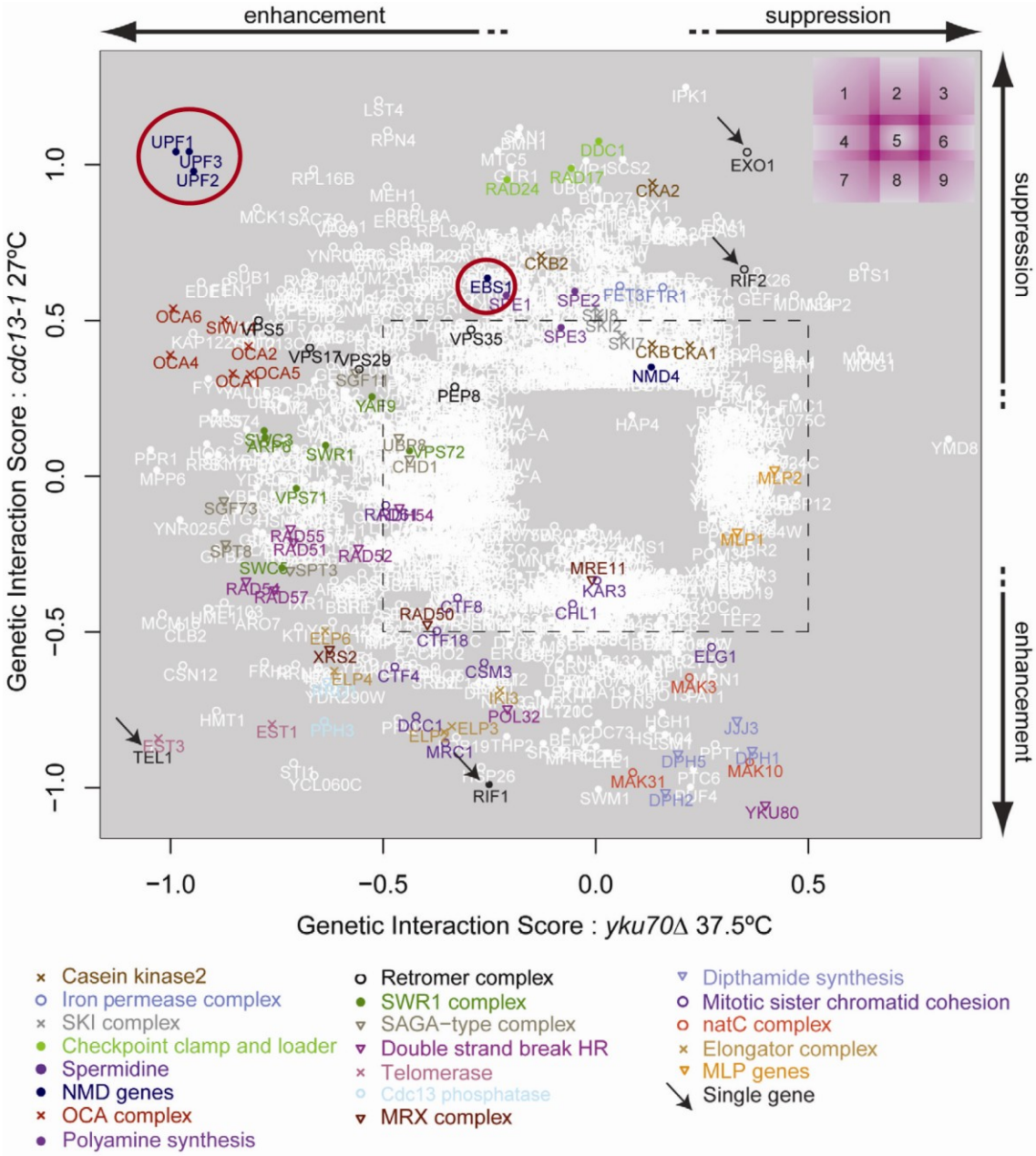

Figure 6. QFA screen for *cdc13-1* and *yku70*Δ

Genes with significant interaction with *cdc13-1* or *yku70*Δ are shown. Location of a gene on the plot is dependent on its genetic interaction score and locations of the NMD genes *UPF1, UPF2, UPF3* and of *EBS1* are highlighted by red circles. Deletion of any of the four genes suppresses *cdc13-1* temperature-sensitivity and enhances *yku70*Δ temperature-sensitivity. Graph is taken and modified from Addinall et al., 2011 (Addinall et al., 2011).

3.2 Results

3.2.1 Ebs1 and Upf2 affect Cdc13- and Yku70-mediated telomere capping

Deletion of NMD genes or *EBS1* suppressed the *cdc13-1* telomere capping defect but enhanced the *yku70*Δ telomere capping defect in the QFA screen (Figure 6) (Addinall *et al.*, 2011). The screen was carried out in S288C budding yeast; to confirm the result of the QFA screen in the W303 background, *upf2*Δ and *ebs1*Δ mutants were crossed with *yku70*Δ or *cdc13-1* mutants in the W303 background in order to obtain double or triple mutants. Maximum Permissive Temperature (MPT) experiments were then performed to investigate the maximum temperature the double or triple mutants can grow on YEPD agar plates. As shown in Figure 7A, all mutants showed comparable growth to wild type at 23°C and *upf2*Δ and *ebs1*Δ single mutants showed no growth defects at 28°C or 36°C. *cdc13-1* mutants, however, had a temperature-sensitive growth phenotype at 28°C and cells were not able to form colonies at the non-permissive temperature of 36°C. Interestingly, deletion of *upf2*Δ dramatically enhanced growth of *cdc13-1* mutants at 28°C. In fact, *upf2*Δ *cdc13-1* mutants grew almost as well as wild-type strains at 28°C. Similar growth phenotypes could be seen for *ebs1*Δ mutants. Deletion of *ebs1*Δ suppresses the temperature-sensitivity of *cdc13-1* mutants at 28°C, but suppression was modest compared to *upf2*Δ. Thus we can conclude that cells lacking Upf2 or Ebs1 suppress the *cdc13-1* capping defect and suppression of *ebs1*Δ was modest compared to *upf2*Δ, which is consistent with the phenotypes observed in the QFA screen (Addinall *et al.*, 2011).

When looking at *yku70*Δ dependent telomere uncapping, *yku70*Δ single mutants showed a temperature-sensitive phenotype at 36°C in W303, which was much more pronounced when *upf2*Δ was deleted (Figure 7B). In fact, whereas *yku70*Δ single mutants showed comparable growth to wild type at 34°C, *upf2*Δ *yku70*Δ double mutants had a temperature-sensitive phenotype. Similarly, deletion of *ebs1*Δ enhanced the temperature-sensitivity of *yku70*Δ mutants at 34°C and 36°C. The growth effects of deleting NMD genes were much more pronounced for *upf2*Δ in *yku70*Δ mutants compared to *ebs1*Δ in the W303 background. In conclusion, cells lacking Upf2 or Ebs1 in the W303 background suppressed the *cdc13-1* telomere capping defect but enhanced the *yku70*Δ telomere capping defect. Similar to the QFA screen, the growth effects of *upf2*Δ mutation were much more pronounced compared to *ebs1*Δ. Hence, the

phenotypes observed in the QFA screen were consistent in two different genetic backgrounds.

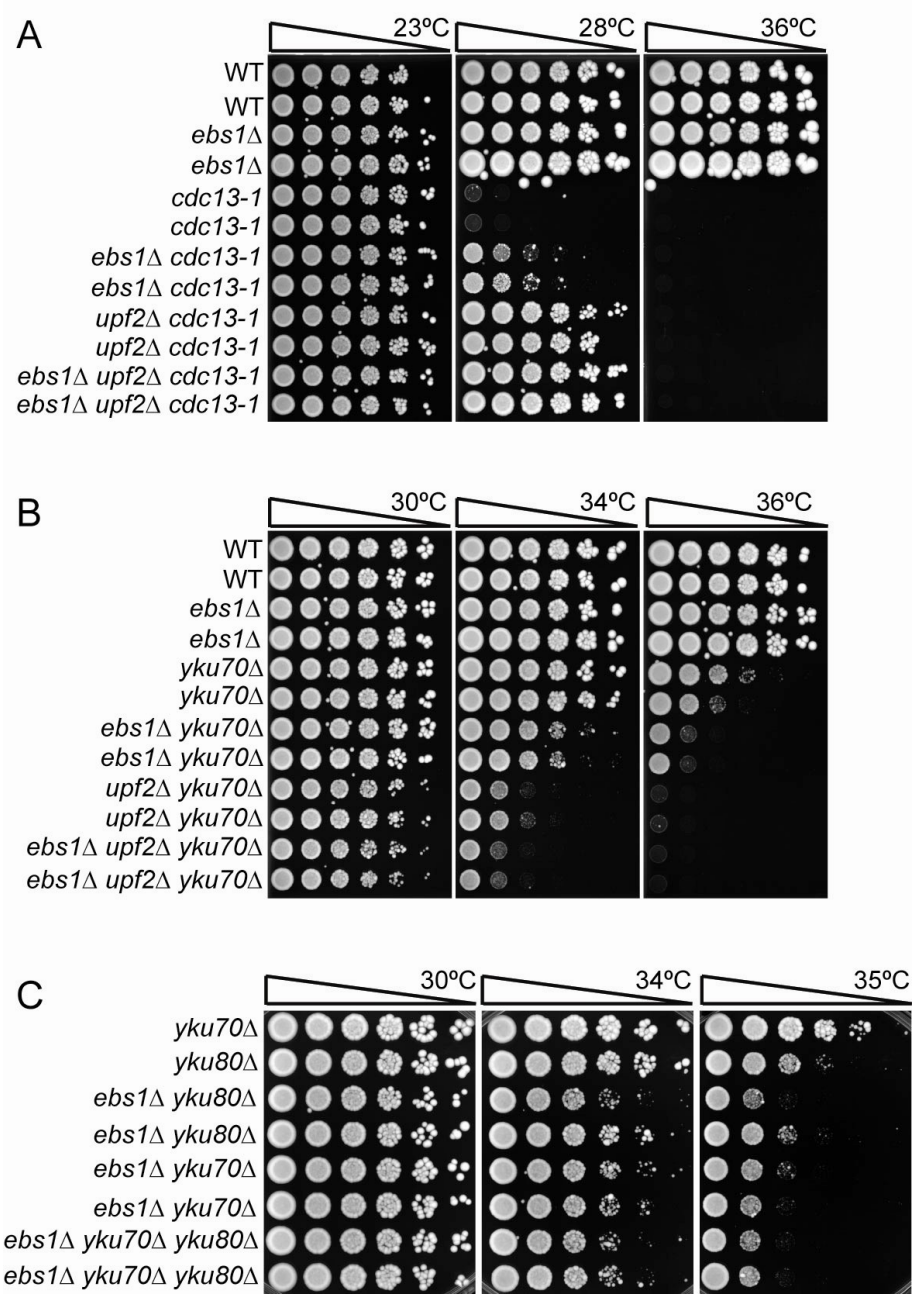

Figure 7. Ebs1 and Upf2 inhibit growth of *cdc13-1* mutants and enhance growth of *yku70*Δ mutants.

A-C. Serial dilutions of saturated cultures of the indicated genotypes were grown for 2 days on YEPD plates at the temperature indicated.

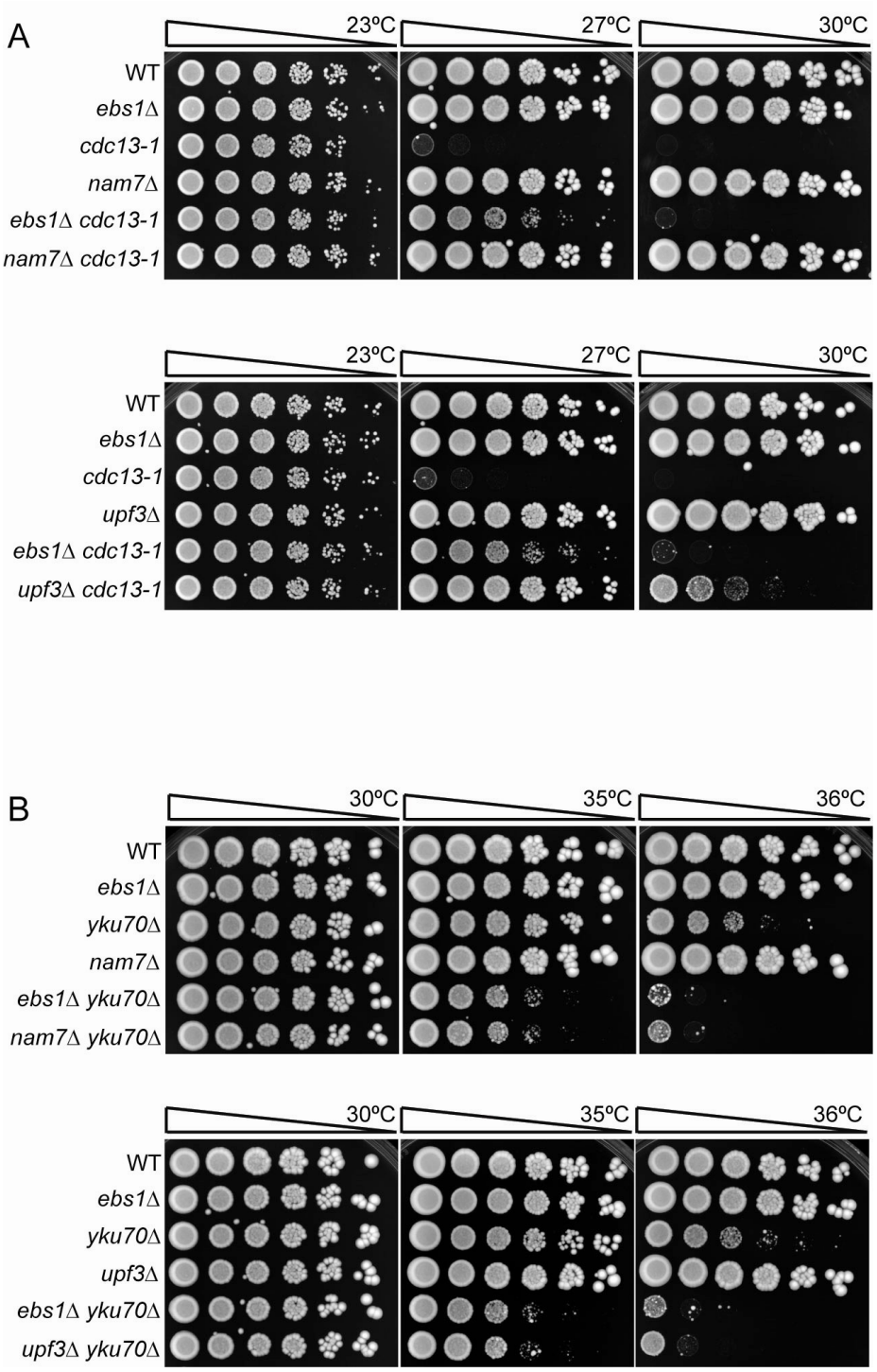

Figure 8. Nam7 and Upf3 inhibit growth of *cdc13-1* mutants and enhance growth of *yku70*Δ mutants.

A and **B.** Serial dilutions of saturated cultures of the indicated genotypes were grown for 2 days on YEPD plates at the temperature indicated.

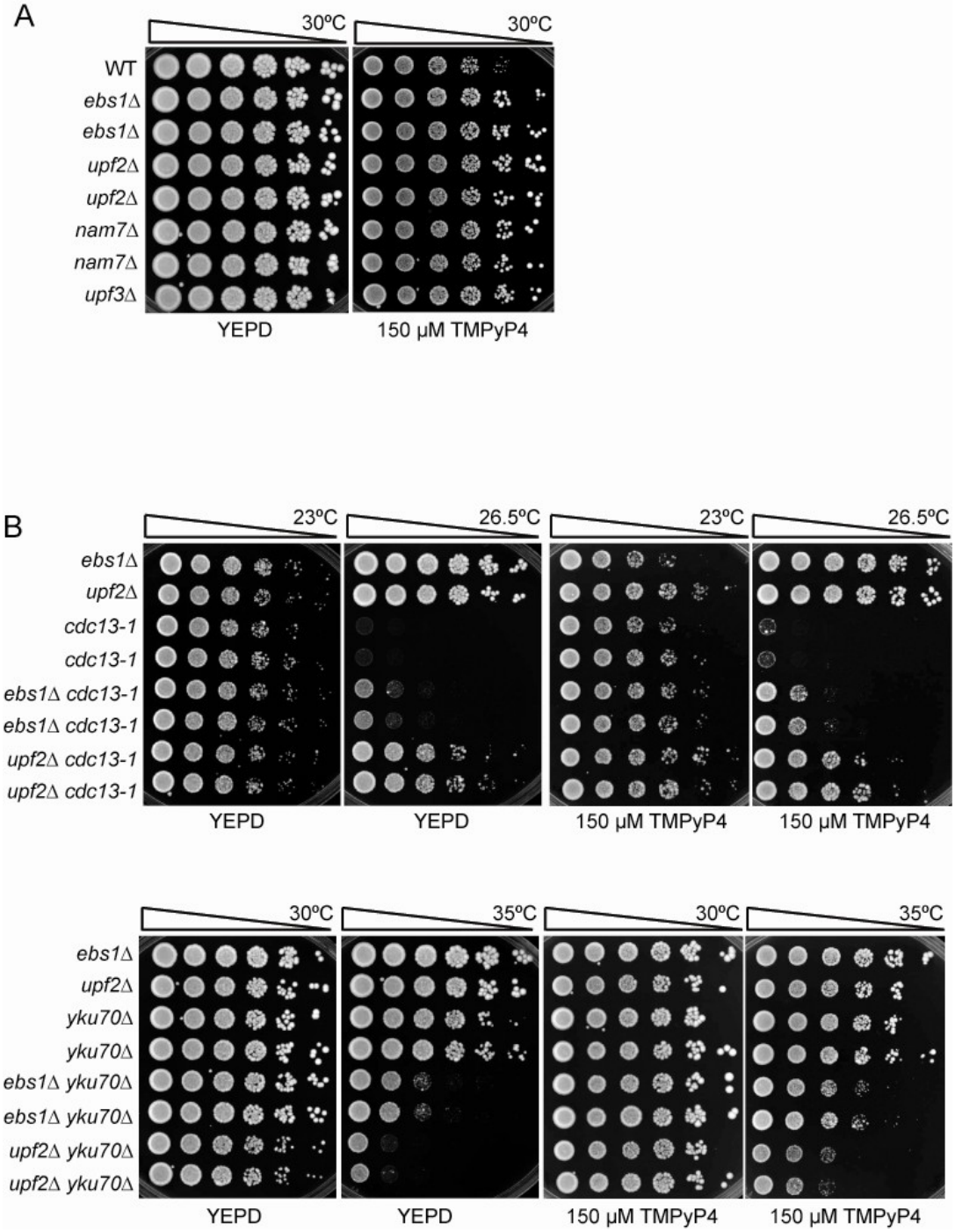

Figure 9. Growth in the presence of the G-quadruplex stabilizer TMPyP4

Saturated cultures of the genotypes indicated were serially diluted across agar plates containing YEPD or YEPD and TMPyP4. Strains were allowed to grow for 3 days at the temperature indicated.

To investigate if the growth phenotypes seen in *yku70*Δ mutants are true for the whole Yku complex, growth of cell lacking the Yku80 subunit was tested. As shown in Figure 7C, growth of *ebs1*Δ *yku80*Δ mutants could not be distinguished from growth of *ebs1*Δ *yku70*Δ strains. Furthermore, no additional growth defect could be seen in *ebs1*Δ *yku70*Δ *yku80*Δ mutants compared to *ebs1*Δ *yku70*Δ strains. The indistinguishable growth phenotypes indicate that the observed phenotype of *ebs1*Δ *yku70*Δ strains is true for the whole Yku complex and that deletion of either subunit of the Ku complex has presumably the same effect in *ebs1*Δ strains.

Like Upf2, Nam7 (Upf1) and Upf3 are core components of the NMD pathway. The ability of mutants lacking one of the core NMD genes to grow in the presence of *cdc13-1* or *yku70*Δ uncapped telomeres was investigated. Elimination of either *NAM7* or *UPF3* did not cause a growth defect at 23°C (Figure 8A). However, *nam7*Δ and *upf3*Δ mutation suppressed the *cdc13-1* temperature-sensitivity at 27°C and enhanced the *yku70*Δ growth defect at 35°C. Hence, it can be concluded that cells lacking either Nam7 or Upf3 showed similar growth phenotypes to cells lacking Upf2 or Ebs1.

Similar to *upf2*Δ mutants (Figure 7B), suppression of the *cdc13-1* temperature-sensitivity was much more pronounced for *nam7*Δ and *upf3*Δ in the presence of *cdc13-1* uncapped telomeres compared to *ebs1*Δ (Figure 8A). However, growth of either *nam7*Δ or *upf3*Δ in *yku70*Δ mutants was comparable to *ebs1*Δ (Figure 8B). In conclusion, deletion of any of the three core components of the NMD pathway or *EBS1* in W303 suppresses the *cdc13-1* growth defect, but enhances the *yku70*Δ growth defect, which is consistent with the phenotypes seen in the QFA screen (Addinall *et al.*, 2011).

3.2.2 NMD and Ebs1 do not affect Cdc13- and Yku-70 mediated telomere capping through stabilisation of G-quadruplexes.

A yeast screen from 2008 revealed mutants that are resistant or sensitive to the G-quadruplex-interacting compound NMM (N-methyl mesoporphyrin IX) (Hershman *et al.*, 2008). Interestingly, deletion of any of the three core components of NMD (Upf1, Upf2, Upf3) or Ebs1 resulted in resistance to NMM. Another mutant showing resistance to NMM was *stm1*Δ. *STM1* encodes for a G-Quadruplex-binding protein (Smith and Johnson, 2010; Nelson et al., 2000). Recent studies in yeast demonstrated a link between G-Quadruplex formation and telomere regulation. For instance, Est1 seems to limit telomerase binding to the 3' telomeric overhang by converting single-stranded telomeric DNA to a G-quadruplex structure (Zhang *et al.*, 2010). In addition, Stm1 has been shown to associate with telomeres and subtelomeres, to interact with the telomere-binding protein Cdc13 in a two-hybrid assay and to suppress the *cdc13-1* telomere capping defect, indicating a link between G-quadruplex formation at telomeres and telomere protection (Addinall et al., 2011; Van Dyke et al., 2004; Hayashi and Murakami, 2002; Frantz and Gilbert, 1995). This is further supported by a recent study that demonstrated that overexpression of several G-quadruplex binding proteins or loss of the helicase Sgs1 (role in unwinding G-quadruplexes) also suppress the *cdc13-1* telomere capping defect (Smith et al., 2011). Their work shows that G-quadruplexes supports telomere capping at dysfunctional telomeres by inhibiting telomere resection by Exo1. In conclusion, the results of the yeast screen from Hersman et al., 2008 suggest a role for NMD at G-quadruplexes and NMD proteins may affect telomere protection through interaction with G-quadruplexes at telomeres.

To test whether NMD proteins affect Cdc13- or Yku70-dependent telomere capping through interaction with G-quadruplexes, NMD-deficient mutants and *ebs1*Δ mutants containing a telomere capping-defective *cdc13-1* or *yku70*Δ mutation were grown in the presence of the G-Quadruplex-interacting compound TMPyP4 (150 µM). If suppression of the *cdc13-1* growth defect or enhancement of the *yku70*Δ growth through *upf2*Δ or *ebs1*Δ is due to stabilization of G-quadruplexes at telomeres, then *cdc13-1* mutants should show similar growth to *upf2*Δ *cdc13-1* or *ebs1*Δ *cdc13-1* mutants in the presence of the drug. Similarly, *yku70*Δ mutants should show similar growth to *upf2*Δ *yku70*Δ or *ebs1*Δ *yku70*Δ mutants in the presence of TMPyP4. As shown in Figure 9A, deletion of

any of the three core components of NMD resulted in better growth in the presence of 150 µM TMPyP4 compared to wild-type, reproducing the results of the NMM screen using a different G-quadruplex-interacting compound. However, no difference in growth was detectable for *cdc13-1*, *ebs1*Δ *cdc13-1* or *upf2*Δ *cdc13-1* mutants in presence of TMPyP4 compared to growth in the absence of TMPyP4 (Figure 9B). Similarly, no difference in growth was detectable for *yku70*Δ, *ebs1*Δ *yku70*Δ or *upf2*Δ *yku70*Δ mutants in presence of TMPyP4 compared to growth in the absence of TMPyP4 (Figure9B). In conclusion, NMD-deficient mutants grew better in the presence of 150 µM TMPyP4 compared to wild-type. NMD-deficient mutants containing a telomere capping-defective *cdc13-1* or *yku70*Δ mutation had no significant growth difference in the presence or absence of 150 µM TMPyP4, indicating that suppression of the *cdc13-1* growth defect and enhancement of the *yku70*Δ growth through *upf2*Δ or *ebs1*Δ is not due to interaction with G-quadruplexes at telomeres.

3.2.3 Ebs1 and NMD regulate transcript and protein levels of the telomere binding factors Ten1 and Stn1

One possibility how Ebs1 and NMD proteins could affect telomere capping may be by regulating transcript levels of telomere binding factors through nonsense-mediated decay. NMD factors are known to target aberrant mRNAs containing premature termination codons for decay, thus preventing translation of protein fragments that could be potentially dangerous for the cell (Chang *et al.*, 2007). Dahlseid et al., 2003 demonstrated that in addition to regulating degradation of aberrant mRNAs, NMD regulates transcript levels of various genes encoding for proteins containing telomere function. Altered stochiometry of telomere cap components is one possible mechanism by which NMD genes and Ebs1 could affect telomere capping in *cdc13-1* and *yku70*Δ mutants. To test this hypothesis, transcript levels of three NMD targets with known telomere function were measured in wild-type, *upf2*Δ and *ebs1*Δ strains using RT-PCR. mRNA levels of the telomere capping proteins Stn1 and Ten1 (known to form the CST complex together with Cdc13; shown in Figure 1) and Est2 (the catalytic subunit of telomerase) were determined. Transcript levels of *CDC13* served as a negative control as *CDC13* mRNAs are not a target of NMD (Dahlseid et al., 2003). As shown in Figure 10, no significant increase in transcript levels of *CDC13* could be seen for any of the

mutants compared to wild-type. In contrast, mRNA levels of *STN1* and *TEN1* were significantly increased in *upf2*Δ and *ebs1*Δ strains compared to wild-type. In the case of *EST2*, transcript levels were only significantly higher in *upf2*Δ but not *ebs1*Δ mutants. Similar to growth phenotypes in Figure 7, the effects of *ebs1*Δ strains were modest compared to *upf2*Δ strains. In conclusion, like Upf2, Ebs1 regulates transcript levels of three telomere binding factors.

Data in Figure 10 demonstrated that Stn1 and Ten1 transcript levels are increased in *upf2*Δ and *ebs1*Δ mutants, suggesting that *upf2*Δ and *ebs1*Δ mutants have higher Stn1 and Ten1 protein levels compared to wild type strains. To confirm that the increased *STN1* transcript levels in *upf2*Δ and *ebs1*Δ mutants lead to increased translation of *STN1* mRNA, Stn1 protein levels were analysed by crossing a strain containing myc-tagged Stn1 with *ebs1*Δ and *nmd2*Δ mutants or *ebs1*Δ and *nmd2*Δ mutants containing *cdc13-1* or *yku70*Δ mutations. Analysis of Stn1 protein levels by Western Blot using antibodies against myc-tagged Stn1 demonstrated a significant increase in Stn1 levels in both *upf2*Δ and *ebs1*Δ mutants compared to wild-type (Figure 11). Similar Stn1 protein levels could be detected in double mutants containing either the *cdc13-1* or the *yku70*Δ mutation. Consistent with the *STN1* transcript levels measured in Figure 10, increase in Stn1 proteins levels in *ebs1*Δ mutants were modest compared to Stn1 protein levels in *upf2*Δ mutants. In conclusion, Upf2 and Ebs1 regulate expression of the telomere binding protein Stn1. *STN1* transcript levels (Figure 10) and Stn1 protein levels (Figure 11) are increased in *ebs1*Δ and *upf2*Δ mutants.

Data in Figure 10 demonstrated that Ebs1 regulates expression of several telomere binding proteins, suggesting that *ebs1*Δ mediates a mild NMD defect. If Ebs1 is part of the NMD pathway, then *ebs1*Δ *upf2*Δ *cdc13-1* or *ebs1*Δ *upf2*Δ *yku70*Δ triple mutants would have the same growth phenotypes as *upf2*Δ on its own in the presence of *cdc13-1* or *yku70*Δ telomere uncapping. Furthermore, no additional increase in transcript levels should be detected in *ebs1*Δ *upf2*Δ double mutants compared to *upf2*Δ. As shown in Figure 12, *STN1* transcript levels were not significantly higher in *ebs1*Δ *upf2*Δ mutants compared to *upf2*Δ. However, *ebs1*Δ *upf2*Δ double mutants had slightly stronger growth effects in the presence of either *cdc13-1* or *yku70*Δ uncapped telomeres compared to

*upf2*Δ on its own (Figure 7A and B). In conclusion, *EBS1* and *UPF2* seem to act partially through different pathways.

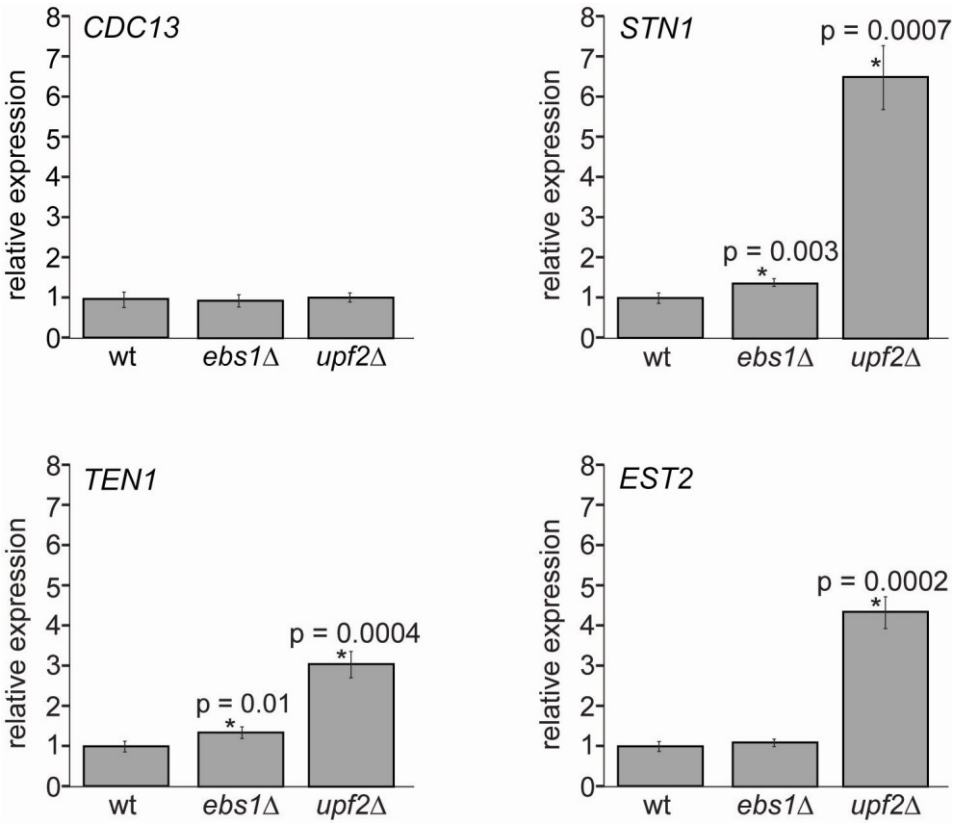

Figure 10. Ebs1 and Upf2 regulate transcript levels of several telomere binding proteins.

Four strains of each genotype were grown exponentially in YEPD medium at 23°C. RNA was isolated and transcript levels were measured using SYBR Green RT-PCR. Measurements were performed in triplicate and error bars indicate standard deviation from four independent measurements. RNA concentration of each sample was normalized to the loading control *BUD6*. A single wild type sample was given the value of 1 and all other values were corrected relative to this. Unpaired t-test using a two-tailed distribution and assuming unequal variance was used to determine p-values.

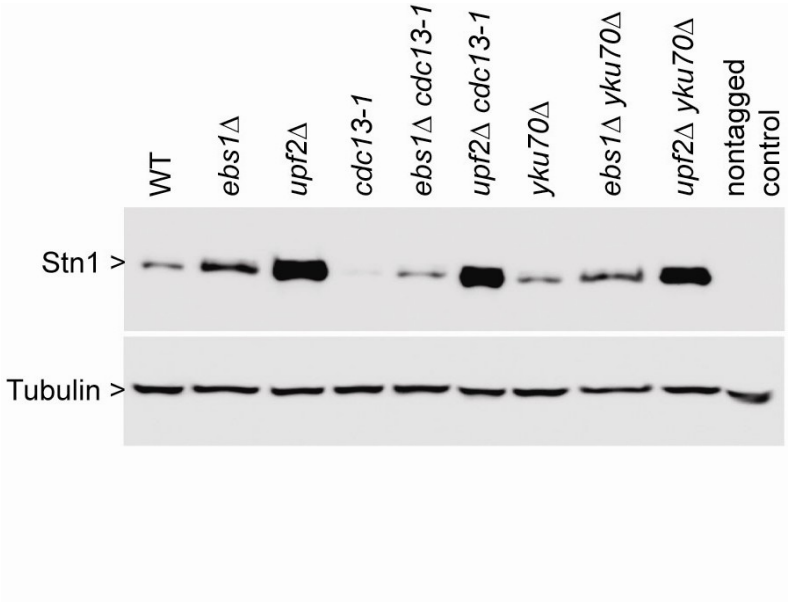

Figure 11. Ebs1 and Upf2 regulate levels of the telomere capping protein Stn1.

Western blot analysis of Stn1 protein levels. Strains contain Stn1-13Myc and antibodies against Myc-tag were used. Antibodies against tubulin were used for loading control.

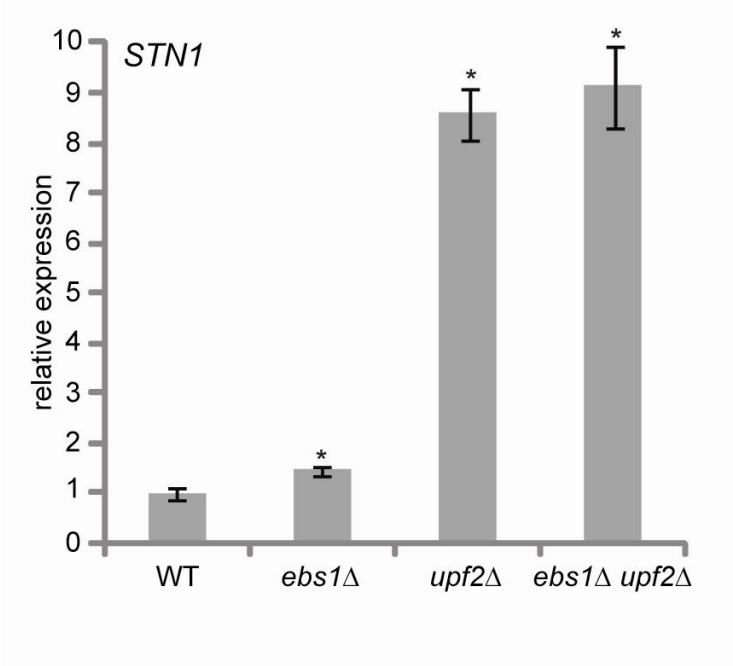

Figure 12. Ebs1 regulates transcript levels of Stn1 through the same pathway as Upf2.

Two strains of each genotype were grown exponentially in YEPD medium at 23°C. RNA was isolated and transcript levels were measured using SYBR Green RT-PCR. Measurements were performed in triplicate and error bars indicate standard deviation from two independent measurements. RNA concentration of each sample was normalized to the loading control *BUD6* and a single wild type sample was given the value of 1 and all other values were corrected relative to this.

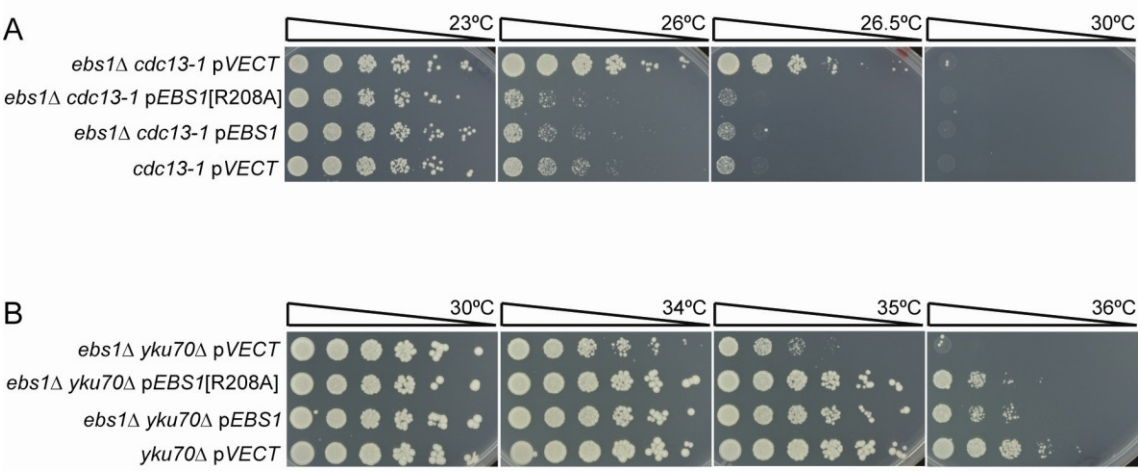

Figure 13. RNA recognition motif in EBS1 is not responsible for Ebs1 inhibiting growth of *cdc13-1* mutants and enhancing growth of *yku70*Δ mutants.

Saturated cultures of the genotypes indicated were serially diluted across agar plates containing synthetic media and grown for 3 days at the temperature indicated.

3.2.4 Ebs1 does not affect Cdc13- and Yku70-mediated telomere capping through an Est1-like RNA recognition motif

A publication from Zhou et al., 2000 showed a significant sequence similarity between Ebs1 and Est1, a core component of telomerase in budding yeast. Sequence similarity is most prominent in a presumed RNA recognition motif (RRM). Est1 is known to bind to the TLC1 RNA of telomerase through an RRM and many RRMs are capable of binding to telomeric single-stranded TG-rich repeats, suggesting that a potential association of Ebs1 with telomerase or telomeres might influence Cdc13- and Yku70-mediated telomere capping (Ding et al., 1999; Johnston et al., 1999; Reim et al., 1999; Lin and Zakian, 1994). The possibility of the Ebs1 RNA recognition motif being responsible for the observed growth phenotypes of cells lacking Ebs1 in the presence of *cdc13-1* and *yku70*Δ uncapped telomeres was tested by using a plasmid encoding for a point mutation in the RRM (Dan Durocher, personal communication) required for interaction with TLC1 RNA.

As shown in Figure 13A, growth of the *ebs1*Δ *cdc13-1* mutant containing a plasmid encoding for a point mutation in the RRM could not be distinguished from growth of the *ebs1*Δ *cdc13-1* mutant containing a plasmid encoding for wild-type *EBS1*. A similar result could be seen in *ebs1*Δ *yku70*Δ mutants (Figure 13B). Growth of *ebs1*Δ *yku70*Δ p*EBS1(R208A)* was indistinguishable from growth of *ebs1*Δ *yku70*Δ p*EBS1*. In conclusion, growth phenotypes of *ebs1*Δ *cdc13-1* or *ebs1*Δ *yku70*Δ mutants do not seem to be due to the Est1-like RNA recognition motif in Ebs1, suggesting that the potential interaction of Ebs1 with telomerase or telomeres through the RRM is not responsible for Ebs1 enhancing the *cdc13-1* capping defect and suppressing the *yku70*Δ capping defect. Further work is required to identify how Ebs1 affects telomere capping in addition to regulation of Stn1 levels.

3.2.5 Sep1 affects Cdc13- and Yku70-mediated telomere capping

The effect of another component of the NMD pathway on Cdc13- and Yku70-mediated telomere capping was tested to determine if the growth phenotypes seen in *upf2*Δ strains are true for other parts of the NMD pathway. The 5'-3' exonuclease Sep1 is known to be responsible for degradation of mRNAs in P-bodies (Sheth and Parker, 2003). The effect of *SEP1* deletion on the ability of *cdc13-1* and *yku70*Δ mutants to grow at the presence of uncapped telomeres was determined by MPT analysis. Similarly to *upf2*Δ and *ebs1*Δ, deletion of the 5'-3' exonuclease Sep1 suppressed the *cdc13-1* growth defect, but enhanced the *yku70*Δ growth defect. As shown in figure 14A, suppression of the *cdc13-1* temperature-sensitivity in *sep1*Δ *cdc13-1* mutants was comparable to suppression in *ebs1*Δ *cdc13-1* mutants. However, the *yku70*Δ growth defect was more pronounced in *ebs1*Δ *yku70*Δ mutants compared to *sep1*Δ *yku70*Δ mutants. As Sep1 is part of the NMD pathway, it seems plausible that *sep1*Δ mutants, like *upf2*Δ mutants, have increased levels of Stn1 compared to wild type strains. Indeed, similarly to *upf2*Δ and *ebs1*Δ (Figure 11), *sep1*Δ mutants expressed more of the telomere capping protein Stn1 compared to wild-type strains and Stn1 levels were comparable to *ebs1*Δ mutants (Figure 14B). In conclusion, cells lacking the NMD protein Sep1 suppressed the *cdc13-1* capping defect, but enhanced the *yku70*Δ capping defect and cells lacking Sep1 have increased protein levels of the telomere binding protein Stn1. Growth phenotypes and regulation of Stn1 levels in cells lacking Sep1 are consistent with the results seen in cells lacking other components of the NMD pathway (Figure 7, 10 and 11), suggesting that not only the proteins responsible for marking mRNAs for decay (Upf1, Upf2, Upf3), but another component of the NMD pathway responsible for degradation of mRNAs, affect Cdc13- and Yku70-mediated telomere capping.

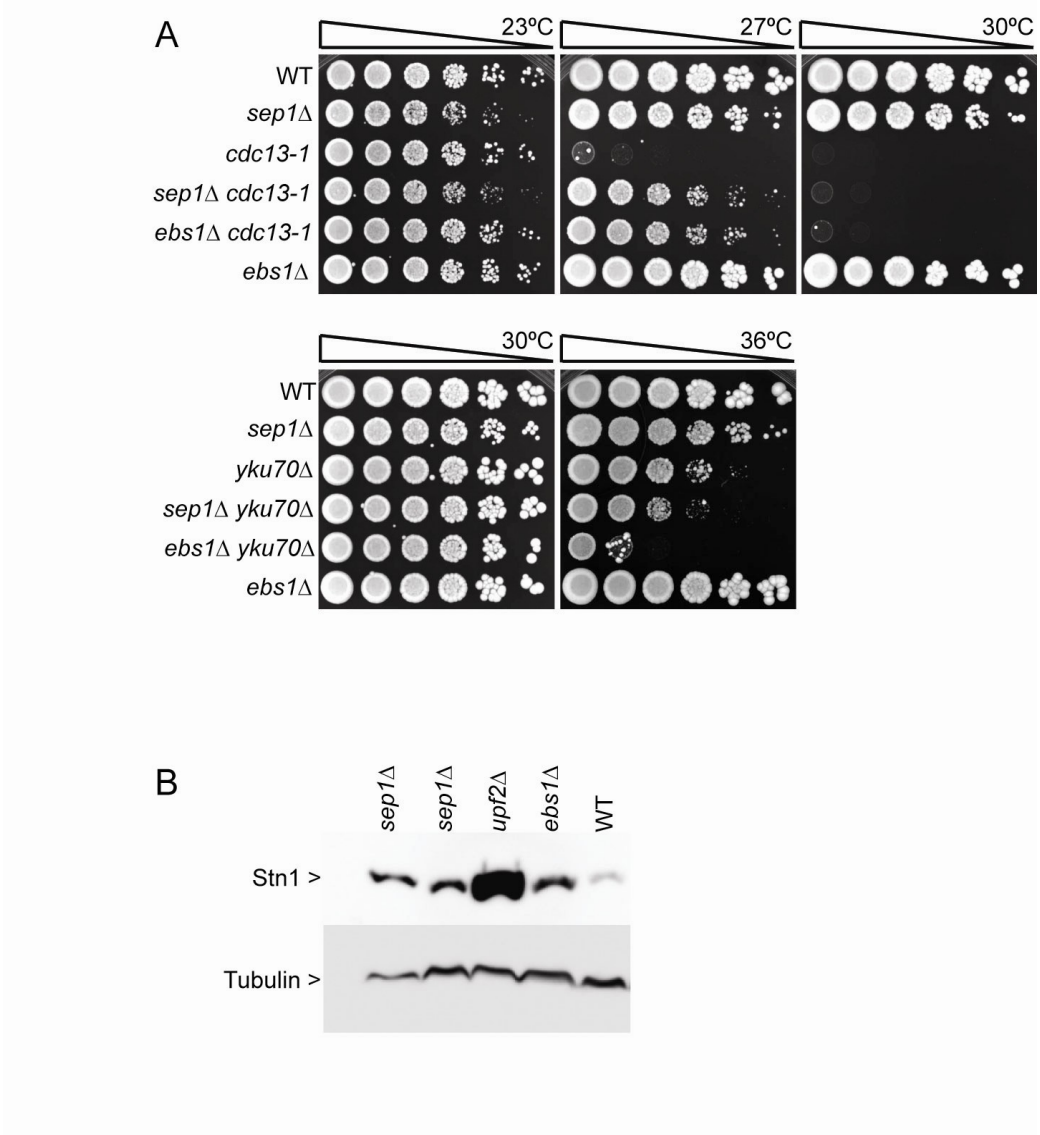

Figure 14. Sep1 inhibits growth of *cdc13-1* mutants, enhances growth of *yku70*Δ mutants and regulate Stn1 protein levels.

A. Saturated cultures of the genotypes indicated were serially diluted across YEPD plates and grown for 2 days at the temperature indicated.

B. Western blot analysis of Stn1 protein levels. Strains contain Stn1-13Myc and antibodies against Myc-tag were used. Antibodies against tubulin were used for loading control.

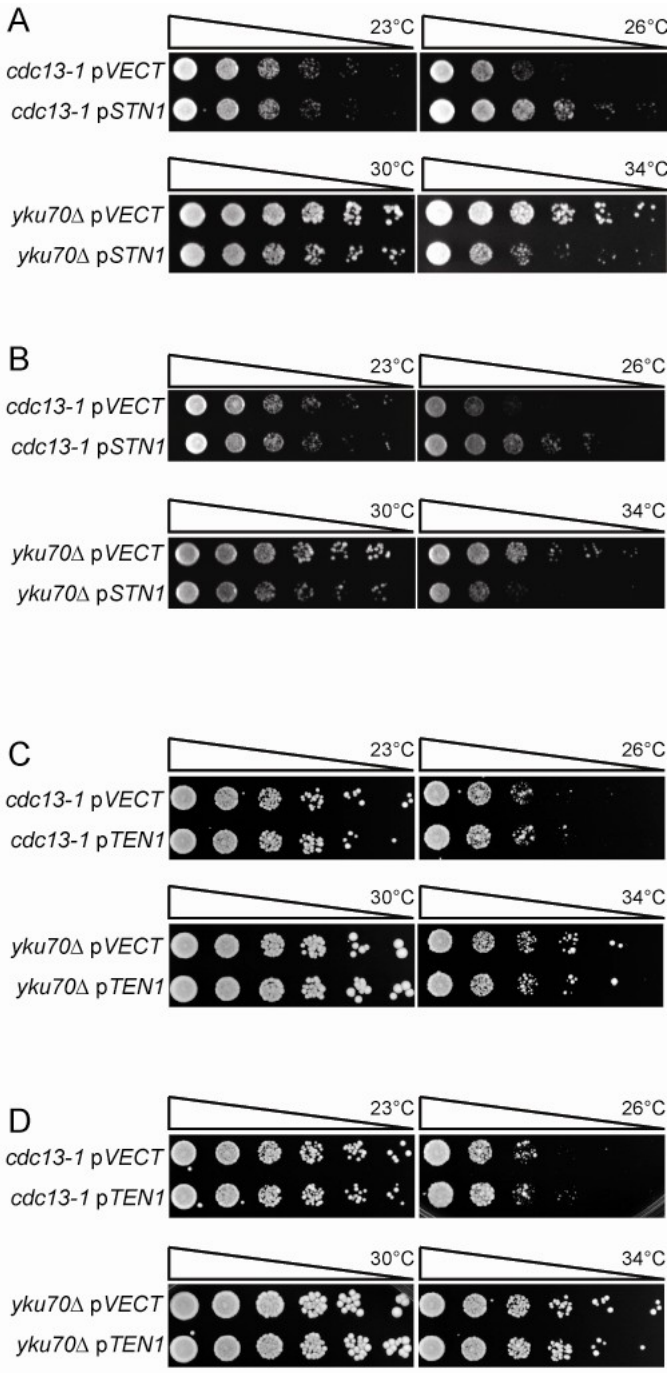

Figure 15. Over-expression of *STN1* enhances growth of *cdc13-1* mutants and suppresses growth of *yku70*Δ mutants.

Saturated cultures of the genotypes indicated were serially diluted across agar plates containing synthetic media and grown for 3 days at the temperature indicated. Plasmids used: **A.** the centromeric Stn1-expressing plasmid pVL1045 and the empty vector YCplac111, **B.** the 2µ Stn1-expressing plasmid pVL1066 and the empty vector YEplac181. **C.** The centromeric Ten1-expressing plasmid pCN284 and the empty vector YCplac22, **D.** the 2µ Ten1-expressing plasmid pPC4 and the empty vector YEplac195.

3.2.6 Alterations in Stn1 protein levels affect Cdc13- and Yku70-mediated telomere capping

Deletion of *UPF2, EBS1* or *SEP1* leads to an increase in the telomere capping protein Stn1 (Figure 10), raising the question if high levels of Stn1 could be responsible for suppression of the *cdc13-1* growth defect and enhancement of the *yku70*Δ growth defect seen in strains lacking NMD components (Figure 7A and B). Previous studies demonstrated that over-expression of Stn1 suppresses the *cdc13-1* growth defect (Enomoto et al., 2004; Grandin et al., 2000). However, the effect of increased levels of Stn1 on the *yku70*Δ growth defect has not been shown before. To test the effect of higher levels of Stn1 in *cdc13-1* and *yku70*Δ telomere capping mutants on their ability to grow, Stn1 was over-expressed in *cdc13-1* and *yku70*Δ mutants using single copy (centromeric) as well as high copy (2μ) Stn1-expressing plasmids. As shown in Figure 15A, strains containing either centromeric or 2μ Stn1-expressing plasmids suppressed the *cdc13-1* temperature-sensitivity at 26°C, which is consistent with previous studies (Enomoto et al., 2004; Grandin et al., 2000). Remarkably, over-expression of Stn1 in *yku70*Δ mutants had the opposite growth effect and resulted in enhancement of the *yku70*Δ defect (Figure 15B). Stn1 is part of the CST complex, consisting of Stn1, Ten1 and Cdc13. As *TEN1* transcript levels are increased in *upf2*Δ mutants (Figure 10), the growth effect of over-expressing Ten1 was also measured. Interestingly, over-expression of Ten1 did not lead to any growth changes in either *cdc13-1* or *yku70*Δ mutants (Figure 15C and D). In conclusion, data in Figure 15 indicate that components of the NMD pathway influence Cdc13- and Yku70- mediated telomere capping through regulation of *STN1* but not *TEN1* expression.

3.2.7 Modification of Stn1 levels alters composition of the CST complex

Results in section 3.2.6 demonstrated that over-expression of Stn1 suppressed the *cdc13-1* telomere capping defect, but enhanced the *yku70*Δ telomere capping defect, raising the question how increased levels of the telomere capping protein Stn1 has opposite effects on two forms of telomere uncapping. I hypothesized that elevated levels of Stn1 lead to increased binding of Stn1 to the telomere, thereby contributing to telomere capping in the absence of functional Cdc13, resulting in suppression of the *cdc13-1* capping defect. Stn1 is part of the CST complex and more Stn1 binding to telomeres might stabilize the complex.

In the case of *yku70*Δ capping defect, I hypothesized that the known reduction in telomerase recruitment in *yku70*Δ mutants may be even further reduced when combined with elevated levels of Stn1. Indeed, Stn1 has been shown to negatively regulate telomerase recruitment through Cdc13 (Li et al., 2009; Grandin et al., 2000). Telomerase not only elongates telomeres, but also plays a role in telomere capping in budding yeast, suggesting that potential reduced telomerase association with telomeres might contribute to the *yku70*Δ capping defect (Tong et al., 2011; Zhang et al., 2010; Hackett and Greider, 2003).

Both hypotheses were tested using Chromatin Immunoprecipiation (ChIP) analysis to compare association of the CST complex and telomerase to telomeres in wild-type and in *upf2*Δ strains.

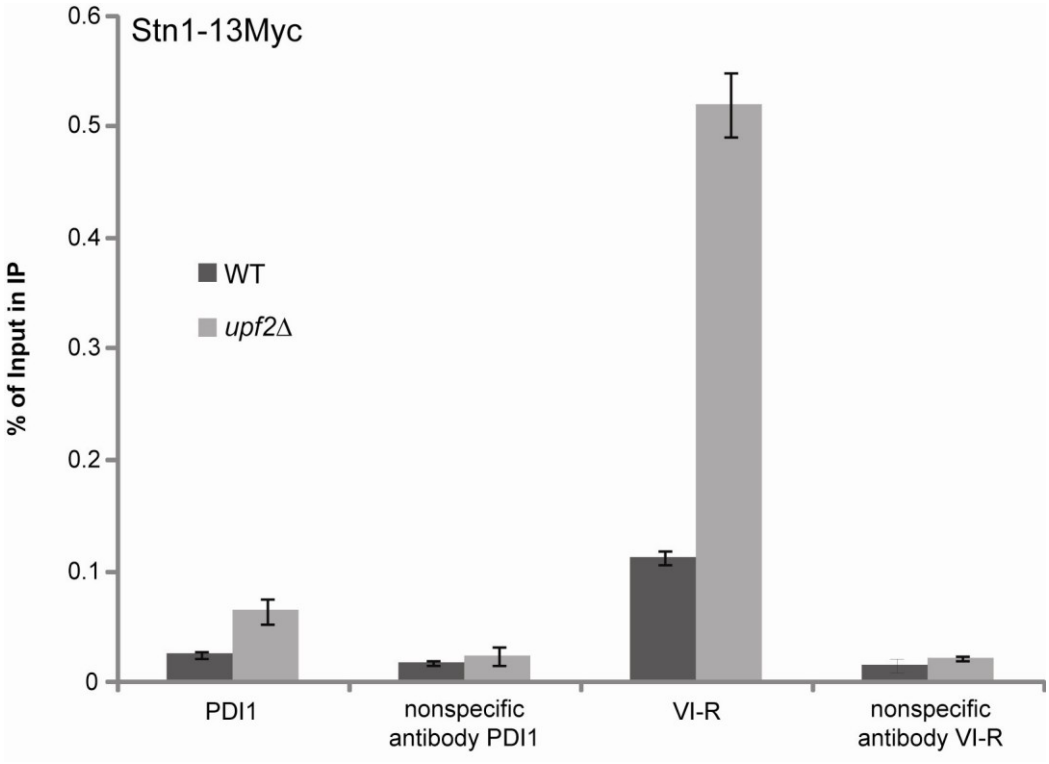

Figure 16. Upf2-dependent association of Stn1 with telomeres.

ChIP analysis of Stn1-13Myc association to the VI-R telomere and the internal locus PDI1 on Chromosome III. Primers used are described in Bianchi and Shore, 2007. Duplicate cultures of each genotype were grown at 23°C and cells were harvested in exponential phase. ChIP samples were measured in triplicate and group means are shown with error bars indicating standard deviation from three independent measurements. A 4.4-fold (WT) and an 8-fold (*upf2*Δ) enrichment was measured relative to the *PDI1* control.

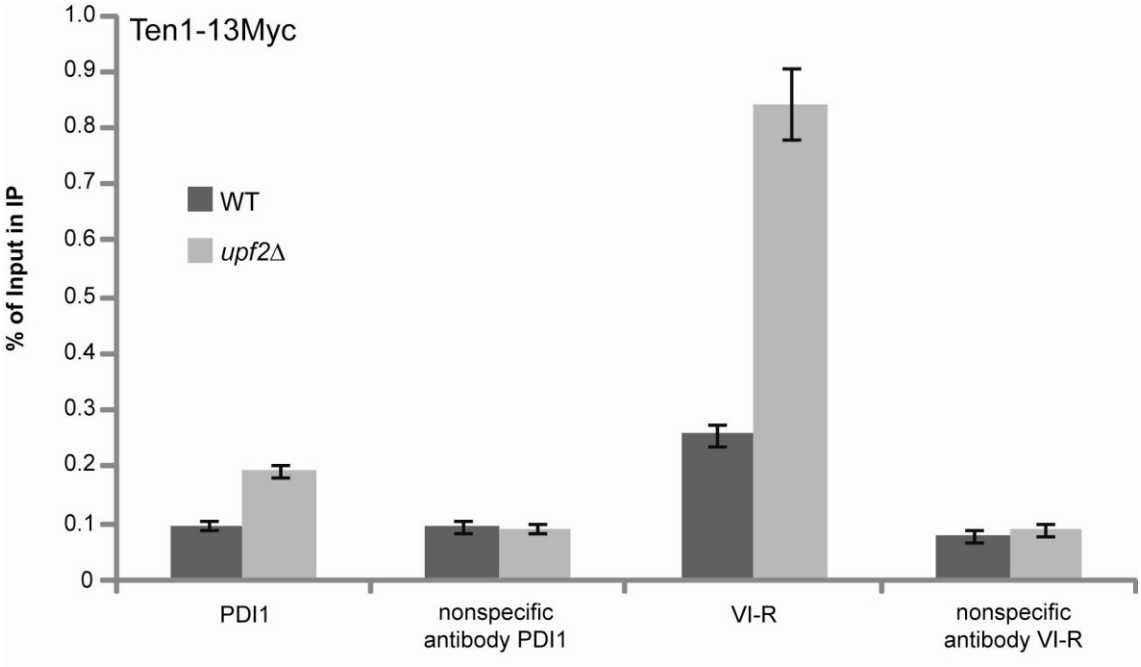

Figure 17. Upf2-dependent association of Ten1 with telomeres.

ChIP analysis of Ten1-13Myc association to the VI-R telomere and the internal locus PDI1 on Chromosome III. Primers used are described in Bianchi and Shore, 2007. Duplicate cultures of each genotype were grown at 23°C and cells were harvested in exponential phase. ChIP samples were measured in triplicate and group means are shown with error bars indicating standard deviation from three independent measurements. A 2.7-fold (WT) and a 4.3-fold (*upf2*Δ) enrichment was measured relative to the *PDI1* control.

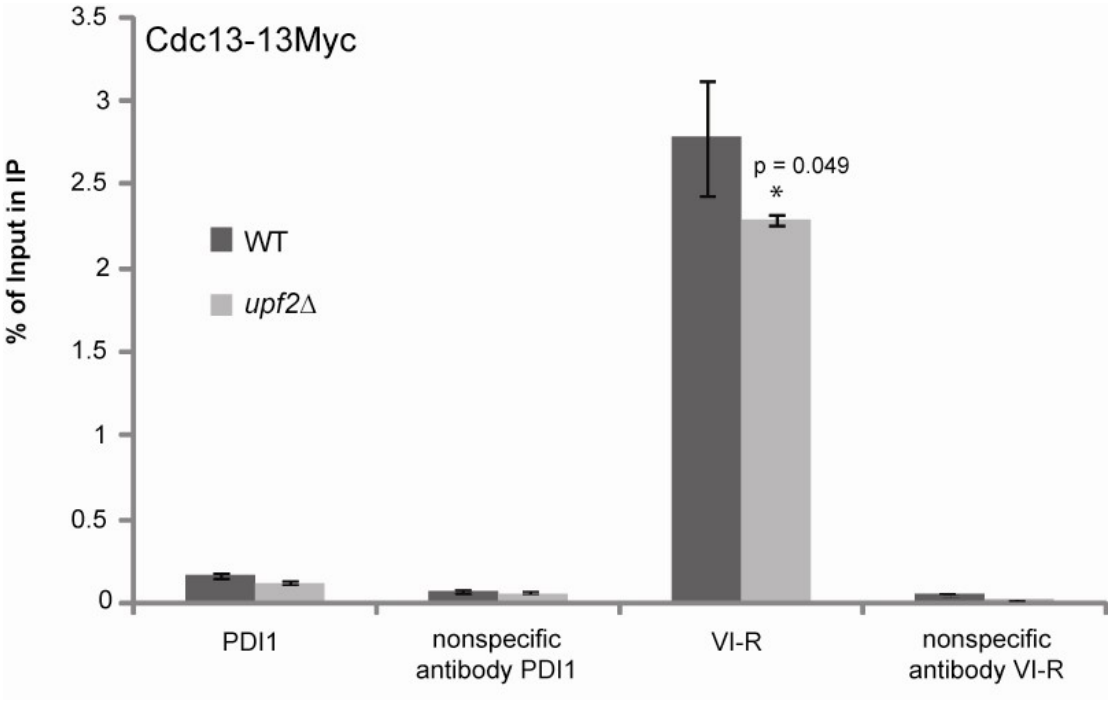

Figure 18. Upf2-dependent association of Cdc13 with telomeres.

ChIP analysis of Cdc13-13Myc association to the VI-R telomere and the internal locus PDI1 on Chromosome III. Primers used are described in Bianchi and Shore, 2007. Duplicate cultures of each genotype were grown at 23°C and cells were harvested in exponential phase. ChIP samples were measured in triplicate and group means are shown with error bars indicating standard deviation from three independent measurements. A 16.5-fold (WT) and a 21-fold (*upf2*Δ) enrichment was measured relative to the *PDI1* control. Unpaired t-test using a two-tailed distribution and assuming equal variance was used to determine p-values.

To test potential alterations in the CST complex composition, myc-tagged Stn1, Ten1 or Cdc13 binding to telomeres were monitored by qPCR measurement using monoclonal anti-myc antibody (9E10, Sigma). First, association of Stn1 to telomeres was measured at chromosome VI-R. As shown in Figure 16, a significant increase in Stn1 binding could be seen in *upf2*Δ strains compared to wild-type strains at chromosome VI-R. The chromosomal locus *PDI1* (50 kb from left telomere of chromosome III) was used as an internal control and showed little Stn1 binding in both wild-type and *upf2*Δ strains.

A similar result could be seen when looking at Ten1 association to chromosome VI-R (Figure 17). A significant increase in Ten1 association was detected in *upf2*Δ strains compared to wild-type strains. A 2-fold increase in Ten1 association was monitored at the internal *PDI1* locus in *upf2*Δ strains compared to wild-type strains, suggesting that, like Stn1, Ten1 can associate with the chromosome beyond the telomere region.

Ten1 and Stn1 are both part of the CST complex, suggesting that the increased association of both telomere capping proteins would result in an increased binding of the third factor, Cdc13. However, ChIP analysis of myc-tagged Cdc13 demonstrated a reduction of Cdc13 association at VI-R in *upf2*Δ strains compared to wild-type, whereas binding at *PDI1* was insignificantly low (Figure 18).

In conclusion, high expression of *STN1* and *TEN1*, due to inactivation of the NMD pathway, leads to increased levels of Stn1 and Ten1 and reduced levels of Cdc13 at the telomeres. Altered composition of telomere-binding factors at *upf2*Δ *cdc13-1* telomeres may support telomere capping in the absence of functional Cdc13, thus suppressing the *cdc13-1* growth defect.

However, the question still remains how increased levels of Stn1 suppress the *cdc13-1* telomere capping defect but enhance the *yku70*Δ telomere capping defect. The hypothesis that telomerase recruitment is even further reduced in *upf2*Δ *yku70*Δ mutants compared to *yku70*Δ and that loss of telomere capping through telomerase contributes to the *yku70*Δ defect was tested using ChIP analysis. Binding of Est2, the catalytic subunit

of telomerase, was determined in wild-type, *upf2*Δ*, yku70*Δ and *upf2*Δ *yku70*Δ double mutants. As shown in Figure 19, Est2 association with the telomere at chromosome VI-R was significantly reduced in *yku70*Δ mutants, which is consistent with data from previous studies (Fisher *et al.*, 2004). Interestingly, deletion of *UPF2* also resulted in reduced telomerase binding to telomeres, although the measured 4.3-fold increase in *EST2* transcript in *upf2*Δ strains would suggest increased levels of Est2 at telomeres (Figure 10). Although Est2 binding in *upf2*Δ *yku70*Δ double mutants was slightly further reduced compared to the single mutants, the reduction was not significant (Figure 19). In conclusion, the hypothesis of further reduced telomerase recruitment in *upf2*Δ *yku70*Δ double mutants compared to *yku70*Δ on its own could not be proven and does not seem to be responsible for the enhanced capping defect in the double mutant.

The reduced binding of the telomere capping protein Cdc13 to telomeres in *upf2*Δ strains raises the question if Cdc13 association with telomeres is reduced in *upf2*Δ strains in the presence of *yku70*Δ uncapped telomeres as reduction in Cdc13 binding to telomeres in *upf2*Δ *yku70*Δ mutants might be responsible for the enhanced growth defect in *upf2*Δ *yku70*Δ mutants compared to *yku70*Δ mutants (Figure 18). To test this hypothesis, Cdc13 binding at telomeres was determined in *upf2*Δ *yku70*Δ double mutants.

A striking increase in Cdc13 binding to the telomere on chromosome VI-R was detected in *yku70*Δ mutants compared to wild-type (Figure 20). The increase in Cdc13 binding in *yku70*Δ mutants is probably due to increased amounts of ssDNA at *yku70*Δ telomeres as a consequence of its telomere capping defect, allowing more Cdc13 to bind to the single-stranded telomere (Fisher et al., 2004). Cdc13 binding at telomeres in *upf2*Δ *yku70*Δ double mutants was significantly reduced compared to Cdc13 binding at telomeres in *yku70*Δ mutants, supporting the idea that Cdc13 might be displaced from telomeres in *upf2*Δ mutants.

Cells lacking Upf2 have higher levels of the telomere binding protein Stn1 (Figure 11), suggesting that the increase in Stn1 binding to telomeres may displace Cdc13. To test this hypothesis, single copy plasmids expressing *STN1* were transformed into wild-type

strains containing myc-tagged Cdc13 protein and Cdc13 association to the telomere at chromosome VI-R was determined. Indeed, ChIP analysis demonstrated a 32% reduction in association of Cdc13 to the telomere on chromosome VI-R compared to the control strain containing an empty vector (Figure 21). In conclusion, high levels of Stn1 at telomeres seem to be capable of displacing Cdc13 from the telomere.

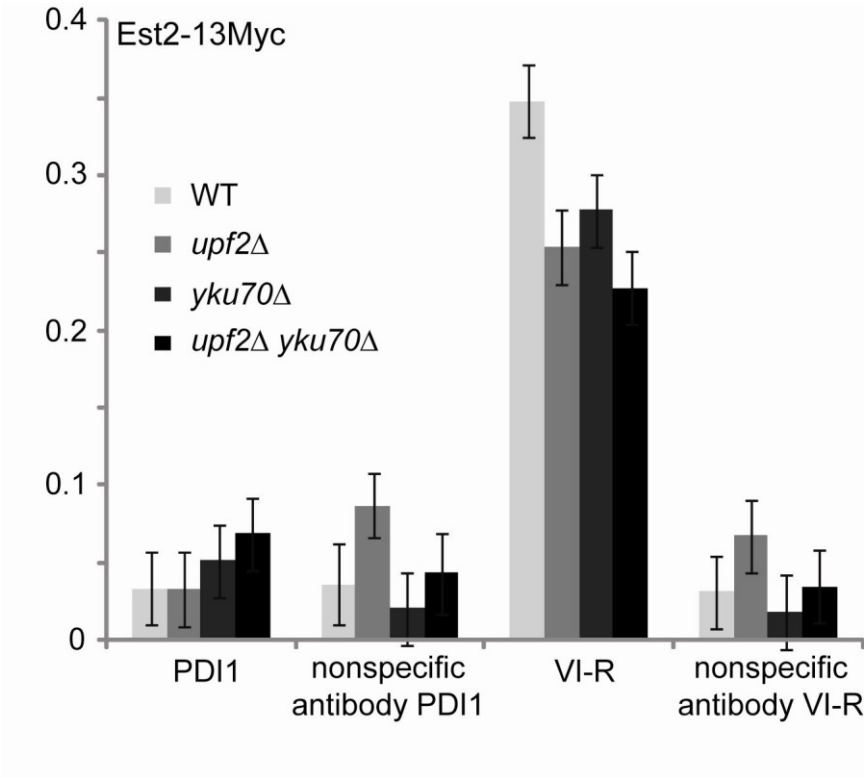

Figure 19. Upf2- and Yku70-dependent association of Est2 with telomeres.

ChIP analysis of Est2-13Myc association to the VI-R telomere and the internal locus PDI1 on Chromosome III. Primers used are described in Bianchi and Shore, 2007. Duplicate cultures of each genotype were grown at 23°C and cells were harvested in exponential phase. ChIP samples were measured in triplicate and group means are shown with 95% confidence bars derived from a two-way ANOVA. A 10.5-fold (WT), a 7.7-fold (*upf2*Δ), a 5.4-fold (*yku70*Δ) and a 3.3-fold (*upf2*Δ *yku70*Δ) enrichment was measured relative to the *PDI1* control.

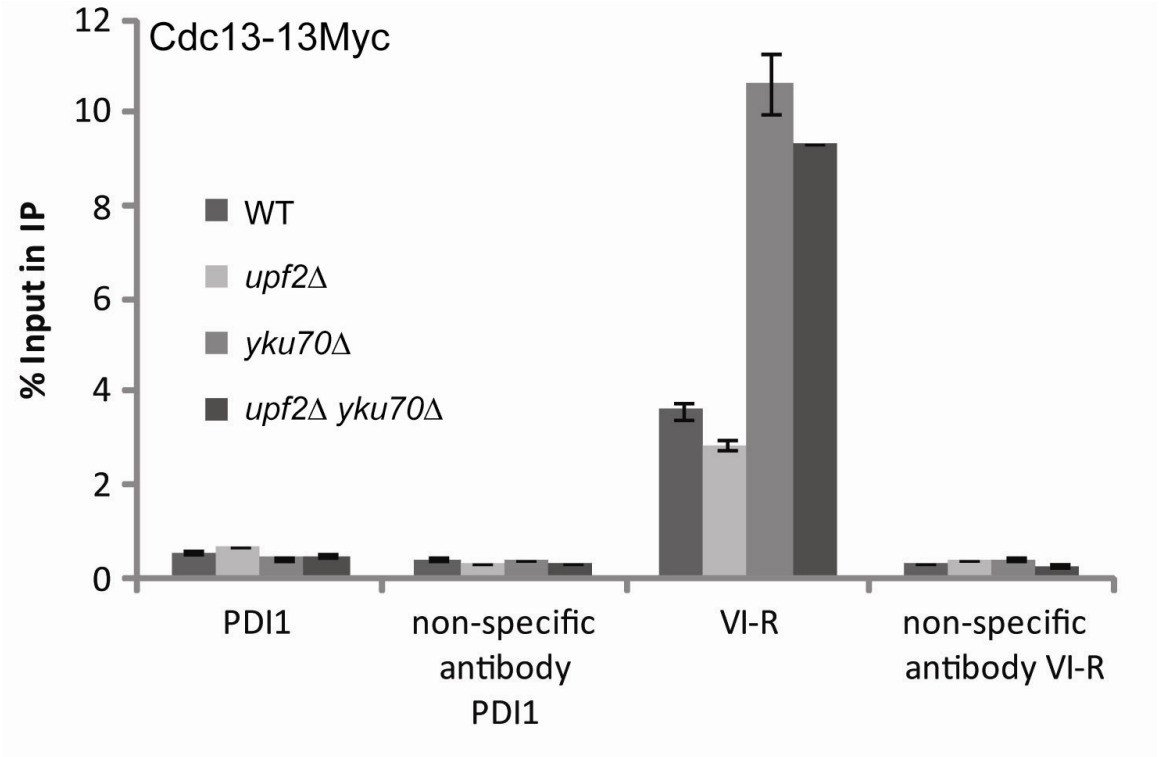

Figure 20. Upf2- and Yku70-dependent association of Cdc13 with telomeres.

ChIP analysis of Cdc13-13Myc association to the VI-R telomere and the internal locus PDI1 on Chromosome III. Primers used are described in Bianchi and Shore, 2007. Duplicate cultures of each genotype were grown at 37°C and cells were harvested in exponential phase. ChIP samples were measured in triplicate and group means are shown with error bars indicating standard deviation from three independent measurements. A 6.8-fold (WT), a 4.3-fold (*upf2*Δ), a 26.4-fold (*yku70*Δ) and a 19.8-fold (*upf2*Δ *yku70*Δ) enrichment was measured relative to the *PDI1* control.

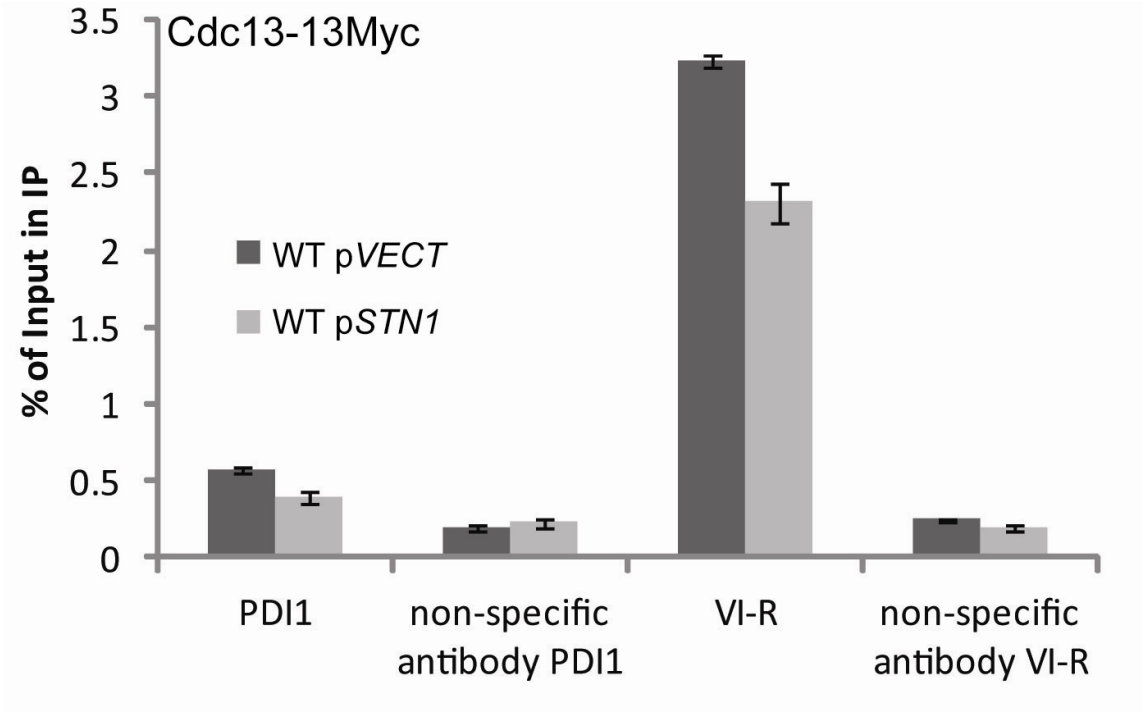

Figure 21. Stn1-dependent association of Cdc13 with telomeres.

ChIP analysis of Cdc13-13Myc association to the VI-R telomere and the internal locus PDI1 on Chromosome III. Primers used are described in Bianchi and Shore, 2007. Strains used contain the centromeric Stn1-expressing plasmid pVL1045 and the empty vector YCplac111 was used as control. Two strains of each genotype were grown at 23°C in synthetic media and cells were harvested in exponential phase. ChIP samples were measured in triplicate and group means are shown with error bars indicating standard deviation from three independent measurements. A 5.7-fold (WT) and a 5.8-fold (*upf2*Δ) enrichment was measured relative to the *PDI1* control.

3.2.8 Do increased Stn1 levels explain other genetic interactions in cdc13-1 and yku70Δ mutants?

Data in section 3.2.3 demonstrated that Stn1 transcripts and Stn1 protein levels are increased in strains lacking a core component of the NMD pathway (Figure 10 and 11). In addition, high amounts of Stn1 suppress the *cdc13-1* capping defect, but enhance the *yku70*Δ capping defect (Figure 15), indicating that the NMD pathway affects Yku70- and Cdc13-mediated telomere capping through alteration of Stn1 levels. Quantitative fitness analysis of the SGA screen in the Addinall et al., 2011 study revealed various gene deletions that, similar to deletion of NMD components, suppress the *cdc13-1* capping defect, but enhance the *yku70*Δ capping defect (Figure 6), raising the question if increased Stn1 levels in these strains can explain the observed phenotypes in these gene deletion mutants.

To test this hypothesis, Stn1 levels were measured in various gene deletion mutants that suppressed the *cdc13-1* growth defect, but enhanced the *yku70*Δ growth defect in the Addinall et al., 2011 publication. As shown in (Figure 6), deletion of *BMH1* or *SAN1*, similarly to deletion of NMD genes, suppressed the *cdc13-1* capping defect and enhanced the *yku70*Δ capping defect. *BMH1* encodes for a 14-3-3 protein and is involved in regulation of many processes in the cell, whereas *SAN1* encodes for an ubiquitin-protein ligase and is involved in proteolysis of proteins in the proteasome. To test whether modification of Stn1 levels are responsible for the growth phenotypes seen in *bmh1*Δ and *san1*Δ mutants, *bmh1*Δ and *san1*Δ were crossed with a strain containing myc-tagged Stn1 and Stn1 levels in both mutants were assessed by Western blot analysis using anti-myc antibodies. As shown in Figure 22A, Stn1 levels in *bmh1*Δ and *san1*Δ mutants were modest compared to *upf2*Δ and *ebs1*Δ strains and no increase in Stn1 was detectable in either *bmh1*Δ and *san1*Δ strains compared to wild-type. Two gene deletion mutants with a different growth phenotype in the QFA screen compared to *upf2*Δ mutants were used as controls and showed no increase in Stn1 levels (*chk1*Δ suppresses both *cdc13-1* and *yku70*Δ growth defect. *rif1*Δ enhances both *cdc13-1* and *yku70*Δ growth defect (Addinall *et al.*, 2011). In conclusion, Stn1 protein levels do not seem to be modified in all mutants with similar growth phenotypes as *upf1*Δ, *upf2*Δ and *upf3*Δ strains in response to *cdc13-1*- and *yku70*Δ-mediated telomere uncapping.

In addition, gene deletion mutants with similar growth phenotypes to *upf2*Δ gene deletion strains in the Addinall et al., 2011 SGA screen were ranked by euclidian distance and genetic interaction score space to produce a list of the nearest neighbours of *upf2*Δ strains according to growth (work by Conor Lawless). The four closest neighbours of *upf2*Δ were chosen and transcript levels of *STN1* were analysed for all four gene deletion strains by RT-PCR. As shown in Figure 22B, deletion of none of the four genes (*ede1*Δ*, mck1*Δ*, sac7*Δ, *vps9*Δ) resulted in any increase in *STN1* mRNA compared to wild-type, indicating that the growth phenotype seen in these gene deletion mutants cannot be explained by modifications in Stn1 levels and must be caused by something other than increased levels of the telomere capping protein Stn1.

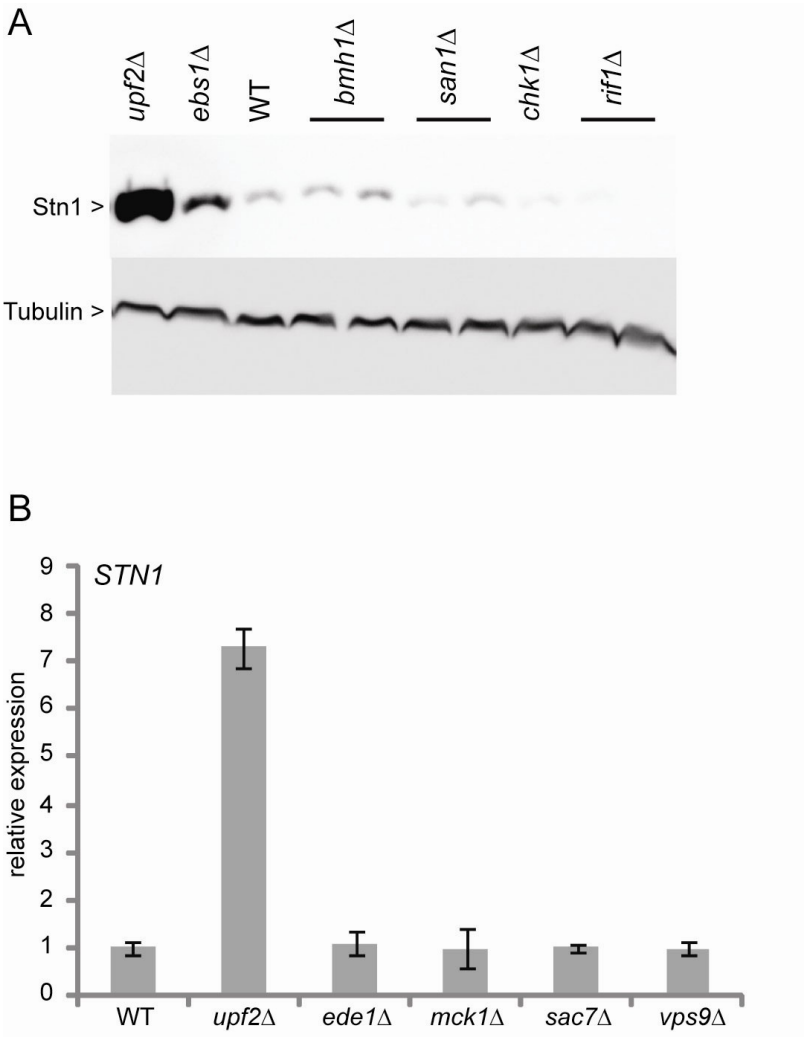

Figure 22. Stn1 transcript and protein levels in mutants suppressing the *cdc13-1* temperature-sensitivity and enhancing the *yku70*Δ temperature-sensitivity.

A. Western blot analysis of Stn1 protein levels. Strains contain Stn1-13Myc and antibodies against Myc-tag were used. Antibodies against tubulin were used for loading control.

B. RT-PCR analysis of *STN1* transcript levels. Two strains of each genotype were grown exponentially in YEPD medium at 23°C. RNA was isolated and transcript levels were measured using SYBR Green RT-PCR. Measurements were performed in triplicate and error bars indicate standard deviation from two independent measurements. RNA concentration of each sample was normalized to the loading control *BUD6* and a single wild type sample was given the value of 1 and all other values were corrected relative to this.

3.3 Discussion

3.3.1 The role of Ebs1 at cdc13-1 and yku70Δ uncapped telomeres

Deletion of any of the NMD genes (*NAM7, UPF2, UPF3, SEP1*) or deletion of *EBS1* suppresses the temperature-sensitive *cdc13-1* growth defect, but enhances the temperature-sensitive *yku70*Δ defect (Figure 7A and B). Data in Chapter 3 demonstrates that Ebs1, like NMD, regulates transcript levels of several genes encoding for telomere binding proteins (Stn1, Ten1), suggesting that Ebs1 is part of the NMD pathway (Figure 10). The hypothesis that Ebs1 is part of the NMD pathway is supported by the fact that deletion of *EBS1* in an *upf2*Δ mutant does not have additive effects regarding transcript levels of *STN1* (Figure 12); however, additive growth effects of *ebs1*Δ *upf2*Δ double mutants in the presence of either *cdc13-1* or *yku70*Δ uncapped telomeres compared to *upf2*Δ on its own (Figure 7) suggest that *EBS1* and *UPF2* act partially through different pathways. One possibility of different roles might be the homology between Ebs1 and Est1, the subunit of telomerase. Homology is most pronounced in a presumed RNA recognition motif, suggesting that Ebs1 might affect Cdc13- or Yku70-mediated telomere capping by binding to telomeres or to telomerase through the RRM. However, elimination of the RRM in Ebs1 had no effect on the ability of an *ebs1*Δ mutant to grow in the presence of either *cdc13-1* or *yku70*Δ uncapped telomeres (Figure 13) and further work will be required to identify if Ebs1 plays a role in telomere protection in addition to regulating Stn1 levels.

3.3.2 NMD and G-quadruplexes

Several studies demonstrated connections between G-quadruplex formation at telomeres and telomere protection. A recent study showed that the telomerase subunit Est1 is able to convert ssDNA telomeric overhangs into a G-quadruplex and that the role of telomerase in telomere protection is dependent on the ability to form G-quadruplexes (Tong *et al.*, 2011). Another study demonstrated that stabilization of G-guadruplexes suppresses the *cdc13-1* capping defect by inhibiting resection at telomeres (Smith et al., 2011). In addition, cells lacking components of NMD were resistant to the G-quadruplex-stabilizing compound TMPyP4, leading to the hypothesis that NMD might affect Cdc13- and Yku70-mediated telomere capping through interaction with G-quadruplex structures at telomeres (Zhang et al., 2010; Hershman et al., 2008).

However, no evidence for NMD influencing Cdc13- and Yku70-dependent telomere capping through interaction with G-quadruplexes at telomeres was found in chapter 3.

3.3.3 NMD, CST complex and Cdc13-dependent telomere protection

Work in chapter 3 demonstrates that NMD and Ebs1 modulate transcript levels of *STN1* and *TEN1* (Figure 10). Data in Figure 15 indicates that NMD and Ebs1 affect Cdc13- and Yku70-mediated telomere capping by modulating expression of *STN1* as increase in Stn1 levels suppressed the temperature-sensitive *cdc13-1* growth defect, but enhanced the temperature-sensitive *yku70*Δ defect, a phenotype seen in *upf2*Δ and *ebs1*Δ mutants. Suppression of the *cdc13-1* growth defect by Stn1 suggests that increased Stn1 (and presumably Ten1) association with telomeres provides efficient telomere protection in the absence of functional Cdc13. Consistent with increased levels of Stn1 suppressing the *cdc13-1* growth defect, it has been demonstrated that over-expression of Stn1 and Ten1 restores the viability of cells lacking Cdc13, indicating that increased levels of Stn1 and Ten1 seen in NMD mutants explain suppression of the *cdc13-1* growth defect (Petreaca *et al.*, 2006). In addition, a previous study has shown that fusion of Stn1 to the DNA binding domain of Cdc13 in cells lacking *CDC13* restores the telomere capping function of Cdc13, but results in telomere shortening (Pennock *et al.*, 2001). However, if Est1 is tethered to telomeres in addition to Stn1, telomere capping and telomere maintenance is fully restored, indicating that Cdc13 function at telomeres is to recruit telomere factors that enable efficient telomere protection and maintenance. In conclusion, increased association of Stn1 and perhaps Ten1 could be capable of efficiently capping telomeres in the absence of functional Cdc13. The fact that deletion of NMD factors results in telomere shortening indicates that despite efficient telomere protection, telomeres are not efficiently maintained in the absence of functional Cdc13 (Askree *et al.*, 2004).

ChIP analysis indicates that the stochiometry of the CST complex at telomeres is altered in NMD mutants (Figures 16-18). Data in Figures 16-18 demonstrates increased association of the telomere capping proteins Stn1 and Ten1, whereas binding of the third factor of the CST complex, Cdc13, was reduced. Reduced Cdc13 binding to telomeres was due to the increase in Stn1 (Figure 21), although it cannot be ruled out

that increase in Ten1 association to telomeres contributes to the reduction in Cdc13 binding. The fact that association of Cdc13 to telomeres was reduced, whilst association of Stn1 and Ten1 were increased, was a surprising result. So far, Cdc13 was thought to bind to telomeres as part of the CST complex, whereas ChIP data in this study implies that Stn1 and Ten1 can bind to the telomere independently of Cdc13. In addition, over-expression of *STN1* also resulted in reduced association of Cdc13 to telomeres (Figure 21), indicating that Stn1 is capable of displacing Cdc13 from telomeres. Previous studies have shown that Stn1 interacts with Ten1 through its N-terminus and is capable of binding telomeric ssDNA (Puglisi et al., 2008; Gao et al., 2007), supporting the idea that Stn1 and Ten1 binding to telomeres may be possible beyond the CST complex.

3.3.4 NMD, CST and Yku70-dependent telomere protection

In the case of the *yku70*Δ capping defect, telomerase recruitment to telomeres was reduced in *yku70*Δ mutants (Figure 19), which is consistent with several publications that demonstrated that Ku recruits telomerase to telomeres in G1 and promotes telomerase activity in late S phase (Fisher et al., 2004; Diede and Gottschling, 1999). A previous study has shown that no Est2 can be detected in G1 in the absence of Ku, and only approximately 50% of Est2 wild type levels are associated with telomeres in late S phase, probably due to Cdc13 (Fisher *et al.*, 2004). Cells lacking *UPF2* have increased levels of the telomere capping protein Stn1 and as Stn1 negatively regulates telomerase recruitment to telomeres (probably due to competing with Est1 for a single recruitment site in Cdc13), I hypothesised that telomerase recruitment is even further reduced in *upf2*Δ *yku70*Δ double mutants (Chandra *et al.*, 2001). Telomerase has been shown to contribute to telomere capping in budding yeast, suggesting that reduction in telomerase association with telomere might contribute to the *yku70*Δ capping defect, hence explaining the enhanced growth defect of *upf2*Δ *yku70*Δ double mutants compared to *yku70*Δ single mutants (Figure 7). In addition, Cdc13 is an important factor for telomerase recruitment. Defects in interaction between Cdc13 and Est1 results in failure of telomerase recruitment (Pennock *et al.*, 2001). Data in Figure 21 demonstrated that Cdc13 association with telomeres is reduced in the presence of increased levels of Stn1, hence supporting the hypothesis that telomerase recruitment might be further reduced in *upf2*Δ *yku70*Δ double mutants compared to *yku70*Δ mutants. Figure 19 showed that Est2 association with telomeres in *upf2*Δ *yku70*Δ double mutants might be reduced compared

to *yku70*Δ single mutants; however, the reduction was not significant. Thus, the question remains how increased levels of Stn1 enhance the *yku70*Δ telomere capping defect. One possibility is that the reduced Cdc13 association with telomeres in cells over-expressing *STN1* contributes to the *yku70*Δ capping defect. This hypothesis is supported by the fact that *yku70*Δ and *yku80*Δ mutants are synthetically sick in combination with *cdc13-1* (Polotnianka *et al.*, 1998). Further experiments will be necessary to better understand the interplay between Stn1, Cdc13 and Ku in telomere protection.

3.3.5 Stn1 and Cdc13- and Yku70-dependent telomere capping

Work in section 3.2.3 and 3.2.6 showed that deletion of NMD components suppresses the temperature-sensitive *cdc13-1* growth defect, but enhances the temperature-sensitive *yku70*Δ defect by modulating expression of *STN1*, suggesting that other gene deletion mutants with similar growth phenotypes as NMD mutants affect Cdc13- and Yku70-mediated telomere capping through regulation of Stn1. However, this is not true for the gene deletion mutants tested during this study. None of the mutants regulated expression of *STN1*, suggesting that the growth phenotypes seen in response to *cdc13-1*- and yku70Δ-mediated telomere uncapping must be caused by something other than increased levels of the telomere capping protein Stn1 (Figure 22). Further experiments will be necessary to understand how these genes affect telomere capping.

3.4 Future Work

Further work will be required to better understand the interplay between nonsense-mediated decay and the CST complex in protecting telomeres. Figure 19 showed that Est2 association with telomeres in *upf2*Δ *yku70*Δ double mutants was reduced compared to *yku70*Δ single mutants, however the observed reduction was not significant. To confirm that loss of telomere capping through absence of telomerase was not responsible for the poor growth of *upf2*Δ *yku70*Δ double mutants, Est2 could be over-expressed in *upf2*Δ *yku70*Δ double mutants using centromeric or 2µ plasmids. Potential better growth would indicate that reduced telomerase association to telomeres at least contributed to the poor growth of *upf2*Δ *yku70*Δ double mutants.

To address the question if the reduced Cdc13 association with telomeres in *upf2*Δ mutants or cells over-expressing *STN1* contributes to the *yku70*Δ capping defect (Figure 21), Cdc13 could be over-expressed in *upf2*Δ *yku70*Δ double mutants to test if the over-expression suppresses the growth defect caused by deletion of *UPF2*.

Western blot and ChIP analysis were performed using C-terminally myc-tagged Stn1. It has been shown that mRNAs containing long 3'UTRs are potential targets of the NMD pathway. Tagging Stn1 on the C-terminus alters the structure of 3' UTR, however, Stn1 still seemed to be a target of NMD as less Stn1 protein levels were detected in wild-type strains compared to *upf2*Δ mutants. This suggests that there must be another way of how some mRNAs become a target of NMD.

Work in Chapter 3 indicate that Stn1 and Ten1 are able to bind to telomeres without Cdc13 and that Stn1 is capable of displacing Cdc13 from the telomere (Figures 16-18 and 21). It would be of interest to test if the ability of Stn1 to bind to telomeres in the absence of Cdc13 and to alter the stochiometry of the CST complex is conserved in other eukaryotes.

4 Upf2 contributes to single-stranded DNA generation at uncapped telomeres

4.1 Introduction

Components of the NMD pathway influence Cdc13- or Yku70-mediated telomere capping as shown in Chapter 3. Telomere structure is masked by various 'capping' proteins in order to prevent telomeres from being recognized and treated as double-strand breaks. Interestingly, although capped telomeres restrain DNA repair, recombination and checkpoint pathways, proteins with roles in these pathways are found at telomeres and have been shown to support telomere capping and telomere maintenance. For instance, Yku70/Yku80 have a role in NHEJ at double-strand breaks besides their function in telomere protection (Ramsden and Gellert, 1998; Pang et al., 1997; Wilson et al., 1997). A DNA damage checkpoint protein found at telomeres is the checkpoint kinase Tel1, which not only mediates cell cycle arrest in response to DNA damage, but has a role in telomere length regulation (Goudsouzian et al., 2006; Tseng et al., 2006; Ritchie and Petes, 2000; Lustig and Petes, 1986). Other DNA damage checkpoint proteins with roles in telomere maintenance include the checkpoint kinase Rad53 or the Rad17-Mec3-Ddc1 complex (Longhese *et al.*, 2000). All of these examples suggest that components of the NMD pathway not only influence Cdc13- or Yku70-mediated telomere capping as shown in Chapter 3, but that they could have a potential role in the DNA damage response. This is further supported by a study showing that over-expression of the telomere-binding protein Stn1 results in sensitivity to the DNA replication inhibitors HU and MMS and inhibits S phase checkpoint response in the presence of DNA replication stress (Gasparyan *et al.*, 2009). Regulation of Stn1 protein levels through NMD suggests that Upf2 and Ebs1 may influence S phase checkpoint in response to DNA replication stress (Chapter 3). In addition, depletion of the human NMD factor SMG1 leads to DNA damage, cell cycle arrest in early S phase an induction of an ATR-dependent DNA damage response (Brumbaugh *et al.*, 2004).

A study by Azzalin and Lingner in 2006 demonstrated that phosphorylation of the DNA damage marker γH2AX (H2AX in yeast) is increased in human cells lacking the NMD

component UPF1 (Azzalin and Lingner, 2006). Increase in H2AX phosphorylation could be an indicator of stalled DNA replication forks in S phase, suggesting that NMD in *Saccharomyces cerevisiae* might contribute to efficient DNA replication. An increase in phosphorylated γH2AX in mammalian cells lacking UPF1 could also be an indicator of ongoing resection, raising the possibility that NMD affects nuclease activity at uncapped telomeres. In *S. cerevisiae*, the 5'-3' exonuclease Exo1 has been shown to be solely responsible for single-stranded DNA generation at telomeres dysfunctional in Ku, whereas resection at *cdc13-1* uncapped telomeres is dependent on Exo1 and a Rad24-dependent nuclease and a potential third still unknown nuclease (Zubko et al., 2004; Maringele and Lydall, 2002).

The aim of this work was to define if NMD has a role in DNA damage response or checkpoint activation in response to uncapped telomeres.

4.2 Results

4.2.1 Upf2 and Ebs1 are required for efficient G1 to S phase progression in the presence of cdc13-1 uncapped telomeres

To test the role of Upf2 and Ebs1 in checkpoint control, maintenance of cell viability and ssDNA production, *cdc15-2* and *bar1*Δ mutations were introduced to *ebs1*Δ *cdc13-1* and *upf2*Δ *cdc13-1* strains. *BAR1* encodes for a protease that cleaves and inactivates the mating pheromone α factor. Hence, *bar1*Δ mutation allows cells to be synchronized by efficiently arresting strains in G1 phase of the cell cycle in the presence of low levels of α factor. *CDC15* encodes for a protein kinase required for mitotic exit. Cells containing the *cdc15-2* mutation cannot finish mitosis and arrest during late nuclear division, allowing to study processes occurring during a single cell cycle (Zubko *et al.*, 2006).

Cell cycle progression of *ebs1*Δ and *upf2*Δ strains in the presence or absence of *cdc13-1* uncapped telomeres was monitored over a single cell cycle. Cells were shifted from 23°C to 36°C after α factor release to induce telomere uncapping in *cdc13-1* mutants. As shown in Figure 23, wild-type, *ebs1*Δ and *upf2*Δ strains progressed through S phase and G2 phase at a similar rate and arrested in late nuclear division due to the *cdc15-2* mutation. In the wild-type, 98% of cells were arrested at late nuclear division 200 min after the release. Similarly, 97% of *ebs1*Δ cells and 95% of *upf2*Δ cells were arrested in G2/M phase 200 min after alpha factor release. *cdc13-1* capping defective mutants progressed through S phase at a similar rate as wild-type cells but did not reach late nuclear division due to activation of the G2/M checkpoint in response to uncapped telomeres (Zubko *et al.*, 2004). Instead, 94% of *cdc13-1* cells were arrested in medial nuclear division 120 min after alpha factor release. Deletion of *UPF2* or *EBS1* in *cdc13-1* mutants did not affect checkpoint arrest of *cdc13-1* mutants at medial nuclear division and 90% of *ebs1*Δ and 89% of *upf2*Δ *cdc13-1* were arrested at the 200 min time point. However, cell cycle progression from G1 to S phase was delayed by approximately 20 min compared to *cdc13-1*, *upf2*Δ or *ebs1*Δ single deletion mutants and only 76% of *ebs1*Δ *cdc13-1* and 43% of *upf2*Δ *cdc13-1* cells had reached medial nuclear division 120 min after α factor release compared to 94% of *cdc13-1* cells at the same time point. As cell cycle position was scored by a combination of number and position of nuclei and bud size, it is possible that the observed delay was due to slower bud growth rather than

a delay in cell cycle progression. To address this, DNA content of the *cdc13-1* mutants were determined using FACS analysis. As demonstrated in Figure 24, *cdc13-1* mutant progressed faster from G1 to S phase (40 min and 80 min time point) compared to *upf2*Δ *cdc13-1* or *ebs1*Δ *cdc13-1* cells. Cell cycle progression was still delayed at later time points for *upf2*Δ *cdc13-1* compared to *cdc13-1* cells, whereas no difference in cell cycle progression was detectable after the 80 min time point for *ebs1*Δ *cdc13-1* cells compared to *cdc13-1* cells. In conclusion, Upf2 and Ebs1 are required for efficient progression from G1 to S phase in the presence of *cdc13-1* uncapped telomeres. However, Upf2 and Ebs1 are not required for efficient G2/M arrest of *cdc13-1* cells.

As over-expression of *STN1* in *upf2*Δ *cdc13-1* mutants is responsible for suppression of the *cdc13-1* growth defect, it might be possible that increased levels of Stn1 cause the delay in cell cycle progression seen in *upf2*Δ *cdc13-1* and *ebs1*Δ *cdc13-1* mutants (Figure 23). The idea is supported by a previous study (Enomoto *et al.*, 2004). The study revealed that senescence is delayed in telomerase-deficient budding yeast cells lacking components of nonsense-mediated decay and the delay can be mimicked by increasing levels of Stn1 and Ten1 in telomerase-deficient cells. The delayed senescence could be due to slower cell cycle progression, hence cells entering senescence at a later time point compared to wild type strains.

To test whether increased levels of Stn1 are responsible for the observed delay in G1 to S phase progression, high copy (2μ) Stn1-expressing plasmids were transformed into *cdc13-1 cdc15-2 bar1*Δ strains and cell cycle progression was monitored over a single cell cycle. As shown in Figure 25, *cdc13-1* cells over-expressing *STN1* progressed through S phase at a similar rate as *cdc13-1* control strains containing an empty vector. No delay was observable and 99% of both *cdc13-1* p*VECT* and *cdc13-1* p*STN1* strains were arrested in medial nuclear division 200 min after alpha factor release, indicating that increased levels of Stn1 were not responsible for the observed cell cycle delay in *upf2*Δ *cdc13-1* mutants (Figure 23).

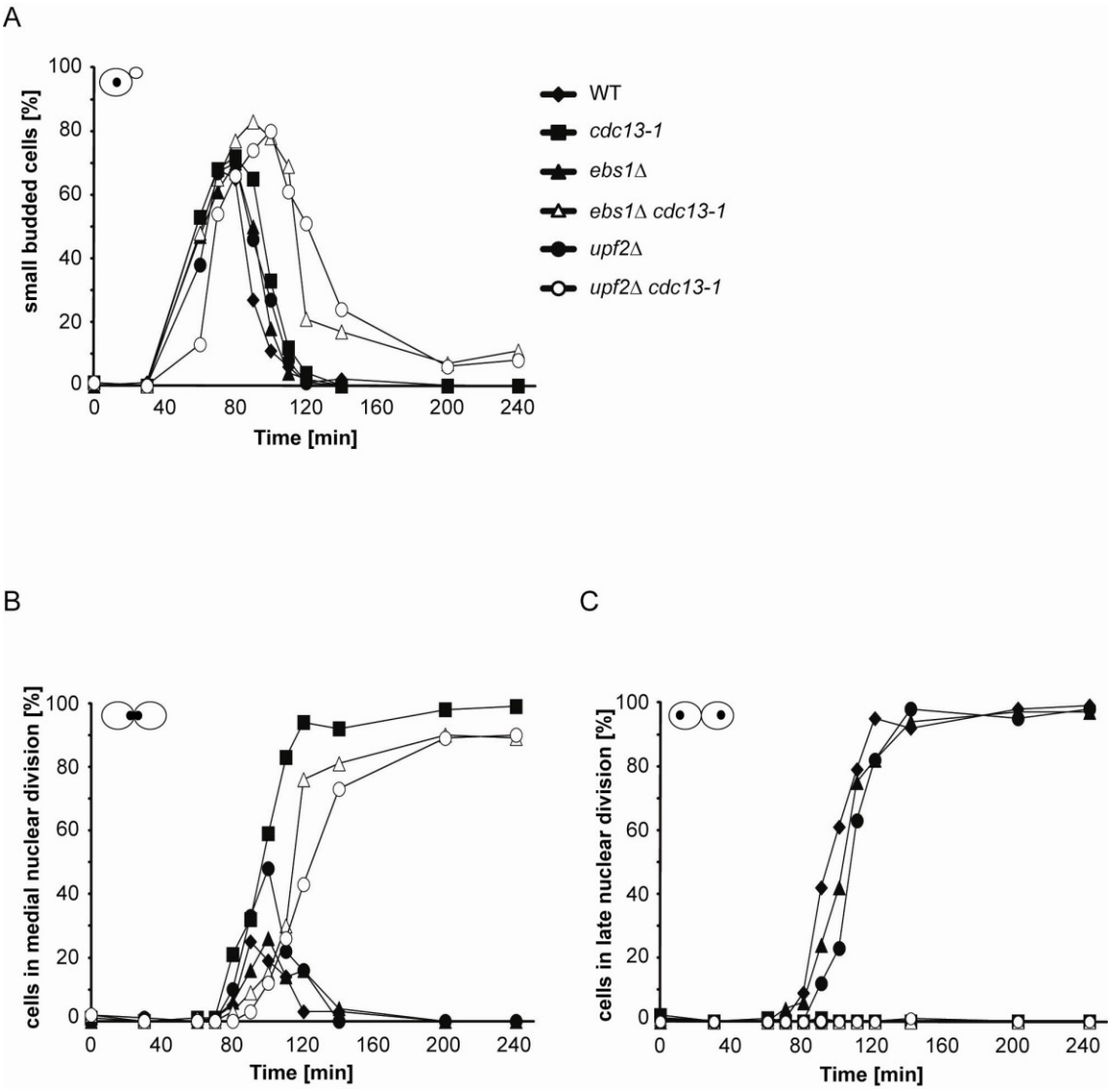

Figure 23. Ebs1 and Upf2 are required for efficient G1 to S phase progression but not for the cell cycle arrest in *cdc13-1* mutants.

A-C. Exponentially dividing cultures containing *bar1*Δ *cdc15-2* mutations were arrested at 23°C in G1 using α factor. Cells were released from arrest and shifted to 36°C to induce telomere uncapping. Samples were taken at indicated times and DAPI staining was used to determine cell cycle position of the cells. Cells that did not arrest in metaphase due to *cdc13-1* uncapped telomeres accumulated at anaphase due to the *cdc15-2* mutation that inhibits mitotic exit.

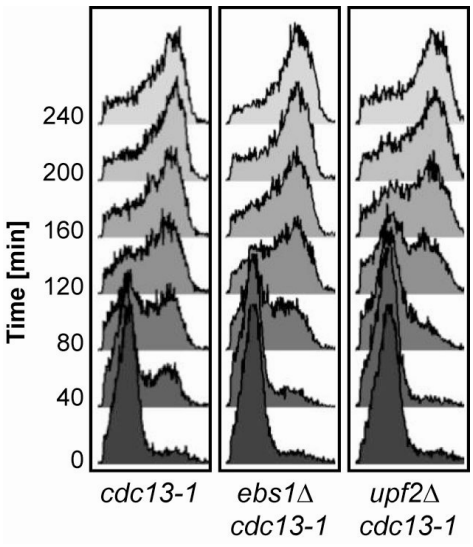

Figure 24 Cell cycle progression of *ebs1*Δ *cdc13-1* and *upf2*Δ *cdc13-1* mutants.

Strains with genotypes indicated were grown exponentially in YEPD at 23°C, arrested in G1 phase using α factor. Cultures were then released from α factor and shifted to 36°C. Samples were taken at time points indicated and cell cycle position was monitored by FACS analysis after nuclei staining with SYTOX green.

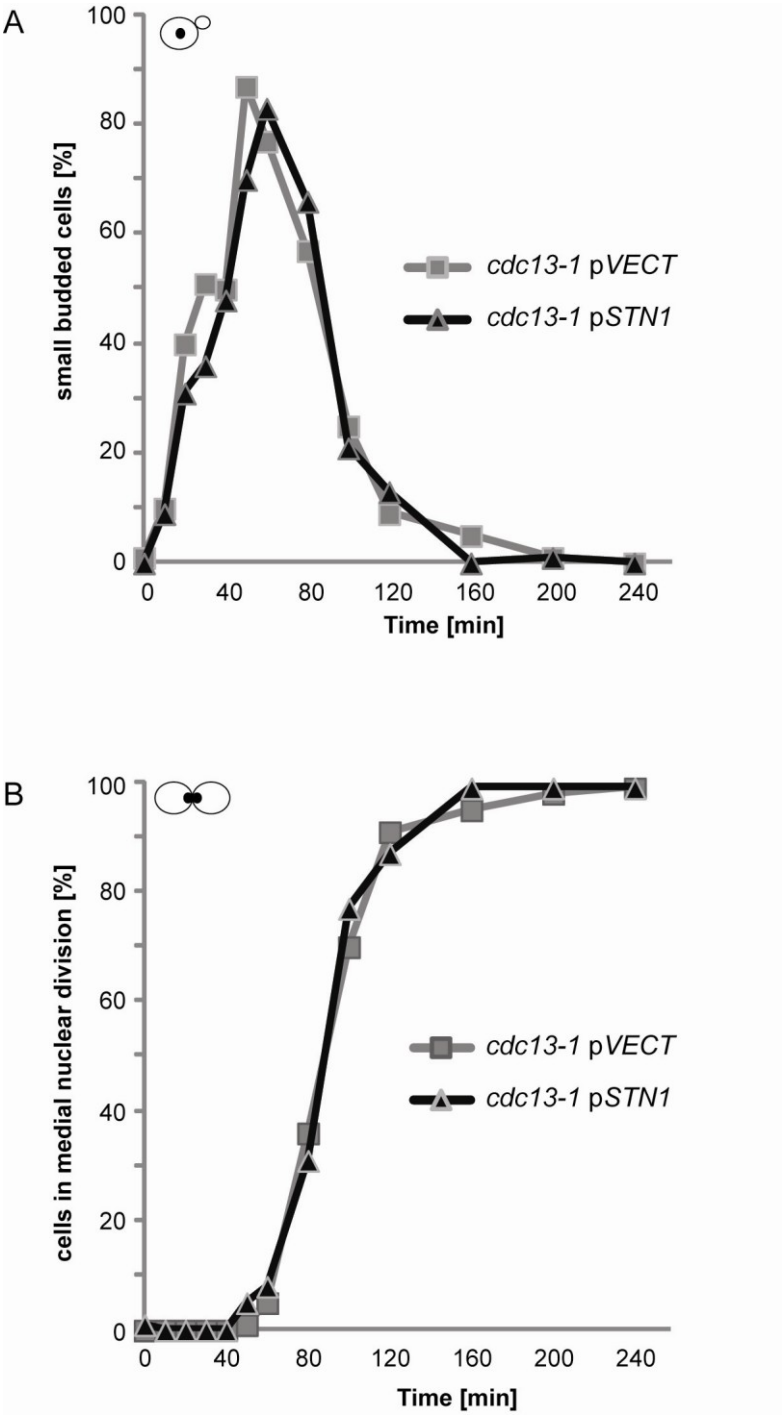

Figure 25. Over-expression of *STN1* does not affect cell cycle progression of *cdc13-1* mutants.

2μ STN1-expressing plasmids were transformed into *cdc13-1 bar1*Δ *cdc15-2* strains. Exponentially dividing cultures were arrested at 23°C in G1 using α factor. Cells were released from arrest and shifted to 36°C to induce telomere uncapping. Samples were taken at indicated times and DAPI staining was used to determine cell cycle position of the cells.

4.2.2 Elimination of EBS1, but not UPF2, induces a Rad9-dependent S phase checkpoint in the presence of cdc13-1-uncapped telomeres

Data in Figure 23 demonstrated that deletion of *EBS1* or *UPF2* caused a delay in cell cycle progression from G1 to S phase in the presence of *cdc13*-1 uncapped telomeres. The delay might be a result of G1/S phase checkpoint activation due to DNA damage or ssDNA accumulation in *ebs1*Δ *cdc13-1* and *upf2*Δ *cdc13-1* mutants. It has been shown that DNA damage during G1 phase leads to phosphorylation of histone H2AX and the checkpoint protein Rad9 is thought to interact with phosphorylated H2AX to induce a delay in G1 to S phase progression (Hammet et al., 2007; Javaheri et al., 2006; Gerald et al., 2002; Paulovich et al., 1997). In addition, TERRA has been shown to be displaced from mammalian telomeres by the NMD component UPF1 during S phase to support efficient progression of the DNA replication fork and a recent paper demonstrated that TERRA upregulation results in telomere shortening due to Exo1-dependent resection (Pfeiffer and Lingner, 2012; Azzalin et al., 2007). The aim was to test whether the observed cell cycle delay in *ebs1*Δ *cdc13-1* and *upf2*Δ *cdc13-1* mutants is a result of Rad9-dependent checkpoint activation in response to DNA damage

To test whether Rad9-dependent delay in G1 to S phase progression is responsible for the observed cell cycle delay, the S-phase and G2/M checkpoint protein Rad9 was deleted in *ebs1*Δ *cdc13-1* and *upf2*Δ *cdc13-1* mutants and cell cycle progression of synchronized cells (in G1 using α factor) was monitored over a single cell cycle at 36°C when *cdc13-1* telomeres are uncapped. As shown in Figure 26, *ebs1*Δ *cdc13-1* mutants exhibited an approximate 20 min delay in cell cycle progression from G1 to S phase compared to *cdc13-1* on its own and cells arrested in medial nuclear division, which is consistent with previous data in Figure 23. *rad9*Δ *cdc13-1* progressed through S phase in a similar pattern as *cdc13-1*, but did not arrest in medial nuclear division due to the abolished DNA damage checkpoint (Figure 26). Instead, cells continued cycling until late nuclear division. 120 min after alpha factor release, 94% of *rad9*Δ *cdc13-1* cells were arrested at late nuclear division due to the *cdc15-2*. Interestingly, deletion of *RAD9* in an *ebs1*Δ *cdc13-1* mutant allowed cells to continue cycling until late nuclear division and the G1 to S delay seen in *ebs1*Δ *cdc13-1* was completely abolished, indicating that checkpoint activation through Rad9 was responsible for the observed cell cycle delay in *ebs1*Δ *cdc13-1* cells. 85% of *ebs1*Δ *rad9*Δ *cdc13-1* cells were arrested in late nuclear

division at the 120 min time point and 99% of the cells were arrested 240 min after α factor release.

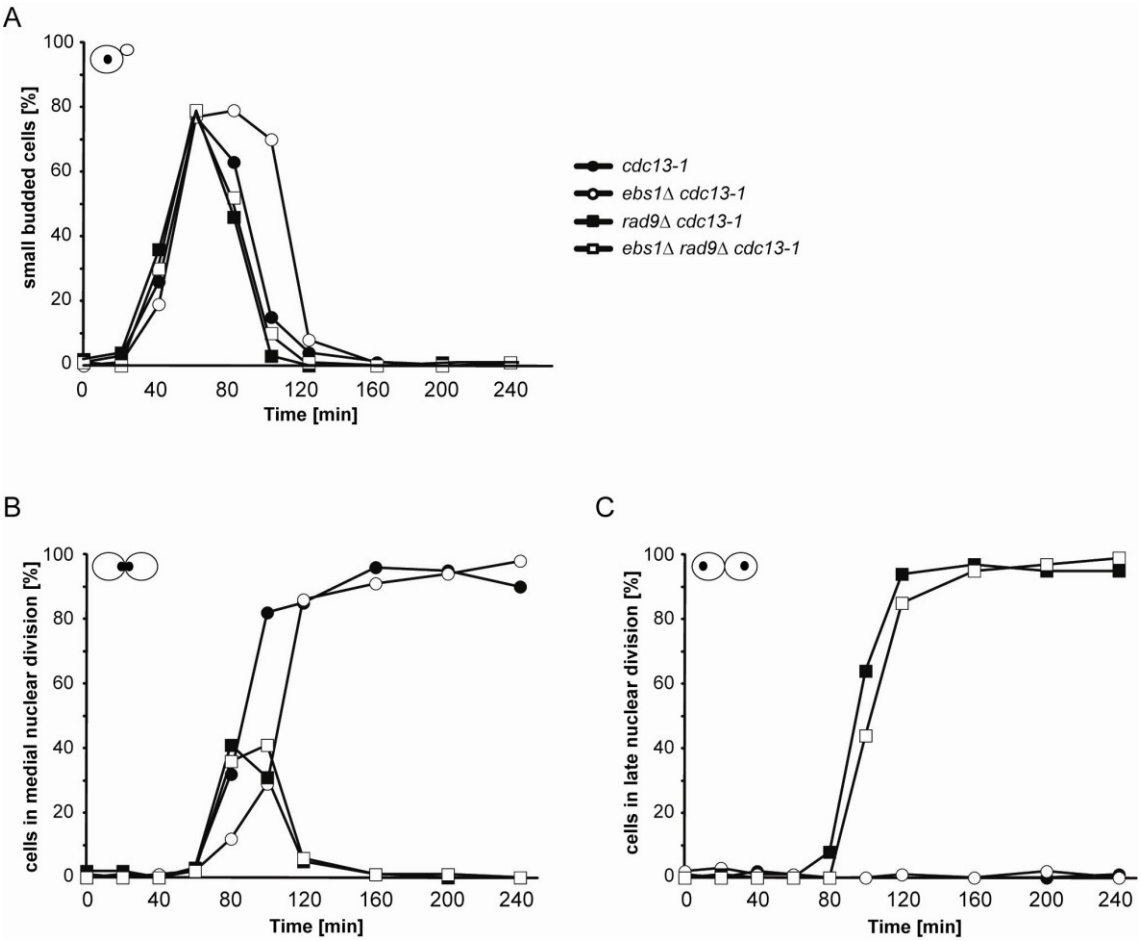

Figure 26. Ebs1 is required to prevent Rad9-dependent S phase checkpoint activation

Exponentially dividing cultures containing *bar1*Δ *cdc15-2* mutations were arrested at 23°C in G1 using α factor. Cells were released from arrest and shifted to 36°C to induce telomere uncapping. Samples were taken at indicated times and DAPI staining was used to determine cell cycle position of the cells.

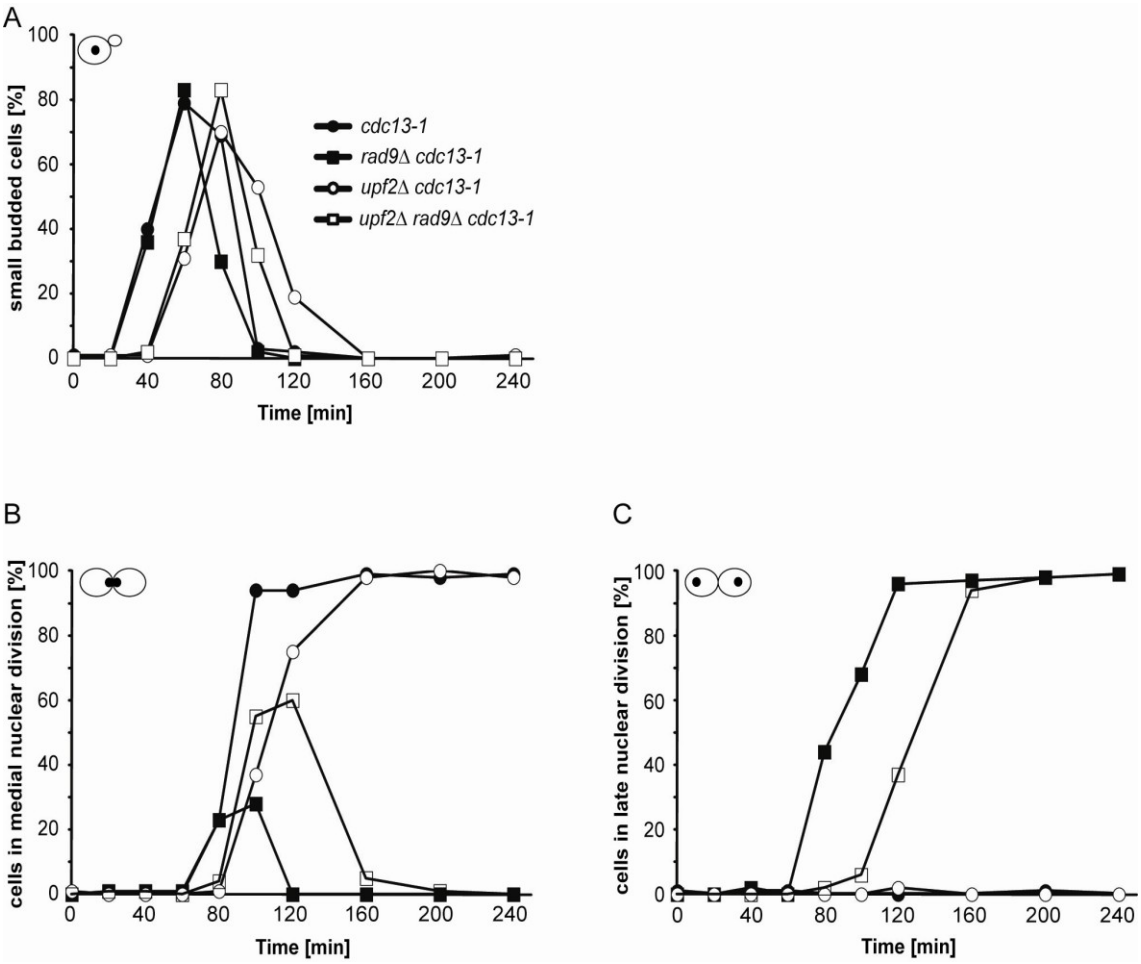

Figure 27. Rad9 is not responsible for the delay in G1 to S phase cell cycle progression in *upf2*Δ *cdc13-1* mutants.

Exponentially dividing cultures containing *bar1*Δ *cdc15-2* mutations were arrested at 23°C in G1 using α factor. Cells were released from arrest and shifted to 36°C to induce telomere uncapping. Samples were taken at indicated times and DAPI staining was used to determine cell cycle position of the cells.

When looking at *upf2*Δ *cdc13-1* cells, cell cycle progression from G1 to S phase was delayed by approximately 20 min compared to *cdc13-1* cells, which is consistent with previous data from Figure 23. However, unlike *ebs1*Δ *rad9*Δ *cdc13-1* cells in Figure 26, deletion of *RAD9* in *upf2*Δ *cdc13-1* did not abolish the G1 to S delay in cell cycle progression and delay was comparable to *upf2*Δ *cdc13-1* mutants containing a functional Rad9 checkpoint (Figure 27). 120 min after alpha factor release, 96% of *rad9*Δ *cdc13-1* cells were arrested at late nuclear division, whereas only 37% of *upf2*Δ *rad9*Δ *cdc13-1* cells were arrested at this time point. 240 min after alpha factor release, 99% of both *rad9*Δ *cdc13-1* and *upf2*Δ *rad9*Δ *cdc13-1* cells were arrested. The above results suggest that the delay in cell cycle progression from G1 to S phase of *ebs1*Δ *cdc13-1* mutants was caused by activation of a Rad9-dependent G1/S phase checkpoint, whereas the observed delay in *upf2*Δ *cdc13-1* mutants seemed to be independent of Rad9 and must have been caused by a different mechanism.

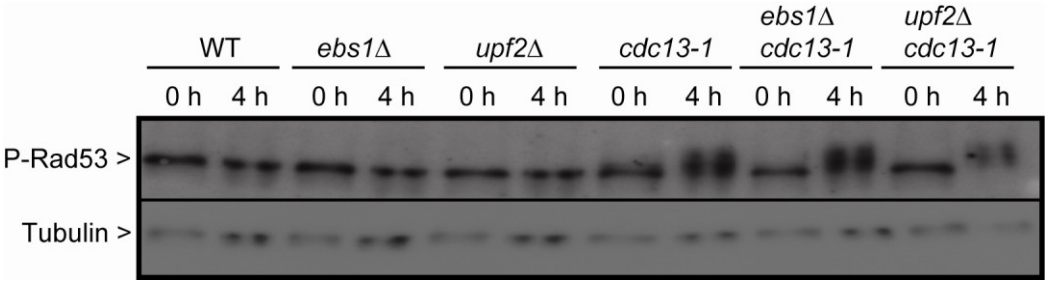

Figure 28. Deletion of *EBS1* or *UPF2* does not induce Rad53 phosphorylation

Exponentially dividing cultures of the indicated genotypes were grown at 23°C and then shifted to 36°C to induce telomere uncapping. Samples were taken before the temperature shift and after 4 hours at 36°C. Western blot was probed with antibodies against phosphorylated Rad53, membrane was stripped and reprobed with anti-tubulin antibody for loading control.

4.2.3 Cells lacking UPF2 or EBS1 do not induce a DNA damage response and do not exhibit sensitivity in response to DNA replication stress caused by HU and MMS

Data in section 4.2.2 suggest that the delay in cell cycle progression from G1 to S phase in *ebs1*Δ *cdc13-1* mutants was dependent on the checkpoint protein Rad9, whereas the delay in *upf2*Δ *cdc13-1* mutants was independent of Rad9. To test whether the observed delay is due to induction of a DNA damage response, phosphorylation of the well-known DNA damage marker Rad53 was measured in *ebs1*Δ *cdc13-1* and *upf2*Δ *cdc13-1* mutants (Allen *et al.*, 1994; Weinert *et al.*, 1994). As shown in Figure 28, neither *ebs1*Δ nor *upf2*Δ mutants induced phosphorylation of the protein kinase Rad53. Furthermore, no increase in phosphorylated Rad53 was detectable in *upf2*Δ *cdc13-1* or *ebs1*Δ *cdc13-1* mutants compared to Rad53 phosphorylation in *cdc13-1* strains in the presence of uncapped telomeres. In conclusion, neither *ebs1*Δ nor *upf2*Δ mutants seem to induce a DNA damage response and phosphorylation in the presence of *cdc13-1*-induced telomere uncapping was comparable to *cdc13-1* on its own.

A recent study revealed that over-expression of the telomere-binding protein Stn1 results in sensitivity to the DNA replication inhibitors HU and MMS and inhibits S phase checkpoint response in the presence of DNA replication stress (Gasparyan *et al.*, 2009). As shown in this study, Upf2- and Ebs1-deficient cells have increased levels of *STN1* transcripts and Stn1 protein (Figure 10), suggesting that Upf2 and Ebs1 may influence S phase checkpoint in response to DNA replication stress through Stn1. To test this hypothesis, viability of *upf2*Δ and *ebs1*Δ mutants was determined in the presence of Methyl methanesulfonate (MMS) and Hydroxyurea (HU). MMS is a DNA alkylating agent and methylation of N^3-deoxyadenine by MMS results in a cytotoxic lesion leading to reduced replication fork progression (Beranek, 1990). Replication of the damaged DNA results in collapse of the replication fork in checkpoint-deficient mutants, eventually causing cell death (Tercero and Diffley, 2001; Paulovich and Hartwell, 1995; Weinert et al., 1994). Hydroxurea is an inhibitor of the ribonucleotide reductase, an enzyme required for DNA synthesis. Treatment of cells with HU leads to activation of the replication checkpoint and stalled replication forks. Checkpoint-deficient cells continue dividing in the presence of HU and rapidly loose viability (Hartman and Tippery, 2004; Koc et al., 2004; Tanaka and Shimizu, 2000; Desany et al., 1998; Yarbro, 1992). Hence, potential sensitivity to the replication inhibitors MMS

and/or HU of Upf2- or Ebs1-deficient cells may indicate a role for Upf2 or Ebs1 in S phase checkpoint control in response to DNA replication damage. All mutants showed growth comparable to wild-type in the absence of HU (Figure 29A). *upf2*Δ and *ebs1*Δ showed no sensitivity in the presence of 100mM HU compared to wild-type, whereas known HU-sensitive mutants Rad24, Mec1 and Sgs1 were not able to grow (Mec1), showed poor growth (Sgs1) or showed reduced growth compared to wild-type (Rad24) (Figure 29A) (Fasullo and Sun, 2008; Woolstencroft et al., 2006; Hartman and Tippery, 2004). Rad9 is known to be sensitive to MMS, but not HU and growth of *rad9*Δ mutant was comparable to wild-type (Chang *et al.*, 2002; Hanway *et al.*, 2002). In conclusion, elimination of neither Upf2 nor Ebs1 caused significant noticeable sensitivity to HU.

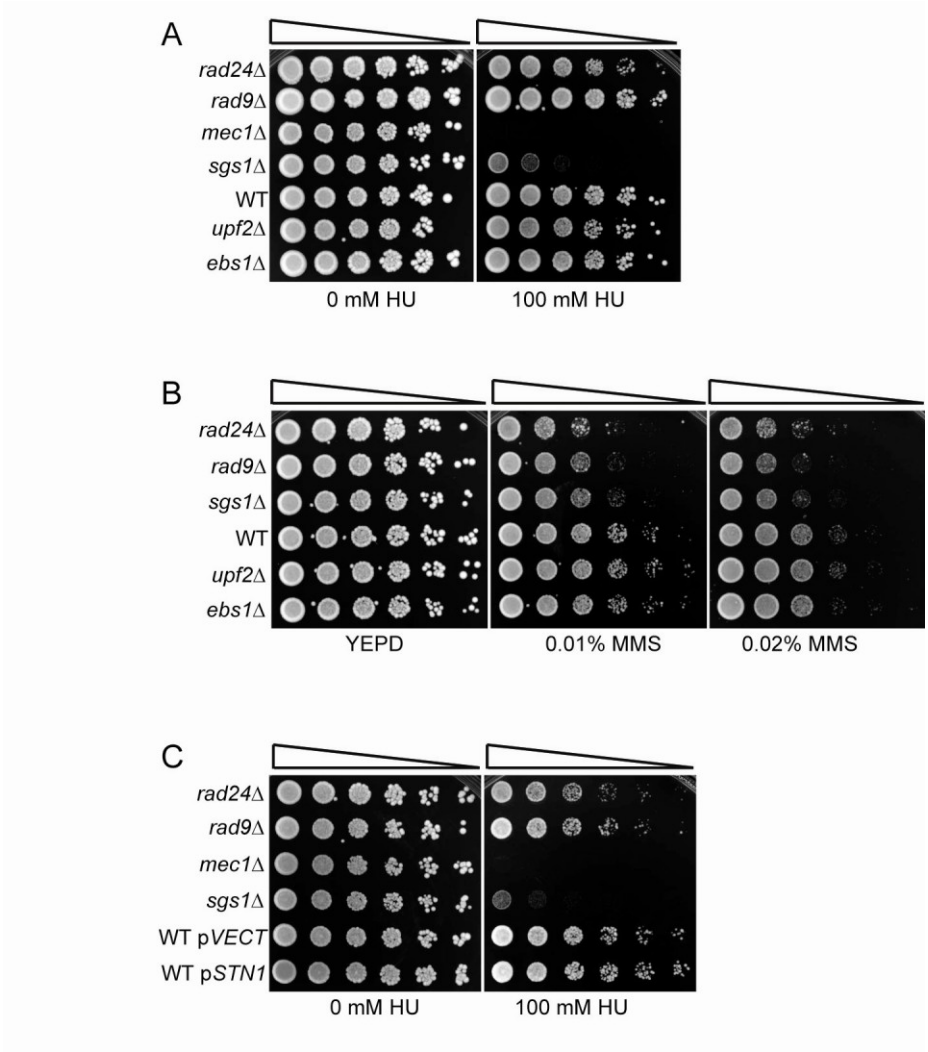

Figure 29. Cells over-expressing *STN1*, lacking *EBS1* or *UPF2* are not sensitive to HU or MMS.

A and **B**. Saturated cultures of the genotypes indicated were serially diluted across agar plates containing YEPD and HU or MMS. Colonies were allowed to form for 3 days at 23°C.

C. Saturated cultures of the genotypes indicated were serially diluted across agar plates containing synthetic media with HU. Colonies were allowed to form for 3 days at 23°C.

A similar result can be seen in presence of 0.01% and 0.02% MMS (Figure 29B). Neither *upf2*Δ, nor *ebs1*Δ showed any sensitivity to MMS compared to wild-type strain. Rad9-, Rad24- and Sgs1-deficient strains were used as positive controls and showed sensitivity in the presence of both 0.01% and 0.02% MMS, but grew comparable to wild-type in the absence of MMS (Murakami-Sekimata *et al.*, 2010). In conclusion, deletion of either *UPF2* or *EBS1* did not result in sensitivity in response to the replication inhibitors HU and MMS, suggesting that Ebs1 and Upf2 are not part of the S phase checkpoint response to DNA replication stress. Interestingly, over-expression of *STN1* using a high copy (2μ) Stn1-expressing plasmid (Figure 29C) did not result in any sensitivity to HU at a concentration that was considerably higher (100 mM) compared to the concentration used in the publication of Gasparyan et al. (2009) (25 mM HU).

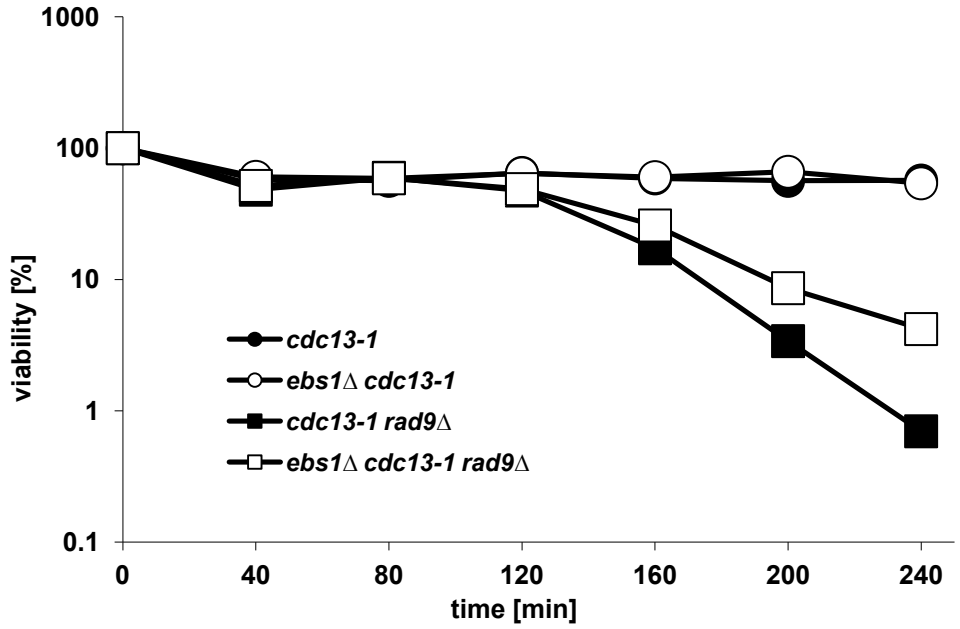

Figure 30. Deletion of *EBS1* increases viability in *cdc13-1* cells in the absence of a Rad9-dependent checkpoint.

Exponentially dividing cultures containing *bar1*Δ *cdc15-2* mutations were arrested at 23°C in G1 using α factor. Cells were released from arrest and shifted to 36°C to induce telomere uncapping. Samples were taken at indicated time points, diluted, plated onto YEPD in duplicate and grown at 23°C for 3 days. Colony forming units were counted and viability was calculated using the dilution factor.

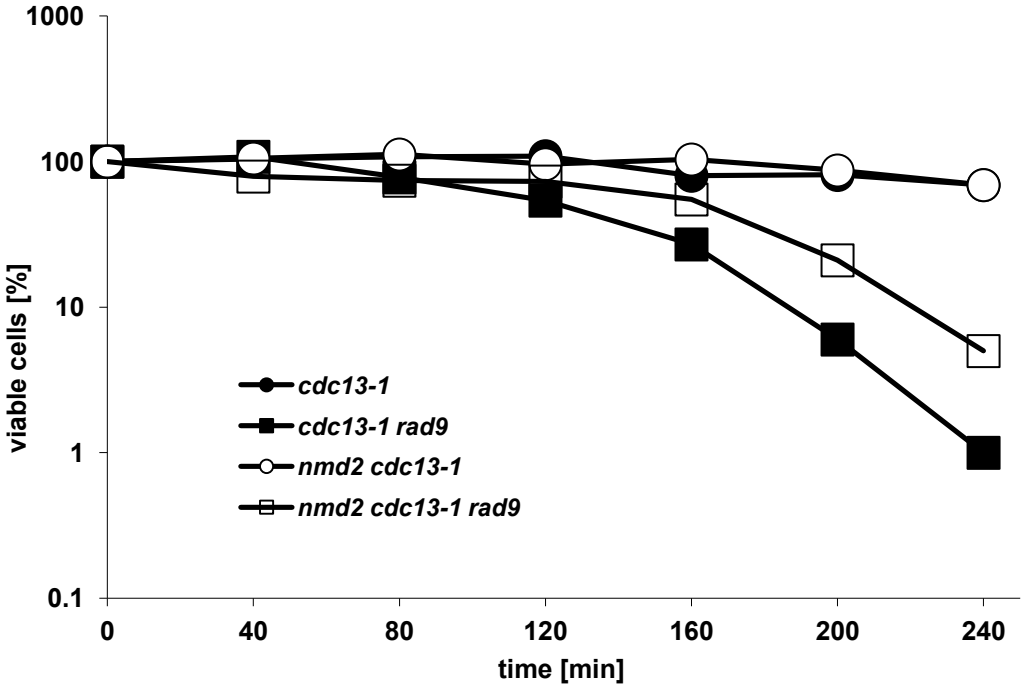

Figure 31. Deletion of *UPF2* increases viability in *cdc13-1* cells in the absence of a Rad9-dependent checkpoint.

Exponentially dividing cultures containing *bar1*Δ *cdc15-2* mutations were arrested at 23°C in G1 using α factor. Cells were released from arrest and shifted to 36°C to induce telomere uncapping. Samples were taken at indicated time points, diluted, plated onto YEPD in duplicate and grown at 23°C for 3 days. Colony forming units were counted and viability was calculated using the dilution factor.

4.2.4 Upf2 and Ebs1 maintain viability in the presence of cdc13-1 uncapped telomeres, but reduce viability in the absence of a Rad9-dependent checkpoint

One form of DNA damage response to telomere uncapping is checkpoint activation and another form is resection. Data in Figure 23 demonstrated that Ebs1 and Upf2 do not affect checkpoint activation in response to *cdc13-1* uncapped telomeres, but were required for efficient G1 to S phase progression. The following work looked into the possibility of Ebs1 and/or Upf2 playing a role in resection at *cdc13-1* uncapped telomeres.

To test this hypothesis, the ability of Upf2 and Ebs1 to maintain viability of *cdc13-1* mutants in the presence or absence of the checkpoint protein Rad9 was determined. Checkpoint activation in response to telomere uncapping allows *cdc13-1* mutants to maintain viability over a 4 hour time course. Deletion of the checkpoint gene *RAD9* however, abolishes checkpoint activation in *cdc13-1* strains in the presence of uncapped telomeres. *rad9*Δ *cdc13-1* mutants continue cycling through mitosis and accumulation of DNA damage eventually leads to cell death (Jia *et al.*, 2004; Zubko *et al.*, 2004). In the absence of the checkpoint, growth is only limited by the amount of resection occurring at the uncapped telomeres. Hence, viability of *upf2*Δ *rad9*Δ *cdc13-1* mutants or *ebs1*Δ *rad9*Δ *cdc13-1* compared to *rad9*Δ *cdc13-1* is a good indicator if Upf2 or Ebs1 contributes to resection at uncapped telomeres.

To directly measure the role of Upf2 and Ebs1 in maintaining viability in the presence of *cdc13-1* uncapped telomeres at 36°C, samples from the synchronous culture experiments (Figure 26 and 27) were taken and colonies were allowed to form on YEPD plates at the permissive temperature of 23°C. Cell viability was then measured by counting the viable colonies. Elimination of *EBS1* in *cdc13-1* strains containing uncapped telomeres did not decrease viability compared to *cdc13-1* on its own (Figure 30), whereas the *rad9*Δ *cdc13-1* mutant showed an approximate one hundred-fold loss in viability over the 4 hour time course. As mentioned before, deletion of the checkpoint gene *RAD9* abolishes checkpoint activation in *cdc13-1* strains in the presence of uncapped telomeres. *rad9*Δ *cdc13-1* mutants continue cycling through mitosis and accumulation of DNA damage then leads to loss in viability (Jia *et al.*, 2004). Deletion

of *EBS1* in *rad9*Δ *cdc13-1* mutants rescued viability to some extent (Figure 30). Similarly to Ebs1, deletion of *UPF2* did not decrease viability in *cdc13-1* strains over a 4 hour time course, but increased viability of *rad9*Δ *cdc13-1* strains to a certain degree (Figure 31). In conclusion, Ebs1 and Upf2 did not affect cell cycle arrest in G2/M (Figure 23) or viability (Figure 30 and 31) in response to *cdc13-1*-induced telomere uncapping, indicating that Ebs1 and Upf2 are not required to activate or maintain checkpoint arrest in response to telomere uncapping in *cdc13-1* strains. Viability of *rad9*Δ *cdc13-1* strains over one cell cycle was increased when *EBS1* or *UPF2* were deleted, suggesting that Ebs1 and Upf2 may contribute to single-stranded DNA generation at *cdc13-1* uncapped telomeres.

The results in Figures 30 and 31 indicate that Upf2 and Ebs1 may contribute to nuclease activity at *cdc13-1* uncapped telomeres. To further test this hypothesis, viability was examined using an up-down assay. Viability of *cdc13-1* strains can be tested by repeatedly growing cells at 36°C (4 hours at 36°C, then 4 hours at 23°C). Checkpoint-proficient *cdc13-1* strains undergo cell cycle arrest at 36°C and cells lose viability to some extent when repeatedly cultured at 36°C due to nuclease activities (such as Exo1) at the uncapped telomeres (Zubko *et al.*, 2004). However, checkpoint-deficient *rad9*Δ *cdc13-1* mutants continue cycling at 36°C and rapidly loose viability even after only one 4 hour cycle at 36°C. As mentioned above, in the absence of the checkpoint growth is only limited by the amount of resection occurring at the uncapped telomeres.

To test whether Upf2 may contribute to nuclease activity at *cdc13-1* uncapped telomeres, *upf2*Δ *cdc13-1* cells were repeatedly cultured at 36°C (three 4 hour cycles). As shown in Figure 32, *cdc13-1* mutants lost viability to a certain degree after three cycles at 36°C, while *upf2*Δ *cdc13-1* cells did not lose a great amount of viability in comparison to wild-type cells, suggesting that Upf2 may contribute to nuclease activity at uncapped telomeres. A similar result can be seen when looking at cells lacking Ebs1. Viability of *ebs1*Δ *cdc13-1* cells was considerably higher compared to *cdc13-1* cells.

Next, growth of *upf2*Δ *rad9*Δ *cdc13-1* mutants in comparison to *rad9*Δ *cdc13-1* mutants was studied. As shown in Figure 32, *rad9*Δ *cdc13-1* mutants showed little growth after

three 4 hour cycles at 36°C, due to extensive resection of telomeres, whereas *upf2*Δ *rad9*Δ *cdc13-1* mutants were able to grow to some extent, indicating that Upf2 most likely contributes to nuclease activity at uncapped telomeres (Zubko *et al.*, 2004). *ebs1*Δ *rad9*Δ *cdc13-1* mutants were not able to grow after three 4 hour cycles at 36°C. In conclusion, Upf2 seems to contribute to loss in viability in checkpoint-deficient *rad9*Δ mutants in the presence of *cdc13-1* uncapped telomeres, suggesting that Upf2 contributes to nuclease activity at *rad9*Δ *cdc13-1* uncapped telomeres. Viability of *ebs1*Δ *rad9*Δ *cdc13-1* mutants was increased compared to *rad9*Δ *cdc13-1* mutants when measured over a single cell cycle. However, no increase in viability was observed when measured over several cell cycles.

It was further tested whether the increase in viability in *upf2*Δ *rad9*Δ *cdc13-1* mutants compared to *rad9*Δ *cdc13-1* mutants was due to increased levels of Stn1. Figure 33 shows that the observed growth of *upf2*Δ *rad9*Δ *cdc13-1* mutants after three 4 hour cycles at 36°C seems to be independent of the increased Stn1 protein levels as *rad9*Δ *cdc13-1* mutants over-expressing *STN1* using a high copy (2μ) Stn1-expressing plasmid did not show any growth in the UP-DOWN assay. However, *rad9*Δ *cdc13-1* cells over-expressing *STN1* using high copy (2μ) Stn1-expressing plasmids did show stronger suppression of the *cdc13-1* temperature-sensitivity at 27°C compared to *rad9*Δ *cdc13-1* mutants. In conclusion, viability of *upf2*Δ *rad9*Δ *cdc13-1* mutants is independent of increased Stn1 protein levels as a result of eliminated NMD pathway.

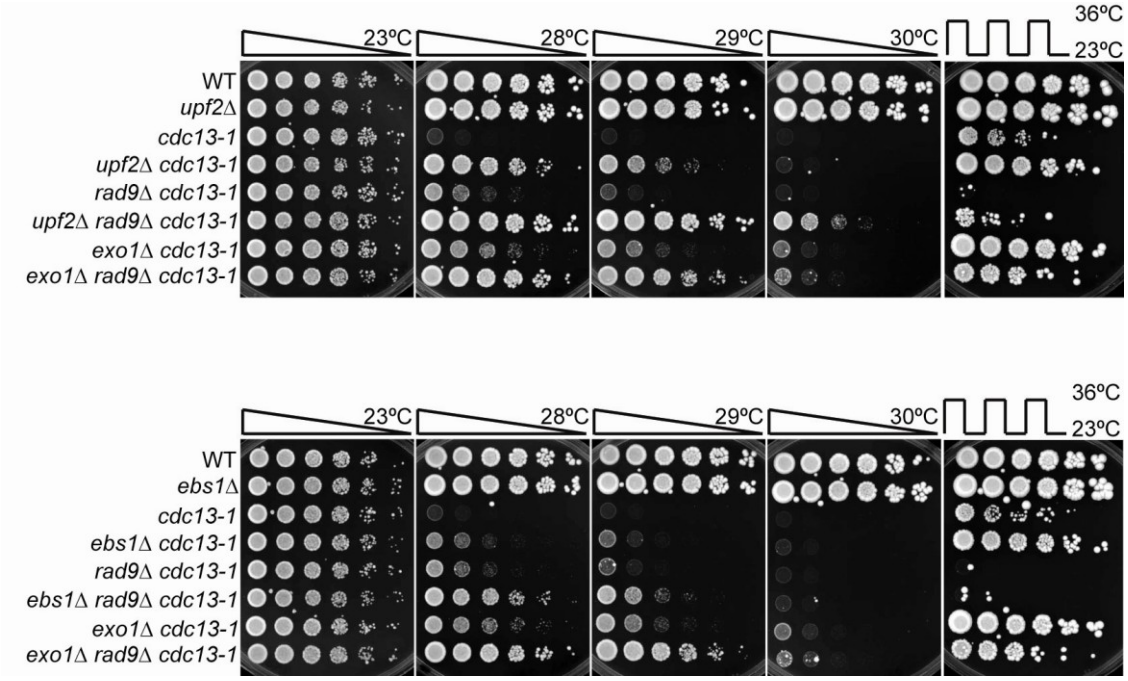

Figure 32. Upf2, but not Ebs1, decrease viability in *rad9*Δ *cdc13-1* mutants

Saturated cultures of the genotypes indicated were serially diluted across agar plates containing YEPD and were grown either at the temperature indicated for 2 days or cycled 3 times from 23°C for 4 hours to 36°C for 4 hours and then allowed to form colonies at 23°C for 3 days.

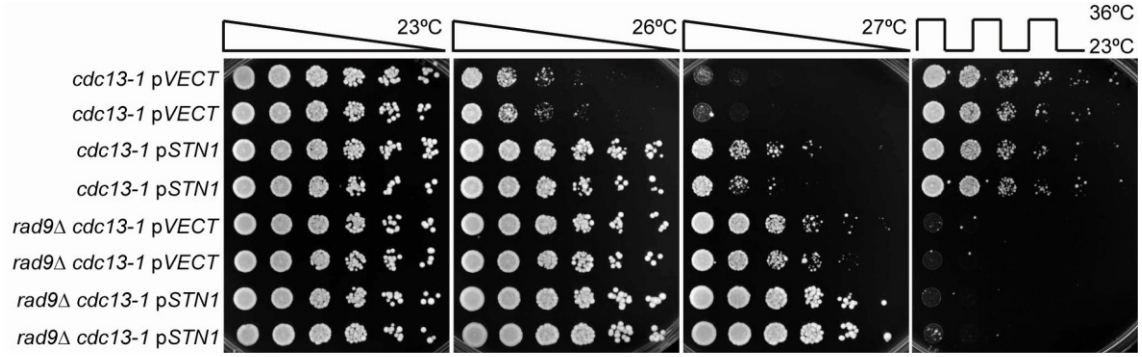

Figure 33. Over-expression of *STN1* does not rescue loss of viability in *rad9*Δ *cdc13-1* mutants

Saturated cultures of the genotypes indicated were serially diluted across agar plates containing synthetic medium and were grown either at the temperature indicated for 3 days or cycled 3 times from 23°C for 4 hours to 36°C for hours and then allowed to form colonies at 23°C for 3 days.

4.2.5 Upf2 contributes to ssDNA generation at cdc13-1 uncapped telomeres

Data from section 4.2.4 suggest that Upf2 may contribute to single-stranded DNA generation at *cdc13-1* uncapped telomeres. To test this hypothesis, the amount of telomeric ssDNA was measured using two methods. To start with, quantitative amplification of single-stranded DNA (QAOS) by RT-PCR was used to determine ssDNA at two loci (*DUG1* and *RET2*) at the right telomere of chromosome VI. *RET1* is located 19.8 kb from the chromosome end, whereas *DUG1* is 30 kb away from the telomere (Booth et al., 2001, Zubko et al., 2006) (Figure 34A). Small amounts of ssDNA could be detected at both the *DUG1* and the *RET2* loci at the TG-strand in *cdc13-1* mutants, with more ssDNA generated at the *RET2* locus (Figure 34B and C). Comparable amounts of ssDNA to *cdc13-1* mutants were detected when *UPF2* was deleted in *cdc13-1* mutants.

A substantial increase in ssDNA generation could be seen when *cdc13-1* mutants lack the checkpoint protein Rad9, which is consistent with previous data (Zubko *et al.*, 2004). *rad9*Δ *cdc13-1* strains keep dividing despite uncapped telomeres, resulting in telomere resection and rapid accumulation of ssDNA (Zubko *et al.*, 2004). Interestingly, deletion of *UPF2* in *rad9*Δ *cdc13-1* mutants significantly decreased the amount of generated ssDNA at both the *DUG1* and the *RET2* loci, showing that Upf2 contributes to ssDNA generation at uncapped telomeres (Figure 34B and C). To confirm that the observed ssDNA was specific for the TG-strand and not a result of unwinding of the dsDNA, the amount of single-stranded DNA occurring on the AC-strand was measured for the *DUG1* and the *RET2* loci. As shown in Figure 34D and E, no significant amount of ssDNA could be detected, confirming that measured ssDNA was specific for the TG-strand. In conclusion, Figure 34 demonstrates that Upf2 contributes to ssDNA generation at *cdc13-1* uncapped telomeres on chromosome VI-R.

No difference in ssDNA generation could be detected at the *DUG1* and the *RET2* loci for *cdc13-1* and *upf2*Δ *cdc13-1* mutants (Figure 34B and C). The amount of generated ssDNA was small for both mutants; however, more ssDNA may be generated closer to the chromosome end and a difference between both mutants may be noticeable when looking at ssDNA generation at all telomeres. To test this, Fluorescent In-Gel Assay

(FIGA) was used to measure ssDNA at telomeric TG strands. As shown in Figure 35, ssDNA accumulated in a *cdc13-1* mutant over a 4 hour time course at 36°C, whereas only a slight increase in ssDNA was detectable in an *upf2*Δ *cdc13-1* strain at the 2 hour time point, indicating that Upf2 contributes to ssDNA generation at *cdc13-1* uncapped telomeres.

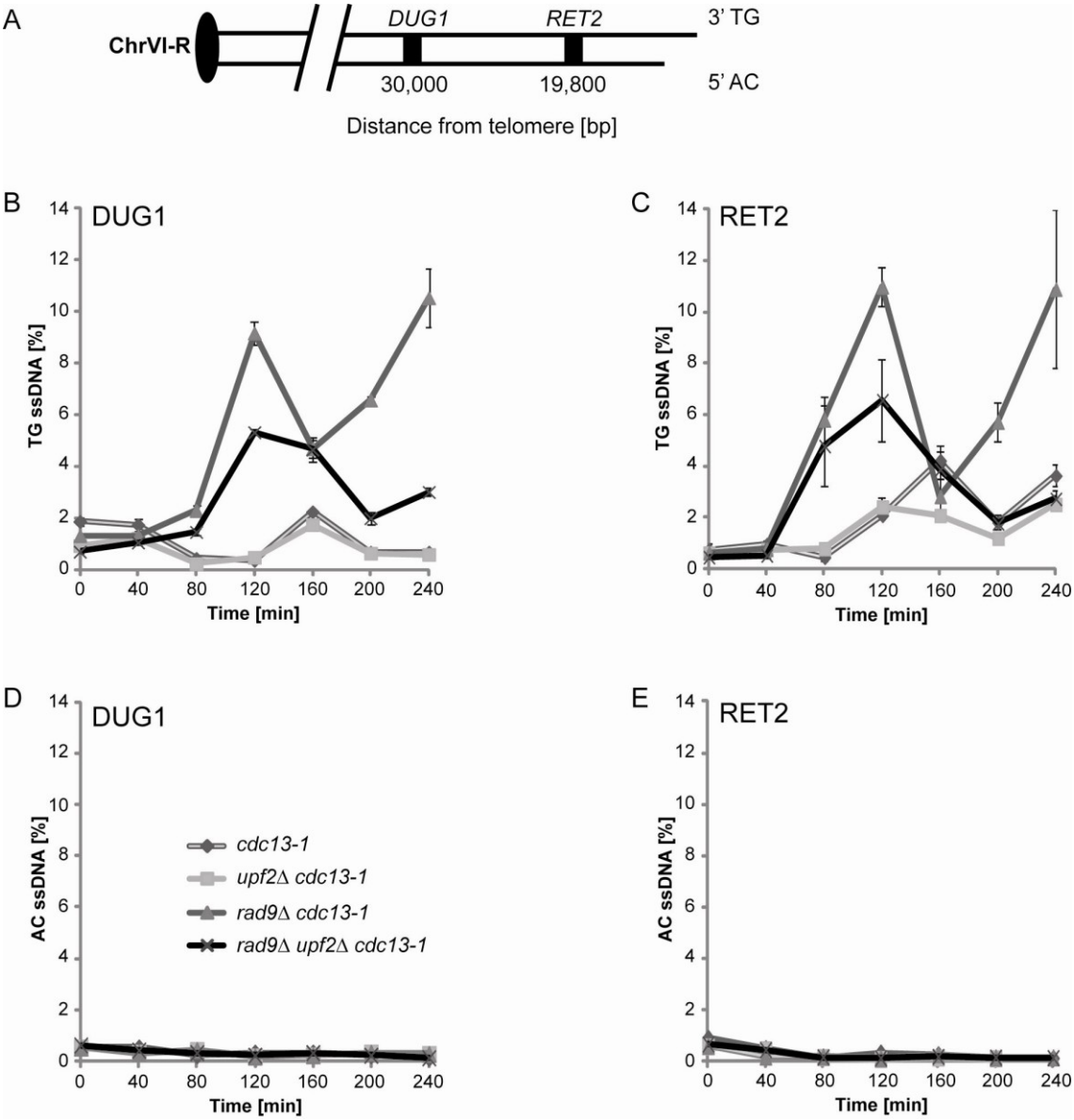

Figure 34. Upf2 contributes to ssDNA generation at *cdc13-1* uncapped telomeres.

Exponentially dividing cells of the genotypes indicated (containing *bar1*Δ and *cdc15*-2) were arrested at 23°C in G1 using α factor. Cultures were released from α factor and shifted to 36°C to induce telomere uncapping. Samples were taken at times indicated and ssDNA was measured by QAOS as described in Holstein and Lydall (in press).

A. Schematic representation of ChrVI-R. **B.** Percentage of ssDNA on the TG strand at the DUG1 locus on Chromosome VI-R **C.** on the TG strand at the RET2 locus on Chromosome VI-R **D.** on the AC strand at the DUG1 locus **E.** on the AC strand at the RET2 locus.

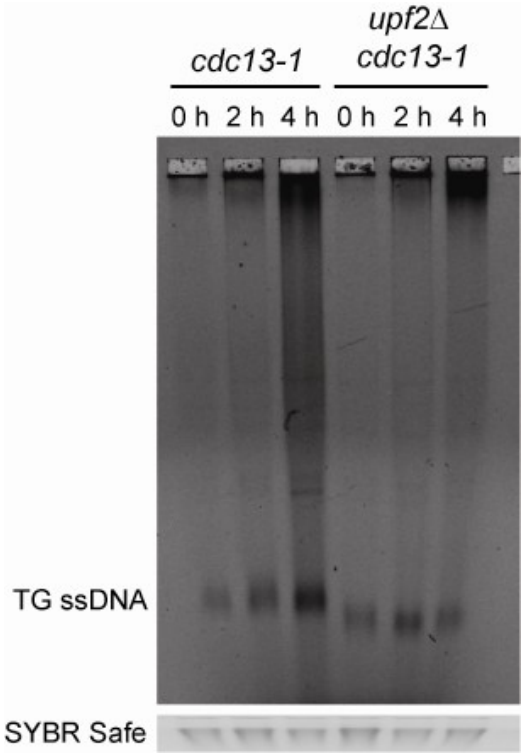

Figure 35. Upf2 contributes to ssDNA generation at *cdc13-1* uncapped telomeres.

Exponentially dividing cells of the genotypes indicated were shifted from 23°C to 36°C. Samples were taken at times indicated and ssDNA was measured in the TG repeats by FIGA. Gel was stained using SYBR Safe for loading control.

4.2.6 Upf2 inhibits growth of cdc13-1 mutants in a parallel pathway to Exo1 and Rad24

The 5'-3' exonuclease Exo1 and a Rad24-dependent nuclease both play a role in resection of *cdc13-1* uncapped telomeres and function in parallel pathways (Zubko *et al.*, 2004). However, even deletion of both nucleases still results in ssDNA being generated at uncapped telomeres, suggesting that other nuclease activities may be active at *cdc13-1* uncapped telomeres (Zubko *et al.*, 2004). Data in Figure 34 and 35 indicate that Upf2 is required for nuclease activity at *cdc13-1* uncapped telomeres. Spot tests were used to determine whether Upf2 functions in the same pathway as Exo1 or Rad24.

As shown in Figure 36, all strains showed similar growth at 23°C. The *exo1*Δ *cdc13-1* mutant and the *upf2*Δ *cdc13-1* mutant were both able to grow to some extent at 29°C with *upf2*Δ *cdc13-1* growing slightly better. In comparison, *exo1*Δ *upf2*Δ *cdc13-1* triple mutant showed wild-type growth at the same temperature (29°C) and was even able to grow to some extent at 36°C, a temperature where neither *upf2*Δ *cdc13-1* nor *exo1*Δ *cdc13-1* mutants were able to grow. In conclusion, the additive growth effect of *exo1*Δ *upf2*Δ *cdc13-1* triple mutant compared to *upf2*Δ *cdc13-1* double mutant demonstrates that Upf2 and Exo1 inhibit growth of *cdc13-1* mutants through different pathways.

The question remained if Upf2 functions in the same pathway as Rad24 or in parallel to both Exo1 and Rad24. As shown in Figure 36, the *rad24*Δ *cdc13-1* mutant was able to grow to some extent at 29°C and was growing slightly better compared to the *upf2*Δ *cdc13-1* mutant. The *rad24*Δ *upf2*Δ *cdc13-1* triple mutant however showed wild-type growth at 29°C and was able to grow to some extent at temperatures as high as 36°C. In addition, the *exo1*Δ *rad24*Δ *upf2*Δ *cdc13-1* quadruple mutant grew considerable better at 36°C compared to the *rad24*Δ *upf2*Δ *cdc13-1* triple mutant. In conclusion, the additive growth effects of *rad24*Δ *upf2*Δ *cdc13-1* triple mutant compared to *rad24*Δ *cdc13-1* double mutant demonstrates that Upf2 and Rad24 inhibit growth of *cdc13-1* mutants through different pathways. Hence, Upf2 functions in parallel pathways to both Exo1 and Rad24.

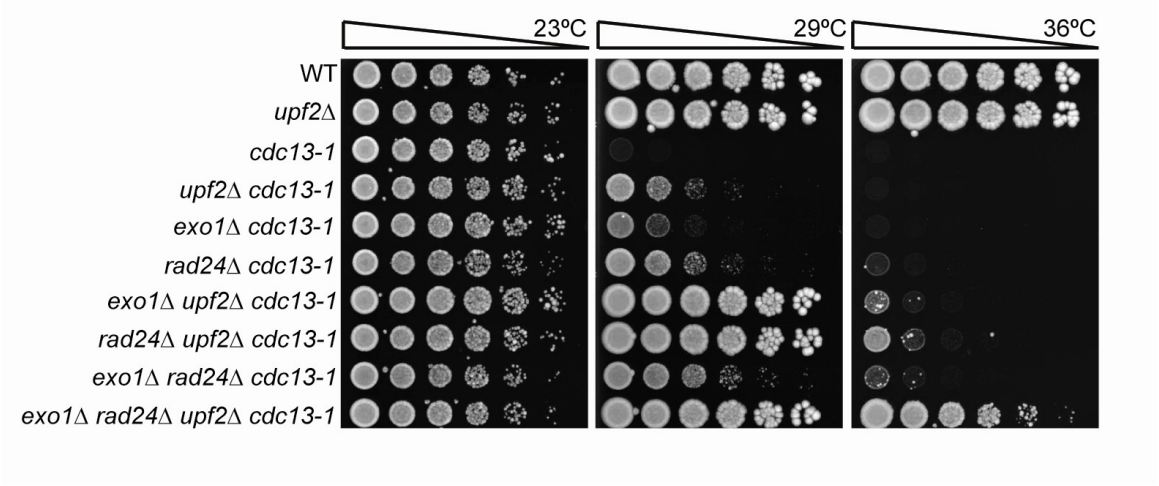

Figure 36. Upf2 inhibits growth of *cdc13-1* mutants in a parallel pathway to Exo1 and Rad24.

Saturated cultures of the genotypes indicated were serially diluted across agar plates containing YEPD and were grown at the temperature indicated for 2 days.

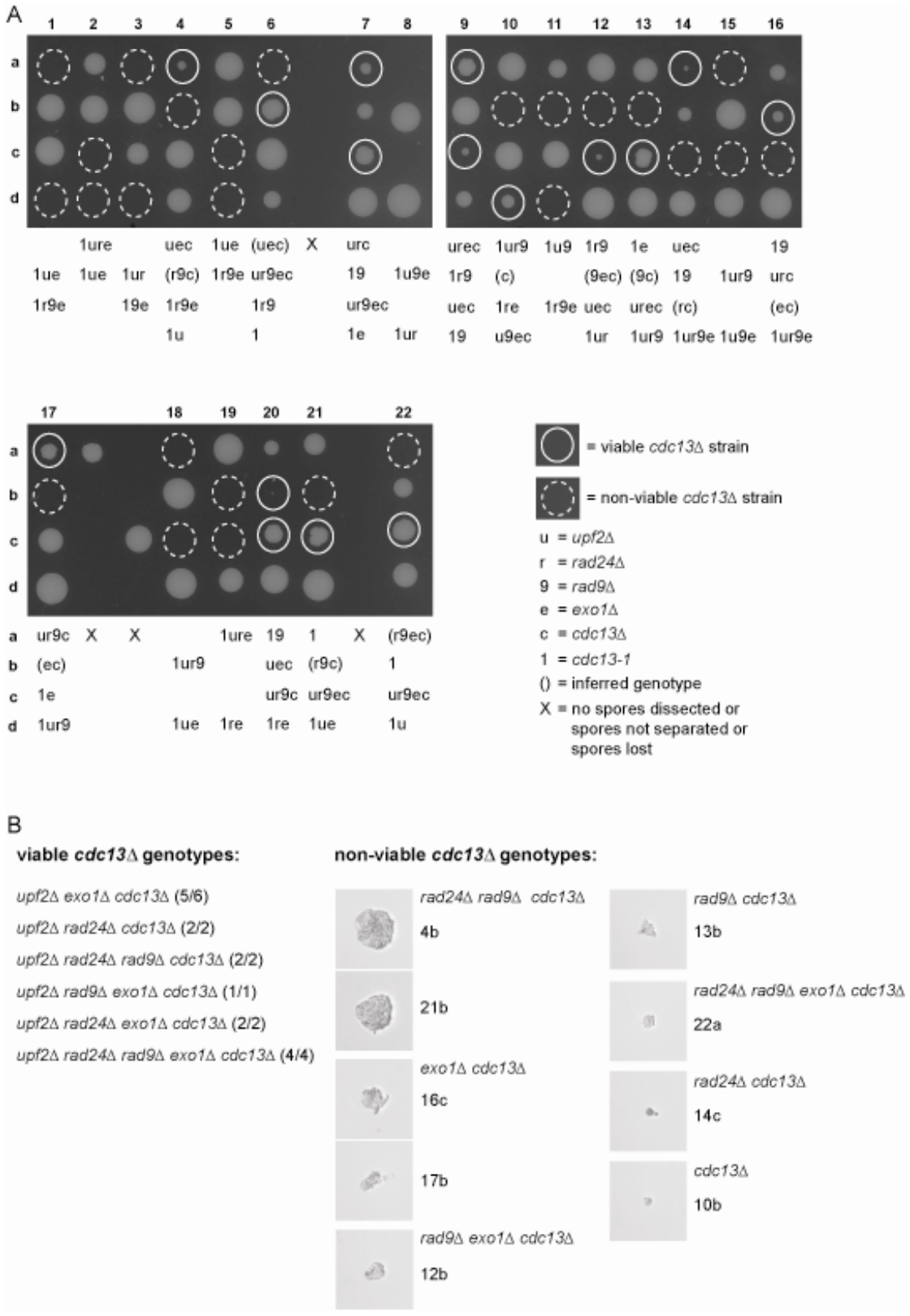

Figure 37. Cdc13 is not required for viability in the absence of Upf2 and Exo1 or Upf2 and Rad24.

upf2Δ/UPF2 exo1Δ/EXO1 rad24Δ/RAD24 rad9Δ/RAD9 cdc13Δ/cdc13-1 diploids were generated and sporulated. The tetrads were dissected and spores were separated apart on agar plates. Spores were allowed to form colonies for 5 days at 23°C.

4.2.7 The essential telomere-binding protein Cdc13 is not required for viability in cells lacking Upf2 and Exo1 or Upf2 and Rad24

Deletion of *UPF2 EXO1* or *UPF2 RAD24* allowed *cdc13-1* mutants to grow at temperatures as high as 36°C (Figure 36), suggesting that the essential telomere-binding protein Cdc13 might not be required for viability. To test whether Cdc13 is non-essential in cells lacking *EXO1* and *UPF2*, or *RAD24* and *UPF2, upf2*Δ*/UPF2 exo1*Δ*/EXO1 rad24*Δ*/RAD24 rad9*Δ*/RAD9 cdc13*Δ*/cdc13-1* diploids were generated and sporulated. The tetrads were then dissected and spores were separated on agar plates. Viable progeny could then form colonies at 23°C. As shown in Figure 37A, *upf2*Δ *exo1*Δ *cdc13*Δ mutants were indeed viable and able to form colonies (4a, 9c, 12c, 14a and 20b, apart from 6a), but growth was poor compared to *upf2*Δ *exo1*Δ *cdc13-1* mutants (1b, 2b, 5a and 21d). Similarly, *upf2*Δ *rad24*Δ *cdc13*Δ mutants were viable and able to form colonies (7a and 16b), but growth was poor compared to *upf2*Δ *rad24*Δ *cdc13-1* mutants (3b, 8d and 12d). Other viable *cdc13*Δstrains include *upf2*Δ *rad24*Δ *rad9*Δ *cdc13*Δ (17a and 20c), *upf2*Δ *exo1*Δ *rad9*Δ *cdc13*Δ (10d), *upf2*Δ *rad24*Δ *exo1*Δ *cdc13*Δ (9a and 13c) and *upf2*Δ *rad24*Δ *exo1*Δ *rad9*Δ *cdc13*Δ (6b, 7c, 21c and 22c). However, no viable strains could be obtained for *upf2*Δ *rad9*Δ *cdc13*Δ mutants or any mutants containing wild-type *UPF2*. In conclusion, elimination of Upf2 together with Exo1 or Rad24 allows viability of cells in the absence of the otherwise essential telomere capping protein Cdc13.

Microscopy was used to look at the cell morphology of the non-viable *cdc13*Δ strain. Interestingly, all strains apart from the *rad24*Δ *cdc13*Δ (14c) and the *cdc13*Δ (10b) strain underwent a couple of divisions (Figure 37B), indicating different degrees of essentiality. Interestingly, viable *cdc13-1* and *cdc13*Δ strains exhibit different colony morphologies and sizes. As shown in Figure 38, all *cdc13-1* colonies featured a round, smooth morphology, but differed in colony sizes. *upf2*Δ *rad24*Δ *cdc13-1* (3b, 8d and 12d) and *upf2*Δ *exo1*Δ *cdc13-1* (1b, 2b, 5a and 21d) colonies were considerably bigger in size compared to *cdc13-1* colonies (6d, 21a and 22b), whereas *rad9*Δ *cdc13-1* colonies (7b, 9d, 14b, 16a and 20a) were smaller in size compared to *cdc13-1* colonies.

Like *cdc13-1* colonies, viable *cdc13*Δ colonies varied in sizes, but exhibited heterogeneous "nibbled" morphologies (Figure 38), a potential indicator for chromosome instability (Admire *et al.*, 2006). As shown in Figure 38, *upf2*Δ *exo1*Δ *cdc13*Δ (4a, 9c, 12c, 14a and 20b) and *upf2*Δ *rad24*Δ *cdc13*Δ colonies (7a and 16b) were considerably smaller compared to other viable *cdc13*Δ or *cdc13-1* strains, indicating a growth defect or cell death. In conclusion, viable *cdc13*Δ colonies exhibited a "nibbled" morphology, whereas *cdc13-1* strains featured a smooth and round morphology. Both, *cdc13*Δ and *cdc13-1* mutants varied in sizes and size variation was genotype-dependent. Most non-viable *cdc13*Δ were able to undergo a couple of divisions. Further work will be required to determine what defects the viable *cdc13*Δ have, such as chromosome instability, senescence, telomere shortening etc.

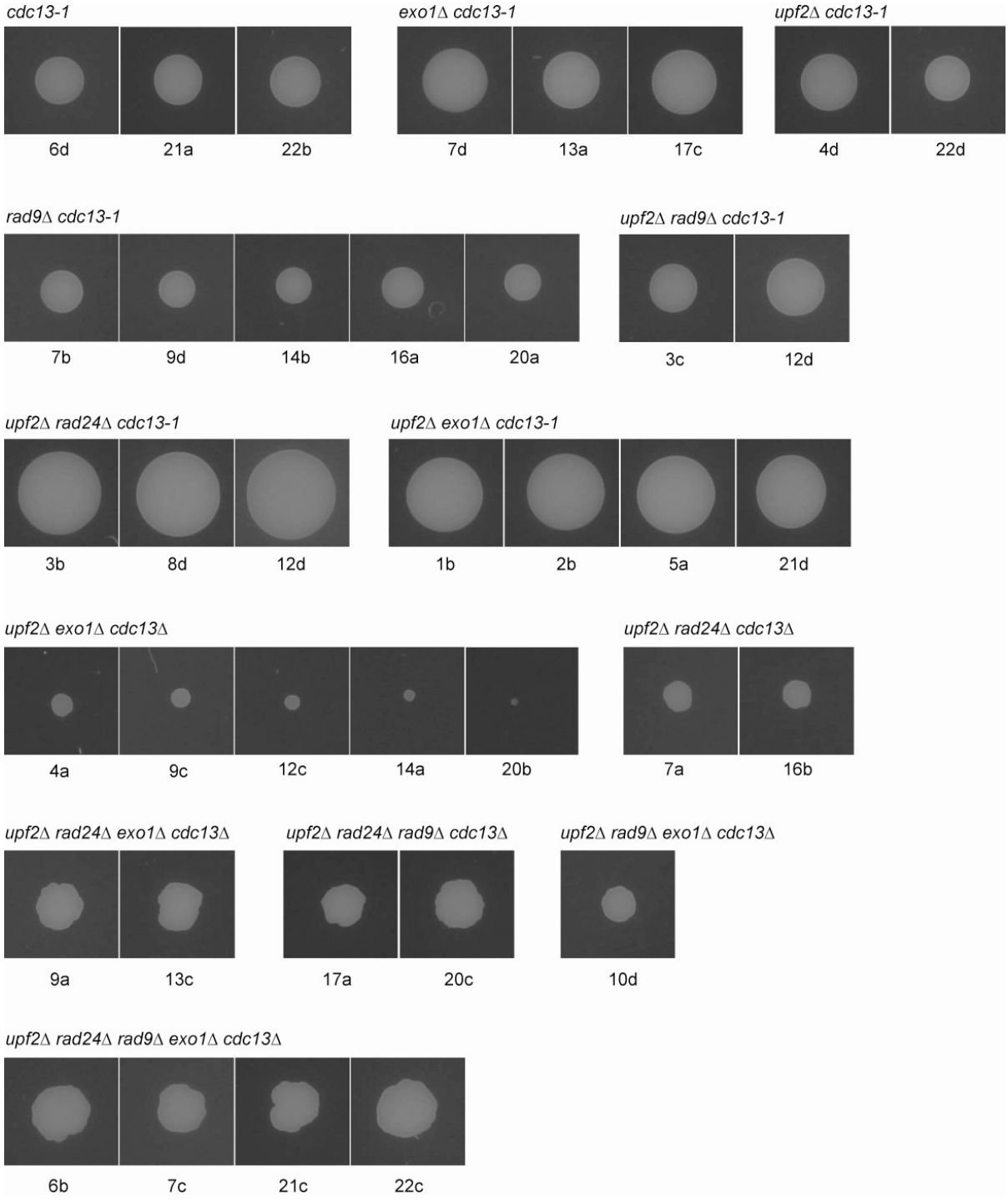

Figure 38. Viable *cdc13*Δ colonies vary in size and morphology

Viable *cdc13*Δ colonies were compared to *cdc13-1* colonies regarding shape and size. Figures of colonies were taken from tetrad dissection experiment shown in Figure 37.

4.3 Discussion

Work in this chapter demonstrated that Ebs1 and Upf2 do not affect checkpoint activation in response to *cdc13-1* uncapped telomeres (Figure 23). However, Figures 23 and 24 demonstrated that Upf2 and Ebs1 are required for efficient G1 to S phase progression in the presence of *cdc13-1* uncapped telomeres. In the absence of Ebs1, the delay was due to the checkpoint protein Rad9, suggesting that activation of the G1/S phase checkpoint might be a response to DNA damage (Figure 26 and Table 3). Figure 28 showed that no increase in phosphorylation of the DNA damage marker Rad53 could be detected in *ebs1*Δ *cdc13-1* mutants compared to *cdc13-1*. However, Rad53 phosphorylation was measured 4 hours after beginning of the experiment. It is possible that Rad53 was completely phosphorylated at the 4 h time point. An increase in Rad53 phosphorylation in *ebs1*Δ *cdc13-1* mutants compared to *cdc13-1* mutants might be detectable at the 80 or 100 min time point, the time when *cdc13-1* and *ebs1*Δ *cdc13-1* mutants progressed through S phase. Interestingly, phosphorylated histone H2AX, a well-known DNA damage marker in mammalian organisms, has been shown to be increased in human cells lacking UPF1, probably due to stalled DNA replication forks in S phase (Azzalin and Lingner, 2006). These data suggest that lack of NMD components in budding yeast might indeed induce a DNA damage response, which would explain the observed delay in cell cycle progression from G1 to S phase in Figure 23. The hypothesis that lack of NMD induces a DNA damage response is further supported by another study that demonstrated that depletion of mammalian NMD factor SMG1 leads to DNA damage, cell cycle arrest in early S phase and induction of an ATR-dependent DNA damage response (Brumbaugh *et al.*, 2004). In addition, mammalian UPF1 physically interacts with the DNA polymerase δ and accumulates at chromatin during S phase, suggesting a role for UPF1 in DNA replication (Azzalin and Lingner, 2006). Further work will be required to test this hypothesis.

cdc13-1	*ebs1*Δ	*upf2*Δ	*rad9*Δ	G1/S delay
+	-	-	-	-
-	+	-	-	-
+	+	-	-	+
+	+	-	+	-
-	-	+	-	-
+	-	+	-	+
+	-	+	+	+

Table 4 Mutations affecting G1/S progression

Similar to in the absence of Ebs1, cells lacking Upf2 did not show any increase in phosphorylation of Rad53 at the presence of *cdc13-1* uncapped telomeres (Figure 28). However, the delay in G1 to S phase progression was not Rad9-dependent (Table 4 and Figure 27), suggesting that the delay was caused by a different mechanism than the delay observed in *ebs1*Δ *cdc13-1* mutants. A recent study in *S. cerevisiae* demonstrated that NMD regulates transcript levels of telomeric repeat-containing RNA (TERRA) (Feuerhahn *et al.*, 2010). In addition, several components of NMD were found to be concentrated at telomeres in mammalian cells (Azzalin *et al.*, 2007). UPF1 was shown to accumulate on chromatin during S phase, to promote dissociation of TERRA from telomeric chromatin during that cell cycle stage and to interact with DNA polymerase δ (Porro et al., 2010; Azzalin and Lingner, 2006; Carastro et al., 2002). This data and the fact that TERRA is a direct negative regulator of telomerase activity by acting as a competitor for telomeric DNA suggests that dissociation of TERRA from telomeres through NMD during S phase may support efficient progression of DNA replication and following telomere elongation through telomerase (Redon *et al.*, 2010). Furthermore, upregulation of TERRA results in telomeric Exo1-dependent resection (Pfeiffer and Lingner, 2012). Hence, the delay in G1 to S phase progression in cells lacking *UPF2* may be a result of increased TERRA levels at telomeres. In addition, TERRA has been shown to associate to telomerase and negatively regulate telomerase activity, which is consistent with the fact that NMD mutants have shorter telomeres (Redon et al., 2010; Askree et al., 2004).

Data in Figures 31-32 demonstrated that Upf2 contributes to loss in viability in *cdc13-1* mutants in the absence of the checkpoint protein Rad9. *rad9*Δ *cdc13-1* mutants have

been shown to not be able to arrest in response to telomere uncapping due to the abolished G2/M checkpoint (Garvik *et al.*, 1995; Lydall and Weinert, 1995). In the absence of the checkpoint, only the level of resection at *cdc13-1* uncapped telomeres limits growth. *rad9*Δ *cdc13-1* mutants feature extensive telomere resection resulting in rapid loss in viability. However, deletion of *UPF2*, but not *EBS1*, in *rad9*Δ *cdc13-1* mutants allows cells to grow to some extent (Figure 32), indicating that Upf2 contributes to nuclease activity at uncapped telomeres. QAOS and FIGA experiments further supported this hypothesis by demonstrating that Upf2 contributes to ssDNA generation at *cdc13-1* uncapped telomeres (Figure 34 and 35). A previous study showed that resection at *cdc13-1* uncapped telomeres is dependent on a Rad24-dependent nuclease, the Exo1 nuclease and possibly a third unknown nuclease (Zubko *et al.*, 2004). Data in Figure 36 demonstrated that Upf2 does not work in the same pathways as Exo1 or Rad24 regarding telomere resection in *cdc13-1* mutants as deletion of *UPF2* in *exo1*Δ *rad24*Δ *cdc13-1* mutants significantly increased the ability to grow at 36°C (Figure 36) As ssDNA generation in *cdc13-1* mutants lacking Rad24 and Exo1 is not completely abolished, it might be possible that Upf2 contributes to resection at uncapped telomeres through a third nuclease (Zubko *et al.*, 2004). It would be of interest to test if ssDNA generation is completely abolished in *upf2*Δ *exo1*Δ *rad24*Δ *cdc13-1* mutants. It can however not be ruled out that the observed delay in G1 to S phase progression in Figure 23 contributed to a delay in ssDNA generation and delay in loss in viability.

Remarkably, data in Figure 37 demonstrated that cells lacking Upf2 and Exo1 or Upf2 and Rad24 do not require the usually essential telomere-binding protein Cdc13 for viability. Two recent publications demonstrated that Cdc13 is not required in cells lacking Sgs1, Exo1 and Rad9, or Pif1 and Exo1 (Dewar and Lydall, 2010; Ngo and Lydall, 2010). Sgs1 and Pif1 are both DNA helicases that contribute to resection at *cdc13-1* uncapped telomeres and the attenuated resection activities in *sgs1*Δ *exo1*Δ *rad9*Δ or *pif1*Δ *exo1*Δ mutants allowed cells to survive in the absence of Cdc13. Like Exo1 and Rad24, Upf2 contributes to ssDNA generation at *cdc13-1* uncapped telomeres (Figure 34 and 35), suggesting that strongly reduced resection activities in *upf2*Δ *exo1*Δ or *upf2*Δ *rad24*Δ mutants allows the cells to be viable and grow in the absence of the otherwise essential Cdc13. The results also indicate that the essential function of the telomere capping protein Cdc13 is to counteract resection activities at telomeres.

Results in Figure 36 suggest that resection might be even further reduced in *upf2*Δ *exo1*Δ *rad24*Δ *cdc13*Δ quadruple mutants compared to either *upf2*Δ *exo1*Δ *cdc13*Δ or *upf2*Δ *rad24*Δ *cdc13*Δ triple mutant. Interestingly, colonies with the quadruple mutations were able to form bigger colonies compared to colonies with triple mutations (Figure 38), supporting the hypothesis that Cdc13 counteracts resection activities at telomeres. Additional inactivation of the DNA damage checkpoint control protein Rad9 in any of these mutants, also allows bigger colony formation, suggesting that besides resection, Cdc13 functions in counteracting the checkpoint control. However, in the absence of Rad9 and Cdc13, cells can only survive if Upf2 and either Rad24 or Exo1 are also eliminated, indicating that Cdc13 counteracts checkpoint control at telomeres, but the essential function of Cdc13 seems to be to counteract resection activities.

However, the viable *cdc13*Δ mutants did feature severe growth defects and a "nibbled" phenotype, a potential indicator for chromosome instability. A study from 2006 argues that formation of unstable chromosomes, caused by stalled replication forks and increased by defects in DNA replication or cell cycle checkpoint controls, led to a "nibbled" phenotype of *Saccharomyces cerevisiae* colonies (Admire *et al.*, 2006). Dissociation of TERRA from telomeres during S phase (promoted by Upf2) has been shown to support efficient progression of the DNA replication fork, suggesting that a potential defect in DNA replication in cells lacking Upf2 could have caused the "nibbled" phenotype (Porro et al., 2010; Azzalin and Lingner, 2006; Carastro et al., 2002). This is supported by a publication from 2006, where Azzalin and Lingner measured an increase in phosphorylated histone γH2AX in human cells in the absence of UPF1 (Azzalin and Lingner, 2006). The group claims that the increase was caused by stalled DNA replication forks in S phase. In contrast, a recent publication showed that cells lacking the DNA helicase Pif1 and the exonuclease Exo1 are viable in the absence of Cdc13 and the viable colonies featured a "nibbled" phenotype, however, maintained their telomeres (Dewar and Lydall, 2010). Future experiments will clarify if telomere alterations occur in the viable *cdc13*Δ used in this study.

4.4 Future work

QAOS and FIGA showed that Upf2 contributes to ssDNA generation at *cdc13-1* uncapped telomeres (Figure 34 and 35) and data in Figure 36 demonstrated that Upf2 functions in a parallel pathway to Exo1 and Rad24 regarding ssDNA generation. ssDNA is not completely abolished at *cdc13-1* uncapped telomeres in the absence of Exo1 and Rad24, indicating that at least one other nuclease processes uncapped telomeric DNA (Zubko *et al.*, 2004). It would of interest to determine if ssDNA generation is abolished or at least further reduced if Upf2 is eliminated in *exo1*Δ *rad24*Δ *cdc13-1* mutants. The theory is supported by the fact that *upf2*Δ *exo1*Δ *rad24*Δ *cdc13-1* grow better compared to *exo1*Δ *rad24*Δ *cdc13-1* mutants at 36°C when telomeres are uncapped. It is further supported by the fact that *upf2*Δ *exo1*Δ *rad24*Δ mutants are viable in the absence of the usually essential telomere capping protein Cdc13.

It has previously been shown that cells, at a low rate, can adapt to loss of Cdc13 by altering their telomere structures (Larrivee and Wellinger, 2006). It would be of interest to determine if alterations in telomere structures, in addition to the reduction in ssDNA generation, allow *upf2*Δ *exo1*Δ *cdc13*Δ or *upf2*Δ *rad24*Δ *cdc13*Δ mutants to be viable. Telomere structures could be analysed by Southern blot. In addition, sectoring of viable *cdc13*Δ mutants implies potential chromosome instability. In contrast, Dewar and Lydall (2006) were able to delete Cdc13 in *pif1*Δ *exo1*Δ mutants and despite a "nibbled" phenotype, the cells maintained their telomeres over 11 passages (Dewar and Lydall, 2010). It would be of interest to test if the mutants used in this study are able to maintain their telomeres or feature chromosome instability. This could be tested by chromosome loss assay.

Upf2 has been shown to promote dissociation of TERRA from telomeric chromatin during S phase and to interact with DNA polymerase δ, suggesting that dissociation of TERRA from telomeres during S phase may support efficient progression of the DNA replication fork (Porro et al., 2010; Azzalin et al., 2007; Carastro et al., 2002). Hence, increased TERRA levels in *upf2*Δ *cdc13-1* and perhaps *ebs1*Δ *cdc13-1* mutants may be responsible for the observed delay in G1 to S phase progression (Figure 23). It would be of interest to test this hypothesis. One possibility might be to over-express the 5' to 3'

single-stranded RNA exonuclease Rat1 in cells lacking components of NMD to reduce TERRA levels, as Rat1 has been shown to degrade TERRA (Luke and Lingner, 2009). It would be interesting to see if regulation of TERRA levels affects G1 to S phase progression in *upf2*Δ *cdc13-1* mutants as several publications propose a strong interplay between NMD, TERRA, DNA replication and telomere maintenance (Feuerhahn et al., 2010; Porro et al., 2010; Redon et al., 2010; Azzalin et al., 2007).

The observed delay in G1 to S phase progression in *cdc13-1* mutants lacking *EBS1* was dependent on the checkpoint protein Rad9, a strong indication for checkpoint arrest in response to DNA damage (Figure 23). Detection of Rad53 phosphorylation during S phase progression might allow detection of different levels of phosphorylation in *ebs1*Δ *cdc13-1* mutants compared to *cdc13-1* mutants. In addition, a study from 2006 further supports the hypothesis that the delay is due to a respone to DNA damage (Azzalin and Lingner, 2006). The group showed that the DNA damage marker γH2AX is increased in human cells in the absence of UPF2 and they claim that the increase is due to stalled DNA replication forks in S phase. To address if the observed delay in cell cycle progression from G1 to S phase is due to a DNA damage response, phosphorylation of histone H2AX could be measured in budding yeast lacking NMD components.

5 General Discussion

The aim of this study was to further understand the role of Ebs1 and nonsense-mediated decay pathways at telomeres. In this work I show that Ebs1 and NMD affect Cdc13- and Yku70-mediated telomere capping by modulating expression of the gene encoding for the telomere capping protein Stn1. Like NMD mutants, increased levels of Stn1 suppressed the temperature-sensitive *cdc13-1* growth defect, but enhanced the temperature-sensitive *yku70*Δ defect. Hence, an increase in the amount of Stn1 had opposite effects on two forms of telomere uncapping. In addition, the absence of NMD altered the stochiometry of the CST (Cdc13-Stn1-Ten1) complex at telomeres, with increased association of Stn1 and Ten1, but reduced binding of Cdc13. Reduced Cdc13 association to telomeres was due to the increase in Stn1 and I propose that Stn1 and Ten1 can bind to the telomere independently of the CST complex and that Stn1 is capable of displacing Cdc13 from telomeres. I propose that suppression of the temperature-sensitive *cdc13-1* growth defect in the absence of functional NMD is due to proficient telomere protection through increased binding of Stn1 and Ten1, suggesting that the function of Cdc13 is to recruit other telomere factors that enable efficient telomere protection. I suggest that the reduced Cdc13 association with telomeres in cells over-expressing *STN1* or lacking NMD contributes to the *yku70*Δ capping defect. A decrease in telomerase recruitment might also contribute to the enhanced defect.

In addition, this work demonstrates that NMD contributes to ssDNA generation at *cdc13-1* uncapped telomeres. This study demonstrated that Upf2 functions in a parallel pathway to the exonuclease Exo1 and a Rad24-dependent nuclease. In the absence of Upf2 and Rad24 or Upf2 and Exo1, yeast is able to survive and grow in the absence of the usually essential telomere capping protein Cdc13. I propose that the essential function of Cdc13 is to counteract telomeric resection. I suggest that the reduced ssDNA generation at *cdc13-1* uncapped telomeres in the absence of functional NMD is a result of proficient telomere capping through increased binding of Stn1 and Ten1 to the telomere. This is supported by a previous publication that demonstrated that over-expression of Stn1 and Ten1 restores viability of cells lacking Cdc13 (Petreaca *et al.*, 2006).

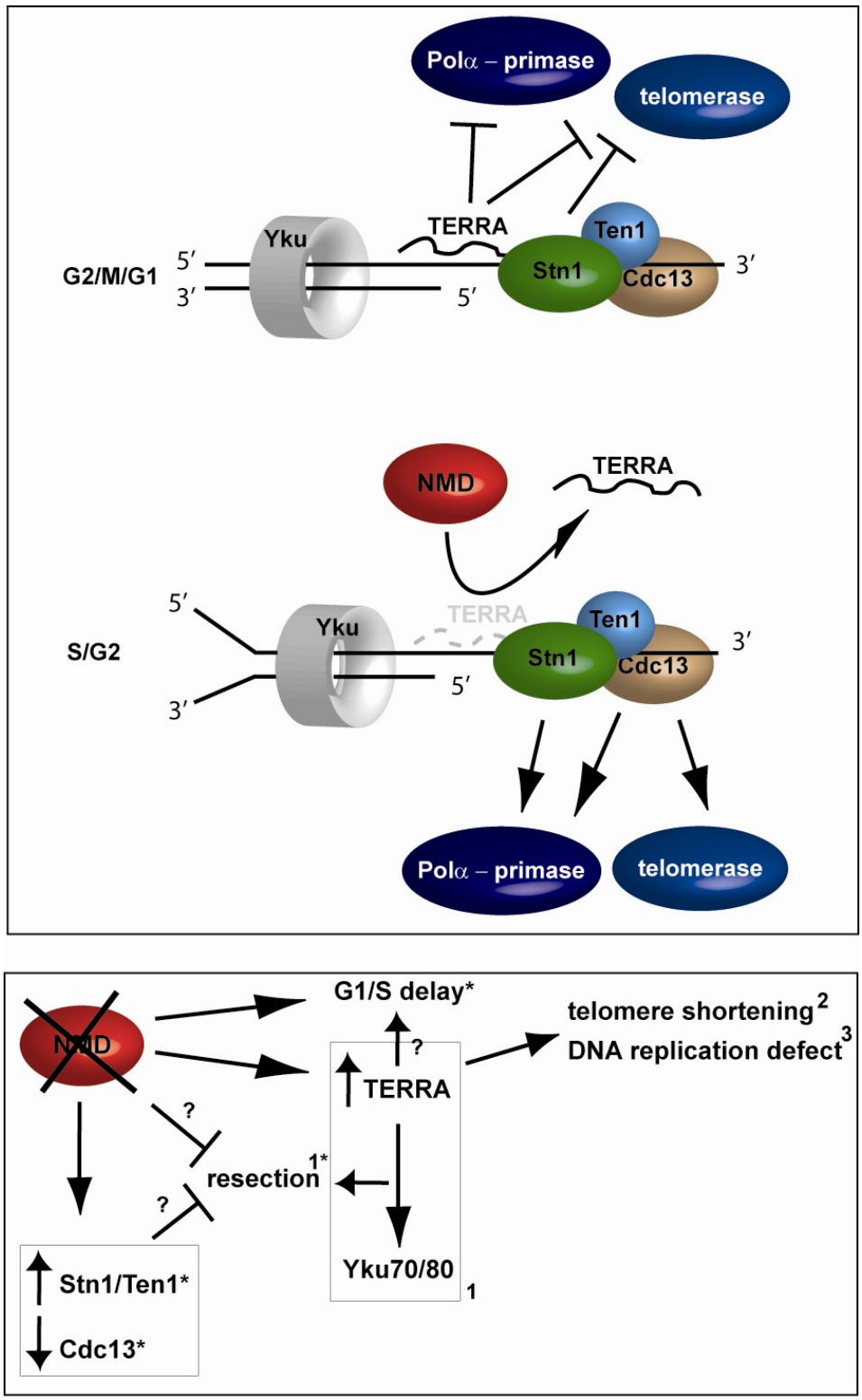

Figure 39. Integrative model for the interplay between NMD, TERRA, DNA replication, telomere capping and telomere maintenance.

The model presented here integrates published interactions and interactions discovered in this study:[1](Pfeiffer and Lingner 2012), [2](Askree, Yehuda et al. 2004), [3](Feuerhahn, Iglesias et al. 2010; Porro, Feuerhahn et al. 2010), * this study and question marks indicate hypotheses. See text for details.

NMD factors Upf1, Upf2 and Upf3 are conserved from yeast to humans and NMD has not only been shown to be connected to telomere metabolism in yeast, but as well in higher eukaryotes, indicating that the results of this work carried out in yeast might be of relevance in other organisms. A role in DNA replication and in DNA damage response has been suggested for human UPF1 (Azzalin and Lingner, 2006; Brumbaugh et al., 2004). In addition, NMD has been proposed to play an important role in protecting organisms from cancer formation. NMD degrades aberrant mRNAs containing a premature translation-termination codon (PTC). Interestingly, a vast amount of mutations in the tumour suppressor genes p53, WT1, BRCA1 and BRCA2 have been shown to contain PTCs and have been suggested to be NMD targets in various studies (Anczukow et al., 2008; Perrin-Vidoz et al., 2002; Reddy et al., 1995). In addition, PTC mutations in the DNA damage response protein MRE11 led to an unstable transcript, indicating that it was targeted for decay and degraded (Pitts et al., 2001; Stewart et al., 1999). Hence, various data in higher eukaryotes demonstrate a link between NMD pathways and telomere protection and suggest an important role for NMD in counteracting cancer formation.

Orthologs of the budding yeast CST complex have been found in plants and humans consisting of CTC1, STN1 and TEN1 and have been linked to telomere replication and telomere maintenance (Gu et al., 2012; Price et al., 2010; Miyake et al., 2009). In addition, mutations in CTC1 have been shown to lead to Coats plus syndrome in humans, a pleiotropic disorder comprising a telomere length defect (Anderson *et al.*, 2012). Furthermore, Dyskeratosis congenita, a syndrome resulting in bone marrow failure and shortened telomeres, has been linked to mutations in several genes involved in telomere regulation, including CTC1 (Keller *et al.*, 2012).

The CST complex in budding yeast has functional and structural similarities with the mammalian RPA complex and POT1 (Sun et al., 2009; Gao et al., 2007; Mitton-Fry et al., 2002). A recent study showed that binding of the mammalian RPA complex and POT1 to telomeric ssDNA is regulated by TERRA (telomeric repeat-containing RNA), leading to displacement of RPA in late S phase and promotion of POT1 binding after S phase (Flynn *et al.*, 2011). Furthermore, human NMD has been indicated to promote dissociation of TERRA from telomeres during S phase to ensure efficient DNA

replication and telomere elongation (Porro *et al.*, 2010; Redon *et al.*, 2010). TERRA has been shown to associate with telomerase and to negatively regulate telomerase activity, suggesting that NMD activity at telomeres may regulate succession of DNA replication and telomere elongation through TERRA. Furthermore, upregulation of TERRA results in telomere shortening due to Exo1-dependent resection through interaction of TERRA with the Yku complex (Pfeiffer and Lingner, 2012). Work in yeast suggests that completion of lagging-strand synthesis by DNA polymerases and telomere elongation by telomerase is co-regulated and mediated by Cdc13 and Stn1 (Puglisi et al., 2008; Grossi et al., 2004; Diede and Gottschling, 1999).

The various discovered roles of TERRA at mammalian and yeast telomeres and their interaction with the NMD pathway suggest that the observed NMD effects on telomere protection might be a result of both Stn1 and TERRA regulation. Work in this study demonstrated that in the absence of functional NMD, Stn1 transcript and protein levels were increased and overexpression of Stn1 suppressed the temperature-sensitive *cdc13-1* growth defect, but enhanced the temperature-sensitive *yku70*Δ defect. As mentioned above, I suggest that the reduced Cdc13 association with telomeres in cells over-expressing *STN1* or lacking NMD contributes to the *yku70*Δ capping defect. Another possibility is that the enhanced temperature-sensitive growth defect in *upf2*Δ *yku70*Δ mutants is caused by TERRA. The interaction of TERRA with the Yku complex has been shown to interfere with the ability of Yku to inhibit Exo1-dependent telomere resection, suggesting that in the absence of functional NMD, increased TERRA levels at telomeres promote telomeric resection (Pfeiffer and Lingner, 2012). In the case of *cdc13-1* dependent telomere uncapping, I propose that increased levels of Stn1 at telomeres allow efficient telomere capping, thereby suppressing the temperature-sensitive *cdc13-1* growth defect. This is consistent with data in this work showing decreased resection in *upf2*Δ *cdc13-1* mutants. Interaction of TERRA with Yku complex facilitates Exo1-dependent resection, suggesting that in the absence of functional NMD resection should be increased. However, I propose that either functional NMD is required for the ability of TERRA to promote resection through interaction with Yku or that increased levels of Stn1 at the telomere in *upf2*Δ mutants counteract resection activities by either interfering with the interaction between TERRA and Yku or through its capping function.

The observed delay in G1/S phase progression in dysfunctional NMD mutants could be a result of a DNA replication defect due to increased TERRA levels at telomeres. As dissociation of TERRA from telomeres in S phase due to UPF1 ensures efficient DNA replication, I propose that in the absence of functional NMD, TERRA remains bound at telomeres, thereby hindering progression of the replication forks and leading to stalled replication forks which would explain the observed delay in G1/S phase progression. TERRA has been shown to negatively regulate telomerase activity, which is consistent with the fact that NMD mutants have shorter telomeres (Redon et al., 2010; Askree et al., 2004).

In summary, I suggest a model where NMD regulates telomere protection and telomere maintenance through TERRA and Stn1 (Figure 39). TERRAs are bound to telomeres throughout most of the cell cycle, thereby limiting access of telomerase to telomeres and contributing to telomere capping. In S phase, TERRAs are displaced from the telomere to allow passage of the DNA replication fork. Phosphorylation of Cdc13 then allows recruitment of telomerase to telomeres through its interaction with the Est1 telomerase subunit and telomeres are elongated until dephosphorylation of Cdc13 results in interaction of Stn1 with Cdc13 and displacement of telomerase. Interaction of the CST complex with DNA polymerase then allows fill-in synthesis of the lagging strand before TERRA rebinds to the telomere. In conclusion, data presented in this work and previous data indicate an intimate connection between NMD, DNA replication, telomere protection and maintenance.

6. References

Addinall, S. G., Downey, M., Yu, M., Zubko, M. K., Dewar, J., Leake, A., Hallinan, J., Shaw, O., James, K., Wilkinson, D. J., Wipat, A., Durocher, D. and Lydall, D. (2008) 'A genomewide suppressor and enhancer analysis of cdc13-1 reveals varied cellular processes influencing telomere capping in Saccharomyces cerevisiae', *Genetics,* 180, (4), pp. 2251-66.

Addinall, S. G., Holstein, E. M., Lawless, C., Yu, M., Chapman, K., Banks, A. P., Ngo, H. P., Maringele, L., Taschuk, M., Young, A., Ciesiolka, A., Lister, A. L., Wipat, A., Wilkinson, D. J. and Lydall, D. (2011) 'Quantitative fitness analysis shows that NMD proteins and many other protein complexes suppress or enhance distinct telomere cap defects', *PLoS Genet,* 7, (4), pp. e1001362.

Admire, A., Shanks, L., Danzl, N., Wang, M., Weier, U., Stevens, W., Hunt, E. and Weinert, T. (2006) 'Cycles of chromosome instability are associated with a fragile site and are increased by defects in DNA replication and checkpoint controls in yeast', *Genes Dev,* 20, (2), pp. 159-73.

Allen, J. B., Zhou, Z., Siede, W., Friedberg, E. C. and Elledge, S. J. (1994) 'The SAD1/RAD53 protein kinase controls multiple checkpoints and DNA damage-induced transcription in yeast', *Genes Dev,* 8, (20), pp. 2401-15.

Amrani, N., Ganesan, R., Kervestin, S., Mangus, D. A., Ghosh, S. and Jacobson, A. (2004) 'A faux 3'-UTR promotes aberrant termination and triggers nonsense-mediated mRNA decay', *Nature,* 432, (7013), pp. 112-8.

Anczukow, O., Ware, M. D., Buisson, M., Zetoune, A. B., Stoppa-Lyonnet, D., Sinilnikova, O. M. and Mazoyer, S. (2008) 'Does the nonsense-mediated mRNA decay mechanism prevent the synthesis of truncated BRCA1, CHK2, and p53 proteins?', *Hum Mutat,* 29, (1), pp. 65-73.

Anderson, B. H., Kasher, P. R., Mayer, J., Szynkiewicz, M., Jenkinson, E. M., Bhaskar, S. S., Urquhart, J. E., Daly, S. B., Dickerson, J. E., O'Sullivan, J., Leibundgut, E. O., Muter, J., Abdel-Salem, G. M., Babul-Hirji, R., Baxter, P., Berger, A., Bonafe, L., Brunstom-Hernandez, J. E., Buckard, J. A., Chitayat, D., Chong, W. K., Cordelli, D. M., Ferreira, P., Fluss, J., Forrest, E. H., Franzoni, E., Garone, C., Hammans, S. R., Houge, G., Hughes, I., Jacquemont, S., Jeannet, P. Y., Jefferson, R. J., Kumar, R., Kutschke, G., Lundberg, S., Lourenco, C. M., Mehta, R., Naidu, S., Nischal, K. K., Nunes, L., Ounap, K., Philippart, M., Prabhakar, P., Risen, S. R., Schiffmann, R., Soh, C., Stephenson, J. B., Stewart, H., Stone, J., Tolmie, J. L., van der Knaap, M. S., Vieira, J. P., Vilain, C. N., Wakeling, E. L., Wermenbol, V., Whitney, A., Lovell, S. C., Meyer, S., Livingston, J. H., Baerlocher, G. M., Black, G. C., Rice, G. I. and Crow, Y. J. (2012) 'Mutations in CTC1, encoding conserved telomere maintenance component 1, cause Coats plus', *Nat Genet,* 44, (3), pp. 338-42.

Artandi, S. E. and DePinho, R. A. (2000) 'A critical role for telomeres in suppressing and facilitating carcinogenesis', *Curr Opin Genet Dev,* 10, (1), pp. 39-46.

Askree, S. H., Yehuda, T., Smolikov, S., Gurevich, R., Hawk, J., Coker, C., Krauskopf, A., Kupiec, M. and McEachern, M. J. (2004) 'A genome-wide screen for Saccharomyces cerevisiae deletion mutants that affect telomere length', *Proc Natl Acad Sci U S A,* 101, (23), pp. 8658-63.

Azzalin, C. M. and Lingner, J. (2006) 'The human RNA surveillance factor UPF1 is required for S phase progression and genome stability', *Curr Biol,* 16, (4), pp. 433-9.

Azzalin, C. M., Reichenbach, P., Khoriauli, L., Giulotto, E. and Lingner, J. (2007) 'Telomeric repeat containing RNA and RNA surveillance factors at mammalian chromosome ends', *Science,* 318, (5851), pp. 798-801.

Barnes, G. and Rio, D. (1997) 'DNA double-strand-break sensitivity, DNA replication, and cell cycle arrest phenotypes of Ku-deficient Saccharomyces cerevisiae', *Proc Natl Acad Sci U S A,* 94, (3), pp. 867-72.

Baumann, P. and Cech, T. R. (2001) 'Pot1, the putative telomere end-binding protein in fission yeast and humans', *Science,* 292, (5519), pp. 1171-5.

Beranek, D. T. (1990) 'Distribution of methyl and ethyl adducts following alkylation with monofunctional alkylating agents', *Mutat Res,* 231, (1), pp. 11-30.

Bertuch, A. A. and Lundblad, V. (2004) 'EXO1 contributes to telomere maintenance in both telomerase-proficient and telomerase-deficient Saccharomyces cerevisiae', *Genetics,* 166, (4), pp. 1651-9.

Bianchi, A., Negrini, S. and Shore, D. (2004) 'Delivery of yeast telomerase to a DNA break depends on the recruitment functions of Cdc13 and Est1', *Mol Cell,* 16, (1), pp. 139-46.

Bianchi, A. and Shore, D. (2007) 'Increased association of telomerase with short telomeres in yeast', *Genes Dev,* 21, (14), pp. 1726-30.

Biessmann, H., Carter, S. B. and Mason, J. M. (1990) 'Chromosome ends in Drosophila without telomeric DNA sequences', *Proc Natl Acad Sci U S A,* 87, (5), pp. 1758-61.

Bitterman, K. J., Medvedik, O. and Sinclair, D. A. (2003) 'Longevity regulation in Saccharomyces cerevisiae: linking metabolism, genome stability, and heterochromatin', *Microbiol Mol Biol Rev,* 67, (3), pp. 376-99, table of contents.

Blasco, M. A. (2007) 'Telomere length, stem cells and aging', *Nat Chem Biol,* 3, (10), pp. 640-9.

Bonetti, D., Martina, M., Clerici, M., Lucchini, G. and Longhese, M. P. (2009) 'Multiple pathways regulate 3' overhang generation at S. cerevisiae telomeres', *Mol Cell,* 35, (1), pp. 70-81.

Booth, C., Griffith, E., Brady, G. and Lydall, D. (2001) 'Quantitative amplification of single-stranded DNA (QAOS) demonstrates that cdc13-1 mutants generate ssDNA in a telomere to centromere direction', *Nucleic Acids Res,* 29, (21), pp. 4414-22.

Botstein, D. and Fink, G. R. (1988) 'Yeast: an experimental organism for modern biology', *Science,* 240, (4858), pp. 1439-43.

Boulton, S. J. and Jackson, S. P. (1998) 'Components of the Ku-dependent non-homologous end-joining pathway are involved in telomeric length maintenance and telomeric silencing', *Embo J,* 17, (6), pp. 1819-28.

Brumbaugh, K. M., Otterness, D. M., Geisen, C., Oliveira, V., Brognard, J., Li, X., Lejeune, F., Tibbetts, R. S., Maquat, L. E. and Abraham, R. T. (2004) 'The mRNA surveillance protein hSMG-1 functions in genotoxic stress response pathways in mammalian cells', *Mol Cell,* 14, (5), pp. 585-98.

Burge, S., Parkinson, G. N., Hazel, P., Todd, A. K. and Neidle, S. (2006) 'Quadruplex DNA: sequence, topology and structure', *Nucleic Acids Res,* 34, (19), pp. 5402-15.

Carastro, L. M., Tan, C. K., Selg, M., Jack, H. M., So, A. G. and Downey, K. M. (2002) 'Identification of delta helicase as the bovine homolog of HUPF1: demonstration of an interaction with the third subunit of DNA polymerase delta', *Nucleic Acids Res,* 30, (10), pp. 2232-43.

Casjens, S. (1999) 'Evolution of the linear DNA replicons of the Borrelia spirochetes', *Curr Opin Microbiol,* 2, (5), pp. 529-34.

Cesare, A. J., Groff-Vindman, C., Compton, S. A., McEachern, M. J. and Griffith, J. D. (2008) 'Telomere loops and homologous recombination-dependent telomeric circles in a Kluyveromyces lactis telomere mutant strain', *Mol Cell Biol,* 28, (1), pp. 20-9.

Cesare, A. J. and Reddel, R. R. (2010) 'Alternative lengthening of telomeres: models, mechanisms and implications', *Nat Rev Genet,* 11, (5), pp. 319-30.

Chai, W., Sfeir, A. J., Hoshiyama, H., Shay, J. W. and Wright, W. E. (2006) 'The involvement of the Mre11/Rad50/Nbs1 complex in the generation of G-overhangs at human telomeres', *EMBO Rep,* 7, (2), pp. 225-30.

Chan, A., Boule, J. B. and Zakian, V. A. (2008) 'Two pathways recruit telomerase to Saccharomyces cerevisiae telomeres', *PLoS Genet,* 4, (10), pp. e1000236.

Chan, S. R. and Blackburn, E. H. (2004) 'Telomeres and telomerase', *Philos Trans R Soc Lond B Biol Sci,* 359, (1441), pp. 109-21.

Chandra, A., Hughes, T. R., Nugent, C. I. and Lundblad, V. (2001) 'Cdc13 both positively and negatively regulates telomere replication', *Genes Dev,* 15, (4), pp. 404-14.

Chang, M., Bellaoui, M., Boone, C. and Brown, G. W. (2002) 'A genome-wide screen for methyl methanesulfonate-sensitive mutants reveals genes required for S phase progression in the presence of DNA damage', *Proc Natl Acad Sci U S A,* 99, (26), pp. 16934-9.

Chang, Y. F., Imam, J. S. and Wilkinson, M. F. (2007) 'The nonsense-mediated decay RNA surveillance pathway', *Annu Rev Biochem,* 76, pp. 51-74.

Chiu, S. Y., Serin, G., Ohara, O. and Maquat, L. E. (2003) 'Characterization of human Smg5/7a: a protein with similarities to Caenorhabditis elegans SMG5 and SMG7 that functions in the dephosphorylation of Upf1', *Rna,* 9, (1), pp. 77-87.

Churikov, D. and Price, C. M. (2008) 'Pot1 and cell cycle progression cooperate in telomere length regulation', *Nat Struct Mol Biol,* 15, (1), pp. 79-84.

Clerici, M., Mantiero, D., Lucchini, G. and Longhese, M. P. (2006) 'The Saccharomyces cerevisiae Sae2 protein negatively regulates DNA damage checkpoint signalling', *EMBO Rep,* 7, (2), pp. 212-8.

Conrad, M. N., Wright, J. H., Wolf, A. J. and Zakian, V. A. (1990) 'RAP1 protein interacts with yeast telomeres in vivo: overproduction alters telomere structure and decreases chromosome stability', *Cell,* 63, (4), pp. 739-50.

Cooper, J. P., Nimmo, E. R., Allshire, R. C. and Cech, T. R. (1997) 'Regulation of telomere length and function by a Myb-domain protein in fission yeast', *Nature,* 385, (6618), pp. 744-7.

Crabbe, L., Verdun, R. E., Haggblom, C. I. and Karlseder, J. (2004) 'Defective telomere lagging strand synthesis in cells lacking WRN helicase activity', *Science,* 306, (5703), pp. 1951-3.

Cross, F. R. (1997) "Marker swap' plasmids: convenient tools for budding yeast molecular genetics', *Yeast,* 13, (7), pp. 647-53.

Cui, Y., Hagan, K. W., Zhang, S. and Peltz, S. W. (1995) 'Identification and characterization of genes that are required for the accelerated degradation of mRNAs containing a premature translational termination codon', *Genes Dev,* 9, (4), pp. 423-36.

Czaplinski, K., Ruiz-Echevarria, M. J., Paushkin, S. V., Han, X., Weng, Y., Perlick, H. A., Dietz, H. C., Ter-Avanesyan, M. D. and Peltz, S. W. (1998) 'The surveillance complex interacts with the translation release factors to enhance termination and degrade aberrant mRNAs', *Genes Dev,* 12, (11), pp. 1665-77.

d'Adda di Fagagna, F., Reaper, P. M., Clay-Farrace, L., Fiegler, H., Carr, P., Von Zglinicki, T., Saretzki, G., Carter, N. P. and Jackson, S. P. (2003) 'A DNA damage checkpoint response in telomere-initiated senescence', *Nature,* 426, (6963), pp. 194-8.

Dahlseid, J. N., Lew-Smith, J., Lelivelt, M. J., Enomoto, S., Ford, A., Desruisseaux, M., McClellan, M., Lue, N., Culbertson, M. R. and Berman, J. (2003) 'mRNAs encoding telomerase components and regulators are controlled by UPF genes in Saccharomyces cerevisiae', *Eukaryot Cell,* 2, (1), pp. 134-42.

Davey, C. A., Sargent, D. F., Luger, K., Maeder, A. W. and Richmond, T. J. (2002) 'Solvent mediated interactions in the structure of the nucleosome core particle at 1.9 a resolution', *J Mol Biol,* 319, (5), pp. 1097-113.

de Bruin, D., Zaman, Z., Liberatore, R. A. and Ptashne, M. (2001) 'Telomere looping permits gene activation by a downstream UAS in yeast', *Nature,* 409, (6816), pp. 109-13.

de Lange, T. (2005) 'Shelterin: the protein complex that shapes and safeguards human telomeres', *Genes Dev,* 19, (18), pp. 2100-10.

Denchi, E. L. and de Lange, T. (2007) 'Protection of telomeres through independent control of ATM and ATR by TRF2 and POT1', *Nature,* 448, (7157), pp. 1068-71.

DePinho, R. A. (2000) 'The age of cancer', *Nature,* 408, (6809), pp. 248-54.

Desany, B. A., Alcasabas, A. A., Bachant, J. B. and Elledge, S. J. (1998) 'Recovery from DNA replicational stress is the essential function of the S-phase checkpoint pathway', *Genes Dev,* 12, (18), pp. 2956-70.

Dewar, J. M. and Lydall, D. (2010) 'Pif1- and Exo1-dependent nucleases coordinate checkpoint activation following telomere uncapping', *EMBO J,* 29, (23), pp. 4020-34.

Diede, S. J. and Gottschling, D. E. (1999) 'Telomerase-mediated telomere addition in vivo requires DNA primase and DNA polymerases alpha and delta', *Cell,* 99, (7), pp. 723-33.

Diffley, J. F. and Labib, K. (2002) 'The chromosome replication cycle', *J Cell Sci,* 115, (Pt 5), pp. 869-72.

Ding, J., Hayashi, M. K., Zhang, Y., Manche, L., Krainer, A. R. and Xu, R. M. (1999) 'Crystal structure of the two-RRM domain of hnRNP A1 (UP1) complexed with single-stranded telomeric DNA', *Genes Dev,* 13, (9), pp. 1102-15.

Ebrahimi, H. and Donaldson, A. D. (2008) 'Release of yeast telomeres from the nuclear periphery is triggered by replication and maintained by suppression of Ku-mediated anchoring', *Genes Dev,* 22, (23), pp. 3363-74.

Enomoto, S., Glowczewski, L., Lew-Smith, J. and Berman, J. G. (2004) 'Telomere cap components influence the rate of senescence in telomerase-deficient yeast cells', *Mol Cell Biol,* 24, (2), pp. 837-45.

Eulalio, A., Behm-Ansmant, I. and Izaurralde, E. (2007) 'P bodies: at the crossroads of post-transcriptional pathways', *Nat Rev Mol Cell Biol,* 8, (1), pp. 9-22.

Evans, S. K. and Lundblad, V. (2000) 'Positive and negative regulation of telomerase access to the telomere', *J Cell Sci,* 113 Pt 19, pp. 3357-64.

Falck, J., Coates, J. and Jackson, S. P. (2005) 'Conserved modes of recruitment of ATM, ATR and DNA-PKcs to sites of DNA damage', *Nature,* 434, (7033), pp. 605-11.

Fasullo, M. and Sun, M. (2008) 'The Saccharomyces cerevisiae checkpoint genes RAD9, CHK1 and PDS1 are required for elevated homologous recombination in a mec1 (ATR) hypomorphic mutant', *Cell Cycle,* 7, (15), pp. 2418-26.

Faure, V., Coulon, S., Hardy, J. and Geli, V. (2010) 'Cdc13 and telomerase bind through different mechanisms at the lagging- and leading-strand telomeres', *Mol Cell,* 38, (6), pp. 842-52.

Feldmann, H. and Winnacker, E. L. (1993) 'A putative homologue of the human autoantigen Ku from Saccharomyces cerevisiae', *J Biol Chem,* 268, (17), pp. 12895-900.

Fellerhoff, B., Eckardt-Schupp, F. and Friedl, A. A. (2000) 'Subtelomeric repeat amplification is associated with growth at elevated temperature in yku70 mutants of Saccharomyces cerevisiae', *Genetics,* 154, (3), pp. 1039-51.

Feuerhahn, S., Iglesias, N., Panza, A., Porro, A. and Lingner, J. (2010) 'TERRA biogenesis, turnover and implications for function', *FEBS Lett,* 584, (17), pp. 3812-8.

Fisher, T. S., Taggart, A. K. and Zakian, V. A. (2004) 'Cell cycle-dependent regulation of yeast telomerase by Ku', *Nat Struct Mol Biol,* 11, (12), pp. 1198-205.

Flynn, R. L., Centore, R. C., O'Sullivan, R. J., Rai, R., Tse, A., Songyang, Z., Chang, S., Karlseder, J. and Zou, L. (2011) 'TERRA and hnRNPA1 orchestrate an RPA-to-POT1 switch on telomeric single-stranded DNA', *Nature,* 471, (7339), pp. 532-6.

Foiani, M., Marini, F., Gamba, D., Lucchini, G. and Plevani, P. (1994) 'The B subunit of the DNA polymerase alpha-primase complex in Saccharomyces cerevisiae executes an essential function at the initial stage of DNA replication', *Mol Cell Biol,* 14, (2), pp. 923-33.

Ford, A. S., Guan, Q., Neeno-Eckwall, E. and Culbertson, M. R. (2006) 'Ebs1p, a negative regulator of gene expression controlled by the Upf proteins in the yeast Saccharomyces cerevisiae', *Eukaryot Cell,* 5, (2), pp. 301-12.

Foster, S. S., Zubko, M. K., Guillard, S. and Lydall, D. (2006) 'MRX protects telomeric DNA at uncapped telomeres of budding yeast cdc13-1 mutants', *DNA Repair (Amst),* 5, (7), pp. 840-51.

Frantz, J. D. and Gilbert, W. (1995) 'A novel yeast gene product, G4p1, with a specific affinity for quadruplex nucleic acids', *J Biol Chem,* 270, (35), pp. 20692-7.

Frischmeyer, P. A. and Dietz, H. C. (1999) 'Nonsense-mediated mRNA decay in health and disease', *Hum Mol Genet,* 8, (10), pp. 1893-900.

Gao, H., Cervantes, R. B., Mandell, E. K., Otero, J. H. and Lundblad, V. (2007) 'RPA-like proteins mediate yeast telomere function', *Nat Struct Mol Biol,* 14, (3), pp. 208-14.

Garneau, N. L., Wilusz, J. and Wilusz, C. J. (2007) 'The highways and byways of mRNA decay', *Nat Rev Mol Cell Biol,* 8, (2), pp. 113-26.

Garvik, B., Carson, M. and Hartwell, L. (1995) 'Single-stranded DNA arising at telomeres in cdc13 mutants may constitute a specific signal for the RAD9 checkpoint', *Mol Cell Biol,* 15, (11), pp. 6128-38.

Gasparyan, H. J., Xu, L., Petreaca, R. C., Rex, A. E., Small, V. Y., Bhogal, N. S., Julius, J. A., Warsi, T. H., Bachant, J., Aparicio, O. M. and Nugent, C. I. (2009) 'Yeast telomere capping protein Stn1 overrides DNA replication control through the S phase checkpoint', *Proc Natl Acad Sci U S A,* 106, (7), pp. 2206-11.

Gelinas, A. D., Paschini, M., Reyes, F. E., Heroux, A., Batey, R. T., Lundblad, V. and Wuttke, D. S. (2009) 'Telomere capping proteins are structurally related to RPA with an additional telomere-specific domain', *Proc Natl Acad Sci U S A,* 106, (46), pp. 19298-303.

Gerald, J. N., Benjamin, J. M. and Kron, S. J. (2002) 'Robust G1 checkpoint arrest in budding yeast: dependence on DNA damage signaling and repair', *J Cell Sci,* 115, (Pt 8), pp. 1749-57.

Gilbert, C. S., Green, C. M. and Lowndes, N. F. (2001) 'Budding yeast Rad9 is an ATP-dependent Rad53 activating machine', *Mol Cell,* 8, (1), pp. 129-36.

Gilley, D., Tanaka, H. and Herbert, B. S. (2005) 'Telomere dysfunction in aging and cancer', *Int J Biochem Cell Biol,* 37, (5), pp. 1000-13.

Goldstein, A. L. and McCusker, J. H. (1999) 'Three new dominant drug resistance cassettes for gene disruption in Saccharomyces cerevisiae', *Yeast,* 15, (14), pp. 1541-53.

Goudsouzian, L. K., Tuzon, C. T. and Zakian, V. A. (2006) 'S. cerevisiae Tel1p and Mre11p are required for normal levels of Est1p and Est2p telomere association', *Mol Cell,* 24, (4), pp. 603-10.

Grandin, N., Damon, C. and Charbonneau, M. (2000) 'Cdc13 cooperates with the yeast Ku proteins and Stn1 to regulate telomerase recruitment', *Mol Cell Biol,* 20, (22), pp. 8397-408.

Grandin, N., Damon, C. and Charbonneau, M. (2001) 'Ten1 functions in telomere end protection and length regulation in association with Stn1 and Cdc13', *Embo J,* 20, (5), pp. 1173-83.

Grandin, N., Reed, S. I. and Charbonneau, M. (1997) 'Stn1, a new Saccharomyces cerevisiae protein, is implicated in telomere size regulation in association with Cdc13', *Genes Dev,* 11, (4), pp. 512-27.

Gravel, S., Larrivee, M., Labrecque, P. and Wellinger, R. J. (1998) 'Yeast Ku as a regulator of chromosomal DNA end structure', *Science,* 280, (5364), pp. 741-4.

Greenall, A., Lei, G., Swan, D. C., James, K., Wang, L., Peters, H., Wipat, A., Wilkinson, D. J. and Lydall, D. (2008) 'A genome wide analysis of the response to uncapped telomeres in budding yeast reveals a novel role for the NAD+ biosynthetic gene BNA2 in chromosome end protection', *Genome Biol,* 9, (10), pp. R146.

Greider, C. W. and Blackburn, E. H. (1985) 'Identification of a specific telomere terminal transferase activity in Tetrahymena extracts', *Cell,* 43, (2 Pt 1), pp. 405-13.

Griffith, J. D., Comeau, L., Rosenfield, S., Stansel, R. M., Bianchi, A., Moss, H. and de Lange, T. (1999) 'Mammalian telomeres end in a large duplex loop', *Cell,* 97, (4), pp. 503-14.

Grossi, S., Puglisi, A., Dmitriev, P. V., Lopes, M. and Shore, D. (2004) 'Pol12, the B subunit of DNA polymerase alpha, functions in both telomere capping and length regulation', *Genes Dev,* 18, (9), pp. 992-1006.

Groth, A., Rocha, W., Verreault, A. and Almouzni, G. (2007) 'Chromatin challenges during DNA replication and repair', *Cell,* 128, (4), pp. 721-33.

Gu, P., Min, J. N., Wang, Y., Huang, C., Peng, T., Chai, W. and Chang, S. (2012) 'CTC1 deletion results in defective telomere replication, leading to catastrophic telomere loss and stem cell exhaustion', *EMBO J.*

Haber, J. E. (2000a) 'Lucky breaks: analysis of recombination in Saccharomyces', *Mutat Res,* 451, (1-2), pp. 53-69.

Haber, J. E. (2000b) 'Partners and pathwaysrepairing a double-strand break', *Trends Genet,* 16, (6), pp. 259-64.

Hackett, J. A. and Greider, C. W. (2003) 'End resection initiates genomic instability in the absence of telomerase', *Mol Cell Biol,* 23, (23), pp. 8450-61.

Hall, G. W. and Thein, S. (1994) 'Nonsense codon mutations in the terminal exon of the beta-globin gene are not associated with a reduction in beta-mRNA accumulation: a mechanism for the phenotype of dominant beta-thalassemia', *Blood,* 83, (8), pp. 2031-7.

Hammet, A., Magill, C., Heierhorst, J. and Jackson, S. P. (2007) 'Rad9 BRCT domain interaction with phosphorylated H2AX regulates the G1 checkpoint in budding yeast', *EMBO Rep,* 8, (9), pp. 851-7.

Hanway, D., Chin, J. K., Xia, G., Oshiro, G., Winzeler, E. A. and Romesberg, F. E. (2002) 'Previously uncharacterized genes in the UV- and MMS-induced DNA damage response in yeast', *Proc Natl Acad Sci U S A,* 99, (16), pp. 10605-10.

Hardy, C. F., Sussel, L. and Shore, D. (1992) 'A RAP1-interacting protein involved in transcriptional silencing and telomere length regulation', *Genes Dev,* 6, (5), pp. 801-14.

Hartman, J. L. t. and Tippery, N. P. (2004) 'Systematic quantification of gene interactions by phenotypic array analysis', *Genome Biol,* 5, (7), pp. R49.

Hayashi, N. and Murakami, S. (2002) 'STM1, a gene which encodes a guanine quadruplex binding protein, interacts with CDC13 in Saccharomyces cerevisiae', *Mol Genet Genomics,* 267, (6), pp. 806-13.

He, F., Li, X., Spatrick, P., Casillo, R., Dong, S. and Jacobson, A. (2003) 'Genome-wide analysis of mRNAs regulated by the nonsense-mediated and 5' to 3' mRNA decay pathways in yeast', *Mol Cell,* 12, (6), pp. 1439-52.

Hediger, F., Neumann, F. R., Van Houwe, G., Dubrana, K. and Gasser, S. M. (2002) 'Live imaging of telomeres: yKu and Sir proteins define redundant telomere-anchoring pathways in yeast', *Curr Biol,* 12, (24), pp. 2076-89.

Hefferin, M. L. and Tomkinson, A. E. (2005) 'Mechanism of DNA double-strand break repair by non-homologous end joining', *DNA Repair (Amst),* 4, (6), pp. 639-48.

Hershman, S. G., Chen, Q., Lee, J. Y., Kozak, M. L., Yue, P., Wang, L. S. and Johnson, F. B. (2008) 'Genomic distribution and functional analyses of potential G-quadruplex-forming sequences in Saccharomyces cerevisiae', *Nucleic Acids Res,* 36, (1), pp. 144-56.

Hirano, Y. and Sugimoto, K. (2007) 'Cdc13 telomere capping decreases Mec1 association but does not affect Tel1 association with DNA ends', *Mol Biol Cell,* 18, (6), pp. 2026-36.

Hockemeyer, D., Daniels, J. P., Takai, H. and de Lange, T. (2006) 'Recent expansion of the telomeric complex in rodents: Two distinct POT1 proteins protect mouse telomeres', *Cell,* 126, (1), pp. 63-77.

Holbrook, J. A., Neu-Yilik, G., Hentze, M. W. and Kulozik, A. E. (2004) 'Nonsense-mediated decay approaches the clinic', *Nat Genet,* 36, (8), pp. 801-8.

Houghtaling, B. R., Cuttonaro, L., Chang, W. and Smith, S. (2004) 'A dynamic molecular link between the telomere length regulator TRF1 and the chromosome end protector TRF2', *Curr Biol,* 14, (18), pp. 1621-31.

Huffman, K. E., Levene, S. D., Tesmer, V. M., Shay, J. W. and Wright, W. E. (2000) 'Telomere shortening is proportional to the size of the G-rich telomeric 3'-overhang', *J Biol Chem,* 275, (26), pp. 19719-22.

Hug, N. and Lingner, J. (2006) 'Telomere length homeostasis', *Chromosoma,* 115, (6), pp. 413-25.

Hughes, T. R., Weilbaecher, R. G., Walterscheid, M. and Lundblad, V. (2000) 'Identification of the single-strand telomeric DNA binding domain of the Saccharomyces cerevisiae Cdc13 protein', *Proc Natl Acad Sci U S A,* 97, (12), pp. 6457-62.

Iftode, C., Daniely, Y. and Borowiec, J. A. (1999) 'Replication protein A (RPA): the eukaryotic SSB', *Crit Rev Biochem Mol Biol,* 34, (3), pp. 141-80.

Javaheri, A., Wysocki, R., Jobin-Robitaille, O., Altaf, M., Cote, J. and Kron, S. J. (2006) 'Yeast G1 DNA damage checkpoint regulation by H2A phosphorylation is independent of chromatin remodeling', *Proc Natl Acad Sci U S A,* 103, (37), pp. 13771-6.

Jia, X., Weinert, T. and Lydall, D. (2004) 'Mec1 and Rad53 inhibit formation of single-stranded DNA at telomeres of Saccharomyces cerevisiae cdc13-1 mutants', *Genetics,* 166, (2), pp. 753-64.

Johnston, S. D., Lew, J. E. and Berman, J. (1999) 'Gbp1p, a protein with RNA recognition motifs, binds single-stranded telomeric DNA and changes its binding specificity upon dimerization', *Mol Cell Biol,* 19, (1), pp. 923-33.

Kelleher, C., Kurth, I. and Lingner, J. (2005) 'Human protection of telomeres 1 (POT1) is a negative regulator of telomerase activity in vitro', *Mol Cell Biol,* 25, (2), pp. 808-18.

Keller, R. B., Gagne, K. E., Usmani, G. N., Asdourian, G. K., Williams, D. A., Hofmann, I. and Agarwal, S. (2012) 'CTC1 Mutations in a patient with dyskeratosis congenita', *Pediatr Blood Cancer*.

Kerr, T. P., Sewry, C. A., Robb, S. A. and Roberts, R. G. (2001) 'Long mutant dystrophins and variable phenotypes: evasion of nonsense-mediated decay?', *Hum Genet,* 109, (4), pp. 402-7.

Kim, S. H., Kaminker, P. and Campisi, J. (1999) 'TIN2, a new regulator of telomere length in human cells', *Nat Genet,* 23, (4), pp. 405-12.

Koc, A., Wheeler, L. J., Mathews, C. K. and Merrill, G. F. (2004) 'Hydroxyurea arrests DNA replication by a mechanism that preserves basal dNTP pools', *J Biol Chem,* 279, (1), pp. 223-30.

Larrivee, M., LeBel, C. and Wellinger, R. J. (2004) 'The generation of proper constitutive G-tails on yeast telomeres is dependent on the MRX complex', *Genes Dev,* 18, (12), pp. 1391-6.

Larrivee, M. and Wellinger, R. J. (2006) 'Telomerase- and capping-independent yeast survivors with alternate telomere states', *Nat Cell Biol,* 8, (7), pp. 741-7.

Leeds, P., Wood, J. M., Lee, B. S. and Culbertson, M. R. (1992) 'Gene products that promote mRNA turnover in Saccharomyces cerevisiae', *Mol Cell Biol,* 12, (5), pp. 2165-77.

Lejeune, F. and Maquat, L. E. (2005) 'Mechanistic links between nonsense-mediated mRNA decay and pre-mRNA splicing in mammalian cells', *Curr Opin Cell Biol,* 17, (3), pp. 309-15.

Lendvay, T. S., Morris, D. K., Sah, J., Balasubramanian, B. and Lundblad, V. (1996) 'Senescence mutants of Saccharomyces cerevisiae with a defect in telomere replication identify three additional EST genes', *Genetics,* 144, (4), pp. 1399-412.

Levy, D. L. and Blackburn, E. H. (2004) 'Counting of Rif1p and Rif2p on Saccharomyces cerevisiae telomeres regulates telomere length', *Mol Cell Biol,* 24, (24), pp. 10857-67.

Lew, J. E., Enomoto, S. and Berman, J. (1998) 'Telomere length regulation and telomeric chromatin require the nonsense-mediated mRNA decay pathway', *Mol Cell Biol,* 18, (10), pp. 6121-30.

Li, B. and de Lange, T. (2003) 'Rap1 affects the length and heterogeneity of human telomeres', *Mol Biol Cell,* 14, (12), pp. 5060-8.

Li, S., Makovets, S., Matsuguchi, T., Blethrow, J. D., Shokat, K. M. and Blackburn, E. H. (2009) 'Cdk1-dependent phosphorylation of Cdc13 coordinates telomere elongation during cell-cycle progression', *Cell,* 136, (1), pp. 50-61.

Lin, J. J. and Zakian, V. A. (1994) 'Isolation and characterization of two Saccharomyces cerevisiae genes that encode proteins that bind to (TG1-3)n single strand telomeric DNA in vitro', *Nucleic Acids Res,* 22, (23), pp. 4906-13.

Lin, Y. S., Kieser, H. M., Hopwood, D. A. and Chen, C. W. (1993) 'The chromosomal DNA of Streptomyces lividans 66 is linear', *Mol Microbiol,* 10, (5), pp. 923-33.

Linger, B. R. and Price, C. M. (2009) 'Conservation of telomere protein complexes: shuffling through evolution', *Crit Rev Biochem Mol Biol,* 44, (6), pp. 434-46.

Lingner, J., Cech, T. R., Hughes, T. R. and Lundblad, V. (1997a) 'Three Ever Shorter Telomere (EST) genes are dispensable for in vitro yeast telomerase activity', *Proc Natl Acad Sci U S A,* 94, (21), pp. 11190-5.

Lingner, J., Hughes, T. R., Shevchenko, A., Mann, M., Lundblad, V. and Cech, T. R. (1997b) 'Reverse transcriptase motifs in the catalytic subunit of telomerase', *Science,* 276, (5312), pp. 561-7.

Liu, D., O'Connor, M. S., Qin, J. and Songyang, Z. (2004a) 'Telosome, a mammalian telomere-associated complex formed by multiple telomeric proteins', *J Biol Chem,* 279, (49), pp. 51338-42.

Liu, D., Safari, A., O'Connor, M. S., Chan, D. W., Laegeler, A., Qin, J. and Songyang, Z. (2004b) 'PTOP interacts with POT1 and regulates its localization to telomeres', *Nat Cell Biol,* 6, (7), pp. 673-80.

Loayza, D. and De Lange, T. (2003) 'POT1 as a terminal transducer of TRF1 telomere length control', *Nature,* 423, (6943), pp. 1013-8.

Longhese, M. P., Mantiero, D. and Clerici, M. (2006) 'The cellular response to chromosome breakage', *Mol Microbiol,* 60, (5), pp. 1099-108.

Longhese, M. P., Paciotti, V., Neecke, H. and Lucchini, G. (2000) 'Checkpoint proteins influence telomeric silencing and length maintenance in budding yeast', *Genetics,* 155, (4), pp. 1577-91.

Longtine, M. S., McKenzie, A., 3rd, Demarini, D. J., Shah, N. G., Wach, A., Brachat, A., Philippsen, P. and Pringle, J. R. (1998) 'Additional modules for versatile and economical PCR-based gene deletion and modification in Saccharomyces cerevisiae', *Yeast,* 14, (10), pp. 953-61.

Louis, E. J. (1995) 'The chromosome ends of Saccharomyces cerevisiae', *Yeast,* 11, (16), pp. 1553-73.

Luger, K., Mader, A. W., Richmond, R. K., Sargent, D. F. and Richmond, T. J. (1997) 'Crystal structure of the nucleosome core particle at 2.8 A resolution', *Nature,* 389, (6648), pp. 251-60.

Luke, B., Azzalin, C. M., Hug, N., Deplazes, A., Peter, M. and Lingner, J. (2007) 'Saccharomyces cerevisiae Ebs1p is a putative ortholog of human Smg7 and promotes nonsense-mediated mRNA decay', *Nucleic Acids Res,* 35, (22), pp. 7688-97.

Luke, B. and Lingner, J. (2009) 'TERRA: telomeric repeat-containing RNA', *EMBO J,* 28, (17), pp. 2503-10.

Lundblad, V. and Blackburn, E. H. (1993) 'An alternative pathway for yeast telomere maintenance rescues est1- senescence', *Cell,* 73, (2), pp. 347-60.

Lundblad, V. and Szostak, J. W. (1989) 'A mutant with a defect in telomere elongation leads to senescence in yeast', *Cell,* 57, (4), pp. 633-43.

Lustig, A. J. and Petes, T. D. (1986) 'Identification of yeast mutants with altered telomere structure', *Proc Natl Acad Sci U S A,* 83, (5), pp. 1398-402.

Lydall, D. and Weinert, T. (1995) 'Yeast checkpoint genes in DNA damage processing: implications for repair and arrest', *Science,* 270, (5241), pp. 1488-91.

Lykke-Andersen, J., Shu, M. D. and Steitz, J. A. (2000) 'Human Upf proteins target an mRNA for nonsense-mediated decay when bound downstream of a termination codon', *Cell,* 103, (7), pp. 1121-31.

Majka, J., Binz, S. K., Wold, M. S. and Burgers, P. M. (2006) 'Replication protein A directs loading of the DNA damage checkpoint clamp to 5'-DNA junctions', *J Biol Chem,* 281, (38), pp. 27855-61.

Makovets, S., Herskowitz, I. and Blackburn, E. H. (2004) 'Anatomy and dynamics of DNA replication fork movement in yeast telomeric regions', *Mol Cell Biol,* 24, (9), pp. 4019-31.

Mangus, D. A., Evans, M. C. and Jacobson, A. (2003) 'Poly(A)-binding proteins: multifunctional scaffolds for the post-transcriptional control of gene expression', *Genome Biol,* 4, (7), pp. 223.

Marcand, S., Wotton, D., Gilson, E. and Shore, D. (1997) 'Rap1p and telomere length regulation in yeast', *Ciba Found Symp,* 211, pp. 76-93; discussion 93-103.

Maringele, L. and Lydall, D. (2002) 'EXO1-dependent single-stranded DNA at telomeres activates subsets of DNA damage and spindle checkpoint pathways in budding yeast yku70Delta mutants', *Genes Dev,* 16, (15), pp. 1919-33.

Mendell, J. T., Sharifi, N. A., Meyers, J. L., Martinez-Murillo, F. and Dietz, H. C. (2004) 'Nonsense surveillance regulates expression of diverse classes of mammalian transcripts and mutes genomic noise', *Nat Genet,* 36, (10), pp. 1073-8.

Mimitou, E. P. and Symington, L. S. (2008) 'Sae2, Exo1 and Sgs1 collaborate in DNA double-strand break processing', *Nature,* 455, (7214), pp. 770-4.

Mitchell, M. T., Smith, J. S., Mason, M., Harper, S., Speicher, D. W., Johnson, F. B. and Skordalakes, E. (2010) 'Cdc13 N-terminal dimerization, DNA binding, and telomere length regulation', *Mol Cell Biol,* 30, (22), pp. 5325-34.

Mitton-Fry, R. M., Anderson, E. M., Hughes, T. R., Lundblad, V. and Wuttke, D. S. (2002) 'Conserved structure for single-stranded telomeric DNA recognition', *Science,* 296, (5565), pp. 145-7.

Miyake, Y., Nakamura, M., Nabetani, A., Shimamura, S., Tamura, M., Yonehara, S., Saito, M. and Ishikawa, F. (2009) 'RPA-like mammalian Ctc1-Stn1-Ten1 complex binds to

single-stranded DNA and protects telomeres independently of the Pot1 pathway', *Mol Cell,* 36, (2), pp. 193-206.

Miyoshi, T., Kanoh, J., Saito, M. and Ishikawa, F. (2008) 'Fission yeast Pot1-Tpp1 protects telomeres and regulates telomere length', *Science,* 320, (5881), pp. 1341-4.

Moser, B. A., Subramanian, L., Chang, Y. T., Noguchi, C., Noguchi, E. and Nakamura, T. M. (2009) 'Differential arrival of leading and lagging strand DNA polymerases at fission yeast telomeres', *EMBO J,* 28, (7), pp. 810-20.

Muhlrad, D. and Parker, R. (1999) 'Aberrant mRNAs with extended 3' UTRs are substrates for rapid degradation by mRNA surveillance', *RNA,* 5, (10), pp. 1299-307.

Murakami-Sekimata, A., Huang, D., Piening, B. D., Bangur, C. and Paulovich, A. G. (2010) 'The Saccharomyces cerevisiae RAD9, RAD17 and RAD24 genes are required for suppression of mutagenic post-replicative repair during chronic DNA damage', *DNA Repair (Amst),* 9, (7), pp. 824-34.

Murnane, J. P. (2006) 'Telomeres and chromosome instability', *DNA Repair (Amst),* 5, (9-10), pp. 1082-92.

Nakada, D., Shimomura, T., Matsumoto, K. and Sugimoto, K. (2003) 'The ATM-related Tel1 protein of Saccharomyces cerevisiae controls a checkpoint response following phleomycin treatment', *Nucleic Acids Res,* 31, (6), pp. 1715-24.

Nakamura, M., Masutomi, K., Kyo, S., Hashimoto, M., Maida, Y., Kanaya, T., Tanaka, M., Hahn, W. C. and Inoue, M. (2005) 'Efficient inhibition of human telomerase reverse transcriptase expression by RNA interference sensitizes cancer cells to ionizing radiation and chemotherapy', *Hum Gene Ther,* 16, (7), pp. 859-68.

Nautiyal, S., DeRisi, J. L. and Blackburn, E. H. (2002) 'The genome-wide expression response to telomerase deletion in Saccharomyces cerevisiae', *Proc Natl Acad Sci U S A,* 99, (14), pp. 9316-21.

Nelson, L. D., Musso, M. and Van Dyke, M. W. (2000) 'The yeast STM1 gene encodes a purine motif triple helical DNA-binding protein', *J Biol Chem,* 275, (8), pp. 5573-81.

Ngo, H. P. and Lydall, D. (2010) 'Survival and growth of yeast without telomere capping by Cdc13 in the absence of Sgs1, Exo1, and Rad9', *PLoS Genet,* 6, (8), pp. e1001072.

Noensie, E. N. and Dietz, H. C. (2001) 'A strategy for disease gene identification through nonsense-mediated mRNA decay inhibition', *Nat Biotechnol,* 19, (5), pp. 434-9.

Nott, A., Le Hir, H. and Moore, M. J. (2004) 'Splicing enhances translation in mammalian cells: an additional function of the exon junction complex', *Genes Dev,* 18, (2), pp. 210-22.

Nugent, C. I., Hughes, T. R., Lue, N. F. and Lundblad, V. (1996) 'Cdc13p: a single-strand telomeric DNA-binding protein with a dual role in yeast telomere maintenance', *Science,* 274, (5285), pp. 249-52.

Nugent, C. I. and Lundblad, V. (1998) 'The telomerase reverse transcriptase: components and regulation', *Genes Dev,* 12, (8), pp. 1073-85.

Ohnishi, T., Yamashita, A., Kashima, I., Schell, T., Anders, K. R., Grimson, A., Hachiya, T., Hentze, M. W., Anderson, P. and Ohno, S. (2003) 'Phosphorylation of hUPF1 induces formation of mRNA surveillance complexes containing hSMG-5 and hSMG-7', *Mol Cell,* 12, (5), pp. 1187-200.

Pang, D., Yoo, S., Dynan, W. S., Jung, M. and Dritschilo, A. (1997) 'Ku proteins join DNA fragments as shown by atomic force microscopy', *Cancer Res,* 57, (8), pp. 1412-5.

Parker, R. and Song, H. (2004) 'The enzymes and control of eukaryotic mRNA turnover', *Nat Struct Mol Biol,* 11, (2), pp. 121-7.

Parkinson, G. N., Lee, M. P. and Neidle, S. (2002) 'Crystal structure of parallel quadruplexes from human telomeric DNA', *Nature,* 417, (6891), pp. 876-80.

Paulovich, A. G. and Hartwell, L. H. (1995) 'A checkpoint regulates the rate of progression through S phase in S. cerevisiae in response to DNA damage', *Cell,* 82, (5), pp. 841-7.

Paulovich, A. G., Margulies, R. U., Garvik, B. M. and Hartwell, L. H. (1997) 'RAD9, RAD17, and RAD24 are required for S phase regulation in Saccharomyces cerevisiae in response to DNA damage', *Genetics,* 145, (1), pp. 45-62.

Pennock, E., Buckley, K. and Lundblad, V. (2001) 'Cdc13 delivers separate complexes to the telomere for end protection and replication', *Cell,* 104, (3), pp. 387-96.

Perlick, H. A., Medghalchi, S. M., Spencer, F. A., Kendzior, R. J., Jr. and Dietz, H. C. (1996) 'Mammalian orthologues of a yeast regulator of nonsense transcript stability', *Proc Natl Acad Sci U S A,* 93, (20), pp. 10928-32.

Perrin-Vidoz, L., Sinilnikova, O. M., Stoppa-Lyonnet, D., Lenoir, G. M. and Mazoyer, S. (2002) 'The nonsense-mediated mRNA decay pathway triggers degradation of most BRCA1 mRNAs bearing premature termination codons', *Hum Mol Genet,* 11, (23), pp. 2805-14.

Peterson, S. E., Stellwagen, A. E., Diede, S. J., Singer, M. S., Haimberger, Z. W., Johnson, C. O., Tzoneva, M. and Gottschling, D. E. (2001) 'The function of a stem-loop in telomerase RNA is linked to the DNA repair protein Ku', *Nat Genet,* 27, (1), pp. 64-7.

Petreaca, R. C., Chiu, H. C., Eckelhoefer, H. A., Chuang, C., Xu, L. and Nugent, C. I. (2006) 'Chromosome end protection plasticity revealed by Stn1p and Ten1p bypass of Cdc13p', *Nat Cell Biol,* 8, (7), pp. 748-55.

Petreaca, R. C., Chiu, H. C. and Nugent, C. I. (2007) 'The role of Stn1p in Saccharomyces cerevisiae telomere capping can be separated from its interaction with Cdc13p', *Genetics,* 177, (3), pp. 1459-74.

Pfeiffer, V. and Lingner, J. (2012) 'TERRA Promotes Telomere Shortening through Exonuclease 1-Mediated Resection of Chromosome Ends', *PLoS Genet,* 8, (6), pp. e1002747.

Pitts, S. A., Kullar, H. S., Stankovic, T., Stewart, G. S., Last, J. I., Bedenham, T., Armstrong, S. J., Piane, M., Chessa, L., Taylor, A. M. and Byrd, P. J. (2001) 'hMRE11: genomic structure and a null mutation identified in a transcript protected from nonsense-mediated mRNA decay', *Hum Mol Genet,* 10, (11), pp. 1155-62.

Polo, S. E. and Almouzni, G. (2006) 'Chromatin assembly: a basic recipe with various flavours', *Curr Opin Genet Dev,* 16, (2), pp. 104-11.

Polotnianka, R. M., Li, J. and Lustig, A. J. (1998) 'The yeast Ku heterodimer is essential for protection of the telomere against nucleolytic and recombinational activities', *Curr Biol,* 8, (14), pp. 831-4.

Porro, A., Feuerhahn, S., Reichenbach, P. and Lingner, J. (2010) 'Molecular dissection of telomeric repeat-containing RNA biogenesis unveils the presence of distinct and multiple regulatory pathways', *Mol Cell Biol,* 30, (20), pp. 4808-17.

Porter, S. E., Greenwell, P. W., Ritchie, K. B. and Petes, T. D. (1996) 'The DNA-binding protein Hdf1p (a putative Ku homologue) is required for maintaining normal telomere length in Saccharomyces cerevisiae', *Nucleic Acids Res,* 24, (4), pp. 582-5.

Price, C. M., Boltz, K. A., Chaiken, M. F., Stewart, J. A., Beilstein, M. A. and Shippen, D. E. (2010) 'Evolution of CST function in telomere maintenance', *Cell Cycle,* 9, (16), pp. 3157-65.

Pryde, F. E. and Louis, E. J. (1997) 'Saccharomyces cerevisiae telomeres. A review', *Biochemistry (Mosc),* 62, (11), pp. 1232-41.

Puglisi, A., Bianchi, A., Lemmens, L., Damay, P. and Shore, D. (2008) 'Distinct roles for yeast Stn1 in telomere capping and telomerase inhibition', *EMBO J,* 27, (17), pp. 2328-39.

Qi, H. and Zakian, V. A. (2000) 'The Saccharomyces telomere-binding protein Cdc13p interacts with both the catalytic subunit of DNA polymerase alpha and the telomerase-associated est1 protein', *Genes Dev,* 14, (14), pp. 1777-88.

Qian, W., Wang, J., Jin, N. N., Fu, X. H., Lin, Y. C., Lin, J. J. and Zhou, J. Q. (2009) 'Ten1p promotes the telomeric DNA-binding activity of Cdc13p: implication for its function in telomere length regulation', *Cell Res,* 19, (7), pp. 849-63.

Ramsden, D. A. and Gellert, M. (1998) 'Ku protein stimulates DNA end joining by mammalian DNA ligases: a direct role for Ku in repair of DNA double-strand breaks', *EMBO J,* 17, (2), pp. 609-14.

Reddy, J. C., Morris, J. C., Wang, J., English, M. A., Haber, D. A., Shi, Y. and Licht, J. D. (1995) 'WT1-mediated transcriptional activation is inhibited by dominant negative mutant proteins', *J Biol Chem,* 270, (18), pp. 10878-84.

Redon, S., Reichenbach, P. and Lingner, J. (2010) 'The non-coding RNA TERRA is a natural ligand and direct inhibitor of human telomerase', *Nucleic Acids Res,* 38, (17), pp. 5797-806.

Rehwinkel, J., Letunic, I., Raes, J., Bork, P. and Izaurralde, E. (2005) 'Nonsense-mediated mRNA decay factors act in concert to regulate common mRNA targets', *RNA,* 11, (10), pp. 1530-44.

Rehwinkel, J., Raes, J. and Izaurralde, E. (2006) 'Nonsense-mediated mRNA decay: Target genes and functional diversification of effectors', *Trends Biochem Sci,* 31, (11), pp. 639-46.

Reichenbach, P., Hoss, M., Azzalin, C. M., Nabholz, M., Bucher, P. and Lingner, J. (2003) 'A human homolog of yeast Est1 associates with telomerase and uncaps chromosome ends when overexpressed', *Curr Biol,* 13, (7), pp. 568-74.

Reim, I., Stanewsky, R. and Saumweber, H. (1999) 'The puff-specific RRM protein NonA is a single-stranded nucleic acid binding protein', *Chromosoma,* 108, (3), pp. 162-72.

Riethman, H., Ambrosini, A. and Paul, S. (2005) 'Human subtelomere structure and variation', *Chromosome Res,* 13, (5), pp. 505-15.

Ritchie, K. B. and Petes, T. D. (2000) 'The Mre11p/Rad50p/Xrs2p complex and the Tel1p function in a single pathway for telomere maintenance in yeast', *Genetics,* 155, (1), pp. 475-9.

Roy, R., Meier, B., McAinsh, A. D., Feldmann, H. M. and Jackson, S. P. (2004) 'Separation-of-function mutants of yeast Ku80 reveal a Yku80p-Sir4p interaction involved in telomeric silencing', *J Biol Chem,* 279, (1), pp. 86-94.

Sabourin, M., Tuzon, C. T. and Zakian, V. A. (2007) 'Telomerase and Tel1p preferentially associate with short telomeres in S. cerevisiae', *Mol Cell,* 27, (4), pp. 550-61.

Saint Girons, I., Norris, S. J., Gobel, U., Meyer, J., Walker, E. M. and Zuerner, R. (1992) 'Genome structure of spirochetes', *Res Microbiol,* 143, (6), pp. 615-21.

Sayani, S., Janis, M., Lee, C. Y., Toesca, I. and Chanfreau, G. F. (2008) 'Widespread impact of nonsense-mediated mRNA decay on the yeast intronome', *Mol Cell,* 31, (3), pp. 360-70.

Schramke, V., Luciano, P., Brevet, V., Guillot, S., Corda, Y., Longhese, M. P., Gilson, E. and Geli, V. (2004) 'RPA regulates telomerase action by providing Est1p access to chromosome ends', *Nat Genet,* 36, (1), pp. 46-54.

Sealey, D. C., Kostic, A. D., LeBel, C., Pryde, F. and Harrington, L. (2011) 'The TPR-containing domain within Est1 homologs exhibits species-specific roles in telomerase interaction and telomere length homeostasis', *BMC Mol Biol,* 12, pp. 45.

Sen, D. and Gilbert, W. (1988) 'Formation of parallel four-stranded complexes by guanine-rich motifs in DNA and its implications for meiosis', *Nature,* 334, (6180), pp. 364-6.

Serin, G., Gersappe, A., Black, J. D., Aronoff, R. and Maquat, L. E. (2001) 'Identification and characterization of human orthologues to Saccharomyces cerevisiae Upf2 protein and Upf3 protein (Caenorhabditis elegans SMG-4)', *Mol Cell Biol,* 21, (1), pp. 209-23.

Sheth, U. and Parker, R. (2003) 'Decapping and decay of messenger RNA occur in cytoplasmic processing bodies', *Science,* 300, (5620), pp. 805-8.

Sheth, U. and Parker, R. (2006) 'Targeting of aberrant mRNAs to cytoplasmic processing bodies', *Cell,* 125, (6), pp. 1095-109.

Shiloh, Y. (2006) 'The ATM-mediated DNA-damage response: taking shape', *Trends Biochem Sci,* 31, (7), pp. 402-10.

Shin, J. S., Hong, A., Solomon, M. J. and Lee, C. S. (2006) 'The role of telomeres and telomerase in the pathology of human cancer and aging', *Pathology,* 38, (2), pp. 103-13.

Smith, C. D., Smith, D. L., DeRisi, J. L. and Blackburn, E. H. (2003) 'Telomeric protein distributions and remodeling through the cell cycle in Saccharomyces cerevisiae', *Mol Biol Cell,* 14, (2), pp. 556-70.

Smith, J. S., Chen, Q., Yatsunyk, L. A., Nicoludis, J. M., Garcia, M. S., Kranaster, R., Balasubramanian, S., Monchaud, D., Teulade-Fichou, M. P., Abramowitz, L., Schultz, D. C. and Johnson, F. B. (2011) 'Rudimentary G-quadruplex-based telomere capping in Saccharomyces cerevisiae', *Nat Struct Mol Biol,* 18, (4), pp. 478-85.

Smith, J. S. and Johnson, F. B. (2010) 'Isolation of G-quadruplex DNA using NMM-sepharose affinity chromatography', *Methods Mol Biol,* 608, pp. 207-21.

Smogorzewska, A. and de Lange, T. (2004) 'Regulation of telomerase by telomeric proteins', *Annu Rev Biochem,* 73, pp. 177-208.

Smogorzewska, A., van Steensel, B., Bianchi, A., Oelmann, S., Schaefer, M. R., Schnapp, G. and de Lange, T. (2000) 'Control of human telomere length by TRF1 and TRF2', *Mol Cell Biol,* 20, (5), pp. 1659-68.

Snow, B. E., Erdmann, N., Cruickshank, J., Goldman, H., Gill, R. M., Robinson, M. O. and Harrington, L. (2003) 'Functional conservation of the telomerase protein Est1p in humans', *Curr Biol,* 13, (8), pp. 698-704.

Stansel, R. M., de Lange, T. and Griffith, J. D. (2001) 'T-loop assembly in vitro involves binding of TRF2 near the 3' telomeric overhang', *Embo J,* 20, (19), pp. 5532-40.

Stellwagen, A. E., Haimberger, Z. W., Veatch, J. R. and Gottschling, D. E. (2003) 'Ku interacts with telomerase RNA to promote telomere addition at native and broken chromosome ends', *Genes Dev,* 17, (19), pp. 2384-95.

Stewart, G. S., Maser, R. S., Stankovic, T., Bressan, D. A., Kaplan, M. I., Jaspers, N. G., Raams, A., Byrd, P. J., Petrini, J. H. and Taylor, A. M. (1999) 'The DNA double-strand break repair gene hMRE11 is mutated in individuals with an ataxia-telangiectasia-like disorder', *Cell,* 99, (6), pp. 577-87.

Sun, J., Yu, E. Y., Yang, Y., Confer, L. A., Sun, S. H., Wan, K., Lue, N. F. and Lei, M. (2009) 'Stn1-Ten1 is an Rpa2-Rpa3-like complex at telomeres', *Genes Dev,* 23, (24), pp. 2900-14.

Surovtseva, Y. V., Churikov, D., Boltz, K. A., Song, X., Lamb, J. C., Warrington, R., Leehy, K., Heacock, M., Price, C. M. and Shippen, D. E. (2009) 'Conserved telomere maintenance component 1 interacts with STN1 and maintains chromosome ends in higher eukaryotes', *Mol Cell,* 36, (2), pp. 207-18.

Sweeney, F. D., Yang, F., Chi, A., Shabanowitz, J., Hunt, D. F. and Durocher, D. (2005) 'Saccharomyces cerevisiae Rad9 acts as a Mec1 adaptor to allow Rad53 activation', *Curr Biol,* 15, (15), pp. 1364-75.

Taddei, A. and Gasser, S. M. (2004) 'Multiple pathways for telomere tethering: functional implications of subnuclear position for heterochromatin formation', *Biochim Biophys Acta,* 1677, (1-3), pp. 120-8.

Taggart, A. K., Teng, S. C. and Zakian, V. A. (2002) 'Est1p as a cell cycle-regulated activator of telomere-bound telomerase', *Science,* 297, (5583), pp. 1023-6.

Tamaru, H. (2010) 'Confining euchromatin/heterochromatin territory: jumonji crosses the line', *Genes Dev,* 24, (14), pp. 1465-78.

Tanaka, T. and Shimizu, N. (2000) 'Induced detachment of acentric chromatin from mitotic chromosomes leads to their cytoplasmic localization at G(1) and the micronucleation by lamin reorganization at S phase', *J Cell Sci,* 113 (Pt 4), pp. 697-707.

Teixeira, M. T., Arneric, M., Sperisen, P. and Lingner, J. (2004) 'Telomere length homeostasis is achieved via a switch between telomerase- extendible and -nonextendible states', *Cell,* 117, (3), pp. 323-35.

Teng, S. C. and Zakian, V. A. (1999) 'Telomere-telomere recombination is an efficient bypass pathway for telomere maintenance in Saccharomyces cerevisiae', *Mol Cell Biol,* 19, (12), pp. 8083-93.

Teo, S. H. and Jackson, S. P. (2001) 'Telomerase subunit overexpression suppresses telomere-specific checkpoint activation in the yeast yku80 mutant', *EMBO Rep,* 2, (3), pp. 197-202.

Tercero, J. A. and Diffley, J. F. (2001) 'Regulation of DNA replication fork progression through damaged DNA by the Mec1/Rad53 checkpoint', *Nature,* 412, (6846), pp. 553-7.

Tham, W. H., Wyithe, J. S., Ko Ferrigno, P., Silver, P. A. and Zakian, V. A. (2001) 'Localization of yeast telomeres to the nuclear periphery is separable from transcriptional repression and telomere stability functions', *Mol Cell,* 8, (1), pp. 189-99.

Tomaska, L., Willcox, S., Slezakova, J., Nosek, J. and Griffith, J. D. (2004) 'Taz1 binding to a fission yeast model telomere: formation of telomeric loops and higher order structures', *J Biol Chem,* 279, (49), pp. 50764-72.

Tong, X. J., Li, Q. J., Duan, Y. M., Liu, N. N., Zhang, M. L. and Zhou, J. Q. (2011) 'Est1 protects telomeres and inhibits subtelomeric y'-element recombination', *Mol Cell Biol,* 31, (6), pp. 1263-74.

Torigoe, H. (2007) 'Fission yeast telomeric DNA binding protein Pot1 has the ability to unfold tetraplex structure of telomeric DNA', *Nucleosides Nucleotides Nucleic Acids,* 26, (10-12), pp. 1255-60.

Tsai, Y. C., Qi, H. and Liu, L. F. (2007) 'Protection of DNA ends by telomeric 3' G-tail sequences', *J Biol Chem,* 282, (26), pp. 18786-92.

Tseng, S. F., Lin, J. J. and Teng, S. C. (2006) 'The telomerase-recruitment domain of the telomere binding protein Cdc13 is regulated by Mec1p/Tel1p-dependent phosphorylation', *Nucleic Acids Res,* 34, (21), pp. 6327-36.

Tsubouchi, H. and Ogawa, H. (2000) 'Exo1 roles for repair of DNA double-strand breaks and meiotic crossing over in Saccharomyces cerevisiae', *Mol Biol Cell,* 11, (7), pp. 2221-33.

Tsukamoto, Y., Kato, J. and Ikeda, H. (1997) 'Silencing factors participate in DNA repair and recombination in Saccharomyces cerevisiae', *Nature,* 388, (6645), pp. 900-3.

Tuteja, R. and Tuteja, N. (2000) 'Ku autoantigen: a multifunctional DNA-binding protein', *Crit Rev Biochem Mol Biol,* 35, (1), pp. 1-33.

Usui, T., Ogawa, H. and Petrini, J. H. (2001) 'A DNA damage response pathway controlled by Tel1 and the Mre11 complex', *Mol Cell,* 7, (6), pp. 1255-66.

Van Dyke, M. W., Nelson, L. D., Weilbaecher, R. G. and Mehta, D. V. (2004) 'Stm1p, a G4 quadruplex and purine motif triplex nucleic acid-binding protein, interacts with ribosomes and subtelomeric Y' DNA in Saccharomyces cerevisiae', *J Biol Chem,* 279, (23), pp. 24323-33.

Veldman, T., Etheridge, K. T. and Counter, C. M. (2004) 'Loss of hPot1 function leads to telomere instability and a cut-like phenotype', *Curr Biol,* 14, (24), pp. 2264-70.

Vodenicharov, M. D., Laterreur, N. and Wellinger, R. J. (2010) 'Telomere capping in non-dividing yeast cells requires Yku and Rap1', *EMBO J,* 29, (17), pp. 3007-19.

Vodenicharov, M. D. and Wellinger, R. J. (2006) 'DNA degradation at unprotected telomeres in yeast is regulated by the CDK1 (Cdc28/Clb) cell-cycle kinase', *Mol Cell,* 24, (1), pp. 127-37.

Wan, M., Qin, J., Songyang, Z. and Liu, D. (2009) 'OB fold-containing protein 1 (OBFC1), a human homolog of yeast Stn1, associates with TPP1 and is implicated in telomere length regulation', *J Biol Chem,* 284, (39), pp. 26725-31.

Wang, S. S. and Zakian, V. A. (1990) 'Sequencing of Saccharomyces telomeres cloned using T4 DNA polymerase reveals two domains', *Mol Cell Biol,* 10, (8), pp. 4415-9.

Wang, W., Czaplinski, K., Rao, Y. and Peltz, S. W. (2001) 'The role of Upf proteins in modulating the translation read-through of nonsense-containing transcripts', *Embo J,* 20, (4), pp. 880-90.

Weinert, T. A. and Hartwell, L. H. (1993) 'Cell cycle arrest of cdc mutants and specificity of the RAD9 checkpoint', *Genetics,* 134, (1), pp. 63-80.

Weinert, T. A., Kiser, G. L. and Hartwell, L. H. (1994) 'Mitotic checkpoint genes in budding yeast and the dependence of mitosis on DNA replication and repair', *Genes Dev,* 8, (6), pp. 652-65.

Wellinger, R. J. and Sen, D. (1997) 'The DNA structures at the ends of eukaryotic chromosomes', *Eur J Cancer,* 33, (5), pp. 735-49.

Wellinger, R. J., Wolf, A. J. and Zakian, V. A. (1993) 'Saccharomyces telomeres acquire single-strand TG1-3 tails late in S phase', *Cell,* 72, (1), pp. 51-60.

Wilson, T. E., Grawunder, U. and Lieber, M. R. (1997) 'Yeast DNA ligase IV mediates non-homologous DNA end joining', *Nature,* 388, (6641), pp. 495-8.

Wold, M. S. (1997) 'Replication protein A: a heterotrimeric, single-stranded DNA-binding protein required for eukaryotic DNA metabolism', *Annu Rev Biochem,* 66, pp. 61-92.

Wolf, M., Edgren, H., Muggerud, A., Kilpinen, S., Huusko, P., Sorlie, T., Mousses, S. and Kallioniemi, O. (2005) 'NMD microarray analysis for rapid genome-wide screen of mutated genes in cancer', *Cell Oncol,* 27, (3), pp. 169-73.

Woolstencroft, R. N., Beilharz, T. H., Cook, M. A., Preiss, T., Durocher, D. and Tyers, M. (2006) 'Ccr4 contributes to tolerance of replication stress through control of CRT1 mRNA poly(A) tail length', *J Cell Sci,* 119, (Pt 24), pp. 5178-92.

Wright, W. E., Tesmer, V. M., Huffman, K. E., Levene, S. D. and Shay, J. W. (1997) 'Normal human chromosomes have long G-rich telomeric overhangs at one end', *Genes Dev,* 11, (21), pp. 2801-9.

Wu, L., Multani, A. S., He, H., Cosme-Blanco, W., Deng, Y., Deng, J. M., Bachilo, O., Pathak, S., Tahara, H., Bailey, S. M., Behringer, R. R. and Chang, S. (2006) 'Pot1 deficiency initiates DNA damage checkpoint activation and aberrant homologous recombination at telomeres', *Cell,* 126, (1), pp. 49-62.

Yarbro, J. W. (1992) 'Mechanism of action of hydroxyurea', *Semin Oncol,* 19, (3 Suppl 9), pp. 1-10.

Ye, J. Z., Donigian, J. R., van Overbeek, M., Loayza, D., Luo, Y., Krutchinsky, A. N., Chait, B. T. and de Lange, T. (2004a) 'TIN2 binds TRF1 and TRF2 simultaneously and stabilizes the TRF2 complex on telomeres', *J Biol Chem,* 279, (45), pp. 47264-71.

Ye, J. Z., Hockemeyer, D., Krutchinsky, A. N., Loayza, D., Hooper, S. M., Chait, B. T. and de Lange, T. (2004b) 'POT1-interacting protein PIP1: a telomere length regulator that recruits POT1 to the TIN2/TRF1 complex', *Genes Dev,* 18, (14), pp. 1649-54.

Zaug, A. J., Podell, E. R. and Cech, T. R. (2005) 'Human POT1 disrupts telomeric G-quadruplexes allowing telomerase extension in vitro', *Proc Natl Acad Sci U S A,* 102, (31), pp. 10864-9.

Zhang, M. L., Tong, X. J., Fu, X. H., Zhou, B. O., Wang, J., Liao, X. H., Li, Q. J., Shen, N., Ding, J. and Zhou, J. Q. (2010) 'Yeast telomerase subunit Est1p has guanine quadruplex-promoting activity that is required for telomere elongation', *Nat Struct Mol Biol,* 17, (2), pp. 202-9.

Zhou, J., Hidaka, K. and Futcher, B. (2000) 'The Est1 subunit of yeast telomerase binds the Tlc1 telomerase RNA', *Mol Cell Biol,* 20, (6), pp. 1947-55.

Zhu, Z., Chung, W. H., Shim, E. Y., Lee, S. E. and Ira, G. (2008) 'Sgs1 helicase and two nucleases Dna2 and Exo1 resect DNA double-strand break ends', *Cell,* 134, (6), pp. 981-94.

Zou, L. and Elledge, S. J. (2003) 'Sensing DNA damage through ATRIP recognition of RPA-ssDNA complexes', *Science,* 300, (5625), pp. 1542-8.

Zubko, M. K., Guillard, S. and Lydall, D. (2004) 'Exo1 and Rad24 differentially regulate generation of ssDNA at telomeres of Saccharomyces cerevisiae cdc13-1 mutants', *Genetics,* 168, (1), pp. 103-15.

Zubko, M. K., Maringele, L., Foster, S. S. and Lydall, D. (2006) 'Detecting repair intermediates in vivo: effects of DNA damage response genes on single-stranded DNA accumulation at uncapped telomeres in budding yeast', *Methods Enzymol,* 409, pp. 285-300.

7. Publications

Holstein, E.M., and Lydall, D. (in preparation). 'Control of the telomere cap by nonsense-mediated decay'.

Holstein, E. M. and Lydall, D. (in press). 'Quantitative amplification of single-stranded DNA (QAOS)', book chapter in *DNA Repair Protocols*.

Weile, J., Pocock, M., Cockell, S. J., Lord, P., Dewar, J. M., Holstein, E. M., Wilkinson, D., Lydall, D., Hallinan, J. and Wipat, A. (2011) 'Customizable views on semantically integrated networks for systems biology', *Bioinformatics,* 27, (9), pp. 1299-306.

Addinall, S. G.[8], Holstein, E. M.[*], Lawless, C.[8], Yu, M., Chapman, K., Banks, A. P., Ngo, H. P., Maringele, L., Taschuk, M., Young, A., Ciesiolka, A., Lister, A. L., Wipat, A., Wilkinson, D. J. and Lydall, D. (2011) 'Quantitative fitness analysis shows that NMD proteins and many other protein complexes suppress or enhance distinct telomere cap defects', *PLoS Genet,* 7, (4), pp. e1001362.

[8]contributed equally

Quantitative Amplification of Single Stranded DNA (QAOS)

Eva-Maria Holstein and David Lydall

Institute for Cell & Molecular Biosciences, Newcastle University, Medical School, Framlington Place, Newcastle upon Tyne, NE2 4HH, UK.

Phone: 0044 (0) 191 2225318; Email: d.a.lydall@ncl.ac.uk

Running head: QAOS

Quantitative Amplification of Single Stranded DNA (QAOS)

i. Summary

Single-stranded DNA (ssDNA) intermediates play an important role in processes such as DNA replication and homologous recombination, DNA damage responses and DNA repair. Using QAOS, ssDNA arising during various cellular processes in complex genomes can be quantified at numerous single-copy and repetitive loci. QAOS is a useful tool to gain insights into the cellular processes that involve ssDNA and the roles of proteins in regulating ssDNA production and responses to ssDNA.

ii. Key Words

QAOS, single-stranded DNA, telomere, CST, nuclease, PCR, resection

1. Introduction

Single-stranded DNA (ssDNA) intermediates occur during various normal cellular processes such as DNA replication and recombination. In addition, ssDNA is crucial for stimulating checkpoint pathways to activate cell cycle arrest in response to DNA damage and ssDNA plays an important role in DNA repair pathways (*1-3*).

Telomeres, located at the end of linear eukaryotic chromosomes, terminate in a 3' single-stranded overhang that resembles a DNA double-strand break. However, telomeres do not usually activate checkpoint or DNA repair pathways as the chromosome ends are masked by various telomere-capping proteins that bind to the telomeric ends. Examples for telomere-capping proteins are the Cdc13-Stn1-Ten1 or the Yku complex in budding yeast (*4, 5*). Loss of any of these proteins can lead to extensive ssDNA accumulation near telomere ends which in turn induces cell cycle arrest and DNA repair pathways (*1, 5-8*). Similarly, loss of the Pot1 telomere-capping protein in *Schizosaccharomyces pombe* leads to telomeric 5' resection and DNA damage checkpoint activation (*9*).

Combining telomere capping mutations (e.g. temperature-sensitive allele *cdc13-1*, null-mutant *yku70*Δ) with mutations in DNA damage response genes allows identification of the roles of the corresponding checkpoint or DNA damage repair proteins in stimulating or inhibiting production of ssDNA at uncapped telomeres and in activating cell cycle arrest (*1, 8, 10-16*).

The QAOS method described here uses qPCR to measure single-stranded DNA accumulation at various single-copy and repetitive loci near the telomeric ends in budding yeast telomere capping mutants. QAOS is a fast and reproducible approach to identify and quantify ssDNA

intermediates arising during cellular processes (*8*). QAOS should in principal work in other yeasts, bacteria and mammalian cells.

Using high quality DNA purified from yeast, QAOS is initiated by annealing of a tagging primer to ssDNA at low temperature. The tagging primer consists of a locus-specific sequence at the 3' end and an artificial sequence (tag) at the 5' end (Figure 1A). Primer extension then creates a novel tagged sequence whose amount is proportional to the initial amount of ssDNA. The hybrid sequence is amplified by qPCR at temperatures that allow binding of specific primers (Reverse and Tag), but not the initial tagging primer. A fluorescent qPCR probe that hybridizes to the target DNA is used to help quantify the ssDNA at the measured locus. The quantity of ssDNA is calculated relative to the amount of ssDNA in a reference sample (ssDNA standards), using a standard curve.

Here we describe in detail the protocol and primers to detect ssDNA on both strands of chromosome V-R and VI-L in budding yeast.

2. Materials

1. Isopropanol.

2. 70% (V/V) ethanol in water.

3. TE buffer: 10 mM Tris-HCl (pH 8.0), 1 mM EDTA.

4. Nuclei isolation buffer (NIB): 17% (V/V) glycerol, 50 mM MOPS, 150 mM potassium acetate, 2 mM $MgCl_2$, 500 µM spermidine, 150 µM spermine. For 1 litre: 170 ml glycerol, 10.463 g MOPS, 14.72 g potassium acetate, 2 ml 1 M $MgCl_2$, 0.55 ml 0.9 M spermidine (stored at -70°C), 52 mg spermine (added as dry powder); adjust to 1 litre by water, dissolve all components, adjust pH to 7.2, filter-sterilize and store in 50 ml aliquots in the dark at 4°C.

5. Sodium azide: 10% (V/V) in water, store at RT.

6. RNAse A: Dissolve pancreatic RNAse at 10 mg/ml in 0.01 M sodium acetate (pH 5.2). Place in boiling water bath for 15 min and then allow to cool to room temperature. Adjust pH by adding 0.1 volume of 1 M Tris-HCl (pH 7.4). Aliqot and store at -20°C. Do not freeze/thaw.

7. G2 with RNAse: 800 mM guanidine hydrochloride, 30 mM EDTA, 30 mM Tris-HCl, 5% Tween 20, 0.5% Triton X-100 (pH 8.0), 200 µg/ml RNAse A (1 ml of 10 mg/ml RNAse per 50 ml tube of G2, add RNAse before use. Buffer should then be stable for 6 months when stored at 4°C).

8. Proteinase K: Dissolve lyophilized powder in sterile water to a 20 mg/ml concentration and store in aliquots at -20 or -80°C.

9. QBT: 750 mM NaCl, 50 mM MOPS, 15% isopropanol, 0.15% Triton X-100 (pH 7.0).

10. QC: 1 M NaCl, 50 mM MOPS, 15% isopropanol (pH 7.0).

11. QF: 1.25 M NaCl, 50 mM Tris-HCl, 15% isopropanol (pH 8.5).

12. Ice cold acid-washed glass beads (Stratech). 0.425 to 0.6 mm in diameter, washed for 1 h in concentrated nitric acid, rinsed with milliQ water until pH is neutral, baked to dryness and stored at 4°C.

13. Qiagen Genomic Tip 20/G kit (catalogue no. 10223).

14. TaKaRa Ex Taq DNA Polymerase kit containing Ex taq DNA polymerase (5 units/µl), 10X Ex taq buffer (contains 20 mM $MgCl_2$) and dNTP Mixture (2.5 mM each dNTP).

3. Methods

This chapter is an update of the Zubko et al., 2006 protocol (*17*). In addition we describe ssDNA measurement on both strands of chromosome VII-L (Figure 1B).

Yeast cells are cultured exactly as described in the Zubko et al., 2006 protocol. In short, 25 ml yeast cell cultures containing approximately 2 x 10^7 buds/ml are collected for each DNA preparation. Cells are centrifuged for 5 min at 2000 rpm at 4°C. The pellet is resuspended in 1 ml of ice-cold sterile water and transferred to a 1.5 ml Eppendorf tube. Cells are spun for 10 s at 13200 rpm. Supernatant is discarded and pellet is frozen at -80°C until DNA extraction (*see* **Note 1**).

3.1 DNA Isolation

All steps are performed on ice unless otherwise stated.

1. Thaw cell pellet (previously kept at -80°C) on ice and re-suspend the pellet in 1.0 ml NIB.
2. Transfer the mixture to a 2 ml screw cap tube with skirt (catalogue no. 72694006, Sarstedt) and spin 8 s in a micro-centrifuge at 13200 rpm.
3. Discard supernatant and re-suspend in 600 µl of NIB by vortexing.
4. Add cold acid-washed glass beads to about 1.5 ml mark on the tube.
5. Lyse cells through repeated breakage cycles in a tissue homogenizer (Precellys24 lysis and homogenization ribolyser, Bertin technologies) for 5 s at 5500 power setting per cycle. Remove from homogenizer and place in ice-water in-between cycles (at

least 1 min). 90% cell breakage is required and breakage efficiency is examined by phase contrast microscopy (*see* **Note 2**).

6. For each lysate prepare a 1.5 ml Eppendorf tube. Remove caps and bottoms from tubes using a dog nail clipper or razor blade (Figure 2).
7. Use a 21 gauge syringe needle to puncture the bottom of Sarstedt tubes containing the cell lysate and glass beads and place the tubes securely on the top of the clipped Eppendorf tubes (Figure 2).
8. Put pairs of tubes in a round bottomed 15 ml Falcon tube (catalogue no. 352059, BD Biosciences) (Figure 2).
9. Spin in pre-cooled swing out centrifuge (CS 6R centrifuge, 2000 rpm, 2 min) (Figure 2).
10. Wash the beads twice by adding 1 ml NIB to the top of the 2 ml screw cap Sarstedt tube and spinning at 2000 rpm for 2 min.
11. Remove and discard the Sarstedt/Eppendorf pair of tubes using tweezers.
12. Vortex the 15 ml Falcon tube containing the cell debris for 2 s.
13. Remove lids from the Falcon tubes (they do not fit in the rotor. Keep them in a clean place) and spin tubes in a fixed angle F0850 rotor (containing appropriate sleeves) in a Beckman Allegra 64R centrifuge for 20 min at 6500g and 4°C.
14. Remove the supernatant by aspiration and re-suspend nuclear/cell pellet in 2 ml G2 buffer containing RNAse by vortexing.
15. Place the lids back on the tubes. Incubate at 37°C for 30 min in a water bath and mix every 10 min by gently shaking the tubes.
16. Add 50 µl of 20 mg/ml proteinase K to each tube. Incubate for one hour at 37°C and every 20 min by gently shaking the tubes.
17. Remove lids from the tubes and spin in F0850 rotor for 10 min at 6500g at 4°C.

18. While spinning add 1 ml of QBT solution to top of Qiagen 20/G columns (one for each sample) and let solution flow through the columns by gravity.
19. Place 2 ml QBT solution in new Falcon round bottomed tubes (one for each sample).
20. After spinning pour supernatant into the Falcon tubes containing the 2 ml QBT.
21. Vortex briefly and add part of the supernatant/QBT mix to top of the equilibrated Qiagen 20/G colum.
22. Discard the flow through and repeat step 21 until all supernatant/QBT mix has flown through the column.
23. Wash the column 3 times by adding 3 x 1 ml of QC solution. Discard the flow through.
24. To elute DNA, add 1 ml of 50°C pre-warmed QF solution to column and collect flow through in a fresh 15 ml Falcon.
25. Add another 1 ml of 50°C pre-warmed QF solution to column.
26. Precipitate DNA at room temperature by adding 1.4 ml of isopropanol to the Falcon tube containing the DNA eluted in QF.
27. Vortex gently and spin in F0850 rotor for 20 min at 7700g and 4°C. A small pellet is visible in most cases (*see* **Note 3**).
28. Carefully discard supernatant and remove as much liquid as possible by inverting the tube onto a paper towel for 1 minute.
29. Wash the pellet by adding 1 ml of 70% ethanol, vortex gently for 1 s.
30. Spin in F0850 rotor for 20 min at 7700g and 4°C.
31. Carefully discard supernatant and re-spin tubes for 1 min. Remove the rest of the liquid by aspiration.
32. Dissolve DNA by adding 400-600 µl TE to DNA pellet, tightly cap the tube and incubate on New Brunswick TC7 roller at 23°C overnight. Then store samples at 4°C.

33. Dilute 10 µl of each DNA prep to 90 µl of TE, vortex and leave overnight at 4°C to equilibrate. The diluted DNA will be used in 3.2 to measure yield of DNA by qPCR.

3.2 qPCR

3.2.1 Measuring Yield of DNA by qPCR

1. Measure all samples in triplicate in a 96-well PCR plate. Pipette 10 µl of each sample to the bottom of a 96-well PCR plate according to Table 1. Use TE for the no template control (NTC) and use concentrations of 0.4 ng/µl, 2 ng/µl and 4 ng/µl of genomic DNA standards (STD) (3.3.1) (*see* **Note 4**).
2. Make PCR master mix as described in Table 2. Use *PAC2* forward and reverse primers and the fluorescent probe shown in Table 3 for quantification of DNA samples.
3. Add sterile water and all primers and probes to a 2 ml screw cap Eppendorf tube and incubate at 95^{o}C for 5 min. Place on ice water for 3 min.
4. Add the Ex Taq buffer, dNTPs and the Ex Taq Polymerase according to Table 2. Close the tube and mix the components by inverting the tube for about 20 times. Spin briefly and keep the tube on ice.
5. Add 15 µl of the PCR master mix to each 10 µl DNA sample using an automatic single-channel pipette. Use a single filter-protected tip to add the mastermix to all 96 samples. Hold the pipette at the same position for loading every well and direct the master mix onto internal wall of wells to minimize cross-contamination.
6. Cover the 96-well plate with adhesive film and centrifuge for a couple of seconds to settle the reaction mixtures.

7. PCR conditions for amplification of the *PAC2* locus are:

   Step 1: 94^{o}C for 5 min (1 cycle). Step 2 : 95^{o}C for 15 s; 63^{o}C for 1 min (40 cycles).

3.2.2 Analysis of Real Time PCR Data and Concentration Adjustment

1. After PCR is finished omit any individual samples from analysis that differ by more than 1 C_t from other replicates (<5 omissions per experiment).
2. Export the data into an excel spreadsheet and determine the concentration of DNA samples using the DNA standards. Use the mean value of the triplicates to estimate the DNA concentration.
3. Adjust concentration of the non-diluted samples (3.1 step 32) to 2 ng/µl using TE. Vortex and leave overnight at 4°C to equilibrate.
4. Confirm the DNA concentration by repeating the *PAC2* real time PCR measurement (3.2.1). For measurement of ssDNA, the concentration of all samples should be close to 2 ng/µl and definitely between 1.5 and 3 ng/µl.
5. Generate the mean value of the measured DNA concentrations for each triplicate. Divide 2 by that number to generate a correction factor for that triplicate (e.g. if the mean value of the DNA is 2.5 ng/µl, the correction factor would be 2/2.5 = 0.8). The correction factors will be used for analysis of the ssDNA measurement in 3.2.3.
6. Prepare 96-well plates by pipetting 10µl of the adjusted DNA samples in rows A to G as described in Table 1 using a multi-channel pipettor. Add ssDNA standards to row H.
7. Cover the plates with adhesive film and store at –20^{o}C or –80^{o}C until used for QAOS described below (3.2.3).

3.2.3 Measuring ssDNA by QAOS

ssDNA qPCR measurements are similar to quantification of DNA content in 3.2.1, except that the standards are all at 2 ng/µl but contain different amounts of ssDNA. In addition, a tagging primer is used that binds specifically to ssDNA at the measured genomic locus and a different temperature profile is used for PCR (Table 3 and 4). A schematic outline of QAOS and the locations of the loci used is shown in Figure 1.

1. Thaw 96-well plates containing the DNA samples and ssDNA standards on ice.
2. For the PCR master mix add primers and probes to sterile water as described in Table 2 and incubate at 95^{o}C for 5 min followed by 3 min on ice. Primers to detect ssDNA on the TG (3') strand near telomeres are shown in Table 3 and to detect ssDNA on the AC (5') in Table 4.
3. Add the Ex Taq buffer, dNTPs and the Ex Taq Polymerase according to Table 2. Close the tube and mix the components by inverting the tube for about 20 times. Spin briefly and keep the tube on ice.
4. Add 15 µl of the PCR master mix to each 10 µl DNA sample
5. Cover the 96-well plate with adhesive film and centrifuge for a couple of seconds to settle the reaction mixtures.
6. PCR conditions for measuring ssDNA are:

   Step 1: 40^{o}C for 5 min (1 cycle). Step 2 : ramp to 72^{o}C at 2^{o}C/ min (1 cycle). Step 3 : 94^{o}C for 4 min (1 cycle). Step 4 : 95^{o}C for 15 s; 67^{o}C for 1 min (40 cycles).
7. After PCR has finished omit any individual samples from analysis that differ by more than 1 C_t from other duplicates (*see* **Note 5**).

8. Export the data into an excel spreadsheet and calculate the mean value for each triplicate.
9. Multiply the mean value of each triplicate times the corresponding correction factor (generated in 3.2.2 step 5) to get the true level of ssDNA.
10. Calculate the 95% confidence interval as a measure of error:

    95% confidence interval of the standard error of the mean = 1.96*(STD/√n)

    with STD = Standard deviation

        n = number of samples (as samples were measured in triplicate: n = 3)

3.3 Preparation of Standards and Primers

3.3.1 Prepare Yeast Genomic DNA Standards

1. Arrest Wild-type cells (DLY62: *MATa bar1*Δ) containing *bar1*Δ mutation using α factor to 20 nM.
2. Prepare DNA as described in 3.1 and adjust to 4 ng/µl, 2 ng/µl and 0.4 ng/µl in TE buffer to use as genomic DNA standards.
3. Determine concentration of the initial gold standard by measuring the 260 nm/280 nm ratio using a spectrophotometer.
4. Prepare at least 1600 µl of 2 ng/µl DNA to make ssDNA standards as described in (3.3.2).

3.3.2 Prepare ssDNA Standards

1. Boil 300 µl of the 2 ng/µl genomic DNA in a screw cap Eppendorf tube for 7 min at 98°C.
2. Place tube on ice water and every 15 s vortex for 2 s. Return to ice water in between vortexing and repeat this step 3 times. Then leave on ice for at least 5 min.
3. Mix boiled and non-boiled DNA according to Table 5 to make 51.2%, 3.2% and 0.8% ssDNA standards.
4. Vortex standards for 1 min and centrifuge briefly. Vortex briefly and centrifuge again, then leave standards on ice for 30 min.
5. Vortex standards for 1 min, centrifuge briefly and use for RT-PCR measurements. Store standards at -80°C, thawed on ice and vortex for 20 s prior to use.

3.3.3 Preparation of Oligonucleotides

1. Make 200 µM stocks of lyophilised oligonucleotides (Sigma Genosys). Resuspended stock is stored at -20^0 C.
2. Make working (100X) stocks by diluting oligonucleotides further with TE according to Table 6.

3.3.4 Probe Design

All probes are labelled with FAM at the 5'end and are quenched with TAMRA at the 3' end.

1. Ideal T_M = 76-78°C
2. GC content: 20-80%
3. Length: 9-40 bases. Generally pick the shortest probe.
4. No G on the 5' end
5. <4 contiguous G's
6. Must not have more G's than C's

3.3.5 Primer Design

Primers to detect ssDNA on the TG (3') strand near telomeres are shown in Table 3 and to detect ssDNA on the AC (5') in Table 4 (*see* **Note 6**). A list of tested tags is shown in Table 7.

1. Ideal T_M = 66-69°C for tag and reverse primer
2. Ideally there is <2°C difference in T_M between the two primers
3. GC content: 20-80%
4. Length: 9-40 bases
5. Maximum of 2 G/C in the last 5 basepairs at the 3' end
6. Tagging primers contain the tag and a 10-15 bp long tail with the T_M of the tail being between 20 and 43°C, but preferably about 30°C. Tail and tag contain a 3bp overlapping sequence.

3.3.6 Amplicon Design

1. Length: 50-150 bp
2. 3’ end of primer as close to the probe as possible without overlapping

Primer design for the *PDA1* locus to amplify ssDNA on the 3’ TG strand is shown in figure 3. Test primers by using boiled (ssDNA) and non-boiled (dsDNA) as templates in QAOS. Aim to have a more than 10 C_T difference between ssDNA and dsDNA samples.

4. Notes

1. The number of DNA preparations that can be done at a time mainly depends on the space in the fixed angle centrifuge rotor. Using a Beckman Allegra 64R centrifuge with a fixed angle F0850 rotor we are readily able to perform two batches of 8 DNA preparations at a time, over an 8 h working day.
2. The number of required sessions to obtain more than 90% cell breakage is dependent on the experiment. We typically perform synchronous culture experiments using telomere capping deficient and temperature-sensitive *cdc13-1* mutants. Cells are synchronized in G1 at 36°C using α factor. After release from α factor, cultures are shifted to 36°C and cells containing the *cdc13-1* mutations arrest over a time course of 4 h. Unbudded alpha factor arrested cells are more difficult to break than large budded mitotic cells. ≥8 sessions are used for time points 0-40 min, 6 sessions for time points 80-120 min and 5 sessions for time points 160-240 min. Breakage efficiency is examined by phase contrast microscopy.

3. When precipitating the DNA with isopropanol, a small pellet is not in all cases visible. It is useful to mark the tube with a pen for orientation in the centrifuge to help detect the position of the pellet.
4. Filter-protected tips are used for all qPCR experiments. Use a separate filter-protected tip for each triplicate when adding the DNA samples to the 96-well plate. Use a single filter-protected tip to add the qPCR master mix to all wells using an automatic single-channel pipette.
5. When measuring ssDNA using ssDNA standards, the difference in C_T between the 51.2% and the 3.2% standard should theoretically be 4, between the 3.2% and 0.8% standard 2.
6. Primer Express is used for primer and probe design. There is no strong need to use Primer Express, but other software may use a different algorithm.

5. References

1. Maringele, L., and Lydall, D. (2002) EXO1-dependent single-stranded DNA at telomeres activates subsets of DNA damage and spindle checkpoint pathways in budding yeast yku70Delta mutants, *Genes Dev 16*, 1919-1933.
2. Niu, H., Chung, W. H., Zhu, Z., Kwon, Y., Zhao, W., Chi, P., Prakash, R., Seong, C., Liu, D., Lu, L., Ira, G., and Sung, P. (2010) Mechanism of the ATP-dependent DNA end-resection machinery from Saccharomyces cerevisiae, *Nature 467*, 108-111.
3. Zou, L., and Elledge, S. J. (2003) Sensing DNA damage through ATRIP recognition of RPA-ssDNA complexes, *Science 300*, 1542-1548.
4. Bertuch, A. A., and Lundblad, V. (2003) The Ku heterodimer performs separable activities at double-strand breaks and chromosome termini, *Mol Cell Biol 23*, 8202-8215.
5. Grandin, N., Damon, C., and Charbonneau, M. (2001) Ten1 functions in telomere end protection and length regulation in association with Stn1 and Cdc13, *EMBO J 20*, 1173-1183.
6. Dewar, J. M., and Lydall, D. (2010) Pif1- and Exo1-dependent nucleases coordinate checkpoint activation following telomere uncapping, *EMBO J 29*, 4020-4034.
7. Foster, S. S., Zubko, M. K., Guillard, S., and Lydall, D. (2006) MRX protects telomeric DNA at uncapped telomeres of budding yeast cdc13-1 mutants, *DNA Repair (Amst) 5*, 840-851.
8. Booth, C., Griffith, E., Brady, G., and Lydall, D. (2001) Quantitative amplification of single-stranded DNA (QAOS) demonstrates that cdc13-1 mutants generate ssDNA in a telomere to centromere direction, *Nucleic Acids Res 29*, 4414-4422.
9. Pitt, C. W., and Cooper, J. P. (2010) Pot1 inactivation leads to rampant telomere resection and loss in one cell cycle, *Nucleic Acids Res 38*, 6968-6975.
10. Addinall, S. G., Holstein, E.-M., Lawless, C., Yu, M., Chapman, K., Banks, P., Ngo, H.-P., Maringele, L., Taschuk, M., Young, A., Ciesiolka, A., Lister, A. L., Wipat, A., Wilkinson, D. J., and Lydall, D. (In Press) Quantitative Fitness Analysis shows that NMD proteins and many other protein complexes suppress or enhance distinct telomere cap defects, *PLoS Genet*.
11. Lee, K., Zhang, Y., and Lee, S. E. (2008) Saccharomyces cerevisiae ATM orthologue suppresses break-induced chromosome translocations, *Nature 454*, 543-546.
12. Negrini, S., Ribaud, V., Bianchi, A., and Shore, D. (2007) DNA breaks are masked by multiple Rap1 binding in yeast: implications for telomere capping and telomerase regulation, *Genes Dev 21*, 292-302.
13. Ngo, H. P., and Lydall, D. (2010) Survival and growth of yeast without telomere capping by Cdc13 in the absence of Sgs1, Exo1, and Rad9, *PLoS Genet 6*, e1001072.
14. Jia, X., Weinert, T., and Lydall, D. (2004) Mec1 and Rad53 inhibit formation of single-stranded DNA at telomeres of Saccharomyces cerevisiae cdc13-1 mutants, *Genetics 166*, 753-764.
15. Lazzaro, F., Sapountzi, V., Granata, M., Pellicioli, A., Vaze, M., Haber, J. E., Plevani, P., Lydall, D., and Muzi-Falconi, M. (2008) Histone methyltransferase Dot1 and Rad9 inhibit single-stranded DNA accumulation at DSBs and uncapped telomeres, *EMBO J 27*, 1502-1512.
16. Zubko, M. K., Guillard, S., and Lydall, D. (2004) Exo1 and Rad24 differentially regulate generation of ssDNA at telomeres of Saccharomyces cerevisiae cdc13-1 mutants, *Genetics 168*, 103-115.
17. Zubko, M. K., Maringele, L., Foster, S. S., and Lydall, D. (2006) Detecting repair intermediates in vivo: effects of DNA damage response genes on single-stranded DNA accumulation at uncapped telomeres in budding yeast, *Methods Enzymol 409*, 285-300.

Fig. 1. Schematic diagram of QAOS. (A) (1) Tagging primer, containing an artificial tag, binds to ssDNA with a locus-specific sequence during the first step at 40°C. The primer does not bind to dsDNA. (2) Ex Taq Polymerase extends the tagging primer during a slow ramp from 40 to 72°C, creating a hybrid sequence containing the tag. Primer extension increases the hybrid products length and therefore affinity for ssDNA allowing it to stay annealed to the ssDNA sequence as temperature increases. (3) The hybrid sequence is amplified using tag and reverse primer and stringent PCR temperatures. A fluorescent probe is used to quantify the amount of amplified DNA. (B) Location of loci used in QAOS on chromosome V-R and VI-L.

Fig. 2. Collection of lysate after cell breakage. (1) Caps and bottoms from 1.5 ml Eppendorf tube are removed. (2) Bottom of 2 ml screw cap Sarstedt tubes containing the lysates are punctured using a 21 gauge syringe needle. (3) The Sarstedt tube is fitted into the Eppendorf tube and both tubes are put into a 15 ml round bottomed Falcon tube. (4) Lysate accumulates at the bottom of the 15 ml Falcon tube during centrifugation.

Fig. 3. Primer design for QAOS at the *PDA1* locus on chromosome V-R. (A) Primers used to measure ssDNA on the TG-strand. (B) Primers used to measure ssDNA on the AC-strand. The same probe is used for measurement of both DNA strands. For tagging primers the lower case sequence corresponds to the region that hybridises to the genome. The bold regions overlap between the tag and the tagging primer.

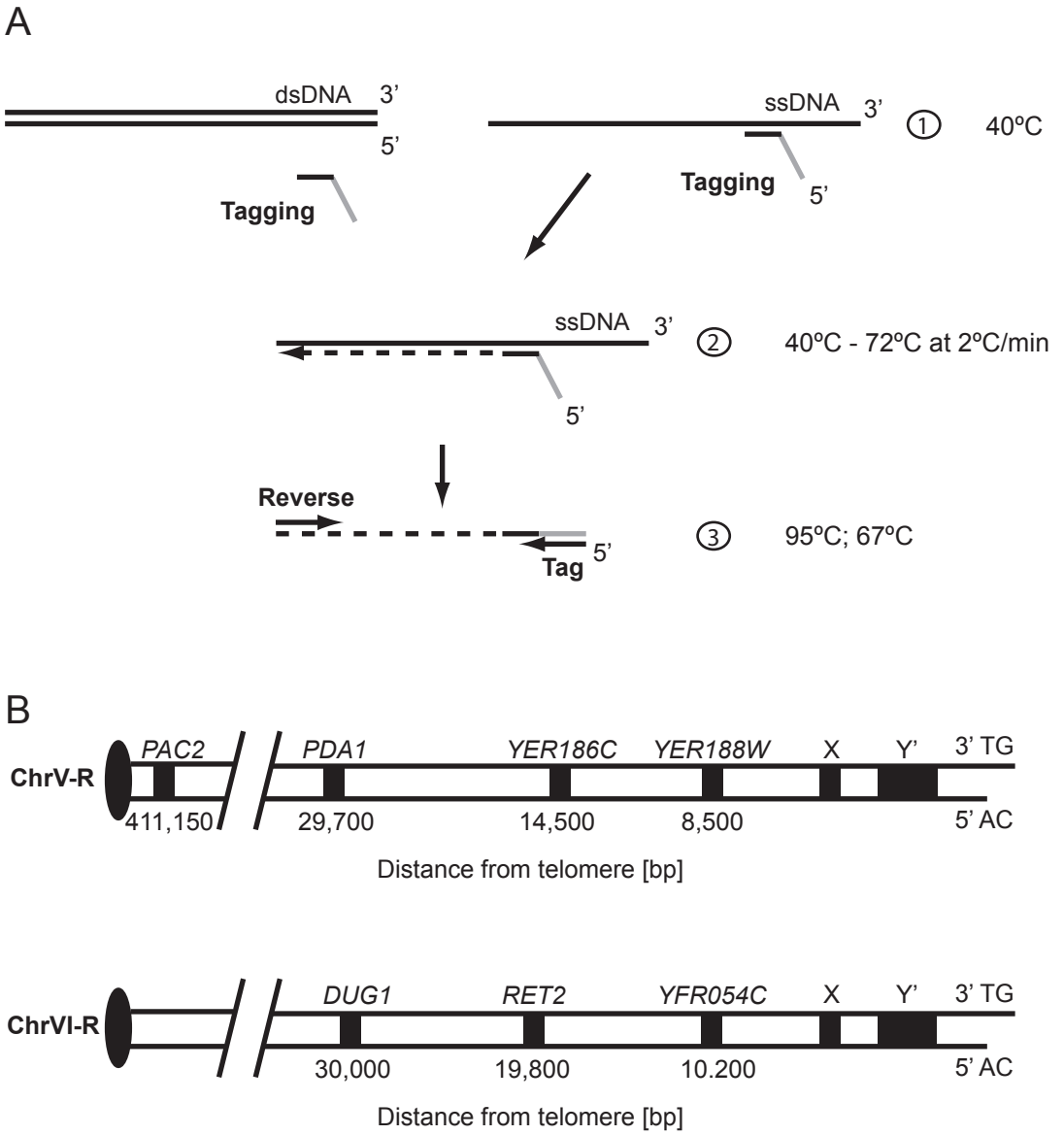
A
dsDNA
3'
5'
Tagging
ssDNA
3'
1
40ºC
Tagging
5'
ssDNA
3'
2
40ºC - 72ºC at 2ºC/min
5'
Reverse
3
95ºC; 67ºC
5'
Tag
B
ChrV-R
PAC2
PDA1
YER186C
YER188W
X
Y'
3' TG
411,150
29,700
14,500
8,500
5' AC
Distance from telomere [bp]
ChrVI-R
DUG1
RET2
YFR054C
X
Y'
3' TG
30,000
19,800
10.200
5' AC
Distance from telomere [bp]

Figure 1

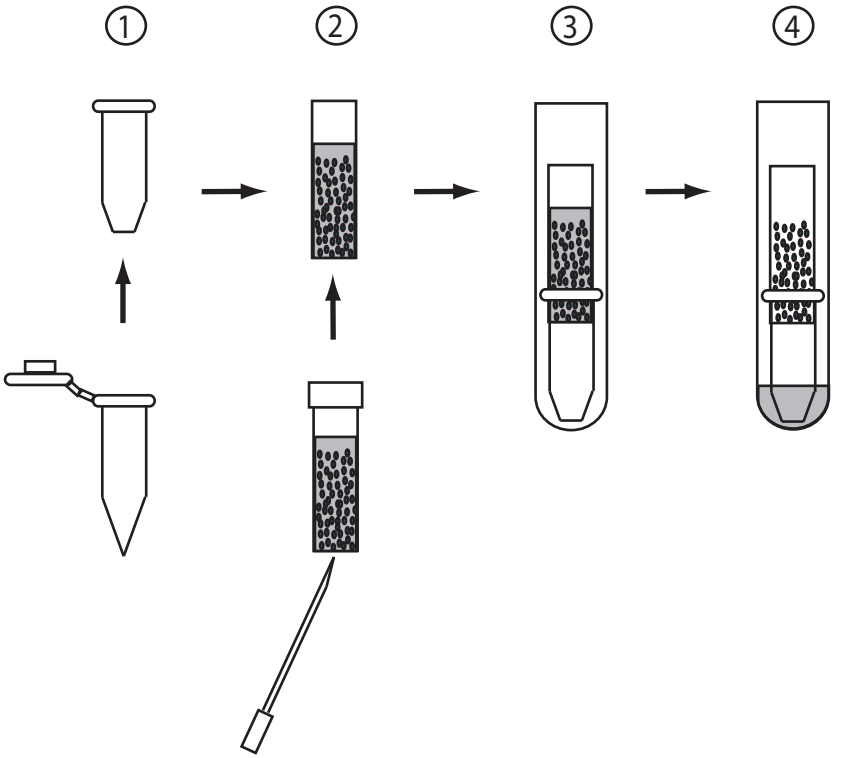

Figure 2

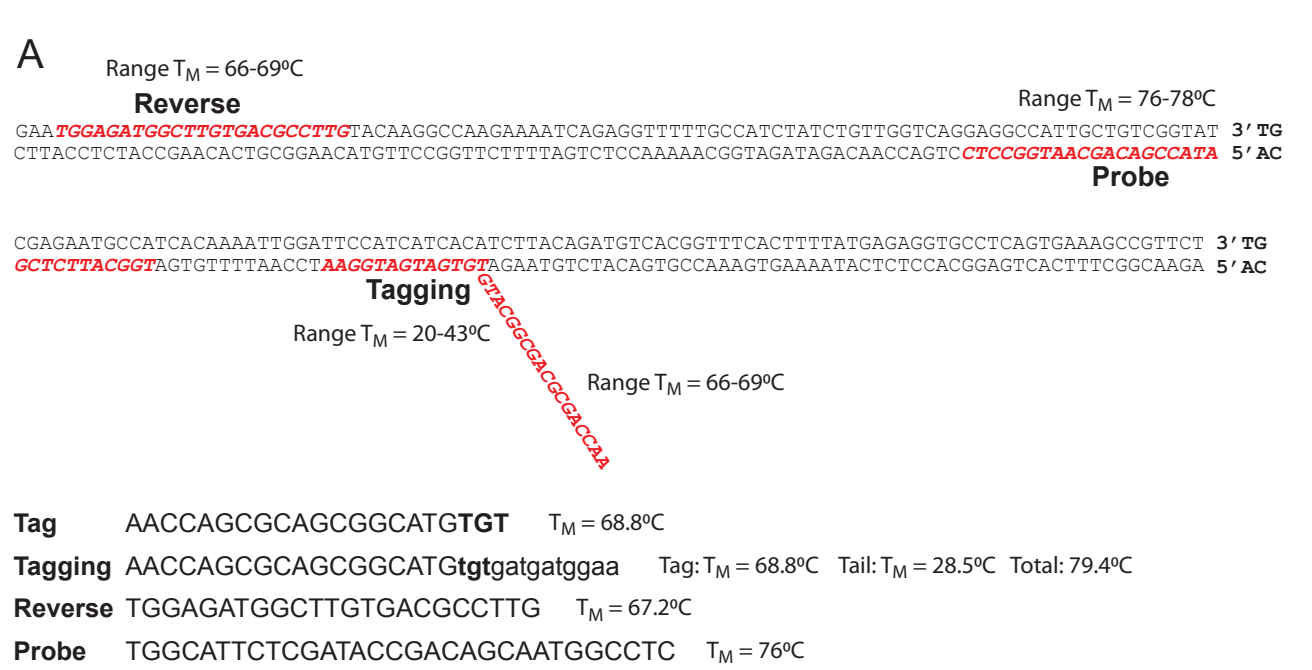
A
Range T_M = 66-69ºC
Reverse
Range T_M = 76-78ºC
GAATGGAGATGGCTTGTGACGCCTTGTACAAGGCCAAGAAAATCAGAGGTTTTTGCCATCTATCTGTTGGTCAGGAGGCCATTGCTGTCGGTAT 3'TG
CTTACCTCTACCGAACACTGCGGAACATGTTCCGGTTCTTTTAGTCTCCAAAAACGGTAGATAGACAACCAGTC 5'AC
Probe
CGAGAATGCCATCACAAAATTGGATTCCATCATCACATCTTACAGATGTCACGGTTTCACTTTTATGAGAGGTGCCTCAGTGAAAGCCGTTCT 3'TG
AGTGTTTTAACCT 5'AC
Tagging
Range T_M = 20-43ºC
Range T_M = 66-69ºC
Tag AACCAGCGCAGCGGCATGTGT T_M = 68.8ºC
Tagging AACCAGCGCAGCGGCATGtgtgatgatggaa Tag: T_M = 68.8ºC Tail: T_M = 28.5ºC Total: 79.4ºC
Reverse TGGAGATGGCTTGTGACGCCTTG T_M = 67.2ºC
Probe TGGCATTCTCGATACCGACAGCAATGGCCTC T_M = 76ºC
B
Tagging
GAATGGAGATGGCTTGTGACGCCTTGTACAAGGCCAAGAAAATCAGAGGTTTTTG
GTCAGGAGGCCATTGCTGTCGGTAT 3'TG
CTTACCTCTACCGAACACTGCGGAACATGTTCCGGTTCTTTTAGTCTCCAAAAACGGTAGATAGACAACCAGTC 5'AC
Probe
CGAGAATGCCATCACAAAATTGGATTCCATCATCACATCTTACAGATGTCACGGTTTCACTTTTATGAGAGGTGCCTCAGTGAAAGCCGTTCT 3'TG
GCTCTTACGGTAGTGTTTTAACCTAAGGTAGTAGTGTAGAATGTCTACAGTGCCAAAGTGAAAATA
AGA 5'AC
Reverse
Tag AAGGAGCGCAGCGCCTGTACCA T_M = 68.8ºC
Tagging AAGGAGCGCAGCGCCTGTAccaccatctatctgttg Tag: T_M = 68.8ºC Tail: T_M = 42.1ºC Total: 77.9ºC
Reverse ACGGCTTTCACTGAGGCACCTCTC T_M = 65.8ºC
Probe TGGCATTCTCGATACCGACAGCAATGGCCTC T_M = 76ºC

Figure 3

	1	2	3	4	5	6	7	8	9	10	11	12
A	A/0	A/0	A/0	A/40	A/40	A/40	A/80	A/80	A/80	A/120	A/120	A/120
B	A/160	A/160	A/160	A/200	A/200	A/200	A/240	A/240	A/240	B/0	B/0	B/0
C	B/40	B/40	B/40	B/80	B/80	B/80	B/120	B/120	B/120	B/160	B/160	B/160
D	B/200	B/200	B/200	B/240	B/240	B/240	C/0	C/0	C/0	C/40	C/40	C/40
E	C/80	C/80	C/80	C/120	C/120	C/120	C/160	C/160	C/160	C/200	C/200	C/200
F	C/240	C/240	C/240	D/0	D/0	D/0	D/40	D/40	D/40	D/80	D/80	D/80
G	D/120	D/120	D/120	D/160	D/160	D/160	D/200	D/200	D/200	D/240	D/240	D/240
H	STD1	STD1	STD1	STD2	STD2	STD2	STD3	STD3	STD3	NTC	NTC	NTC

Table 1. 96 well plate set up for PCR to measure total DNA or ssDNA from 4 yeast strains (A,B,C and D) sampled every 40 minutes. Each PCR is performed in triplicate. STD wells contain standards. NTC contain no template control.

	Final Conc.	Stock Conc.	Volume (µL) [QPCR]	Volume (µL) [QAOS]
Water			985	960
Tagging primer	30 nM	3 µM (100X)	-	25
Tag	300 nM	30 µM (100X)	25	25
Reverse primer	300 nM	30 µM (100X)	25	25
Probe	200 nM	20 µM (100X)	25	25
Ex Taq buffer	0.97X	10X	245	245
dNTPs	194 nM	2.5 mM	195	195
Ex Taq Polymerase	0.024 u/µL	5 u/ µL	12	12
Total			1512	1512

Table 2. PCR master mix for *PAC2* DNA quantification and QAOS. The above mixture is sufficient to add 15µL master mix to 96 individual 10 µL DNA samples (and contains 5% extra, to cover pipetting errors). This recipe permits each 250 unit batch of Takara Ex Taq polymerase to be used for 4 individual 96 well plates.

Primer	Loci	Sequence	Type of primer
M 442	*PAC2*	AATAACGAATTGAGCTATGACACCAA	Forward
M 573	*PAC2*	AGCTTACTCATATCGATTTCATACGACTT	Reverse
M 326	*PAC2*	CTGCCGCGTTGGTCAAGCCTCAT	Probe
M 239		AACCAGCGCAGCGGCATG**TGT**	Tag
M 272	*PDA1*	AACCAGCGCAGCGGCATG**tgt**gatgatggaa	Tagging
M 320	*PDA1*	TGGAGATGGCTTGTGACGCCTTG	Reverse
M 698	*PDA1*	TGGCATTCTCGATACCGACAGCAATGGCCTC	Probe
M 313		GATCTCGAGCTCGATATCGGATCC**ATT**	Tag
M 314	*YER186C*	GATCTCGAGCTCGATATCGGATCC**att**tacggcgga	Tagging
M 96	*YER186C*	AATCTCGCCTAACAAAAAAAGGCTTCTTAGTG	Reverse
M 325	*YER186C*	AGGCAAATAACGGCAAGCCCTCTCC	Probe
M 315		AAGGAGCGCAGCGCCTGTA**CCA**	Tag
M 444	*YER188W*	AAGGAGCGCAGCGCCTGTA**cca**tagcgtgat	Tagging
M 319	*YER188W*	AACGTACAGGTTACGATCGCGTCATTTTA	Reverse
M 427	*YER188W*	TAGCCGTTATCATCGGGCCCAAAACCGTATTCATTG	Probe
M 315		AAGGAGCGCAGCGCCTGTA**CCA**	Tag
M 513	*X-repeat*	AAGGAGCGCAGCGCCTGTA**cca**cattttaatatct	Tagging
M 512	*X-repeat*	ATTGAGTGGATAGTAGATGGTGAAAAAGTGGTATAACG	Reverse

M 510	*X-repeat*	TCATTCGGCGGCCCCAAATATTGTATAACTGCCC	Probe
M 520		TGCCCTCGCATCGCTCTC**GAA**	Tag
M 521	*Y'-5000*	TGCCCTCGCATCGCTCTC**gaa**acaaagtcagtga	Tagging
M 517	*Y'-5000*	GTCCTGGAACGTTGTCACGAAAAAGC	Reverse
M 516	*Y'-5000*	TGCTAGGCCGAACGACAGCTCTACGATGCGTACTT	Probe
M 316		TGCCCTCGCATCGCTCTC**ACA**	Tag
M 243	*Y'-600*	TGCCCTCGCATCGCTCTC**aca**gccctatcag	Tagging
M 237	*Y'-600*	GAGATCAGCTTGCGCTGGGAGTTACC	Reverse
M 526	*Y'-600*	ACAGGAATGCCGTCCAATGCGGCACTTTAGA	Probe
M827		AAGGAGCGCAGCGCCTGTA**CCA**	Tag
M1517	*DUG1*	AAGGAGCGCAGCGCCTGTA**cca**agatgcctt	Tagging
M1513	*DUG1*	AAGCAGCCATCGTCTTCATACCACCA	Reverse
M1515	*DUG1*	AATGAGCACCATCATCGCCTCTAC	Probe
M1252		TGTTGCGTGCAGGGTGGA**ACC**	Tag
M1512	*RET2*	TGTTGCGTGCAGGGTGGA**acc**tccattaagat	Tagging
M1508	*RET2*	AATGCATCTTCATATGGAGCTTCGATAGTGAAT	Reverse
M1510	*RET2*	AGCGCACCTGCATCGTTGGCAGCAA	Probe
M313		GATCTCGAGCTCGATATCGGATCC**ATT**	Tag
M1701	*YFR054C*	GATCTCGAGCTCGATATCGGATTC**att**tcattttcagtaa	Tagging
M1503	*YFR054C*	AATTGATCTGATTCAGCTGCAATAATATCGGTATTT	Reverse

M1505	*YFR054C*	TGGTACCTTCCATGCTCTTTGCCGAACTGCA	Probe

Table 3. Oligonucleotides for measuring total DNA and ssDNA on the TG-strand near telomeres. Oligonucleotides are classified as tags, tagging primers, probes and reverse primers (see Fig. 1A). For tagging primers the lower case sequence corresponds to the region that hybridises to the genome. The bold regions overlap between the tag and the tagging primer.

Primer	Loci	Sequence	Type of primer
M 315		AAGGAGCGCAGCGCCTGTA**CCA**	Tag
M 271	*PDA1*	AAGGAGCGCAGCGCCTGTA**cca**tctatctgttg	Tagging
M 288	*PDA1*	ACGGCTTTCACTGAGGCACCTCTC	Reverse
M 698	*PDA1*	TGGCATTCTCGATACCGACAGCAATGGCCTC	Probe
M 313		GATCTCGAGCTCGATATCGGATCC**ATT**	Tag
M 311	*YER186C*	GATCTCGAGCTCGATATCGGATCC**att**ctctcctta	Tagging
M 321	*YER186C*	GCAAGTAGGAAGCATCCCTTCAAGTCATT	Reverse
M 325	*YER186C*	AGGCAAATAACGGCAAGCCCTCTCC	Probe
M 233		ATGCCCGCACCGCCTCA**TTG**	Tag
M 242	*Y'-600*	ATGCCCGCACCGCCTCA**ttg**cgctggga	Tagging
M 236	*Y'-600*	CCGAAATGTTTTATTGCAGAACAGCCCTAT	Reverse
M 526	*Y'-600*	ACAGGAATGCCGTCCAATGCGGCACTTTAGA	Probe
M418		ATGCTCGCAGAGCCCCTGGA**TCT**	Tag
M1516	*DUG1*	ATGCTCGCAGAGCCCCTGGA**tct**tcataccacca	Tagging
M1514	*DUG1*	TGACTTTCCAAGATGCCTTGAACACTAGTGTC	Reverse
M1515	*DUG1*	AATGAGCACCATCATCGCCTCTAC	Probe

M417		ATGGGCGCAGGGCCTGGA**TTC**	Tag
M1511	*RET2*	ATGGGCGCAGGGCCTGGA**ttc**atatggagctt	Tagging
M1509	*RET2*	CAAGAAATGGGAACCTCCATTAAGATTAGCAA	Reverse
M1510	*RET2*	AGCGCACCTGCATCGTTGGCAGCAA	Probe

M417		ATGGGCGCAGGGCCTGGA**TTC**	Tag
M1506	*YFR054C*	ATGGGCGCAGGGCCTGGA**ttc**agctgcaata	Tagging
M1504	*YFR054C*	TCCTGCAATTTGCAGACGCAGGTT	Reverse
M1505	*YFR054C*	TGGTACCTTCCATGCTCTTTGCCGAACTGCA	Probe

Table 4. Oligonucleotides for ssDNA on the AC-strand near telomeres. Oligonucleotides are classified as tags, tagging primers, probes and reverse primers (see Fig. 1A). For tagging primers the lower case sequence corresponds to the region that hybridises to the genome. The bold regions overlap between the tag and the tagging primer.

ssDNA (%)	Total	Boiled DNA (μl)	Non boiled DNA (μl)
51.2	500	256	244
3.2	500	16	484
0.8	500	4	496

Table 5. Preparation of ssDNA standards.

	100x Stock (µM)	200 µM stock (µL)	TE (µL)
Tagging primers	3	6	394
Tags	30	60	340
Forward/Reverse primers	30	60	340
Probes	20	40	360

Table 6. qPCR primer preparation.

Primer	Sequence
M97	GATCTCGAGCTCGATATCGGATCCATT
M137	TCTTGCGTGCAGGGTCCGCACC
M139	TGTTGCGTGCAGGGTGGAACC
M233	ATGCCCGCACCGCCTCATTG
M234	AAGGAGCGCAGCGCCTGTACCA
M235	TGCCCTCGCATCGCTCTCACA
M239	AACCAGCGCAGCGGCATGTGT
M417	ATGGGCGCAGGGCCTGGATTC
M418	ATGCTCGCAGAGCCCCTGGATCT
M514	ATCCAGCGCAGCGGCATGTG
M520	TGCCCTCGCATCGCTCTCGAA

Table 7. List of tested tags that are used to design tagging primers.

BIOINFORMATICS ORIGINAL PAPER Vol. 27 no. 9 2011, pages 1299–1306
doi:10.1093/bioinformatics/btr134

Systems biology

Advance Access publication March 16, 2011

Customizable views on semantically integrated networks for systems biology

Jochen Weile[1], Matthew Pocock[1], Simon J. Cockell[2], Phillip Lord[1], James M. Dewar[3], Eva-Maria Holstein[3], Darren Wilkinson[3,4], David Lydall[3,5], Jennifer Hallinan[1] and Anil Wipat[1,3,*]

[1]School of Computing Science, Faculty of Science Agriculture and Engineering, Newcastle University, Newcastle upon Tyne NE1 7RU, [2]Bioinformatics Support Unit, Institute for Cell and Molecular Biosciences, Faculty of Medical Sciences, Newcastle University, Newcastle upon Tyne NE2 4HH, [3]Centre for Integrative Systems Biology of Ageing and Nutrition, Institute for Ageing and Health, Faculty of Medical Sciences, Newcastle University, Newcastle upon Tyne NE4 5PL, [4]School of Mathematics and Statistics, Faculty of Science Agriculture and Engineering, Newcastle University, Newcastle upon Tyne NE1 7RU and [5]Institute for Cell and Molecular Biosciences, Faculty of Medical Sciences, Newcastle University, Newcastle upon Tyne NE2 4HH, UK

Associate Editor: Olga Troyanskaya

ABSTRACT

Motivation: The rise of high-throughput technologies in the post-genomic era has led to the production of large amounts of biological data. Many of these datasets are freely available on the Internet. Making optimal use of these data is a significant challenge for bioinformaticians. Various strategies for integrating data have been proposed to address this challenge. One of the most promising approaches is the development of semantically rich integrated datasets. Although well suited to computational manipulation, such integrated datasets are typically too large and complex for easy visualization and interactive exploration.

Results: We have created an integrated dataset for *Saccharomyces cerevisiae* using the semantic data integration tool Ondex, and have developed a view-based visualization technique that allows for concise graphical representations of the integrated data. The technique was implemented in a plug-in for Cytoscape, called OndexView. We used OndexView to investigate telomere maintenance in *S. cerevisiae*.

Availability: The Ondex yeast dataset and the OndexView plug-in for Cytoscape are accessible at http://bsu.ncl.ac.uk/ondexview.

Contact: anil.wipat@ncl.ac.uk

Supplementary information: Supplementary data is available at *Bioinformatics* online.

Received on August 27, 2010; revised on February 10, 2011; accepted on March 9, 2011

1 INTRODUCTION

1.1 Systems biology and integrative bioinformatics

Systems biology considers multiple aspects of an organism's structure and function at the same time, using the plethora of data that is publicly available online. Biologists have access to heterogeneous data covering many different aspects of biology; 1230 entries are listed in the 2010 database issue of *Nucleic Acids Research* (http://nar.oxfordjournals.org/content/38/suppl_1). For model organisms such as *Saccharomyces cerevisiae*, the abundance of freely available data has long since exceeded the point at which it can be analysed manually.

Most data sources still exist in isolation, each with its own specialization and focus (Stein, 2002). In many cases, databases lack semantic links to each other, even when they are providing data about the same entities. This partitioning of knowledge is a particular problem for systems biology, hampering the examination of the emergent behaviours inherent in complex biological systems. The problem of using distributed, heterogeneous datasets is addressed by the subdiscipline of integrative bioinformatics. There are many different approaches to the integration and querying of large heterogeneous datasets. Early XML-based approaches (Achard *et al.*, 2001) were soon replaced by more sophisticated methods. Federated approaches, such as the distributed annotation system (DAS) (Prlić *et al.*, 2007) establish a central view on the data by translating each internal query into a set of external queries in order to retrieve the required data from the outside sources on the fly (Heimbigner and McLeod, 1985). Semantic web approaches, as endorsed by the Open Biological and Biomedical Ontologies foundry (OBO) (Smith *et al.*, 2007) or as implemented in YeastHub (Cheung *et al.*, 2005), establish a network of interlinked ontologies using a set of controlled vocabularies (Brinkley *et al.*, 2006). Data warehousing approaches such as BioMART (Haider *et al.*, 2009) EcoCyc (Keseler *et al.*, 2010) and SAMBA (Tanay *et al.*, 2004), convert and incorporate data from their external sources into their own database schema and provide custom queries.

1.2 Ondex

Ondex is a graph-based data integration framework (Kohler *et al.*, 2006), which takes a semantic warehousing approach. Links between entities in different datasets may be directly extracted from the available data sources, inferred as part of the integration, or generated by external tools, such as BLAST (Altschul *et al.*, 1990). These data can subsequently be matched and interlinked with each other semantically. The result is a semantically enriched dataset, with which users can interact and also visualize.

*To whom correspondence should be addressed.

Ondex incorporates data into a network of entities termed 'concepts', connected by 'relations', all of which can carry 'attributes'. All concepts, relations and attributes have 'types', which are organized in a hierarchical fashion. For example, the concept type `Protein` is a subtype of `Molecule`, which is itself a subtype of `Thing`. This hierarchy means that every `Protein` concept is also a `Molecule` and a `Thing`. Similarly, the relation type *catalyzes* is a subtype of *actively_participates_in*. Therefore, every statement that *p*::`Protein` *catalyzes r*::`Reaction` means that *p actively_participates_in r*. Adding this type of information means that the computer stores not only data, but also its meaning, providing a 'semantic representation' of the data.

A special kind of attribute that all concepts in the an Ondex graph have is the cross-reference (called 'concept accession' in Ondex). Concept accessions make it easy to connect concepts originating from different sources. For example, if an Ondex dataset contains two `Gene` concepts which have been imported from two different data sources, but which share the same concept accession, Ondex can connect these concepts with a new relation of type *same_as*, and can at a later time merge these concepts into a single concept. All concepts and relations also have attached provenance information stating their origin and any associated evidence codes.

The process of integrating data into this data structure is performed by the Ondex workflow engine, which employs a plugin architecture. Parsers, mapping methods and other plugins can be developed using an open API (Taubert *et al.*, 2007) and can subsequently be used in workflows.

In this work, we describe a mechanism to collapse groups of concepts into a simpler, more easily visualized and conceptualized representation. We have implemented this mechanism as a plugin for Cytoscape, called OndexView, which facilitates the focused analysis of parts of a large, complex network. We demonstrate the value of this approach by applying it to an investigation into the systems biology of telomere maintenance in the baker's yeast *S. cerevisiae*.

1.3 Telomere maintenance and *BMH1/2*

Telomeres are structures composed of the ends of eukaryotic chromosomes together with their capping nucleoprotein complexes. These structures appear to play a major role in the ageing process (Blasco, 2007; Cheung and Deng, 2008). Without the capping proteins, chromosome ends appear as double-stranded breaks to the cell's DNA damage detection mechanism, triggering a checkpoint response and ultimately cell cycle arrest (Longhese, 2008; Sandell and Zakian, 1993). With each cell division, telomeres shorten (Longhese, 2008). When telomere length falls under a certain threshold, the checkpoint response is triggered. This mechanism appears to contribute to the establishment of a cell's finite lifespan.

Saccharomyces cerevisiae is an excellent subject for studying telomere biology, because it is one of the simplest and most well-studied eukaryotic model organisms, and telomere biology is highly conserved across eukaryotes. In *S. cerevisiae*, an important component of the telomere maintenance mechanism is the protein Cdc13, which binds to the single-stranded DNA overhangs of telomeres. Cdc13 has two major functions: capping the telomeric DNA and recruiting telomerase (Garvik *et al.*, 1995; Nugent *et al.*, 1996), which is part of the telomere repair mechanism.

CDC13 is an essential gene, so it is difficult to characterize using knock-out mutants. However, there is a temperature-sensitive mutant called *cdc13-1*. This mutant has a wild-type phenotype below 26°C, but above this temperature telomeres become uncapped, the checkpoint response is induced and the cells stop dividing (Weinert and Hartwell, 1993).

Epistatic interactions between *cdc13-1* and every non-essential gene of the *S. cerevisiae* genome have been studied (Addinall *et al.*, 2008) using a high-throughput synthetic genetic array (SGA) assay (Tong *et al.*, 2001). Addinall and co-workers identified a large number of genes which appear to genetically interact with *cdc13-1*. The biological function of many of these genes is already understood, but the role of others requires further investigation.

A particularly challenging problem is the phenotype of the two paralogues *BMH1* and *BMH2*. The deletion of the gene *BMH1* strongly suppresses the *cdc13-1* phenotype, while the deletion of its paralogue *BMH2* suppresses *cdc13-1* rather weakly. *BMH1* and *BMH2* share 91.6% sequence identity. They both encode 14-3-3 proteins, a class of proteins which usually occur as dimers and which bind to phosphoproteins (Chaudhri, 2003). Members of the 14-3-3 family have a variety of different functions in eukaryotes, including directly modifying the functionality of their target proteins, mediating and controlling transport processes between the cytoplasm and different organelles and serving as scaffolds for interactions between different proteins (Tzivion *et al.*, 2001). An important role for *BMH1* and *BMH2* in the regulation of carbohydrate metabolism has also been suggested (Bruckmann *et al.*, 2007).

It is not immediately obvious why *BMH1* and *BMH2* behave differently despite their close homology. Clearly, the difference in phenotype between two such closely homologous genes cannot be understood by studying the genes in isolation; a systems biology approach is essential.

In order to investigate this problem, we used Ondex to integrate five publicly available data sources as well as a homology dataset generated from BLAST results. We then enriched this data with semantic links between the concepts from the different data sources. In addition, we developed a novel, view-based visualization approach which we used to analyse this large, complex dataset. This analysis produced several testable hypotheses.

2 METHODS

2.1 Data sources

We integrated six different data sources using Ondex. Genomics data, as well as the latest Gene Ontology (Ashburner *et al.*, 2000) annotations, were obtained from the *Saccharomyces* Genome Database (SGD) (Cherry *et al.*, 1997). A yeast regulatory network was acquired from Balaji *et al.* (2006). A curated model of the yeast metabolic network was sourced from Herrgard *et al.* (2008). A yeast protein–protein interaction (PPI) network and a network of known genetic interactions (GI) were taken from the BioGRID database (Stark *et al.*, 2006). The BioGRID data includes the GIs reported by Addinall *et al.* (2008). Homology links between genes were created using BLAST (Altschul *et al.*, 1990) with an 85% sequence identity threshold (Table 1). Further information regarding the data sources can be found in the Supplementary Material.

2.2 Integration

The source datasets were integrated to form a combined Ondex *Saccharomyces* knowledge network. A metadata model was designed for the knowledge network to capture the semantics of concept and relationship

Table 1. Data sources used in this work

Data	Source	Version/date
Genome	SGD	11/02/2010
GO annotations	SGD	11/02/2010
Interactome	BioGRID	v2.0.61
Regulatory network	Balaji *et al.* (2006)	NA
Metabolic network	Herrgard *et al.* (2008)	v1.0
Homology	BLAST (id.> 85%)	NA

NA = not applicable.

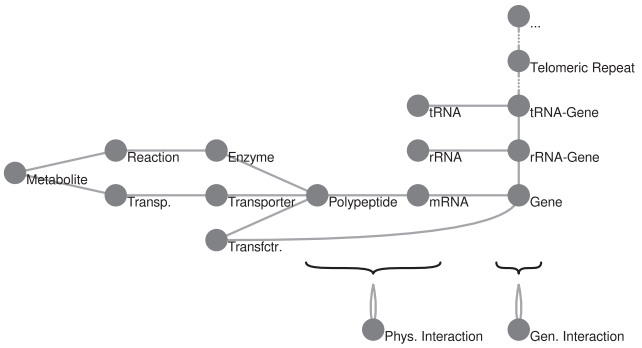

Fig. 1. Simplified schematic of the data structure underlying the Ondex *Saccharomyces* knowledge network. Circles represent concept types, and lines represent relations between them.

types found within the different datasets (Fig. 1). This model provides information about how certain concept types inherit features from one another (for example, an `Enzyme` is always a `Protein`), and allows such concepts to be treated as both concept types in the downstream workflow.

Ondex parsers for each data source produce an Ondex-compatible representation of the data. For example, the BioGRID parser creates an appropriately typed concept for every reported gene, protein and RNA in the database, and an interaction concept of a corresponding type for every interaction. All genes, proteins and RNAs that take part in an interaction are linked to that interaction concept with a *participates_in* relation.

A mapping algorithm based on matching cross-references was used to find identical concepts in the Ondex graph. For example, the protein encoded by the ORF *YDL220C* from BioGRID matches a concept with the same accession number in the metabolic network. When the procedure identifies a group of matching concepts, it merges them into one single concept that captures all of the information that was represented by the group members. The procedure checks whether all concepts in a group have compatible types. If so, it automatically uses the most specific type present in the group for the merged concept. Otherwise it reports the inconsistency. For example, a concept cannot be both a `Gene` and a `Pseudogene`, but a concept can be both a `Protein` and an `Enzyme`, in which case `Enzyme` is the more specific type.

The semantic model reflects current understanding of molecular cell biology: concepts of type `Gene` have *transcription* relations linking them to `mRNA` concepts, which in turn connect to `Polypeptide` concepts via *translation* relations. `Polypeptides` can be *part_of* `Proteins`. `Enzymes`, a subtype of `Proteins`, may *catalyze* `Reactions`, which *consume* and *produce* `Molecules` such as `Metabolites` and `Proteins`.

`Transcription_factors`, a subtype of `Protein`, connect to `Genes` via *regulation* relations. `Genes` in turn are `Nucleotide_features`, which connect via *adjacency* or *overlap* relations, establishing genomic context. All `Nucleotide_features` can *participate_in* various `Genetic_interactions`. Similarly, `Molecules`, such as `RNAs` or `Polypeptides` can *participate_in* `Physical_interactions`.

Non-physical data can also be associated with existing concepts. `Nucleotide_features` can contribute to `Biological_processes`. `Proteins` can have a `Molecular_function`. Various parts of the knowledge network can also be associated with `Publication` concepts.

All of the parsers and mapping methods, as well as the metadata that were created for this work, are available as part of the Ondex suite, which is licensed under the GNU GPL v3, and is downloadable from http://www.ondex.org/. Further details regarding the integration process can be found in the Supplementary Material.

2.3 A novel visualization strategy

The graph produced by the integration is stored in the Ondex XML format OXL (Taubert *et al.*, 2007) and can be browsed in Ondex. The resulting network is large and complex, and contains many types of concepts and relations. In order to present a more succinct and biologically focused view of the data, we developed a plugin for the network visualization tool Cytoscape (Shannon *et al.*, 2003) called OndexView.

This new visualisation allows the user to define 'views' on the data. A view focusses on one type of concept. All concepts of that type found in the knowledge network are visualized as network nodes. The user can query the knowledge network for associations between the concepts. These associations will be visualized as edges between the corresponding nodes. Querying for associations is accomplished by specifying a set of metadata motifs. The instances of these motifs found in the underlying knowledge network are then used to create corresponding associations in the view. Metadata motifs are alternating sequences of concept types and relation types that begin and end on the same concept type (Fig. 2E).

A modified depth-first search algorithm is used to extract motif instances from the underlying Ondex knowledge network. At each depth level, the algorithm checks whether the currently explored path matches the target motif. For example, a user interested in proteins and metabolic pathway relationships between them could specify a motif representing this type of interaction. Applying the algorithm using this motif produces a view on the graph, containing only those elements in which the user is interested (Fig. 2). It is possible to combine multiple motifs to form a view as long as the motifs share the same start point concept type.

2.4 Using OndexView with the *Saccharomyces* knowledge network for generating hypotheses

A semantically collapsed view of a complex network facilitates hypothesis generation by providing a simple representation of genes of interest and their interactions. A subnetwork consisting only of these genes and their neighbours can be generated, and inspected to identify edges of potential interest. Examination of the annotations attached to these edges and their adjacent nodes in the Ondex network provides links to available knowledge about the underlying biology. The semantically collapsed view also provides a way of perusing relevant literature in a focused manner, making hypothesis generation considerably more efficient than the alternative of trawling through large databases of publications.

Using OndexView, we defined five motifs over `Gene` concepts covering genetic and physical interactions, homology, regulation and metabolic precedence (Table 2).

We created a view using all five motifs, querying for the immediate neighbourhood of *BMH1*, *BMH2* and *CDC13*. We then laid out the view, separating all neighbouring genes into groups: Exclusive neighbours of *BMH1*, exclusive neighbours of *BMH2*, joint neighbours of *BMH1* and *BMH2* and others.

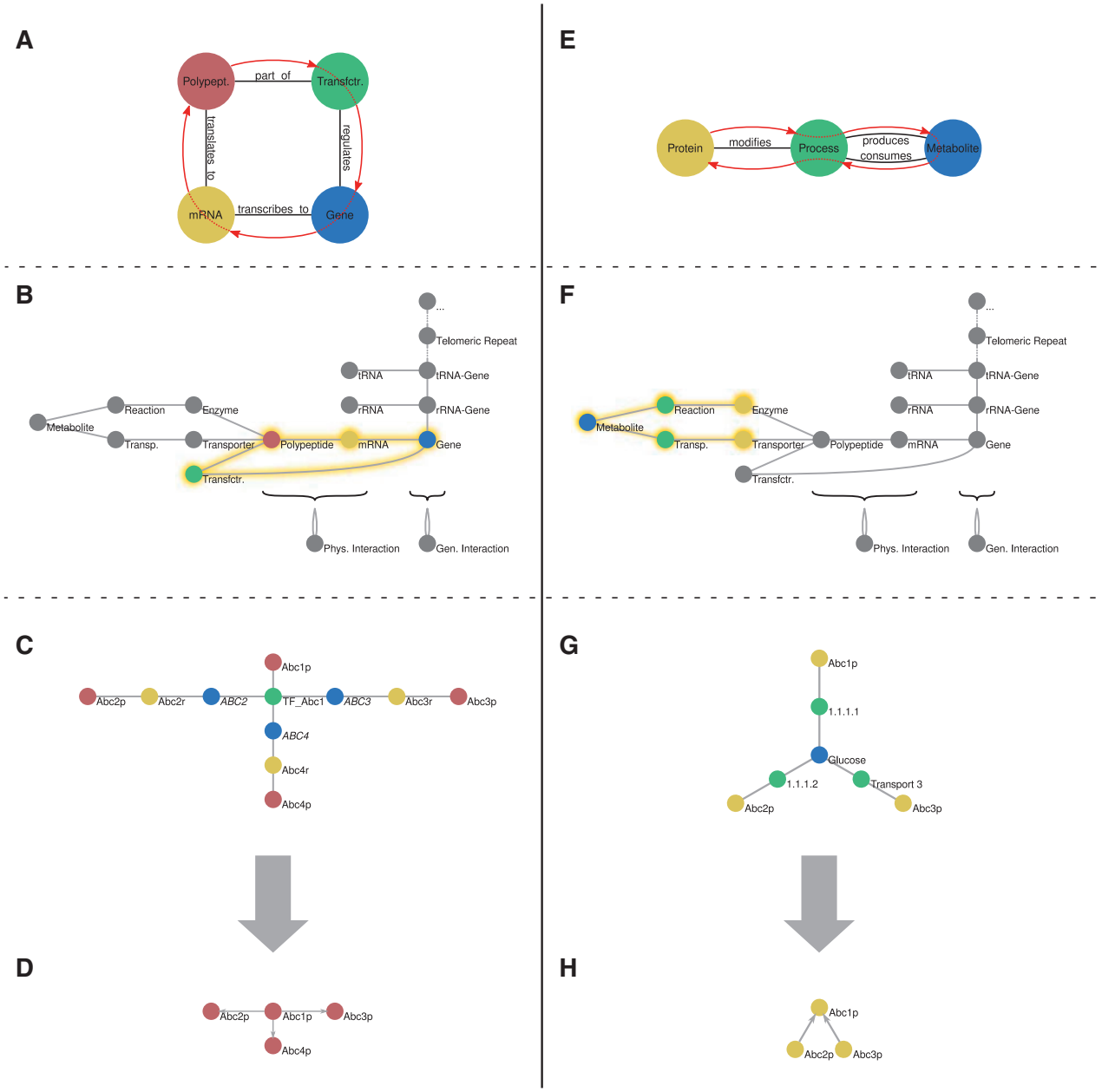

Fig. 2. Schema illustrating two examples for constructing associations based on metadata motifs. (**A**) The motif shown selects all paths from a polypeptide that is part of a transcription factor which regulates a gene that is transcribed to an mRNA which is translated into another polypeptide. (**B**) The motif from (A) is shown in context of the complete metadata structure. (**C**) A small example subnetwork to which the motif can be applied. Finding the motif (A) in the subnetwork, we identify three matching paths. Each element in these paths matches its corresponding element in the motif. (**D**) The view resulting from collapsing the paths identified in (C) according to motifs from (A) contains three edges; one for each matching path. (**E**) The motif selects all paths from a protein that modifies a process that produces a metabolite which is then consumed by another process back to another protein that modifies that process. Such a motif could be described as 'precedence in a metabolic pathway'. (**F**) The motif from (E) is shown in context of the complete metadata structure. (**G**) A small example subnetwork to which the motif can be applied. Finding the motif (E) in the subnetwork, we identify two matching paths. Each element in these paths either matches or is a subtype of the corresponding element in the motif. (**H**) The views resulting from collapsing the paths identified in (G) according to motifs from (E) contains two edges; one for each matching path.

Table 2. Motif definitions used in this work

Association name	Motif
homologue	`Gene` *is_homologue* `Gene`
metabolic path	`Gene` *encodes* `Polypeptide` *is_part_of* `Protein` *participates_actively_in* `Process` *gives* `Metabolite` *taken_by* `Process` *has_active_participant* `Protein` *has_part* `Polypeptide` *encoded_by* `Gene`
ph. interaction	`Gene` *encodes* `Polypeptide` *participates_actively_in* `Physical_Interaction` *has_passive_participant* `Polypeptide` *encoded_by* `Gene`
regulation	`Gene` *encodes* `Polypeptide` *is_part_of* `Transcription_Factor` *regulates* `Gene`
gen. interaction	`Gene` *participates_actively_in* `Genetic_Interaction` *has_passive_participant* `Gene`

3 RESULTS AND DISCUSSION

The work described here has four major outcomes: a knowledge network for the yeast *S. cerevisiae*; an algorithm for semantic collapsing of a network; a Cytoscape plugin for visualization of the knowledge network implementing this algorithm; and a set of hypotheses relating to telomere maintenance in *S. cerevisiae*, generated using this approach.

3.1 The Ondex *Saccharomyces* knowledge network

Using the Ondex data integration platform, we integrated five publicly available data sources covering various aspects of *S.cerevisiae* biology into a semantically enriched and interlinked knowledge network. The resulting knowledge network consists of a total of 240964 concepts of 59 different types, connected by 754391 relations of 28 types.

3.2 OndexView: a Cytoscape plugin

We implemented a new method for semantic simplification as the Cytoscape plugin OndexView, that uses views on the underlying data. Users can load integrated Ondex networks into OndexView and open views on them.

A user can invoke predefined views over the knowledge network or define custom views. A built-in motif editor is included in OndexView for this purpose. To apply a view, a concept type is selected from the knowledge network. The user then chooses one or more motifs for the selected concept type. OndexView extracts all the required data from the underlying Ondex graph and constructs associations according to the algorithm outlined in Section 2.3. The program then offers a query interface to the user, which can be used to focus on specific nodes (such as genes) or collections of nodes (such as pathways and complexes) and their neighbourhoods. Once the query has been processed, OndexView displays the selected view in the main Cytoscape window.

3.3 Telomere maintenance in *S. cerevisiae*

BMH1 and *BMH2*, despite their 91.6% sequence identity, have very different interactions with the temperature-sensitive telomere uncapping mutant *cdc13-1*. Our analysis of the Ondex *Saccharomyces* knowledge network, conducted using OndexView, led to the formulation of several hypotheses to explain the different interaction profiles of *BMH1* and *BMH2*.

Table 3. Gene groups in the neighbourhood of *BMH1* and *BMH2* in the created view and their cardinalities

	Total	Cell cycle related	Glucose metabolism related	Histone related
		No. (%)	No. (%)	No. (%)
Neighb. of *BMH1*	68	15 (22.1)	7 (10.3)	4 (5.9)
Neighb. of *BMH2*	79	15 (18.9)	8 (10.1)	4 (5.1)
Intersection of *BMH1/2* neighbourhoods	28	7 (25.0)	3 (10.7)	4 (14.3)
Union of *BMH1/2* neighbourhoods	119	23 (19.3)	12 (10.1)	4 (3.3)

From the semantically collapsed graph, it is apparent that the neighbourhoods of *BMH1* and *BMH2* have only 23.5% of genes in common; *BMH1* and *BMH2* have completely separate sets of transcriptional regulators. This information is not readily apparent in the uncollapsed graph. Analysis of the node description fields reveals that 19.3% of the two genes' combined neighbourhood are cell cycle-related genes, while 10.1% are glucose metabolism related genes. Of the genes that physically interact with both *BMH1* and *BMH2*, 14.3% are histone related (Table 3). An annotated screenshot of this view is available as Supplementary Figure S2.

The over-representation of genes involved in regulation of the cell cycle[1] in the joint neighbourhood of *BMH1* and *BMH2* suggests that *BMH1* and *BMH2* may function as cell cycle regulators. Notably, Rad53, a key element of the cell's checkpoint signalling pathway, interacts physically with Bmh2. Further, two genes that have previously been identified as suppressors of *cdc13-1*: *BNR1* and *CYK3*, are also present in the neighbourhood of *BMH1* and *BMH2*. The joint neighbourhood of *BMH1* and *BMH2* also contains a relatively large number of genes related to regulation of glucose metabolism,[2] indicating that the pair of genes may also play a major role in the regulation of glucose metabolism (Bruckmann *et al.*, 2007).

3.4 Differential regulation of *BMH1* and *BMH2*

The semantically collapsed view of the neighbourhood of *BMH1* and *BMH2* (Section 2.4) shows that Bmh2 physically interacts with the protein Rad53. After selecting Rad53 in the view, we can learn from its description field that Rad53 mediates the activation of the cell-cycle checkpoint (Schwartz *et al.*, 2002), thus interacting with the *cdc13-1* phenotype. Examination of the interaction between Bmh2 and Rad53 reveals an annotation indicating that this interaction was originally reported by Usui and Petrini (2007). These authors showed that both Bmh1 and Bmh2 directly bind to the active (phosphorylated) Rad53 protein, thus enhancing its signalling effect. An edge between *BMH1* and *RAD53* is absent in the Ondex network, since Usui and Petrini experimentally verified only the physical

[1]Over-represented with respect to the distribution of GO terms in the *S.cerevisiae* genome; hypergeometric test, $P = 0.00046$.

[2]Over-represented with respect to the distribution of GO terms in the *S.cerevisiae* genome; hypergeometric test, $P = 0.0079$.

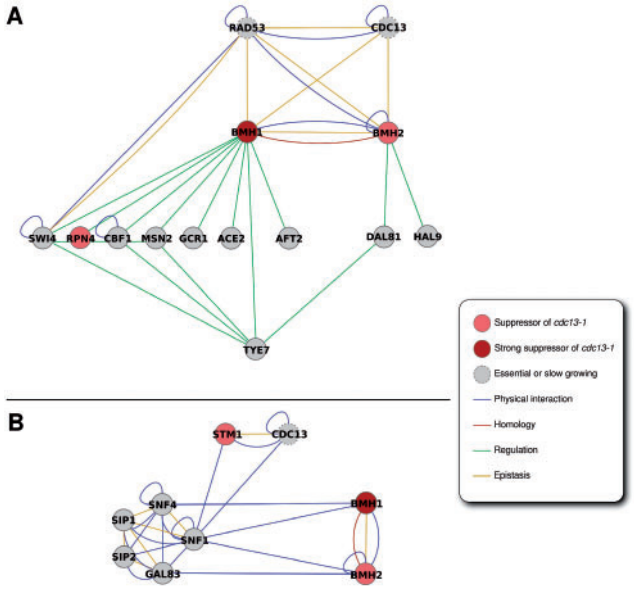

Fig. 3. Screenshots from OndexView, summarizing the hypotheses presented. Edges represent physical interactions (blue), homology (red), regulation (green) and epistasis (yellow). Nodes represent genes, some of which are weak (light red) and some strong (dark red) suppressors of *cdc13-1*. Genes which show lethal or slow growing phenotypes upon deletion are marked with dashed outlines, as knowledge of their epistatic behaviour can be expected to be incomplete.

interaction between Bmh2 and Rad53. However, they hypothesise that Bmh1 interacts with Rad53 in the same way that Bmh2 does.

Accepting Usui and Petrini's assumption, a significant difference in protein abundance during the time of checkpoint induction could explain the different effects of *BMH1* and *BMH2* deletions. The collapsed network neighbourhood of *BMH1* and *BMH2* shows clearly that the two genes are regulated completely independently from one another. Furthermore, according to their description fields in the network, two of *BMH1*'s transcriptional regulators, *ACE2* and *SWI4*, are known to be active during G_1 phase (Andrews and Moore, 1992; McBride *et al.*, 1999). This observation leads us to conjecture that *BMH1* could be more strongly expressed than *BMH2* during the G_1 phase, resulting in a higher abundance of Bmh1 protein during and after G_1 phase.

We hypothesize that due to its independent transcriptional regulation, *BMH1*'s products are present at higher levels than those of *BMH2* at checkpoint time. Thus, deleting *BMH1* would remove the majority of the Bmh1 and Bmh2 protein available as binding partners for Rad53, severely impairing the cell's checkpoint response in the face of uncapped telomeres. Removing *BMH2*, in contrast, removes a smaller proportion of binding partners for Rad53, thus resulting in a milder suppression effect on *cdc13-1*.

The differential regulation hypothesis has been summarized in Figure 3A, by generating a neighbourhood graph of *BMH1* and *BMH2* and removing all nodes except for those mentioned in the above discussion.

Experimental validation of the differential regulation hypothesis could be performed in several ways. Expression profiling of *BMH1* and *BMH2* over the course of the cell cycle could be performed. Consultation of pre-existing data has so far been inconclusive: a time course microarray performed by Spellman and colleagues showed *BMH1* expression levels to be slightly higher than those of *BMH2* throughout the the cell cycle and spiking 4-fold during G_1 phase (Spellman *et al.*, 1998) (Supplementary Fig. S2). However, due to the low resolution of the assay, the observed peak is represented by only one datapoint, rendering its significance rather doubtful. Another possibility would be the examination of an *ace2*Δ*swi4*Δ double mutant, which under the above hypothesis should replicate the *bmh1*Δ phenotype regarding suppression of *cdc13-1*.

3.5 Phosphorylation of Cdc13

A different hypothesis was formed after further examining the OndexView network neighbourhood of *BMH1* and *BMH2*. The network shows a set of edges, indicating that Bmh1 and Bmh2 physically interact with Snf1, Snf4 and Gal83, which according to their node description fields, are members of the AMP-dependent kinase (AMPK) complex. Snf1 also interacts with Cdc13 and Stm1, another telomere-capping protein. The publication linked in the Ondex knowledge network reveals that this interaction is a phosphorylation, (Ptacek *et al.*, 2005).

Publications linked from the nodes reveal that the AMPK complex is a heterotrimer composed of the α-subunit Snf1 (the actual kinase), its activating γ-subunit Snf4 and a third component β-subunit that tethers Snf1 and Snf4 together. Sip1, Sip2 and Gal83 compete for the place of this third component (Jiang and Carlson, 1997). These three competing proteins have been shown to determine the AMPK's substrate specificity and its cellular localization (Lin *et al.*, 2003; Schmidt and McCartney, 2000). For example, the Gal83 variant of the AMPK complex has been shown to be able to enter the nucleus (Vincent *et al.*, 2001).

In the network, two edges exist indicating that Bmh1 and Bmh2 both physically interact with Snf1 (Elbing *et al.*, 2006). However, Bmh1 alone interacts with the γ-subunit Snf4 (Gavin *et al.*, 2002), while Bmh2 alone interacts with the β-subunit Gal83 (Krogan *et al.*, 2006).

The nature of these interactions is currently unknown, but 14-3-3 proteins have been reported to affect kinases in several different ways, including scaffolding and direct alteration of the target's function (Tzivion *et al.*, 2001). If Bmh1/2 are involved in scaffolding for the formation of different AMPK variants, then the deletion of *BMH1* and the subsequent over-representation of Bmh2 dimers could favour the formation of Gal83-AMPK variants which can enter the nucleus to phosphorylate Cdc13. We, therefore, hypothesize that the phosphorylation of Cdc13 could potentially affect its temperature sensitivity and thus the *cdc13-1* phenotype.

The phosphorylation hypothesis has been summarized in Figure 3B, by generating a neighbourhood graph of *BMH1* and *BMH2* and removing all nodes except for those mentioned in the above discussion.

Experimental validation of the phosphorylation hypothesis is more difficult. An examination of the phenotype of *gal83*Δ mutants could offer further insight. If such a test would corroborate the importance of the AMPK complex for the observed phenotype, one could examine whether *in vitro* phosphorylation of Cdc13 by the AMPK is possible. However, without further evidence we have to consider the effect of a potential phosphorylation of Cdc13 on its temperature sensitivity in particular to be mere speculation.

3.6 Impact of noisy data

Like any other data integration approach, the Ondex *Saccharomyces* knowledge network is limited by the state of knowledge contained in its data sources. There are two main types of errors that affect the system. (i) Incorrect information from the databases, such as curator errors, will also be present in the integrated network, unless detectable by Ondex's inconsistency checks as discussed in Section 2.2. For example, contradictions between data sources can be detected and rectified. (ii) Information that is missing from the source databases will also be missing in the integrated dataset. A particular problem in this respect is the lack of negative knowledge recording throughout the systems biology community. In many sources, it is not possible to decide if non-existence of a database entry is indicative of the subject being known not to exist or not being known to exist.

It is obvious that such problems also impact downstream analyses with OndexView. However, by enabling the user to review the evidence underlying the integrated data, she/he can be pointed at the original publications that can be consulted. For example, as described in Section 3.4, the publication linked from the physical interaction edge between Bmh2 and Rad53 clarified the circumstances around the non-existence of an edge between Bmh1 and Rad53. So it can be argued that performing visual analyses with OndexView on the Ondex *Saccharomyces* knowledge network also impacts on missing data, as it allows for clarifications and corrections.

3.7 Comparison to related works

While the Ondex *Saccharomyces* knowledge network in conjunction with OndexView's semantic simplification method shows parallels to previous data integration approaches, there are a number of important differences. Like the work presented in this article, semantic web approaches, such as YeastHub (Cheung *et al.*, 2005) store their integrated data in a machine-interpretable fashion, thus providing flexible platforms that can be adapted for various purposes. However, unlike OndexView, such systems require complex querying language constructs to access them. Data warehousing approaches such as SAMBA (Tanay *et al.*, 2004) and EcoCyc (Keseler *et al.*, 2010), on the other hand, are related to the presented work in that they collect the contents of heterogeneous data sources in one centralized repository. Unlike the Ondex *Saccharomyces* knowledge network, they offer web interfaces, which makes them very easy to query for standard use. However, they are based on less semantically rigorous data structures, rendering them less flexible. In summary, the Ondex *Saccharomyces* knowledge network combines aspects from both semantic web approaches and data warehousing approaches; featuring both their strengths, but also some of their weaknesses.

4 CONCLUSIONS

The data produced by high-throughput approaches has the potential to revolutionize our understanding of biology, but can do so only if the computational techniques necessary to visualize and analyse the data can scale with the amount of data generated. Data integration methods have proven to be a successful way to face this challenge. We have shown that a view-based approach can be a powerful tool to simplify the visualization of the complex knowledge networks generated by semantic data integration, without loss of the underlying information. The view-based approach provides concise visualizations tailored to providing only the information relevant to a particular investigation.

Biological phenomena such as the different phenotypes arising from deletion of *BMH1* and *BMH2* emerge from the interplay of several independent molecular biological networks. OndexView enables users to visualize not only these networks but also the ways in which they dovetail. This visualization serves as a starting point for the user, who can now easily explore genes, their various relationships and the underlying evidence, thus gathering inspirations facilitating the generation of testable hypotheses regarding the functions of these genes.

4.1 Outlook

There are a number of improvements that could be applied to OndexView and the presented knowledge network, as well as a number of ideas that build upon this work. The exploration of evidence trails behind the simplified edges in OndexView could be made more easily accessible. Rather than showing evidence in a textual representation in graph attributes, an option to visualize it graphically on demand would further increase the tool's usefulness. However, due to the limitations of the Cytoscape API, which renders graph views immutable, such new features will more likely be included in a re-implementation of OndexView for Ondex's own graph visualization frontend.

Furthermore, the Ondex *Saccharomyces* knowledge network could be enriched with probabilities on the connections between concepts, which could be inferred from the original data sources as well as the evidence coverage. Then, if more experience can be gathered on molecular pathways that potentially qualify for explaining observed epistasis effects, they could be generalized into a collection of semantic motifs. Instances of these motifs in the graph could be ranked according to their overall probability. The generation of such ranked lists could further assist biologists with the formation of hypotheses.

ACKNOWLEDGEMENTS

J.W. and M.P. created the Ondex yeast dataset and all required Ondex workflow modules not already present in the Ondex distribution; J.W. and A.W. designed the view-based visualization approach; J.W. implemented the OndexView plug-in for Cytoscape; J.W., E.H. and J.D. investigated BMH1/2 epistasis with OndexView and generated the presented hypotheses; J.W., S.J.C., P.L., J.H. and A.W. wrote the paper; S.J.C., P.L., D.W., D.L., J.H. and A.W. supervised the project. Furthermore, the authors would like to thank the Ondex development team and the Newcastle Integrative Bioinformatics writing group for their help.

Funding: The authors are pleased to acknowledge funding from the Biotechnology and Biological Sciences Research Council (BBSRC) Systems Approaches to Biological Research (SABR) initiative [Grant number BB/F006039/1].

Conflict of Interest: none declared.

REFERENCES

Achard,F. *et al.* (2001) XML, bioinformatics and data integration. *Bioinformatics*, **17**, 115–125.

Addinall,S.G. *et al.* (2008) A genomewide suppressor and enhancer analysis of *cdc13-1* reveals varied cellular processes influencing telomere capping in *Saccharomyces cerevisiae*. *Genetics*, **180**, 2251–2266.

Altschul,S.F. *et al.* (1990) Basic local alignment search tool. *J. Mol. Biol.*, **215**, 403–410.

Andrews,B.J. and Moore,L.A. (1992) Interaction of the yeast Swi4 and Swi6 cell cycle regulatory proteins in vitro. *Proc. Natl Acad. Sci. USA*, **89**, 11852–11856.

Ashburner,M. *et al.* (2000) Gene ontology: tool for the unification of biology. The Gene Ontology Consortium. *Nat. Genet*., **25**, 25–29.

Balaji,S. *et al.* (2006) Comprehensive analysis of combinatorial regulation using the transcriptional regulatory network of yeast. *J. Mol. Biol.*, **360**, 213–227.

Blasco,M.A. (2007) Telomere length, stem cells and aging. *Nat. Chem. Biol.*, **3**, 640–649.

Brinkley,J.F. *et al.* (2006) A framework for using reference ontologies as a foundation for the semantic web. *AMIA Annu. Sympos. Proc.*, 96–100.

Bruckmann,A. *et al.* (2007) Post-transcriptional control of the *Saccharomyces cerevisiae* proteome by 14-3-3 proteins. *J. Proteome Res.*, **6**, 1689–1699.

Chaudhri,M. (2003) Mammalian and yeast 14-3-3 isoforms form distinct patterns of dimers *in vivo*. *Biochem. Biophys. Res. Commun.*, **300**, 679–685.

Cherry,J.M. *et al.* (1997) Genetic and physical maps of *Saccharomyces cerevisiae*. *Nature*, **387** (Suppl. 6632), 67–73.

Cheung,A.L.M. and Deng,W. (2008) Telomere dysfunction, genome instability and cancer. *Front. Biosci. J. Virt. Lib.*, **13**, 2075–2090.

Cheung,K.-H. *et al.* (2005) Yeasthub: a semantic web use case for integrating data in the life sciences domain. *Bioinformatics*, **21** (Suppl. 1), i85–i96.

Elbing,K. *et al.* (2006) Purification and characterization of the three Snf1-activating kinases of *Saccharomyces cerevisiae*. *Biochem. J.*, **393**(**Pt 3**), 797–805.

Garvik,B. *et al.* (1995) Single-stranded DNA arising at telomeres in *cdc13* mutants may constitute a specific signal for the RAD9 checkpoint. *Mol. Cell. Biol.*, **15**, 6128–6138.

Gavin,A. *et al.* (2002) Functional organization of the yeast proteome by systematic analysis of protein complexes. *Nature*, **415**, 141–147.

Haider,S. *et al.* (2009) BioMart central portal–unified access to biological data. *Nucleic Acids Res.*, **37** (Suppl. 2), W23–W27.

Heimbigner,D. and McLeod,D. (1985) A federated architecture for information management. *ACM Trans. Inf. Syst.*, **3**, 253–278.

Herrgard,M.J. *et al.* (2008) A consensus yeast metabolic network reconstruction obtained from a community approach to systems biology. *Nat. Biotechnol.*, **26**, 1155–1160.

Jiang,R. and Carlson,M. (1997) The Snf1 protein kinase and its activating subunit, Snf4, interact with distinct domains of the Sip1/Sip2/Gal83 component in the kinase complex. *Mol. Cell. Biol.*, **17**, 2099–2106.

Keseler,I.M. *et al.* (2010) Ecocyc: a comprehensive database of *Escherichia coli* biology. *Nucleic Acids Res.*, 334–337.

Kohler,J. *et al.* (2006) Graph-based analysis and visualization of experimental results with ONDEX. *Bioinformatics*, **22**, 1383–1390.

Krogan,N.J. *et al.* (2006) Global landscape of protein complexes in the yeast *Saccharomyces cerevisiae*. *Nature*, **440**, 637–643.

Lin,S.S. *et al.* (2003) Sip2, an N-myristoylated β-subunit of Snf1 kinase, regulates aging in *Saccharomyces cerevisiae* by affecting cellular histone kinase activity, recombination at rDNA loci, and silencing. *J. Biol. Chem.*, **278**, 13390–13397.

Longhese,M.P. (2008) DNA damage response at functional and dysfunctional telomeres. *Genes Dev.*, **22**, 125–140.

McBride,H.J. *et al.* (1999) Distinct regions of the Swi5 and Ace2 transcription factors are required for specific gene activation. *J. Biol. Chem.*, **274**, 21029–21036.

Nugent,C.I. *et al.* (1996) Cdc13p: a single-strand telomeric DNA-binding protein with a dual role in yeast telomere maintenance. *Science*, **274**, 249–252.

Prlić,A. *et al.* (2007) Integrating sequence and structural biology with DAS. *BMC Bioinformatics*, **8**, 333.

Ptacek,J. *et al.* (2005) Global analysis of protein phosphorylation in yeast. *Nature*, **438**, 679–684.

Sandell,L.L. and Zakian,V.A. (1993) Loss of a yeast telomere: arrest, recovery, and chromosome loss. *Cell*, **75**, 729–739.

Schmidt,M.C. and McCartney,R.R. (2000) β-subunits of Snf1 kinase are required for kinase function and substrate definition. *EMBO J*., **19**, 4936–4943.

Schwartz,M.F. *et al.* (2002) Rad phosphorylation sites couple Rad53 to the *Saccharomyces cerevisiae* DNA damage checkpoint. *Mol. Cell*, **9**, 1055–1065.

Shannon,P. *et al.* (2003) Cytoscape: a software environment for integrated models of biomolecular interaction networks. *Genome Res.*, **13**, 2498–2504.

Smith,B. *et al.* (2007) The OBO foundry: coordinated evolution of ontologies to support biomedical data integration. *Nat. Biotechnol.*, **25**, 1251–1255.

Spellman,P. T. *et al.* (1998) Comprehensive identification of cell cycle-regulated genes of the yeast *Saccharomyces cerevisiae* by microarray hybridization. *Mol. Biol. Cell*, **9**, 3273–3297.

Stark,C. *et al.* (2006) BioGRID: a general repository for interaction datasets. *Nucleic Acids Res.*, **34**, D535–D539.

Stein,L. (2002) Creating a bioinformatics nation. *Nature*, **417**, 119–120.

Tanay,A. *et al.* (2004) Revealing modularity and organization in the yeast molecular network by integrated analysis of highly heterogeneous genomewide data. *Proc. Natl Acad. Sci. USA*, **101**, 2981–2986.

Taubert,J. *et al.* (2007) The OXL format for the exchange of integrated datasets. *J. Integr. Bioinformatics*, **1**, 62.

Tong,A.H.Y. *et al.* (2001) Systematic genetic analysis with ordered arrays of yeast deletion mutants. *Science*, **294**, 2364–2368.

Tzivion,G. *et al.* (2001) 14-3-3 proteins; bringing new definitions to scaffolding. *Oncogene*, **20**, 6331–6338.

Usui,T. and Petrini,J.H.J. (2007) The *Saccharomyces cerevisiae* 14-3-3 proteins Bmh1 and Bmh2 directly influence the DNA damage-dependent functions of Rad53. *Proc. Natl Acad. Sci. USA*, **104**, 2797–2802.

Vincent,O. *et al.* (2001) Subcellular localization of the Snf1 kinase is regulated by specific β subunits and a novel glucose signaling mechanism. *Genes Dev.*, **15**, 1104–1114.

Weinert,T.A. and Hartwell,L.H. (1993) Cell cycle arrest of *cdc* mutants and specificity of the *RAD9* checkpoint. *Genetics*, **134**, 63–80.

OPEN ACCESS Freely available online

PLoS GENETICS

Quantitative Fitness Analysis Shows That NMD Proteins and Many Other Protein Complexes Suppress or Enhance Distinct Telomere Cap Defects

Stephen Gregory Addinall[1,2☯], Eva-Maria Holstein[1,2☯], Conor Lawless[2☯], Min Yu[1,2], Kaye Chapman[1,2¤], A. Peter Banks[1,2], Hien-Ping Ngo[1], Laura Maringele[3], Morgan Taschuk[2,4], Alexander Young[2,5], Adam Ciesiolka[1,2], Allyson Lurena Lister[2,4], Anil Wipat[1,2,4], Darren James Wilkinson[2,5], David Lydall[1,2]*

1 Institute for Cell and Molecular Biosciences, Newcastle University Medical School, Newcastle upon Tyne, United Kingdom, **2** Centre for Integrated Systems Biology of Ageing and Nutrition, Institute for Ageing and Health, Newcastle University Campus for Ageing and Vitality, Newcastle upon Tyne, United Kingdom, **3** Crucible Laboratory, Institute for Ageing and Health, Newcastle University Centre for Life, Newcastle upon Tyne, United Kingdom, **4** School of Computing Science, Newcastle University, Newcastle Upon Tyne, United Kingdom, **5** School of Mathematics and Statistics, Newcastle University, Newcastle upon Tyne, United Kingdom

Abstract

To better understand telomere biology in budding yeast, we have performed systematic suppressor/enhancer analyses on yeast strains containing a point mutation in the essential telomere capping gene *CDC13* (*cdc13-1*) or containing a null mutation in the DNA damage response and telomere capping gene *YKU70* (*yku70*Δ). We performed Quantitative Fitness Analysis (QFA) on thousands of yeast strains containing mutations affecting telomere-capping proteins in combination with a library of systematic gene deletion mutations. To perform QFA, we typically inoculate 384 separate cultures onto solid agar plates and monitor growth of each culture by photography over time. The data are fitted to a logistic population growth model; and growth parameters, such as maximum growth rate and maximum doubling potential, are deduced. QFA reveals that as many as 5% of systematic gene deletions, affecting numerous functional classes, strongly interact with telomere capping defects. We show that, while Cdc13 and Yku70 perform complementary roles in telomere capping, their genetic interaction profiles differ significantly. At least 19 different classes of functionally or physically related proteins can be identified as interacting with *cdc13-1*, *yku70*Δ, or both. Each specific genetic interaction informs the roles of individual gene products in telomere biology. One striking example is with genes of the nonsense-mediated RNA decay (NMD) pathway which, when disabled, suppress the conditional *cdc13-1* mutation but enhance the null *yku70*Δ mutation. We show that the suppressing/enhancing role of the NMD pathway at uncapped telomeres is mediated through the levels of Stn1, an essential telomere capping protein, which interacts with Cdc13 and recruitment of telomerase to telomeres. We show that increased Stn1 levels affect growth of cells with telomere capping defects due to *cdc13-1* and *yku70*Δ. QFA is a sensitive, high-throughput method that will also be useful to understand other aspects of microbial cell biology.

Citation: Addinall SG, Holstein E-M, Lawless C, Yu M, Chapman K, et al. (2011) Quantitative Fitness Analysis Shows That NMD Proteins and Many Other Protein Complexes Suppress or Enhance Distinct Telomere Cap Defects. PLoS Genet 7(4): e1001362. doi:10.1371/journal.pgen.1001362

Editor: Sue Biggins, Fred Hutchinson Cancer Research Center, United States of America

Received September 9, 2010; **Accepted** March 2, 2011; **Published** April 7, 2011

Funding: This work was supported by the Biotechnology and Biological Sciences Research Council UK (B/C008200/1 and BB/F006039/1), a research BBSRC fellowship to DJW (BBF0235451) by the Engineering and Physical Sciences Research Council UK, and the Wellcome Trust (075294). AY was funded by a BBSRC undergraduate vacation bursary. The funders had no role in study design, data collection and analysis, decision to publish, or preparation of the manuscript.

Competing Interests: The authors have declared that no competing interests exist.

* E-mail: d.a.lydall@ncl.ac.uk

☯ These authors contributed equally to this work.

¤ Current address: Health Protection Agency North East, Citygate, Newcastle upon Tyne, United Kingdom

Introduction

Linear chromosome ends must be protected from the DNA damage response machinery and from shortening of chromosome ends during DNA replication [1,2]. Chromosome ends therefore adopt specialized structures called telomeres, distinct from double-stranded DNA breaks elsewhere in the genome. Telomeric DNA is protected, or capped and replicated by a large number of different DNA-binding proteins in all eukaryotic cell types [2,3].

In budding yeast, numerous proteins contribute to telomere capping and amongst these are two critical protein complexes, the Yku70/Yku80 (Ku) heterodimer and the Cdc13/Stn1/Ten1 (CST) heterotrimeric complex [4]. Orthologous protein complexes play roles at telomeres in other eukaryotic cell types suggesting that understanding the function of the Ku and CST protein complexes in budding yeast will be generally informative about key aspects of eukaryotic telomere structure and function.

In budding yeast Yku70 is a non-essential protein that has multiple roles in DNA repair and at telomeres, being involved in the non-homologous end-joining (NHEJ) DNA repair pathway, in the protection of telomeres and the recruitment of telomerase. The mammalian orthologue, Ku70, has similar properties [5]. In budding yeast, deletion of the *YKU70* gene (*yku70*Δ) results in short telomeres and temperature sensitivity [6]. At high temperatures, cells lacking Yku70 accumulate ssDNA at telomeres, which activates the DNA damage response and leads to cell-cycle arrest [7,8,9].

Author Summary

Telomeres, specialized structures at the end of linear chromosomes, ensure that chromosome ends are not mistakenly treated as DNA double-strand breaks. Defects in the telomere cap contribute to ageing and cancer. In yeast, defects in telomere capping proteins can cause telomeres to behave like double-strand breaks. To better understand the telomere and responses to capping failure, we have combined a systematic yeast gene deletion library with mutations affecting important yeast telomere capping proteins, Cdc13 or Yku70. Quantitative Fitness Analysis (QFA) was used to accurately measure the fitness of thousands of different yeast strains containing telomere capping defects and additional deletion mutations. Interestingly, we find that many gene deletions suppress one type of telomere capping defect while enhancing another. Through QFA, we can begin to define the roles of different gene products in contributing to different aspects of the telomere cap. Strikingly, mutations in nonsense-mediated mRNA decay pathways, which degrade many RNA molecules, suppress the *cdc13-1* defect while enhancing the *yku70*Δ defect. QFA is widely applicable and will be useful for understanding other aspects of yeast cell biology.

Cdc13 is a constituent of the essential budding yeast Cdc13-Stn1-Ten1 (CST) protein complex which is analogous to the CST complex found recently in mammalian, plant and fission yeast cells [10,11]. Cdc13 binds to ssDNA overhangs at telomeres and functions in telomerase recruitment and telomere capping [12,13,14]. Acute inactivation of Cdc13 by the temperature sensitive *cdc13-1* allele induces ssDNA generation at telomeres and rapid, potent checkpoint-dependent cell cycle arrest [14].

cdc13-1 or *yku70*Δ mutations each cause temperature dependent disruption of telomere capping that is accompanied by ssDNA production, cell-cycle arrest and cell death [7,15]. Interestingly, the poor growth imparted by each mutation can be suppressed by deletion of *EXO1*, removing the Exo1 nuclease that contributes to ssDNA production when either Cdc13 or Yku70 is defective [7]. However, *cdc13-1* and *yku70*Δ mutations show a synthetic poor growth interaction [8] and different checkpoint pathways are activated by each mutation [7]. These latter observations, along with numerous others, show that CST and Ku complexes perform distinct roles capping budding yeast telomeres and that further clarification of their functions at the telomere is important to help understand how eukaryotic telomeres function.

Many insights into the telomere cap and the DNA damage responses induced when capping is defective were first identified as genetic interactions. For example all DNA damage checkpoint mutations suppress the temperature sensitive growth of *cdc13-1* mutants [16], but only a subset of these suppress the temperature sensitive growth of *yku70*Δ mutants [7]. We reasoned that the roles of Cdc13 and Yku70 at telomeres could be further understood by quantitative, systematic analysis of genetic interactions between telomere capping mutations and a genome-wide collection of gene deletions.

We used standard synthetic genetic array (SGA) approaches to combine the systematic gene deletion collection with *cdc13-1* and *yku70*Δ mutations [17,18]. After this, strain fitnesses were measured at a number of temperatures by quantitative fitness analysis (QFA). For QFA, liquid cultures were spotted onto solid agar plates and culture growth was followed by time course photography. Images were processed and fitted to a logistic growth model to allow an accurate estimation of growth parameters, such as doubling time. In other high-throughput experiments such as SGA or EMAP approaches, culture fitness is determined from colony size [17,18,19]. In QFA, analysis of growth curves of cultures grown on solid agar plates allows us to measure fitness more precisely.

Through QFA we identify hundreds of gene deletions, in numerous different classes, showing genetic interactions with *cdc13-1*, *yku70*Δ or both. One particularly striking example of the type of genetic interactions we measured by QFA is between deletions affecting nonsense mediated RNA decay pathways (*upf1*Δ, *upf2*Δ, *upf3*Δ), *cdc13-1* and *yku70*Δ. Additional experiments show that disabling nonsense mediated mRNA decay pathways, using *upf2*Δ as an example, suppresses the *cdc13-1* defect but enhances the *yku70*Δ defect by increasing the levels of the telomere capping protein Stn1. QFA is generally applicable and will be useful for understanding other aspects of yeast cell biology or studying other microorganisms.

Results

QFA identifies gene deletions that interact with *cdc13-1* and *yku70*Δ

To systematically examine genetic interactions between a genome-wide collection of gene deletion strains (*yfg*Δ, **y**our **f**avorite **g**ene **d**eletion, to indicate any of ~4200 viable systematic gene deletions) and mutations causing telomere capping defects we crossed the knockout library to *cdc13-1* or *yku70*Δ mutations, each affecting the telomere, or to a neutral control query mutation (*ura3*Δ) using SGA methodology [17,18]. Since both *cdc13-1* and *yku70*Δ mutations cause temperature sensitive defects, we generated all double mutants at low, permissive temperatures before measuring the growth of double mutants at a number of semi-permissive or non-permissive temperatures. We cultured *yku70*Δ *yfg*Δ strains at 23°C, 30°C, 37°C and 37.5°C, *cdc13-1 yfg*Δ strains at 20°C, 27°C and 36°C and *ura3*Δ *yfg*Δ strains at 20°C, 27°C and 37°C and measured fitness.

Double mutant fitness was measured after spotting of dilute liquid cultures onto solid agar. We estimate approximately 100 separate cells were placed in each of 384 spots on each agar plate. Fitness of thousands of individual cultures, each derived from spotted cells, was deduced by time course photography of agar plates followed by image processing, data analysis, fitting of growth measurements to a logistic model and determination of quantitative growth parameters (Figure 1) [20,21,22]. We fitted logistic growth model parameters to growth curves allowing us to estimate maximum doubling rate (MDR, population doublings/day) and maximum doubling potential (MDP, population doublings) of approximately 12,000 different yeast genotypes (e.g. *cdc13-1 yfg1*Δ, *yku70*Δ *yfg1*Δ, etc.) at several temperatures. At least eight independent biological replicates for each strain at each temperature were cultured and repeatedly photographed, capturing more than 4 million images in total. To rank fitness we assigned equal importance to maximum doubling rate and maximum doubling potential and defined strain fitness as the product of the MDR and MDP values (Fitness, F, population doublings^2/day). Other measures of fitness can be derived from the sets of logistic parameters available from Text S1.

Figure 1A shows approximately 170 example images, corresponding to eight independent time courses for each of three pairwise combinations of *yku70*Δ, *ura3*Δ and *upf2*Δ mutations. These example images clearly show, qualitatively, that *upf2*Δ *yku70*Δ strains grow less well than *yku70*Δ *ura3*Δ strains, which in turn grow less well than *upf2*Δ *ura3*Δ strains at 37°C. These fitness

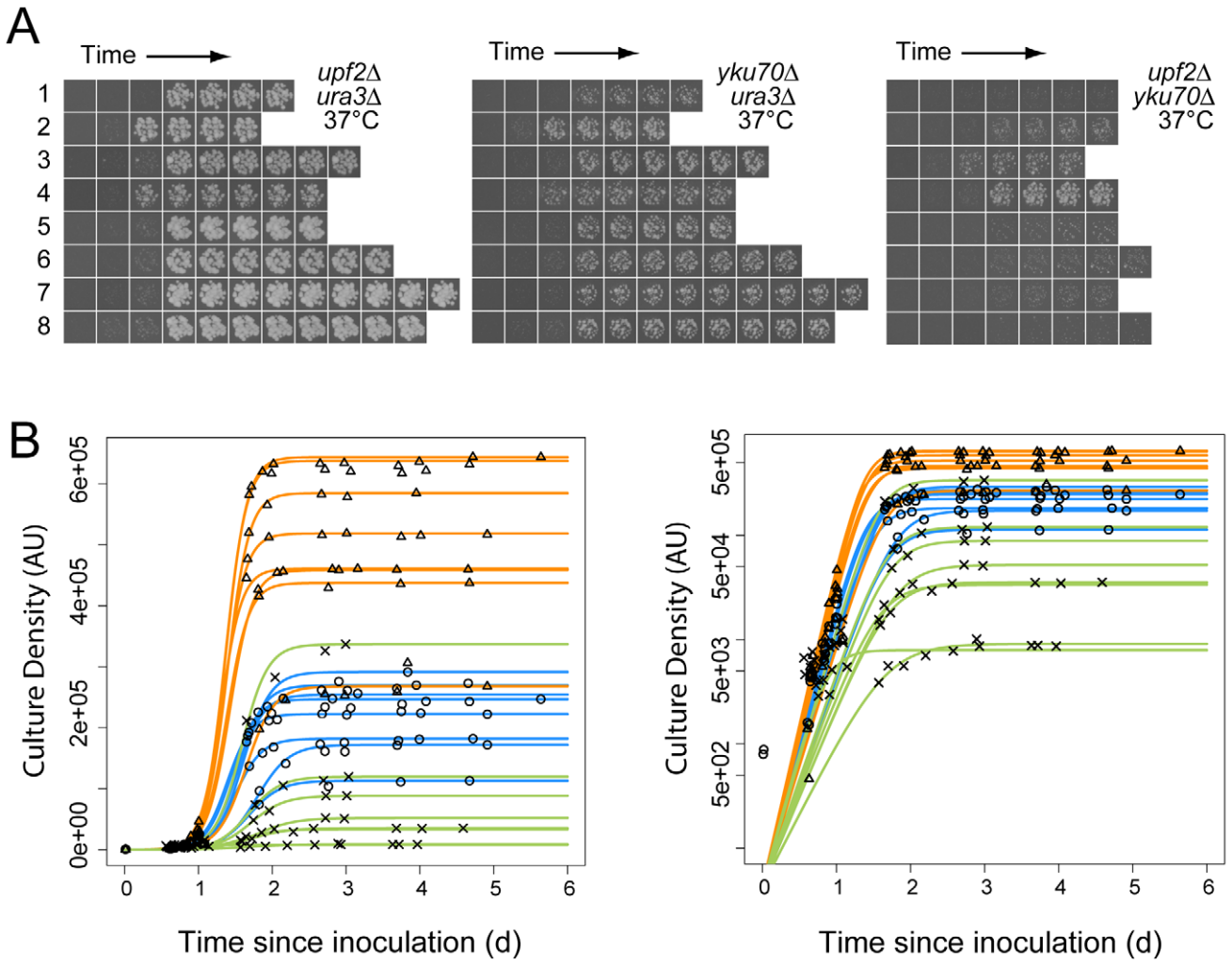

Figure 1. Cell fitness determination from growth on agar plates for quantitative fitness analysis (QFA). A) Time course images of eight independent *upf2*Δ *ura3*Δ, *yku70*Δ *ura3*Δ and *upf2*Δ *yku70*Δ strains at the indicated temperatures; B) Cell density of individual replicate cultures was determined after image-analysis. The logistic growth model is fitted to each culture density time-series. The same data are plotted on linear or logarithmic scales on left and right respectively. C) Average values for Maximum Doubling Rate, Maximum Doubling Potential and Fitness (MDR, MDP and F respectively; see Text S1, experimental procedures), determined from the fitted curves. Data for *yku70*Δ *ura3*Δ is presented here to illustrate epistasis between *yku70*Δ and *upf3*Δ, however this is not how epistasis was calculated (see Figure 2 and Text S1, experimental procedures).
doi:10.1371/journal.pgen.1001362.g001

measures are consistent with numerous earlier studies, showing that *yku70*Δ mutants do not grow well at high temperatures, but also demonstrate a novel observation, that the *upf2*Δ mutation enhances the *yku70*Δ defect and this is further investigated below. Images like those in Figure 1A were processed, quantified, plotted and logistic growth curves fitted to the data (Figure 1B). We applied QFA to all genotypes at each temperature, as the three examples in Figure 1C illustrate.

QFA of telomere capping mutants

QFA of *cdc13-1 yfg*Δ, *yku70*Δ *yfg*Δ and *ura3*Δ *yfg*Δ double mutant libraries was performed at a number of temperatures and therefore a variety of informative comparisons were possible. For example to help identify gene deletions that suppress or enhance the *yku70*Δ temperature dependent growth defect it is useful to compare the fitness of *yku70*Δ *yfg*Δ cells incubated at 37.5°C, with that of control, *ura3*Δ *yfg*Δ, cells incubated at 37°C. In Figure 2, genes which, when deleted, suppress the *yku70*Δ phenotype at 37.5°C will be positioned above the linear regression line and enhancers of *yku70*Δ defects below the line. *yfg*Δ mutations that result in low fitness when combined with the neutral *ura3*Δ mutation will be found on the left and those with high fitness on the right of the x-axis.

The location of each gene in Figure 2 indicates the effect of each deletion on fitness of *yku70*Δ strains versus the effect of the deletion on fitness of *ura3*Δ strains. The regression line drawn through all data points (solid gray line) indicates the expected *yku70*Δ *yfg*Δ

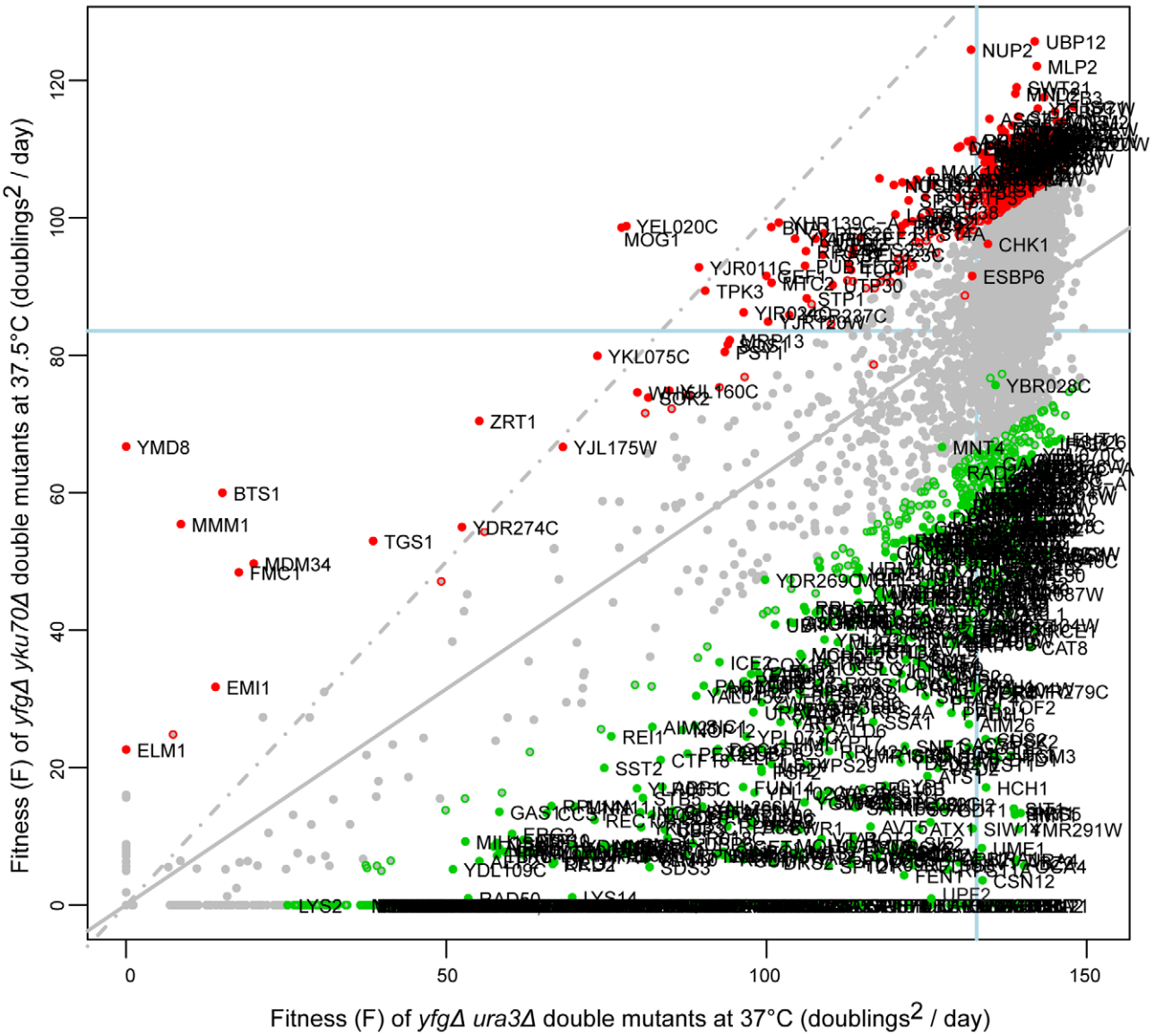

Figure 2. Fitness of *yku70*Δ strains at high temperature. The yeast genome knock out collection was crossed to the *yku70*Δ mutation, or as a control to the *ura3*Δ mutation. 8 replicate crosses were performed and for each, the fitness of all double mutant cultures measured as in Figure 1. Growth of *yku70*Δ *yfg*Δ (“*your favourite gene deletion*”) double mutants was measured at 37.5°C and *ura3*Δ *yfg*Δ strains at 37°C. Gene deletions that significantly enhance (green) or suppress (red) the *yku70*Δ defect, in comparison with the *ura3*Δ mutation are indicated. Those marked by open circles have p-values <0.05 and those filled circles have FDR corrected p-values (q-values) <0.05. The line of equal growth (dashed grey) and a population model of expected fitness (solid grey) are indicated. The average position of *his3*Δ strains are indicated by solid light-blue lines on each axis, as proxy for “wild-type” growth.
doi:10.1371/journal.pgen.1001362.g002

fitness given the fitness of the corresponding *ura3*Δ *yfg*Δ mutant. The line of equal growth (dashed gray line) shows the expected positions of *yku70*Δ *yfg*Δ strains if they grew similarly to *ura3*Δ *yfg*Δ strains. Comparing the linear regression with the line of equal growth, it is clear that *yku70*Δ mutants grow poorly relative to control *ura3*Δ mutants, as expected due to the temperature dependent telomere uncapping observed in *yku70*Δ mutants. Figure 2 also highlights large numbers of *yku70*Δ *yfg*Δ strains growing significantly better than expected, given the fitness of the equivalent *ura3*Δ *yfg*Δ mutation at 37°C (red data points, Figure 2) and these *yfg*Δ genes can be classified as *yku70*Δ suppressors. There are also large numbers of *yku70*Δ *yfg*Δ strains that grow worse than expected and these are classified as *yku70*Δ enhancers (green data points, Figure 2). Three further example plots comparing growth of *yfg*Δ *cdc13-1* versus *yfg*Δ *ura3*Δ at 20°C; *yfg*Δ *cdc13-1* versus *yfg*Δ *ura3*Δ at 27°C and *yfg*Δ *ura3*Δ at 37°C versus *yfg*Δ *ura3*Δ at 20°C are shown in Figure S1 and others can be found on our supporting information data files website.

We estimated genetic interaction strength (GIS) as the vertical displacement of each *yku70*Δ *yfg*Δ normalised mutant fitness from the expected normalised fitness, with expected fitness given by a linear regression model (see Text S1, experimental procedures). GIS is dimensionless. This method is equivalent to defining GIS as the deviation of observed fitness from that expected if a multiplicative model of genetic interaction were correct. In all, more than 30,000 genetic interaction strengths, together with their statistical significances, were calculated (Tables S1, S2, S3, S4, S5, S6). Table 1 summarizes the numbers of statistically significant

Table 1. Percentage of deletions suppressing or enhancing query mutation fitness defects in specific QFA screens.

	Suppressors (%)		Enhancers (%)	
	GIS≥0	GIS≥0.5	GIS≤0	GIS≤−0.5
cdc13-1 20°C	1.65	0.07	2.06	0.22
cdc13-1 27°C	10.11	4.85	7.15	2.60
cdc13-1 36°C	0.53	0.53	0.00	0.00
yku70Δ 23°C	1.46	0.07	3.76	0.61
yku70Δ 30°C	0.61	0.05	4.07	0.73
yku70Δ 37°C	0.92	0.12	7.93	2.52
yku70Δ 37.5°C	3.42	0.12	13.19	5.14

We examined the effects of 4,120 gene deletions, ignoring deletions that were technically problematic (e.g. displayed linkage with query mutation, affected uracil, leucine or histidine biosynthesis). The table above shows percentages classified as significant suppressors (FDR corrected q-value <0.05, +ve GIS) or significant enhancers (FDR corrected q-value <0.05, -ve GIS) and with strong interactions (|GIS| ≥0.5).

doi:10.1371/journal.pgen.1001362.t001

genetic interactions observed under the different conditions of telomere capping. Table 1 clearly illustrates that many more genetic interactions are observed under conditions of mild telomere uncapping (*cdc13-1* strains at 27°C and *yku70*Δ strains at 37.5°C) and that at these temperatures around 5% of gene deletions can show strong suppressing or enhancing interactions (GIS >0.5).

Comparing genetic interactions between *cdc13-1* and *yku70*Δ

In order to compare the effects of gene deletions on cell fitness when combined with *cdc13-1* or *yku70*Δ induced telomere cap defects, it was particularly useful to compare the GIS of each gene with respect to *cdc13-1* or *yku70*Δ after induced telomere uncapping. Figure 3 summarises how different gene deletions interact with the two types of telomere capping defect, suppressing, enhancing or showing no strong interaction with each telomere cap defect. For example, genes that when deleted significantly suppress temperature sensitivity of both *cdc13-1* and *yku70*Δ mutants appear in the top right of this plot (Figure 3, region 3). *EXO1* is in this area as expected because Exo1 generates ssDNA at telomeres in both types of telomere capping mutants (Figure 3, region 2/3, arrow) [7]. Deleting components of the checkpoint sliding clamp (9-1-1 complex) and its clamp loader, suppress *cdc13-1* but have minor effects on growth of *yku70*Δ mutants [7]. *DDC1*, *RAD17* and *RAD24* are in region 2, as expected. *MEC3*, encoding the third component of the sliding clamp was missing from our knock out library and was not tested. Gene deletions that disrupt the telomerase enzyme directly (*est1*Δ, *est3*Δ) enhance the temperature sensitivity of both mutations and so appear in region 7. Genes that, when deleted, suppress *cdc13-1* yet enhance the *yku70*Δ temperature sensitivity (Figure 3, region 1) represent a novel telomere-related phenotype and interestingly include three major components of the nonsense mediated RNA decay pathways (*UPF1, UPF2, UPF3*). It is reassuring that the *UPF* genes cluster so closely in Figure 3 because this strongly suggests that positioning of genes on this plot is an accurate measure of the function of the corresponding gene products in telomere biology.

The position of *YKU80* in the bottom right corner of region 8 is informative. The negative interaction of *yku80*Δ with *cdc13-1* is expected since it is known that *yku80*Δ (and *yku70*Δ) mutations reduce fitness of *cdc13-1* mutants, even at permissive temperatures [8]. However, the positive effect of *yku80*Δ on the growth of *yku70*Δ mutants appears, at first, surprising. The positive epistatic effect simply reflects the fact that *yku70*Δ, *yku80*Δ and *yku70*Δ *yku80*Δ double mutants are all similarly unfit at high temperatures. We have confirmed that in the different W303 genetic background that *yku70*Δ, *yku80*Δ and *yku70*Δ *yku80*Δ double mutants are all similarly unfit at high temperatures. According to the multiplicative model of epistasis the fitness of the *yku70*Δ *yku80*Δ double mutants is significantly higher than expected based on the fitness of the single mutants. Thus, by this criterion, *yku80*Δ suppresses the *yku70*Δ fitness defect. These data can be explained if neither single sub-unit of the Ku comlex retains a telomere capping function in the absence of the other.

It is reasonable to hypothesize, based partly on the behaviour of *UPF1, UPF2* and *UPF3* genes, that genes having similar genetic interactions with *cdc13-1* and *yku70*Δ under particular conditions which are proximal in Figure 3 share similar functions in telomere biology. For example, genes that function similarly to *EXO1* and for example, regulate ssDNA at uncapped telomeres might appear close to *EXO1* in Figure 3. Similarly, genes with strong effects on telomerase function might appear in region 7. Consistent with this hypothesis, it is clear from Figure 3 that many genes encoding members of the same protein complex, or proteins which work together to perform a particular function, often have similar genetic interaction profiles and are located in similar positions on this plot. Examples in Figure 3 include: NMD pathway (*UPF1*, *UPF2*, *UPF3*, region 1); OCA complex (regions 1 & 4); clamp-loader and clamp-like complex (*RAD24*, *DDC1*, *RAD17*, region 2); telomerase (*EST1*, *EST3*, region 7) and dipthamide biosynthesis (*JJJ3*, *DPH1*, *DPH2*, *DPH5*, regions 8 & 9) genes, as well as the numerous other complexes highlighted by the key at the bottom of Figure 3. Table 2 shows the number of genes found in each section of Figure 3. Table 3 lists 19 different sets of genes that are functionally or physically related and that cluster in Figure 3 as well as the single genes *EXO1, RIF1, RIF2* and *TEL1* also found in interesting positions. *EXO1* is in its expected position but it is interesting that *RIF1* and *RIF2* are found in different positions in Figure 3, suggesting they have different functions in telomere biology. Further experiments in the W303 genetic background confirm the different interactions of *RIF1* and *RIF2* with *cdc13-1* (Xue, Rushton and Maringele, submitted). *TEL1* encodes the ATM orthologue and is required for telomere maintenance and it clusters very near components of telomerase, in region 7.

Groupings such as these and their positioning on this type of plot help generate testable, mechanistic predictions about the roles of proteins/protein complexes on telomere capping in budding yeast. For example, we predict that NMD genes (which we examine further in this study) and dipthamide synthesis genes have opposing effects on both Cdc13-mediated and Yku70-mediated telomere capping, because they lie in opposite corners of Figure 3.

The QFA experiments summarised by Figure 3 were performed in a high-throughput manner with the systematic knock out collection in the S288C genetic background and the fitness of different query mutants was measured in slightly different types of media. It was therefore conceivable that some of the genetic interactions scored were due to: defects in the knock out collection, such as incorrect mutations being present or the presence of suppressor mutations, the S288C genetic background, subsets of the cell populations that progressed through the mass mating, sporulation and germination that occur during SGA or media differences.

To test whether genetic interactions identified by QFA with *cdc13-1* or *yku70*Δ strains were robust observations we retested a

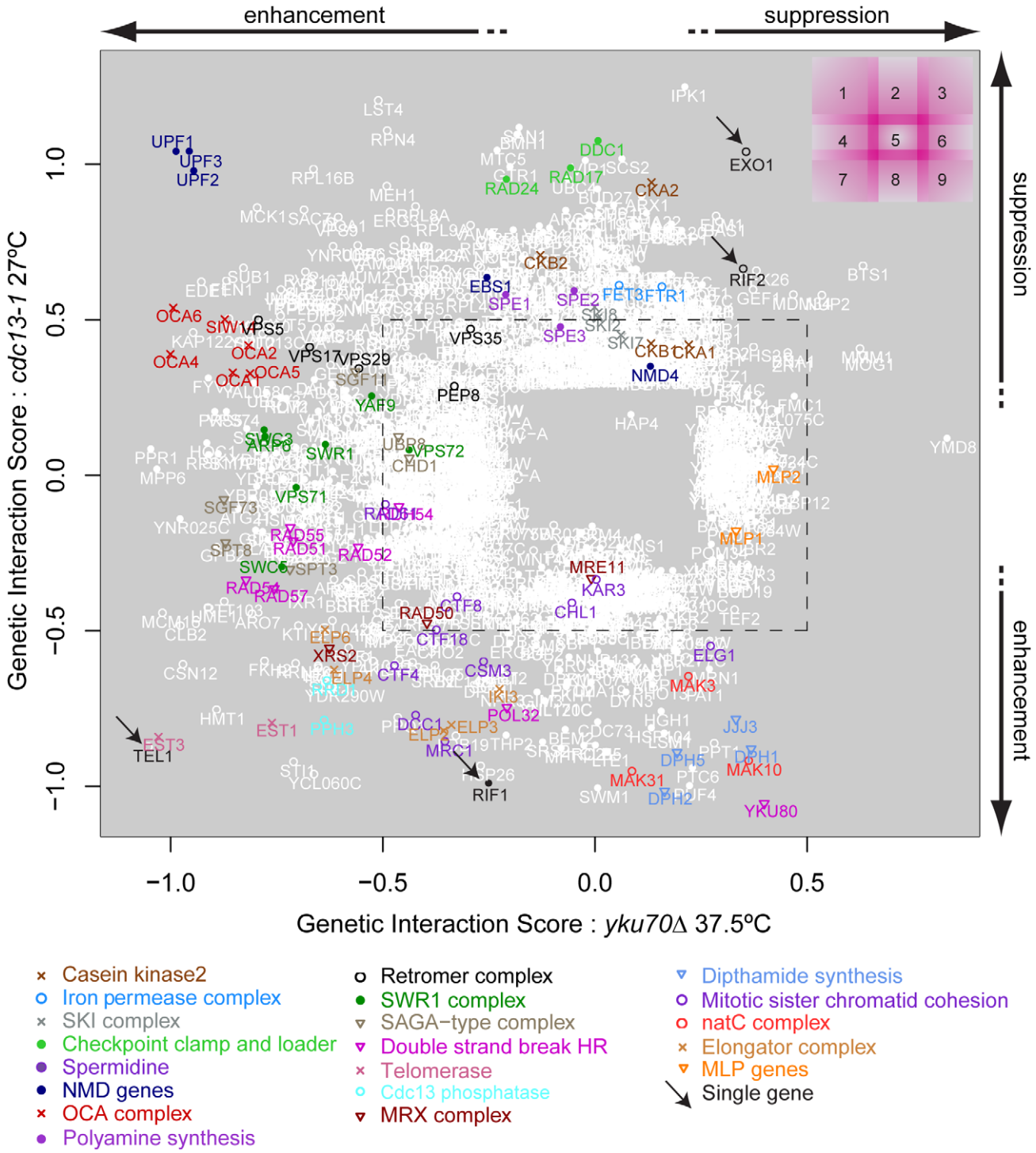

Figure 3. Genetic interaction strength (GIS) comparison between *cdc13-1* and *yku70*Δ. Genes that significantly interacted with *cdc13-1* or *yku70*Δ are shown, most genes did not interact and would be placed in the centre of the plot. Genes encoding components of selected protein complexes (or proteins which work closely together towards the same function) are indicated by colour-co-ordinated text and symbols. Genes that interact with both *cdc13-1* and *yku70*Δ are open white circles, those that interact with just one mutation are filled white circles. Different regions of the plot are indicated on the top right and borders between regions are intentionally blurred/overlapping as there are not precise cut-offs. An arbitrary GIS cutoff of +/−0.5 is indicated by the black dashed rectangle. Also see Figure S3 for further analysis of these data.
doi:10.1371/journal.pgen.1001362.g003

subset of interactions in the W303 genetic background, on rich media, after construction of strains by individual tetrad dissection by manual spot test. Figure 4 and Figure S2 show the behaviour of a number of gene deletions chosen from different regions in Figure 3 to test the effects in W303. In all we measured 26 genetic interactions between 13 gene deletions and *cdc13-1* or *yku70*Δ. Of these we estimate that 20/26 interactions were as expected, 5/26 difficult to classify, and 1/26, due to *elp6*Δ, opposite to that

Table 2. Number and proportion of deletions in each of the nine regions shown in Figure 3.

Region	Number of deletions	% deletions
1	32	0.78
2	34	0.83
3	2	0.05
4	47	1.14
5	70	1.70
6	2	0.05
7	22	0.53
8	25	0.61
9	0	0.00

The number and percentage of gene deletions showing strong genetic interactions (|GIS|≥0.5) in each of the outer regions shown in Figure 3.
doi:10.1371/journal.pgen.1001362.t002

expected after QFA. In particular *exo1*Δ, *mlp1*Δ, *mlp2*Δ, *mak31*Δ and *dph1*Δ mutations suppress the growth defects of *yku70*Δ strains in W303 at 36°C, consistent with their position on the right side of Figure 3 and *exo1*Δ, *rad24*Δ, *upf1*Δ and *upf2*Δ strongly suppress *cdc13-1* at 26°C consistent with their position near the top of Figure 3. *upf1*Δ, *upf2*Δ, *rrd1*Δ and *pph3*Δ mutations all reduced growth of *yku70*Δ strains at 36°C consistent with their position on the left of Figure 3, while *elp6*Δ, *mak31*Δ, *dph2*Δ, *rrd1*Δ and *pph3*Δ mutations all enhanced *cdc13-1* growth defects consistent with their positions near the bottom of Figure 3. Other genes have more subtle effects, the *oca1*Δ and *oca2*Δ mutations had marginal effects on *yku70*Δ strains but improved growth of *cdc13-1* strains (Figure S2). Interestingly the *elp6*Δ mutation enhanced the *cdc13-1* defect at 26°C, as expected, but suppressed the *yku70*Δ strain growth defect at 36°C, the opposite of what was expected from Figure 3. Further experiments will be necessary to clarify the role of Elp6 and other elongator factors in cells with uncapped telomeres. However, overall, it is clear that the majority of genetic interactions identified by QFA are reproducible in smaller scale experiments in a different genetic background.

Analysis of fitness at other temperatures

Suppressors and enhancers of the *cdc13-1* and *yku70*Δ phenotypes were most easily identified at semi-permissive temperatures for the query mutations (Figure 2, Figure 3), however QFA at other temperatures also proved informative. For example, comparison of the fitness of *yfg*Δ *ura3*Δ strains at 37°C versus 20°C, allowed us to identify temperature sensitive mutants (Figure S1C and Table S9). Of the 57 genes which were categorized with a phenotype of "heat sensitivity: increased" in the *Saccharomyces* Genome Database (http://www.yeastgenome.org), as identified by low though-put experiments, which were also present in the knockout library we used, 45 (79% of total) were identified as being significantly heat sensitive by our independent QFA.

2-dimensional GIS plots, like Figure 3, also proved useful for identifying broader patterns of genetic interactions. For example, we observed a difference between the effects of deleting small and large ribosomal subunit genes on the growth of telomere capping mutants (Figure S3A, S3B). Gene deletions which affect the small ribosomal subunit are generally neutral with both *cdc13-1* and *yku70*Δ mutations (Figure S3A, S3B red). In contrast, disruptions of large ribosomal subunit function suppress the effect of *cdc13-1* on average and enhance that of *yku70*Δ (Figure S3A, S3B blue). Although the basis for this novel observation is unknown it may be related to the finding that the large ribosome sub-unit is subject to autophagy upon starvation, whereas the small ribosome sub-unit is not [23]. Positive and negative regulators of telomere length [24,25,26] also showed differing distributions in GIS comparisons – gene deletions which suppress the *yku70*Δ defect are more likely to result in long than short telomeres (Figure S3C). This is perhaps to be expected since *yku70*Δ mutants, on their own, have a short telomere phenotype. Importantly, over 90% of genes identified as suppressors of *cdc13-1* in a previous study [20] showed a positive GIS with *cdc13-1* (Figure S2D), demonstrating that QFA reproduces conclusions derived from qualitatively scored visual inspection. It should be noted however, that the improved sensitivity of QFA has allowed identification of significantly more enhancing mutations than were indentified in the preceding, qualitatively scored study [20].

QFA is sensitive enough to permit identification of genetic interactions even where gene deletions combined with the control *ura3*Δ query mutation impart a poor growth phenotype. For example, deletion of all three *SPE* genes resulted in low fitness that was strongly rescued by *cdc13-1* (Figure S1B, blue, Figure 3 region 2). Interestingly it has recently been reported that increasing spermidine levels increases lifespan in organisms such as yeast, flies and worms [27], but no previous connection with telomeres has been made. Telomere-driven, replicative senescence is thought to be a significant component of the ageing phenotype. Our observations of interactions between *SPE* genes and cells with uncapped telomeres may ultimately lead to experiments to provide insight into the mechanisms by which spermidine affects lifespan.

NMD and telomere capping

One of the most striking results obtained from QFA experiments was the effect of deleting nonsense mediated RNA decay genes on growth of cells with telomere capping mutations. Deletion of any of the NMD genes *UPF1*, *UPF2* or *UPF3* suppresses the *cdc13-1* telomere capping defect but enhances the *yku70*Δ defect (Figure 3, region 1). We wanted to understand the basis of this interesting interaction and decided to further analyze the NMD genes. We also investigated *EBS1*, a gene that has proposed roles in both the NMD pathway and telomere function [28,29,30] and was identified previously as interacting with *CDC13* [20,31]. *EBS1* had less strong, but qualitatively similar GISs to *UPF* genes in our analysis (Figure 3, region 1∼2), suggesting that the position of *EBS1* in Figure 3 was due a partial defect in nonsense mediated RNA decay.

One potential mechanism by which *UPF* genes and *EBS1* affect telomere capping is if they regulate the levels of telomere capping proteins. Indeed, *UPF* genes have been shown to regulate transcripts of genes involved in telomere function [32,33]. The effect of *EBS1* on these transcripts has not so far been reported. Therefore we compared mRNA levels of three NMD targets with roles in telomere regulation (*STN1*, *TEN1* and *EST2*) in *upf2*Δ, *ebs1*Δ and wild-type strains. Transcripts of *STN1* and *TEN1* were increased significantly in *upf2*Δ and *ebs1*Δ, mutants whereas *EST2* transcripts were increased only in *upf2*Δ strains (Figure 5A). We conclude that both *EBS1* and *UPF2* modulate expression of *STN1* and *TEN1*, but the effects of *ebs1*Δ are modest compared to those of *upf2*Δ. Furthermore, elevated levels of Stn1 protein were detected in both *ebs1*Δ and *upf2*Δ mutants (Figure 5B). Consistent with the measured mRNA levels of *STN1*, the increase in Stn1 levels was smaller in *ebs1*Δ strains than *upf2*Δ strains. Thus we concluded that the effects of *UPF2* and *EBS1* could be due to the effects on Stn1 and possibly Ten1 levels.

Table 3. Genes interacting with the telomere cap.

Gene	Comments	Region
EXO1	5′ to 3′ exonuclease, degrades uncapped telomeres in *cdc13-1* and *yku70Δ* mutants.	3
CKA1, CKA2, CKB1, CKB2	Casein kinase 2, a Ser/Thr protein kinase with roles in cell growth and proliferation; holoenzyme contains Cka1, Cka2, Ckb1 and Ckb2	2
FET3, FTR1	Iron permease	2
SKI2, SKI7, SKI8	Ski complex component and putative RNA helicase, mediates 3′-5′ RNA degradation by the cytoplasmic exosome;	2
RAD17, RAD24, DDC1 (MEC3)	Checkpoint sliding clamp and clamp loader. Active in *cdc13-1* mutants, not in *yku70Δ* mutants, affects nuclease activity	2
SPE1, SPE2, SPE3	Spermidine Biosynthesis.	2
UPF1, UPF2, UPF3 [EBS1, NMD4]	ATP-dependent RNA helicase involved in nonsense mediated mRNA decay; required for efficient translation termination at nonsense codons; involved in telomere maintenance	1
OCA1, OCA2, OCA3, OCA4, OCA5, SIW14	Putative protein tyrosine phosphatase, required for cell cycle arrest in response to oxidative damage of DNA	1/4
PEP8, VPS5, VPS17, VPS29, VPS35	Components of the retromer membrane coat complex, essential for endosome-to-Golgi retrograde protein transport	1/4
ARP6, SWC3, SWR1, VPS71, VPS72, YAF9	Components of Swr1 chromatin remodeling complex	4
CHD1, SGF11, SGF73, SPT3, SPT8, UBP8	SAGA nucleosome remodeling complex	4
RAD51, RAD52, RAD54, RAD55, RAD57	Proteins involved in the repair of double-strand breaks in DNA during vegetative growth and meiosis	4
EST1, EST3 (EST2)	Telomerase components	7
TEL1	PI3-like protein kinase. ATM orthologue. Required for telomere length maintenance, interacts with MRX.	7
RRD1, PPH3	Cdc13, serine 306 phosphatase, that affects *de novo* telomere addition at DSB.	7
MRE11, RAD50, XRS2	MRX complex involved in meiosis, telomeres and DSB repair.	7/8
DPH1, DPH2, DPH5, JJJ3	Dph1, Dph2, Kti11, Jjj3 and Dph5, for synthesis of diphthamide, a modified histidine residue of translation elongation factor 2 (Eft1 or Eft2);	8/9
MAK3, MAK10, MAK31	Catalytic subunit of N-terminal acetyltransferase of the NatC type; required for replication of dsRNA virus	8/9
CHL1, CTF4, CTF8, CTF18, DCC1, ELG1, KAR3, MRC1, RAD61	Required for sister chromatid cohesion, replication and/or telomere length maintenance	7/8
ELP2, ELP3, ELP4, ELP6, IKI3	Components of elongator complex, required for modification of wobble nucleosides in tRNA; Recently shown to have a role in DNA replication and at telomeres.	8
RIF1	Rap1 interacting factor 1, long telomeres.	8
RIF2	Rap1 interacting factor 2, long telomeres.	3
MLP1, MLP2	Myosin-like proteins associated with the nuclear envelope	6

Genes that affect growth of *cdc13-1* mutants, *yku70*Δ mutants or both. Genes in ( ) brackets are known components of complexes not co-located. This is either because the deletion is missing from our collection or because the gene deletion is in a different position because, for example, deleting the gene affects the function of the adjacent gene also therefore causing a confounding phenotype. Genes in [ ] brackets are associated with the NMD pathway but have different phenotypes and are located in different positions on the plot.

doi:10.1371/journal.pgen.1001362.t003

Increased Stn1 and Ten1 levels are known to suppress the *cdc13-1* defect [33,34]. To test whether elevated levels of Stn1 or Ten1 proteins could reproduce the enhancement of the *yku70*Δ defect observed in *ebs1*Δ and *upf2*Δ mutants, we over-expressed Stn1 and Ten1 independently of NMD by providing extra copies of *STN1* and *TEN1* on plasmids. Both single copy (centromeric; Figure 5C) and high copy (2 μ) Stn1-expressing plasmids [35] suppressed the temperature sensitivity of *cdc13-1* strains and enhanced the temperature sensitivity of *yku70*Δ strains (Figure S4A), mimicking the *upf2*Δ and *ebs1*Δ phenotypes. In contrast, Ten1-expressing plasmids [35] did not affect the growth of either *cdc13-1* or *yku70*Δ mutants (Holstein; data not shown). We therefore conclude that both *UPF2* and *EBS1* affect telomere capping by modulating expression of *STN1*. However, it is also possible that *UPF2* and *EBS1* affect telomere capping by modulating expression of genes other than *STN1*. To test this and the relative contribution of *STN1* versus any other mechanisms, it would be informative to reduce *STN1* expression in *upf2*Δ mutants. Such experiments might be difficult to perform and interpret since both centromeric single-copy and 2 micron multi-copy *STN1* plasmids suppress the *cdc13-1* defect to similar extents (Figure S4A), suggesting there is not a simple correlation between Stn1 levels and effects on growth of *cdc13-1* and *yku70*Δ mutants.

Since the effect of *ebs1*Δ was milder than that of *upf2*Δ on the fitness of *cdc13-1* and *yku70*Δ cells (Figure 3), we hypothesized that if *ebs1*Δ imparts a mild NMD defect, an *ebs1*Δ *upf2*Δ double mutation would result in the same phenotype as *upf2*Δ on its own. Figure 5D shows that both *upf2*Δ and *ebs1*Δ mutations suppress *cdc13-1* temperature sensitivity and exacerbate *yku70*Δ temperature sensitivity in the W303 genetic background. We also confirmed that *upf1*Δ *upf2*Δ double mutants suppress *cdc13-1*

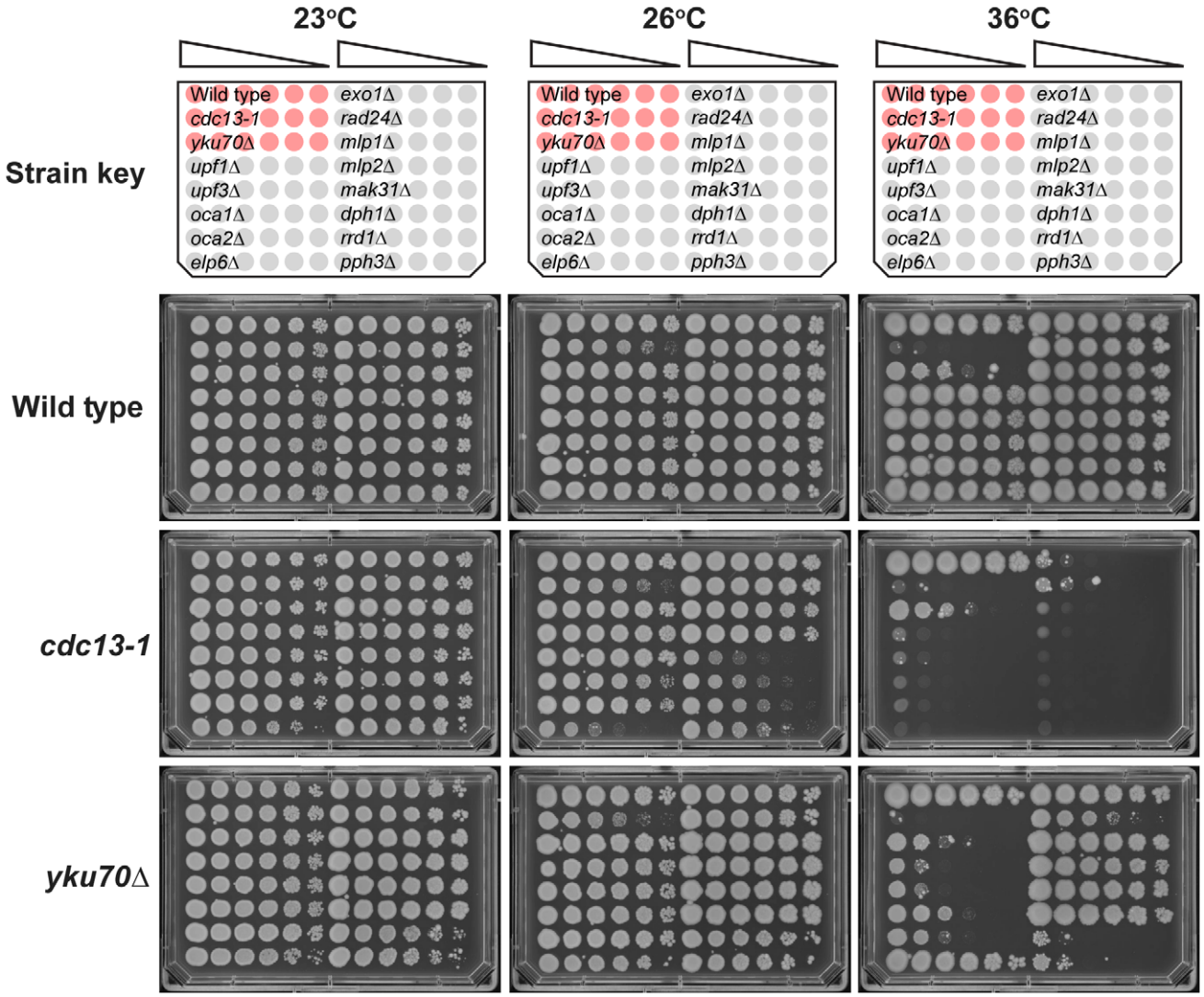

Figure 4. Confirmation of genetic interactions in an alternative genetic background. A selection of genes identified by QFA were combined with either the *yku70*Δ or *cdc13-1* mutations in the W303 genetic background and assessed for growth by manual spot test. Strains were cultured to saturation in 2 ml YPD at 23°C, a six-fold dilution series generated and spotted onto YPD. Strains were incubated at the indicated temperatures for three days before being photographed. All plates contained the reference strains 640 (wild type), 1108 (*cdc13-1*) and 1412 (*yku70*Δ), indicated as red cultures in the key. The "Wild Type" single mutant strains assessed were: 6656, 6811, 3622, 3653, 6620, 1273, 659, 6862, 6927 6951, 6963, 6692 and 6632. The *cdc13-1* double mutant strains assessed were: 6810, 6814, 3624, 3655, 6614, 1296, 1258, 6860, 6928, 6865, 6967, 6694 and 6396. The *yku70*Δ double mutant strains assessed were: 6808, 6812, 4290, 4296, 6628, 1409, 1284, 2413, 2415, 6968, 6971, 6776 and 6763. Growth at other temperatures is shown in Figure S2.
doi:10.1371/journal.pgen.1001362.g004

temperature sensitivity and exacerbate *yku70*Δ temperature similarly to either single mutant (Figure S4B). It is clear that the effects of *ebs1*Δ are less strong than *upf2*Δ mutations and interestingly *upf2*Δ *ebs1*Δ double mutants have slightly stronger effects on growth of both *cdc13-1* and *yku70*Δ mutants, suggesting that *ebs1*Δ effects are not solely due to defects in nonsense mediated RNA decay (Figure 5D). We therefore conclude that, at least with respect to telomere capping, *EBS1* and *UPF2* act partially through different pathways. We do not yet understand these differences, but they may be related to the homology between Ebs1 and the telomerase protein Est1.

It is simple to hypothesize why increased Stn1 levels, caused by inactivation of nonsense mediated mRNA decay pathways, suppress the *cdc13-1* defect, presumably by stabilizing the Cdc13-1/Stn1/Ten1 complex at telomeres. It is less simple to explain why increased Stn1 levels enhance the *yku70*Δ-induced telomere-capping defect. Our hypothesis is based on the facts that the Stn1 protein can inhibit telomerase activity [36,37] and that Yku70 interacts with and helps recruit telomerase to telomeres [38,39]. Thus we hypothesized that *yku70*Δ causes a partial defect in telomerase recruitment, one that is exacerbated by the *upf2*Δ mutation that causes high levels of Stn1, thus inhibiting telomerase activity. To test the simplest version of this hypothesis, that *yku70*Δ and *upf2*Δ mutations reduce the amount of telomerase binding to telomeres, we performed ChIP analyses. We examined binding of the Est2 sub-unit of telomerase in *yku70*Δ, *upf2*Δ and *yku70*Δ *upf2*Δ double mutants. Interestingly we observed a significant reduction in binding of telomerase to telomeres in *yku70*Δ, *upf2*Δ and *yku70*Δ *upf2*Δ mutants (Figure 5E). It is known that *yku70*Δ mutants recruit less telomerase to telomeres [39] but we are unaware of any other

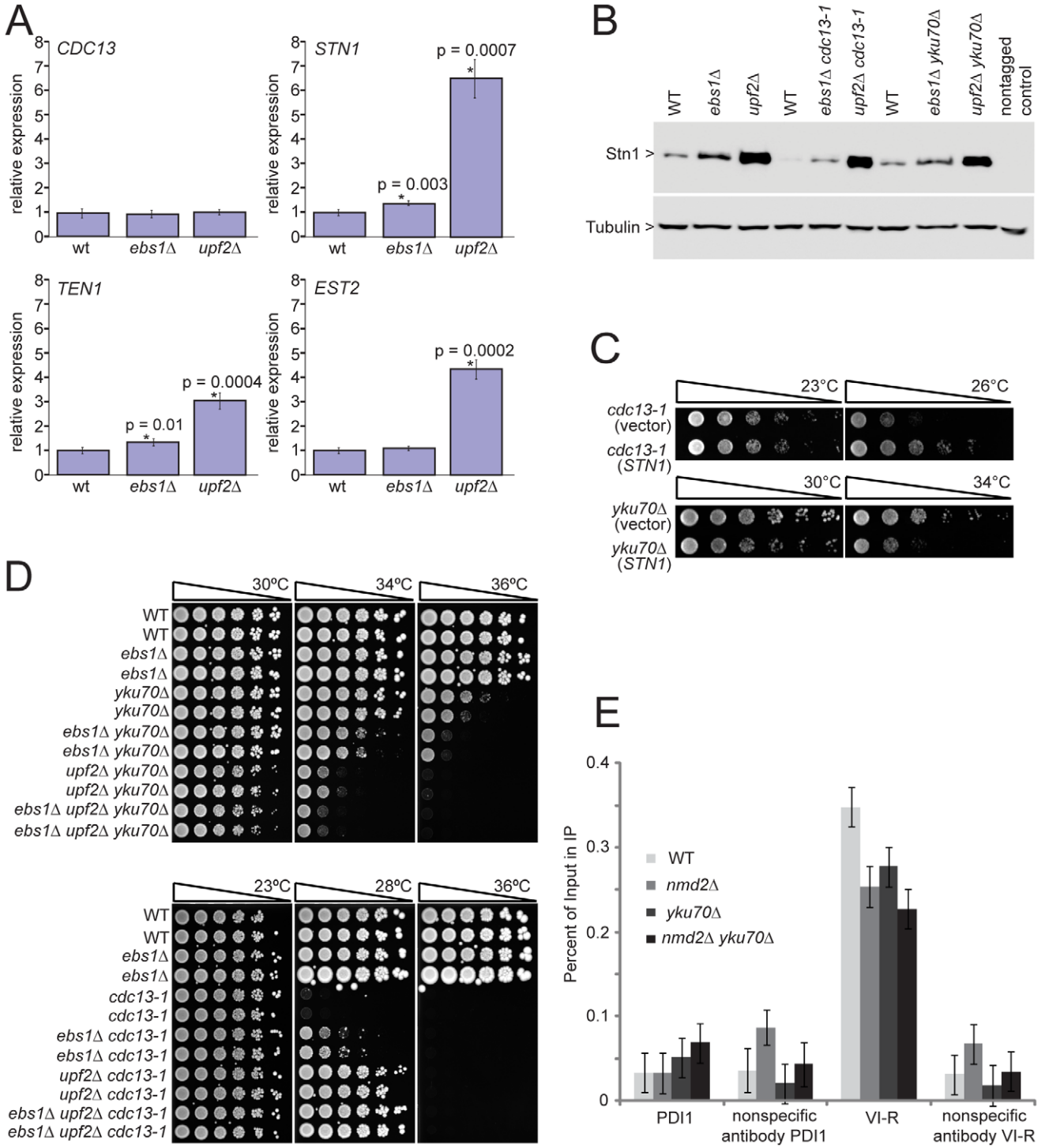

Figure 5. *UPF2* influences telomere capping through *STN1* and telomerase recruitment. A) Transcript levels of four telomere-binding factors measured in *upf2*Δ and *ebs1*Δ mutants. Four strains of each genotype were grown exponentially in liquid culture at 23°C. RNA was isolated and transcript levels were determined by SYBR Green RT-PCR. Each measurement was performed in triplicate and error bars indicate standard deviation from four independent measurements. RNA concentrations of the samples were normalized to the loading control *BUD6*. A single wild type sample was given the value of 1 and all other values were corrected relative to this. Strains measured are 640, 2824, 3001, 4763, 4764, 4765, 4766, 4780, 4781, 4782, 4783 and 4784; B) Western blot analysis of Stn1 protein levels using antibodies against Stn1-13Myc tagged strains. Strains shown are 5757, 5758, 5759, 5760, 5761, 5763, 5764, 5765 and 5766; C) Growth analysis of *yku70*Δ or *cdc13-1* mutants over-expressing *STN1* using the centromeric plasmid pVI1045. The empty vector Ycplac111 was used as a control. Strains 5046, 5047, 5051 and 5052 were spot tested on –LEU medium; D) *upf2*Δ and *ebs1*Δ mutants were combined with *yku70*Δ or *cdc13-1* mutations in the W303 genetic background and assessed for growth by spot test. Strains shown are 640 and 3001 (wild type), 2764 and 2824 (*ebs1*Δ), 2787 and 4309 (*yku70*Δ), 2889 and 2890 (*ebs1*Δ *yku70*Δ), 5007 and 5008 (*nmd2*Δ *yku70*Δ), 5251 and 5242 (*ebs1*Δ *nmd2*Δ *yku70*Δ), 1195 and 4557 (*cdc13-1*), 4576 and 4577 (*ebs1*Δ *cdc13-1*), 4624 and 4625 (*nmd2*Δ *cdc13-1*), 5238 and 5239 (*ebs1*Δ *nmd2*Δ *cdc13-1*); E) ChIP analysis of Est2-13Myc association to the VI-R telomere and the internal locus PDI1 on Chromosome

III using primers previously described [50]. Duplicate cultures were grown and harvested in exponential phase. Individual ChIP samples were measured in triplicate and group means are shown with 95% confidence bars derived from a two-way ANOVA. Strains shown are 6977 (Est2-13Myc), 6978 (*nmd2*Δ Est2-13Myc), 6979 (*nmd2*Δ *yku70*Δ Est2-13Myc) and 6980 (*yku70*Δ Est2-13Myc).
doi:10.1371/journal.pgen.1001362.g005

reports showing that *upf2*Δ mutants recruit less telomerase to telomeres. This observation most likely explains the short telomere phenotype of *upf2*Δ (as well as *yku70*Δ) mutants [24,25]. It is noteworthy that although the *upf2*Δ mutation causes a four-fold increase in the *EST2* transcript, it causes a reduction in the amount of Est2 bound to telomeres. This suggests that the increased levels of Stn1in *upf2*Δ cells more than counteracts any mass action effects on telomerase recruitment to telomeres caused by *EST2* over-expression. However, the simple hypothesis that *yku70*Δ *upf2*Δ mutants show a more severe capping defect because of a reduction in the recruitment of telomerase appears not to be valid. Further experiments will be necessary to better understand the complex interplay between Ku, nonsense mediated decay pathways, Cdc13, Stn1 and telomere capping (Figure 6).

Discussion

Systematic measurement of genetic interactions is a powerful way to help understand how cells and organisms function [40,41]. This is because genetic approaches examine the role of individual gene products, or individual residues in genes, in the context of the whole organism and can help dissect the effects of weak biochemical interactions that are important for cells to function [42]. Systematic SGA and eMAP experiments typically examine millions of genetic interactions and use comparatively crude measures of growth (colony size) to infer genetic interactions [19,41]. Here we have more accurately measured a smaller number of genetic interactions, focusing on interactions that affect budding yeast telomere function. The telomere is an important and interesting subject for systematic genetic analysis because it is a complex, subtle and in some senses paradoxical nucleic acid/protein structure that plays critical roles during human ageing and carcinogenesis. One paradox of telomeres is that many DNA damage response proteins, which induce DNA repair or cell cycle arrest when interacting elsewhere in the genome, induce neither response at telomeres but instead play important roles in telomere physiology.

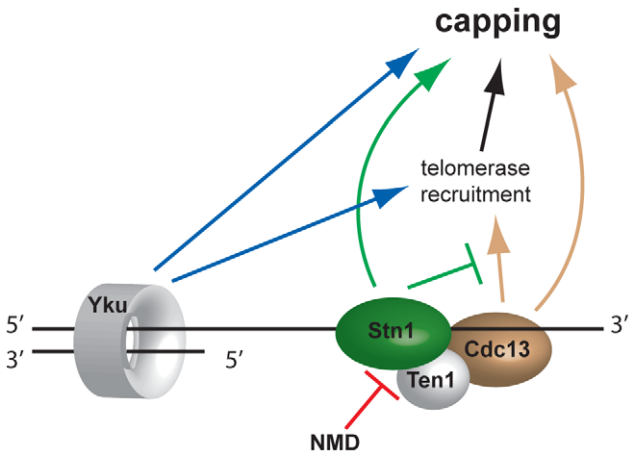

Figure 6. Model of telomere capping activities influenced by NMD. Disruption of NMD activity results in higher Stn1 transcript and protein levels (Figure 5). Stn1 promotes capping directly and is thought to oppose telomerase recruitment through interaction with Cdc13. Since telomerase has telomere capping function, Stn1 therefore both promotes and inhibits telomere capping.
doi:10.1371/journal.pgen.1001362.g006

We used Quantitative Fitness Analysis (QFA) to accurately assess the fitness of many thousands of yeast strains containing mutations that affect telomere function in combination with other deletion mutations. To assess fitness, cells were grown in parallel, in 384 spot arrays on solid agar plates. Photographs of plates were taken, images processed and analysed and growth curves for each culture generated. The growth curves are in essence very similar to those observed in liquid culture, with clear exponential and saturation phases (Figure 2 from Lawless et al. 2010) and can be summarized with as few as three logistic growth parameters. The major advantage of QFA over parallel liquid culture methods to measure yeast fitness is that many more cultures can be examined in parallel. For example we routinely follow the growth of about 18,000 parallel cultures (4,500 yeast strains, incubated at four different temperatures), whereas parallel liquid culture based methods are generally restricted to up to 200 parallel cultures [43].

QFA is similar to SGA or EMAP approaches but typically four times fewer strains per plate are cultured (384 spots versus 1536 colonies) [17,18,19,41]. A further difference between QFA and SGA is that in QFA, which has a liquid growth phase, double mutants are cultured for longer before fitness is assessed. This means that that in QFA, synthetically sick double mutants often show poorer growth than is observed in SGA experiments simply because the more divisions that occur the easier it is to observe growth defects. There is a risk with QFA that during the comparatively long culturing period that suppressors or modifiers will arise. In the experiments we performed in this paper the double mutants show conditional, temperature sensitive defects and were generated in permissive conditions where there was little selection for suppressors/modifiers. The principal advantage of QFA over SGA and EMAP is that QFA provides more accurate fitness measurements that can be measured at higher culture densities. The accuracy of QFA is indicated by the tight clustering of genes affecting particular biochemical pathways/functions in Figure 3.

QFA is also lower throughput than "bar code" based assays where up to 6000 independent strains compete in a single culture [44]. One principal difference between QFA and bar code competition methods is that fitness measures are absolute, rather than comparative.

Comparison of genetic interactions observed in yeast cells containing *cdc13-1* or *yku70*Δ mutations, affecting telomeres in different ways, has generated numerous new insights into telomere biology. For example, we have identified at least 19 groups of genes, each representing a particular protein complex or biological process, that significantly affect growth of cells with telomere capping defects in different ways and these are highlighted in Figure 3. Each of these groups of genes, as well as numerous individual genes, warrant further investigation to characterize how they influence the telomere cap. In this paper we followed up just one striking observation that deletions of NMD pathway genes suppress the *cdc13-1* temperature-sensitive phenotype and enhance the *yku70*Δ temperature sensitive phenotype. In *upf2*Δ strains, levels of *STN1* transcripts and levels of Stn1 protein increased. Our detailed follow-up observations are consistent with the hypothesis that the NMD pathway influences Cdc13- or Yku70-mediated

telomere capping through modification of Stn1 but not Ten1 levels (Figure 6).

As well as helping generate hypotheses about the roles of individual gene products at telomeres QFA will be ideal for developing, constraining and testing dynamic, systems models of the effects of complex biological processes on telomere function. Any model describing cellular growth and division as an outcome of the complex interaction of gene products e.g. [45] could usefully be parameterized and tested by QFA. We expect QFA to be widely applicable to other quantitative phenotypic screens in budding yeast and other microbial systems.

Materials and Methods

Growth media

Library strains created using SGA in this study were cultured in SD/MSG media [17] with appropriate amino-acids and antibiotics added – Canavanine (final concentration, 50 μg/ml); G418 (200 μg/ml); thialysine (50 μg/ml); clonNAT (100 μg/ml); hygromycin B (300 μg/ml). Media were made lacking arginine when using canavanine and lacking lysine when using thialysine. W303 genetic background strains were cultured in YEPD (ade).

Western blot analysis

Cell lysis and western blot analysis were performed as previously described [46]. Antibody 9E10 from Cancer Research UK was used to detect the C-Myc epitope and anti-tubulin antibodies, from Keith Gull, Oxford, UK, used as loading controls.

Quantitiative RT-PCR

RNA extraction and RT-PCR were performed as previously described [47]. RNA concentrations of each sample were normalized relative to the loading control, *BUD6*.

ChIP

Chromatin immunoprecipitation was performed as previously described with minor modifications [48]. Mouse anti-myc (9E10) or goat anti-Mouse antibodies were used for the immunoprecipitations. Immunoprecipitated DNA was quantified by RT-PCR using the SYBR Green qPCR SuperMIX-UDG w/ROX kit (Invitrogen, 11744500).

Plate filling

Rectangular, single chamber, SBS footprint plates (omnitrays; Nunc, Thermo Fisher Scientific) were filled with 35 ml molten agar media using a Perimatic GP peristaltic pump (Jencons (Scientific) Limited, Leighton Buzzard, UK) fitted with a foot switch. 96-well plates (Greiner Bio-One Ltd.) were filled with liquid media or distilled H_2O (200 μl per well) using a Wellmate plate-filler with stacker (Matrix Technologies, Thermo Fisher Scientific).

Robotics

Solid agar to solid agar pinning was performed on a Biomatrix BM3-SC robot (S&P Robotics Inc., Toronto, Canada) using either 384-pin (1 mm diameter) or 1536-pin (0.8 mm diameter) pintools. Inoculation from solid agar to liquid media was performed on the Biomatrix BM3-SC robot using a 96-pin (1 mm diameter) pintool. Resuscitation of frozen strain collections (from liquid to solid agar) was performed on the Biomatrix BM3-SC robot using a 384-pin (1 mm diameter) tool. Re-array procedures were carried out using the BM3-SC robot equipped with a 96-pin rearray pintool. Dilution and spotting of liquid cultures onto solid agar plates was performed on a Biomek FX robot (Beckman Coulter (UK) Limited, High Wycombe, UK) equipped with a pintool magnetic mount and a 96-pin (2 mm diameter) pintool (V&P Scientific, Inc., San Diego, CA, USA). Both the Biomatrix BM3-SC and the Biomek FX were equipped with bar-code readers (Microscan Systems, Inc.) and the bar-codes of plates involved in each experiment were recorded in robot log-files.

Strains, strain collections, oligonucleotide primers, and plasmids

All strains, strain collections oligonucleotide primers and plasmids are described in Text S1. Single gene deletion collections (a gift from C. Boone) were stored at −80°C in 384-well plates (Greiner BioOne) in 15% glycerol and when required, were thawed and pinned onto YEPD + G418 agar. Strains were then routinely pinned onto fresh YEPD + G418 agar plates approximately every two months but were re-pinned from frozen stocks after approximately 6 months. An array containing 6 replicates of 12 telomere-related genes, 14 replicates of *his3*Δ and 6 replicates of 37 randomly chosen genes was created from the original deletion collection (SGAv2). This array (plate 15 in our deletion mutant collections) was designed to quickly check that gene deletions with familiar phenotypes were behaving as expected and to also provide high numbers of replicates for a small number of genes (49) allowing more robust statistical analysis. This collection was SGAv2p15. Collection SGAv3 was made by re-arraying each of the 15 plates of SGAv2p15, randomly, with the exceptions that all *his3*Δ strains on the plate periphery [17] were not moved and genes which were in the corner area of plates in SGAv2p15 were specifically moved to non-corner positions in SGAv3.

Growth assays

Liquid-to-solid agar 384-format robotic spot tests were performed as follows. Colonies were inoculated from solid agar SGA plates into 96-well plates containing 200 μl appropriately supplemented liquid SD/MSG media in each well. These were grown to saturation (usually three days), without shaking, at 20°C. Cultures were resuspended, diluted approximately 1/100 in 200 μl H_2O and spotted onto appropriately supplemented solid SD/MSG media plates which were incubated at different temperatures.

SGA with *cdc13-1* and *yku70*Δ

SGA query strains DLY5688 (*cdc13-1* flanked by *LEU2* and *HPHMX* (Hygromycin^R)), DLY3541 (*yku70*Δ*::URA3*) and DLY4228 (*ura3::NATMX*) were crossed to SDLv2p15 and SDLv3 in quadruplicate, giving eight biological replicate crosses each. Fitness of each strain under different conditions was assayed in 384-spot growth assays. As previously [20], growth at 36°C was used as an indication of failure of the SGA process or spontaneous reversion in SGA screens where *cdc13-1* was the query mutation. In this study, repeats with modeled Trimmed Area >25000 after 6 days at 36°C (provided this included no more than 3 repeats for a single gene deletion) were stripped out. In each SGA experiment, a small number of strains were missing from the starting mutant array (due to mis-pinning, strains being lost, replaced etc.). These experiment-specific missing strains; together with genes affecting selection during SGA; and experiment-specific genes situated within 20 kb of SGA markers; were removed from analysis.

Photography

Solid agar plates were photographed on an spImager (S&P Robotics Inc., Toronto, Canada). The integrated camera

(Canon EOS 40D) was used in manual mode with a pre-set manual focus. Manual settings were as follows: exposure, 0.25 s; aperture, F10; white balance, 3700 K; ISO100; image size, large; image quality, fine; image type, .jpg. Using the spImager software, the plate barcode number and a time stamp (date in year, month, day and time in hour, minute, second) were incorporated as the image name (e.g. DLY00000516-2008-12-24_23-59-59.jpg).

Image analysis

The image analysis tool Colonyzer [21] was used to quantify cell density from captured photographs. Colonyzer corrects for lighting gradients, removing spatial bias from density estimates. It is designed to detect cultures with extremely low cell densities, allowing it to capture a wide range of culture densities after dilute spotting on agar. Colonyzer is available under GPL at http://research.ncl.ac.uk/colonyzer.

384 spot versus 1,536 colony sensitivity

We directly compared QFA of pinned 1536- colony format versus spotted 384- culture format and found that the range of normalized 384 spot fitness is approximately 4 times that estimated from 1,536 colony growth curves (Lawless et al., in prep). We also find that 384 spot fitness estimates adequately captures the strong temperature dependent growth of *cdc13-1* mutants, whereas 1536-format growth estimates do not, and that analysis of growth in 384 spot format captures a much higher dynamic range of cell densities than 1536 colony format (approx 1,000 versus 20 fold, see Fig. 2, Lawless et al, 2010). For these reasons we chose to perform QFA of telomere capping mutants arrayed as 384 spotted cultures.

Sample tracking and data storage

Strain array positions on a 384-spot layout (plate, row, column) were defined in a comma-separated text file and tracked using barcodes reported in robot log-files. Data was stored in a Robot Object Database (ROD) as described previously [20]. Screen data is exported from ROD in tab delimited format (Table S7) ready for modeling and statistical analysis (see below).

Modeling of fitness

Culture density (G) was estimated from captured photographs using the Integrated Optical Density (IOD or Trimmed Area; Table S7) measure of cell density provided by the image-analysis tool Colonyzer (Lawless et al 2010). Observed density time series were summarised with the logistic population model, which is an ODE describing self-limiting population growth. It has an analytical solution *G (t)*:

$$\frac{dG(t)}{dt} = rG(t)\left(1-\frac{G(t)}{K}\right)$$

$$G(t) = \frac{KG_0e^{rt}}{K+G_0(e^{rt}-1)}$$

Modelled inoculum density (G_0, AU) was fixed (at 43 AU in this case), assuming that all liquid cultures reached the same density in stationary phase before water dilution and inoculation onto agar. Logistic parameter values r (growth rate, d^{-1}) and K (carrying capacity, AU) were inferred by least squares fit to observations, using optimization routines in the SciPy Python library (code available from http://sourceforge.net/projects/colonyzer/).

For least-squares minimisation, initial guesses for K were the maximum observed cell density for that culture. For r, we constructed initial guesses by observing that *G'(t)* is at a maximum when $t = t^*$:

$$\frac{d^2G(t^*)}{dt^2} = 0$$

Linearly interpolating between cell density observations we estimated the time of greatest rate of change of density. We then estimated r as:

$$r \approx \frac{\log\left(\frac{K-G_0}{G_0}\right)}{t^*}$$

A quantitative measure of fitness was then constructed from the optimal parameters. The particular measure we used was the product of the maximal doubling rate (*MDR*, doublings.d^{-1}), which is the inverse of the doubling time and the maximal doubling potential (*MDP*, doublings). These phenotypes were quantified using logistic model parameter estimates as follows.

We estimate the minimum doubling time T which the cell population takes to reach a density of $2G_0$ (assuming that the culture is in exponential phase immediately after inoculation):

$$\frac{G(T)}{G(0)} = 2$$

$$\frac{1}{T} = \frac{r}{\log\left(\frac{2(K-G_0)}{K-2G_0}\right)} = MDR$$

MDP is the number of divisions the culture is observed to undergo. Considering cell growth as a geometric progression:

$$G_0 \times 2^{MDP} = K$$

$$MDP = \frac{\log\left(\frac{K}{G_0}\right)}{\log 2}$$

These two phenotypes provide different information about the nature of population fitness and both of them are important, reflecting the rate of growth (*MDR*) and the capacity of the mutant to divide (*MDP*) under given experimental conditions. Our chosen measure of fitness ($F = MDR \times MDP$) places equal importance on these two phenotypes.

Quantifying genetic interaction

To estimate GIS, F is obtained for a particular temperature for both the QFA screen of interest and a second QFA screen using a control query mutation, *ura3*Δ, which is assumed to be neutral under the experimental conditions, approximating wild-type fitness. Experimental and control strain fitnesses are analysed for evidence of epistatic interactions contradicting a multiplicative model of genetic independence [49] (used due to the ratio scale of the phenotype). We denote the fitness of the query (or background) mutation F_{xyz}, that of a typical deletion from the yeast knockout library $F_{yfg\Delta}$ and double mutant fitnesses as $F_{xyz\ yfg\Delta}$. Genetic

independence therefore implies:

$$F_{xyz\ yfg\Delta} \times F_{wild-type} = F_{xyz} \times F_{yfg\Delta}$$

$$F_{ura3\Delta\ yfg\Delta} \times F_{wild-type} = F_{ura3\Delta} \times F_{yfg\Delta}$$

and re-arranging gives:

$$\frac{F_{ura3\Delta\ yfg\Delta} \times F_{wild-type}}{F_{ura3\Delta}} = F_{yfg\Delta}$$

$$\Rightarrow F_{xyz\ yfg\Delta} = F_{xyz} \times \frac{F_{ura3\Delta\ yfg\Delta}}{F_{ura3\Delta}}$$

$$F_{xyz\ yfg\Delta} = M \times F_{ura3\Delta\ yfg\Delta}$$

where $M = F_{xyz}/F_{ura3\Delta}$ is a constant independent of the particular knockout, *yfg*Δ. Thus, after normalising fitnesses ($\tilde{F}$) so that the means across all knockouts for both the experimental (QFA, *xyz yfg*Δ) and control (cQFA, *ura3*Δ *yfg*Δ) mutation strains are equal to 1, evidence that $\tilde{F}_{xyzyfg\Delta}$ is significantly different from $\tilde{F}_{ura3\Delta yfg\Delta}$ is evidence of genetic interaction. Thus for each knockout a model is fitted of the form:

$$\tilde{F}_{ij} = \mu + \gamma_i + \varepsilon_{ij}$$

where $\tilde{F}_{ij}$ $i = 1,2, j = 1,..,n_i$ is the j^{th} normalised fitness for treatment i (cQFA = 1, QFA = 2), μ is the mean fitness for the knockout in the control QFA, $\gamma_1 = 0$, γ_2 represents genetic interaction and ε_{ij} is (normal, iid) random error. Typically n_i is 8 (4 replicates each of SGAv2p15 and SGAv3), but is sometimes a larger multiple of 8 for strains that are repeated in the libraries (e.g. those on plate 15). The model is fitted in R using the lmList command. For each knockout the fitted value of γ_2 is recorded as an estimated measure of the strength of genetic interaction (with the sign indicating suppression or enhancement) and the corresponding *p*-value is used as a measure of statistical significance of the effect. The *p*-value is corrected using the R function p.adjust to give a FDR-corrected *q*-value, and it is this *q*-value which is thresholded to give the lists of statistically significant genetically interacting strains (see Figure 2).

The R code used for the statistical analysis of data from ROD and Colonyzer is available from the authors on request and sample logistic analysis output is presented in Table S8.

Stringent lists of genetic interactors for each query mutation and growth condition (Tables S1, S2, S3, S4, S5, S6) were compiled by imposing a 5% FDR cutoff and arbitrarily removing genes with $-0.5 <$ GIS > 0.5.

Supplementary information data files website

Raw output data and hyperlinked supplementary tables, together with detailed legends for interpretation of data files are available from: http://research.ncl.ac.uk/colonyzer/AddinallQFA/.

Supporting Information

Figure S1 Fitness plots for *cdc13-1 versus ura3*Δ strains at 20°C and 27°C and for *ura3*Δ strains at 20°C versus 37°C. A] Fitness plot showing *cdc13-1* at 20°C, compared with QFA for *ura3*Δ at 20°C. B] Fitness plot showing QFA for of *cdc13-1* at 27°C compared with QFA for *ura3*Δ at 27°C. Note that *SPE1*, *SPE2* and *SPE3* (blue text and symbols) have poor fitness in both conditions but fall above the line of equal growth, hence double mutants with *cdc13-1* grow better than the single deletion strains. Note the tight clustering of the members of the *MRX* complex: *MRE11*, *RAD50* and *XRS2* (blue squares) C] Temperature sensitivity analysis of *ura3*Δ strains comparing fitnesses of *ura3*Δ mutations at 37°C with those at 20°C. A list of stringent temperature sensitive deletion mutations taken from this analysis are presented in Table S9. Figure annotations are as for Figure 2.
Found at: doi:10.1371/journal.pgen.1001362.s001 (1.27 MB TIF)

Figure S2 W303 Spot tests. Strains shown in Figure 4 were incubated at the additional temperatures shown.
Found at: doi:10.1371/journal.pgen.1001362.s002 (2.28 MB TIF)

Figure S3 Genetic interaction strength (GIS) analysis of ribosomal and telomere length maintenance genes. A] Large ribosomal subunit genes [26] (blue) and small ribosomal subunit genes [26] (red) are indicated. B] Contour lines represent the density of large (blue) and small (red) ribosomal subunit genes and all other genes (white). Density was estimated using the kde2d function in the R package MASS (bandwidth = 0.6). Crosses represent the mean location for genes in each group. See also Figure S3. C] Genes identified as affecting telomere length maintenance [24–26] are indicated. Colour represents telomere length, ranging from blue (short telomeres) to red (long telomeres). White indicates telomere length was either wild-type or not measured [24]. D] Genes that were previously identified [20] as suppressors of *cdc13-1* (red) are indicated.
Found at: doi:10.1371/journal.pgen.1001362.s003 (2.22 MB TIF)

Figure S4 Effects of over-expression of *STN1* or Nonsense Mediated Decay genes on telomere capping mutants. A] Spot tests of *yku70*Δ (4413) or *cdc13-1* (1195) mutants over-expressing *STN1* using the centromeric vector pVL1045 and the 2 μ vector pVL1066. The empty centromeric vector Ycplac111 or the 2 μ vector YEplac181 were used as controls. Strains were grown on selective media at the temperatures indicated. B] Spot tests of strains on YEPD at the temperatures indicated. Strains were 2787, 4557, 6656, 4765, 6976, 6808, 5007, 6974, 6975, 6810, 5107, 6867 and 6868.
Found at: doi:10.1371/journal.pgen.1001362.s004 (1.07 MB TIF)

Table S1 List of suppressors and enhancers of *yku70*Δ defect at 23°C. A list of genes which, when deleted, result in suppression or enhancement of the *yku70*Δ phenotype at 23°C. Only included are gene deletions which passed a 5% FDR cutoff and had a GIS of greater than 0.5 (+ or −) in magnitude. http://research.ncl.ac.uk/colonyzer/AddinallQFA/S1_yku70_23.html. See http://research.ncl.ac.uk/colonyzer/AddinallQFA for a list of all significant interactors, a GIS plot showing interactors and raw data.
Found at: doi:10.1371/journal.pgen.1001362.s005 (0.01 MB HTML)

Table S2 List of suppressors and enhancers of *yku70*Δ defect at 30°C. A list of genes which, when deleted, result in suppression or enhancement of the *yku70*Δ phenotype at 30°C. Only included are gene deletions which passed a 5% FDR cutoff and had a GIS of greater than 0.5 (+ or −) in magnitude. http://research.ncl.ac.uk/colonyzer/AddinallQFA/S2_yku70_30.html. See http://research.ncl.ac.uk/colonyzer/AddinallQFA for a list of all significant interactors, a GIS plot showing interactors and raw data.
Found at: doi:10.1371/journal.pgen.1001362.s006 (0.02 MB HTML)

Table S3 List of suppressors and enhancers of *yku70*Δ defect at 37°C. A list of genes which, when deleted, result in suppression or enhancement of the *yku70*Δ phenotype at 37°C. Only included are gene deletions which passed a 5% FDR cutoff and had a GIS of

greater than 0.5 (+ or −) in magnitude. http://research.ncl.ac.uk/colonyzer/AddinallQFA/S3_yku70_37.html. See http://research.ncl.ac.uk/colonyzer/AddinallQFA for a list of all significant interactors, a GIS plot showing interactors and raw data.
Found at: doi:10.1371/journal.pgen.1001362.s007 (0.05 MB HTML)

Table S4 List of suppressors and enhancers of *yku70*Δ defect at 37.5°C. A list of genes which, when deleted, result in suppression or enhancement of the *yku70*Δ phenotype at 37.5°C. Only included are gene deletions which passed a 5% FDR cutoff and had a GIS of greater than 0.5 (+ or −) in magnitude. http://research.ncl.ac.uk/colonyzer/AddinallQFA/S4_yku70_375.html. See http://research.ncl.ac.uk/colonyzer/AddinallQFA for a list of all significant interactors, a GIS plot showing interactors and raw data.
Found at: doi:10.1371/journal.pgen.1001362.s008 (0.10 MB HTML)

Table S5 List of suppressors and enhancers of *cdc13-1* defect at 20°C. A list of genes which, when deleted, result in suppression or enhancement of the *cdc13-1* phenotype at 20°C. Only included are gene deletions which passed a 5% FDR cutoff and had a GIS of greater than 0.5 (+ or −) in magnitude. http://research.ncl.ac.uk/colonyzer/AddinallQFA/S5_cdc131_20.html. See http://research.ncl.ac.uk/colonyzer/AddinallQFA for a list of all significant interactors, a GIS plot showing interactors and raw data.
Found at: doi:10.1371/journal.pgen.1001362.s009 (0.01 MB HTML)

Table S6 List of suppressors and enhancers of *cdc13-1* defect at 27°C. A list of genes which, when deleted, result in suppression or enhancement of the *cdc13-1* phenotype at 27°C. Only included are gene deletions which passed a 5% FDR cutoff and had a GIS of greater than 0.5 (+ or −) in magnitude. http://research.ncl.ac.uk/colonyzer/AddinallQFA/S6_cdc131_27.html. See http://research.ncl.ac.uk/colonyzer/AddinallQFA for a list of all significant interactors, a GIS plot showing interactors and raw data.
Found at: doi:10.1371/journal.pgen.1001362.s010 (0.14 MB HTML)

Table S7 ROD output. Robot log files, metadata and image analysis data are stored in the ROD database, then exported in this format for further analysis. These are text files compressed in. zip format: http://research.ncl.ac.uk/colonyzer/AddinallQFA/RODOutput.zip. See http://research.ncl.ac.uk/colonyzer/AddinallQFA for detailed description of column contents.
Found at: doi:10.1371/journal.pgen.1001362.s011 (131.84 MB ZIP)

Table S8 Logistic data file. ROD output data is subjected to logistic modelling and exported in this format for further analysis. These are text files compressed in .zip format: http://research.ncl.ac.uk/colonyzer/AddinallQFA/Logistic.zip. See http://research.ncl.ac.uk/colonyzer/AddinallQFA for detailed description of column contents.
Found at: doi:10.1371/journal.pgen.1001362.s012 (30.13 MB ZIP)

Table S9 List of suppressors and enhancers of temperature-induced fitness defect at 37°C. A list of genes which, when deleted, result in significantly better or worse growth at 37°C compared to 20°C. Only included are gene deletions which passed a 5% FDR cutoff and had a GIS of greater than 0.5 (+ or −) in magnitude. http://research.ncl.ac.uk/colonyzer/AddinallQFA/S9_cSGA_37_20.html. See http://research.ncl.ac.uk/colonyzer/AddinallQFA for a list of all significant interactors, a GIS plot of these data and raw data.
Found at: doi:10.1371/journal.pgen.1001362.s013 (0.09 MB HTML)

Text S1 Supplemental experimental procedures, strains and strain collections list, supplemental references.
Found at: doi:10.1371/journal.pgen.1001362.s014 (0.12 MB PDF)

Acknowledgments

We would like to thank A. Baryshnikova, C. Boone, M Costanzo, M. Kupiec, C. Myers, and our colleagues in Newcastle for helpful discussions; A Biancchi, C. Boone, B. Chang, M. Downey, D. Durocher, and C. Nugent for providing strains or plasmids; and I Ivanova for advice on CHIP. We are grateful for computational support provided by the Newcastle University Bioinformatics Support Unit.

Author Contributions

Conceived and designed the experiments: SGA EMH CL MY KC APB HPN LM DJW DL. Performed the experiments: SGA EMH CL MY KC APB HPN LM AC. Analyzed the data: SGA EMH CL MY KC APB HPN AY DJW DL. Contributed reagents/materials/analysis tools: LM MT ALL AW DJW. Wrote the paper: SGA EMH CL DJW DL.

References

1. Olovnikov AM (1973) A theory of marginotomy. The incomplete copying of template margin in enzymic synthesis of polynucleotides and biological significance of the phenomenon. J Theor Biol 41: 181–190.
2. Longhese MP (2008) DNA damage response at functional and dysfunctional telomeres. Genes Dev 22: 125–140.
3. Greider CW, Blackburn EH (1985) Identification of a specific telomere terminal transferase activity in *Tetrahymena* extracts. Cell 43: 405–413.
4. Lydall D (2009) Taming the tiger by the tail: modulation of DNA damage responses by telomeres. EMBO J 28: 2174–2187.
5. Fisher TS, Zakian VA (2005) Ku: a multifunctional protein involved in telomere maintenance. DNA Repair (Amst) 4: 1215–1226.
6. Boulton SJ, Jackson SP (1998) Components of the Ku-dependent non-homologous end-joining pathway are involved in telomeric length maintenance and telomeric silencing. EMBO J 17: 1819–1828.
7. Maringele L, Lydall D (2002) *EXO1*-dependent single-stranded DNA at telomeres activates subsets of DNA damage and spindle checkpoint pathways in budding yeast *yku70*Delta mutants. Genes Dev 16: 1919–1933.
8. Polotnianka RM, Li J, Lustig AJ (1998) The yeast Ku heterodimer is essential for protection of the telomere against nucleolytic and recombinational activities. Curr Biol 8: 831–834.
9. Gravel S, Larrivee M, Labrecque P, Wellinger RJ (1998) Yeast Ku as a regulator of chromosomal DNA end structure. Science 280: 741–744.
10. Miyake Y, Nakamura M, Nabetani A, Shimamura S, Tamura M, et al. (2009) RPA-like mammalian Ctc1-Stn1-Ten1 complex binds to single-stranded DNA and protects telomeres independently of the Pot1 pathway. Mol Cell 36: 193–206.
11. Surovtseva YV, Churikov D, Boltz KA, Song X, Lamb JC, et al. (2009) Conserved telomere maintenance component 1 interacts with STN1 and maintains chromosome ends in higher eukaryotes. Mol Cell 36: 207–218.
12. Lin JJ, Zakian VA (1996) The Saccharomyces CDC13 protein is a single-strand TG1-3 telomeric DNA-binding protein in vitro that affects telomere behavior in vivo. Proc Natl Acad Sci U S A 93: 13760–13765.
13. Nugent CI, Hughes TR, Lue NF, Lundblad V (1996) Cdc13p: a single-strand telomeric DNA-binding protein with a dual role in yeast telomere maintenance. Science 274: 249–252.
14. Garvik B, Carson M, Hartwell L (1995) Single-stranded DNA arising at telomeres in *cdc13* mutants may constitute a specific signal for the *RAD9* checkpoint. Mol Cell Biol 15: 6128–6138.
15. Zubko MK, Guillard S, Lydall D (2004) Exo1 and Rad24 differentially regulate generation of ssDNA at telomeres of *Saccharomyces cerevisiae cdc13-1* mutants. Genetics 168: 103–115.
16. Weinert TA, Kiser GL, Hartwell LH (1994) Mitotic checkpoint genes in budding yeast and the dependence of mitosis on DNA replication and repair. Genes Dev 8: 652–665.
17. Tong AH, Boone C (2006) Synthetic genetic array analysis in *Saccharomyces cerevisiae*. Methods Mol Biol 313: 171–192.
18. Tong AH, Evangelista M, Parsons AB, Xu H, Bader GD, et al. (2001) Systematic genetic analysis with ordered arrays of yeast deletion mutants. Science 294: 2364–2368.
19. Collins SR, Miller KM, Maas NL, Roguev A, Fillingham J, et al. (2007) Functional dissection of protein complexes involved in yeast chromosome biology using a genetic interaction map. Nature 446: 806–810.

20. Addinall SG, Downey M, Yu M, Zubko MK, Dewar J, et al. (2008) A genomewide suppressor and enhancer analysis of cdc13-1 reveals varied cellular processes influencing telomere capping in Saccharomyces cerevisiae. Genetics 180: 2251–2266.
21. Lawless C, Wilkinson D, Young A, Addinall S, Lydall D (2010) Colonyzer: automated quantification of micro-organism growth characteristics on solid agar. BMC Bioinformatics 11: 287.
22. Shah NA, Laws RJ, Wardman B, Zhao LP, Hartman JLt (2007) Accurate, precise modeling of cell proliferation kinetics from time-lapse imaging and automated image analysis of agar yeast culture arrays. BMC Syst Biol 1: 3.
23. Kraft C, Deplazes A, Sohrmann M, Peter M (2008) Mature ribosomes are selectively degraded upon starvation by an autophagy pathway requiring the Ubp3p/Bre5p ubiquitin protease. Nat Cell Biol 10: 602–610.
24. Askree SH, Yehuda T, Smolikov S, Gurevich R, Hawk J, et al. (2004) A genome-wide screen for *Saccharomyces cerevisiae* deletion mutants that affect telomere length. Proc Natl Acad Sci U S A 101: 8658–8663.
25. Gatbonton T, Imbesi M, Nelson M, Akey JM, Ruderfer DM, et al. (2006) Telomere length as a quantitative trait: genome-wide survey and genetic mapping of telomere length-control genes in yeast. PLoS Genet 2: e35. doi:10.1371/journal.pgen.0020035.
26. SGD (2008) Saccharomyces Genome Database.
27. Eisenberg T, Knauer H, Schauer A, Buttner S, Ruckenstuhl C, et al. (2009) Induction of autophagy by spermidine promotes longevity. Nat Cell Biol 11: 1305–1314.
28. Ford AS, Guan Q, Neeno-Eckwall E, Culbertson MR (2006) Ebs1p, a negative regulator of gene expression controlled by the Upf proteins in the yeast Saccharomyces cerevisiae. Eukaryot Cell 5: 301–312.
29. Luke B, Azzalin CM, Hug N, Deplazes A, Peter M, et al. (2007) Saccharomyces cerevisiae Ebs1p is a putative ortholog of human Smg7 and promotes nonsense-mediated mRNA decay. Nucleic Acids Res 35: 7688–7697.
30. Zhou J, Hidaka K, Futcher B (2000) The Est1 subunit of yeast telomerase binds the Tlc1 telomerase RNA. Mol Cell Biol 20: 1947–1955.
31. Downey M, Houlsworth R, Maringele L, Rollie A, Brehme M, et al. (2006) A genome-wide screen identifies the evolutionarily conserved KEOPS complex as a telomere regulator. Cell 124: 1155–1168.
32. Dahlseid JN, Lew-Smith J, Lelivelt MJ, Enomoto S, Ford A, et al. (2003) mRNAs encoding telomerase components and regulators are controlled by UPF genes in *Saccharomyces cerevisiae*. Eukaryot Cell 2: 134–142.
33. Enomoto S, Glowczewski L, Lew-Smith J, Berman JG (2004) Telomere cap components influence the rate of senescence in telomerase-deficient yeast cells. Mol Cell Biol 24: 837–845.
34. Grandin N, Damon C, Charbonneau M (2000) Cdc13 cooperates with the yeast Ku proteins and Stn1 to regulate telomerase recruitment. Mol Cell Biol 20: 8397–8408.
35. Petreaca RC, Chiu HC, Nugent CI (2007) The role of Stn1p in Saccharomyces cerevisiae telomere capping can be separated from its interaction with Cdc13p. Genetics 177: 1459–1474.
36. Puglisi A, Bianchi A, Lemmens L, Damay P, Shore D (2008) Distinct roles for yeast Stn1 in telomere capping and telomerase inhibition. EMBO J.
37. Chandra A, Hughes TR, Nugent CI, Lundblad V (2001) Cdc13 both positively and negatively regulates telomere replication. Genes Dev 15: 404–414.
38. Stellwagen AE, Haimberger ZW, Veatch JR, Gottschling DE (2003) Ku interacts with telomerase RNA to promote telomere addition at native and broken chromosome ends. Genes Dev 17: 2384–2395.
39. Chan A, Boule JB, Zakian VA (2008) Two pathways recruit telomerase to Saccharomyces cerevisiae telomeres. PLoS Genet 4: e1000236. doi:10.1371/journal.pgen.1000236.
40. Beltrao P, Cagney G, Krogan NJ (2010) Quantitative genetic interactions reveal biological modularity. Cell 141: 739–745.
41. Costanzo M, Baryshnikova A, Bellay J, Kim Y, Spear ED, et al. (2010) The genetic landscape of a cell. Science 327: 425–431.
42. Gibson TJ (2009) Cell regulation: determined to signal discrete cooperation. Trends Biochem Sci 34: 471–482.
43. Warringer J, Ericson E, Fernandez L, Nerman O, Blomberg A (2003) High-resolution yeast phenomics resolves different physiological features in the saline response. Proc Natl Acad Sci U S A 100: 15724–15729.
44. Hillenmeyer ME, Fung E, Wildenhain J, Pierce SE, Hoon S, et al. (2008) The chemical genomic portrait of yeast: uncovering a phenotype for all genes. Science 320: 362–365.
45. Smallbone K, Simeonidis E, Swainston N, Mendes P (2010) Towards a genome-scale kinetic model of cellular metabolism. BMC Syst Biol 4: 6.
46. Morin I, Ngo HP, Greenall A, Zubko MK, Morrice N, et al. (2008) Checkpoint-dependent phosphorylation of Exo1 modulates the DNA damage response. EMBO J 27: 2400–2410.
47. Greenall A, Lei G, Swan DC, James K, Wang L, et al. (2008) A genome wide analysis of the response to uncapped telomeres in budding yeast reveals a novel role for the NAD+ biosynthetic gene BNA2 in chromosome end protection. Genome Biol 9: R146.
48. Aparicio O, Geisberg JV, Struhl K (2004) Chromatin immunoprecipitation for determining the association of proteins with specific genomic sequences in vivo. Curr Protoc Cell Biol Chapter 17: Unit 17 17.
49. Mani R, St Onge RP, Hartman JLt, Giaever G, Roth FP (2008) Defining genetic interaction. Proc Natl Acad Sci U S A 105: 3461–3466.
50. Bianchi A, Shore D (2007) Early replication of short telomeres in budding yeast. Cell 128: 1051–1062.